UNIVERSIDAD COMPLUTENSE DE MADRID
FACULTAD DE CIENCIAS BIOLÓGICAS

TESIS DOCTORAL

Pulmonary surfactant-related factors in the pathogenesis and therapies of respiratory diseases

Efectos y terapias con surfactante pulmonar en el tratamiento de patologías respiratorias

MEMORIA PARA OPTAR AL GRADO DE DOCTOR

PRESENTADA POR

Chiara Autilio

Directores

Mercedes Echaide Torreguitar
Jesús Pérez Gil

Madrid

UNIVERSIDAD COMPLUTENSE DE MADRID
FACULTAD DE CIENCIAS BIOLÓGICAS
Departamento de Bioquímica y Biología Molecular

PULMONARY SURFACTANT-RELATED FACTORS IN THE PATHOGENESIS AND THERAPIES OF RESPIRATORY DISEASES

EFECTOS Y TERAPIAS CON SURFACTANTE PULMONAR EN EL TRATAMIENTO DE PATOLOGÍAS RESPIRATORIAS

PhD Thesis
CHIARA AUTILIO

PhD Supervisors
MERCEDES ECHAIDE TORREGUITAR
JESÚS PÉREZ GIL

Madrid, Spain 2021

alla mia famiglia

The research for this Thesis has been conducted in the Department of Biochemistry and Molecular Biology of Complutense University of Madrid under the supervision of Prof. Jesús Pérez Gil and Prof. Mercedes Echaide. Clinical data and human samples were obtained in collaboration with Prof. Daniele De Luca, from the Division of Pediatrics and Neonatal Critical Care ("A.Béclère" Medical Center, Paris, France). Part of the experimental work was performed with PhD Jorid Sørli, at the Laboratory of Toxicology (National Research Centre for the Working Environment, Copenhagen, Denmark); with PhD María Carmen Rey Santano at Animal Research Unit (Hospital Universitario Cruces, Bilbao, Spain); with Prof. Maria Antonia Blasco Marhuenda at Spanish National Cancer Research Center (CNIO) (Madrid, Spain). Funding for the stay in Copenhagen and the financial support to complete this Thesis were provided by the Spanish Ministry of Science and Innovation (BES-2016-077009). Additional funding was in part supplied by two grants won by the PhD student from the European Society for Paediatric Research (ESPR) (Young Investigator Start-Up Grant 2017 and Post-Doc Research Grant 2019).

Table of contents

Table of contents

List of abbreviations

ABC: ATP-Binding Cassette
ADSA: Axisymmetric drop shape analysis
AF: Amniotic fluid
ARDS: Acute Respiratory Distress Syndrome
AT-I: Alveolar type I
AT-II: Alveolar type II
AUC: Area under the curve
BAL: Bronchoscopic bronchoalveolar lavage
BPD: Bronchopulmonary dysplasia
CBS: Captive Bubble Surfactometer
CCT: Cytidine triphosphate:phosphocholine cytidylyltransferase
CDP: Cytidine diphosphate
CDS: Constrained Drop Surfactometer
Cdyn: Dynamic compliance
CI: Confidence interval
CMV: Controlled mechanical ventilation
CPAP: Early continuous positive airway pressure
CRD: C-terminal carbohydrate-recognition domain
CRIB-II: Critical Risk Index for Babies II
CRP: C-reactive protein
cryo-EM: Cryogenic Electron Microscopy
DOPG: Dioleoylphosphatidylglycerol
DPPC: Dipalmitoylphosphatidylcholine
DSC: Differential scanning calorimetry
DSPC: disaturated phosphatidylcholine
ELISA: Enzyme-Linked ImmunoSorbent Assay
ER: Endoplasmic reticulum
FAS: Fatty acid synthase
FFAs: Free fatty acids
FiO_2: Fraction of inspired oxygen
fR: Respiratory frequency
G: Gas-like 2D phase
γ: Surface tension
GA: Gestational age
GARD: Global Alliance Against Chronic Respiratory Diseases
GM-CSF: Granulocyte-macrophage colony stimulating factor
γ_{max}: Maximum surface tension
γ_{min}: Minimum surface tension
GSH: Reduced glutathione
GSSG: Oxidised glutathione

HDL: High density lipoproteins

HFOV: High frequency oscillatory ventilation

IPF: Idiopathic Pulmonary Fibrosis

IQR: Interquartile range

Lα: Disordered liquid-crystalline phase

Lβ: Ordered gel phase

LBC: Lamellar body count

LC-HRMS: Liquid chromatography–high-resolution mass spectrometry

Lc: Liquid-condensed phase

Ld: Liquid-disordered phase

LDL: Low density lipoproteins

Le: Liquid-expanded phase

Lo: Liquid-ordered phase

LPC: Lysophosphatidylcholine

LPCAT1: Acyl-CoA:lysophosphatidylcholine acyltransferase

LPLs: Lysophospholipids

LPS: Lipopolysaccharide

LUS: Lung ultrasound score

MAS: Meconium aspiration syndrome

MEC: Size-molecular exclusion chromatography

MSAF: Meconium-stained amniotic fluid

nBAL: Non-bronchoscopic bronchoalveolar lavages

NF-kB: Nuclear factor kappa B

NICU: Neonatal Intensive Care Unit

NLD: No lung disease

NPC1: Niemann-Pick disease type C1 protein

NPC2: Niemann-Pick disease type C2 protein

OI: Oxygenation Index

OI_{adm}: oxygenation index at neonate admission

P63/CKAP4: Cytoskeleton-associated protein 4

$PaCO_2$: Partial pressure of carbon dioxide

PAGE: Polyacrylamide gel electrophoresis

PaO_2: Partial pressure of oxygen

PAP: Pulmonary alveolar proteinosis

Paw: Mean airway pressure

PC: Phosphatidylcholine

PE: Phosphatidylethanolamine

PEEP: Positive end-expiratory pressure

PG: Phosphatidylglycerol

PI: Phosphatidylinositol

PIP: Positive inspiratory pressure
PLA_2: Phospholipase A2
pIPC: Phosphatidylcholine plasmalogen
POPC: Palmitoyloleoylphosphatidylcholine
POPG: Palmitoyloleoylphosphatidylglycerol
PPARγ: Peroxisome proliferator-activated receptor gamma
PS: purified porcine surfactant
PuPC: Polyunsaturated PC
RDS: Neonatal respiratory Distress Syndrome
RFU: relative fluorescence units
ROS: Reactive species of oxygen
RUBAM: Research Unit on BioActive Molecules
SAT: Surfactant Adsorption Test
SE: Standard error
SNAPPE-II: Score for Neonatal Acute Physiology with Perinatal extension II
SP-A: Surfactant Protein A
SP-B: Surfactant Protein B
SP-C: Surfactant Protein C
SP-D: Surfactant Protein D
$sPLA_2$: Secretory PLA2
SR-BI: Scavenger receptor class B type I
SSA: 5-sulfo-salicylic acid dehydrate
StarD10: StAR Related Lipid Transfer Domain Containing 10
TGF-β: Transforming growth factor β
TLR-4: Toll Like Receptor 4
T_m: melting temperature
TNB: 5-thionitrobenzoic acid
TNF-α: Tumour necrosis factor-a
TTF-1: Thyroid transcription factor 1
unPC: Unsaturated phosphatidylcholine
VEI: Ventilator efficiency index
WBH: Whole-body hypothermia
WHO: World Health Organization

Summary

Respiratory diseases are one of the primary causes of death, disability and health costs worldwide. In this framework, the lack and dysfunction of lung surfactant may result in airless collapsed alveoli and difficulty for breathing, being the primary trigger or a contributing factor of severe respiratory disorders, such as neonatal respiratory distress syndrome (RDS) and acute respiratory distress syndrome (ARDS). RDS is a common cause of morbidity in preterm neonates, associated to immature lungs and an impaired secretion of pulmonary surfactant. The latter is, instead, present but inactivated during ARDS, a quickly progressive severe respiratory failure characterised by widespread acute lung inflammation. In both diseases, the leading role of pulmonary surfactant is due to its specific properties, which permit to maintain reduced surface tension values at the alveolar spaces, particularly upon exhalation. To accomplish this function, its lipid-protein complexes are secreted by pneumocyte type II cells and distribute, as a dense network of membranes, at the air liquid-interface that is generated between the aqueous layer covering the pulmonary epithelium and the alveolar air space. The resulting efficient adsorption, spreading and reorganisation of lung surfactant prevent alveolar collapse and depend on its particular composition: ~90% lipids, mainly disaturated phospholipids (~50%), and 10% of hydrophilic (SP-A and SP-D) and highly hydrophobic proteins (SP-B and SP-C).

Since pulmonary surfactant is essential for the process of breathing, exploring its alterations under a lung disease may optimise the diagnostic and therapeutic strategies, supporting clinical interventions. With this in mind, the main objective of this Thesis is to investigate the surfactant-related aspects involved in both the pathogenesis and therapy of several respiratory disorders. Making use of biophysical techniques, this may shed light on the role of pulmonary surfactant as a reliable indicator of changes in the alveolar milieu upon physiological and pathological conditions. In order to achieve this goal, the following specific aims are proposed:

1. Developing quick non-invasive and sensitive diagnostic methods to assay surfactant quality in several lung diseases (i.e. RDS and ARDS due to meconium aspiration (MAS)), using different sample sources (non-bronchoscopic bronchoalveolar lavages (nBALs) or amniotic fluid).

2. Understanding the main mechanisms under the early lung surfactant inactivation during pro-inflammatory acute lung injury (i.e. neonatal ARDS due to meconium aspiration).

3. Proposing new therapeutic strategies to reduce lung inflammation and surfactant disfunction upon an acute lung damage (i.e. whole body hypothermia (WBH) treatment in neonates with ARDS due to meconium aspiration).

4. Elaborating a biophysical *in vitro* model to explain the effects of reducing temperature on surfactant properties and using this model to propose novel therapeutic approaches (i.e. combining WBH and surfactant replacement therapy to enhance restoration of the surfactant system).

5. Exploring the involvement of lung surfactant in chronic and age-related diseases, which may resemble idiopathic pulmonary fibrosis due to telomerase disfunction.

In the present Thesis a biophysical technique, called surfactant adsorption test (SAT), which allows for a rapid screening of surfactant adsorption, was improved to create a rapid bench-to-bedside method. This technique has the potential to test surfactant activity from the lamellar bodies present in amniotic fluids of RDS neonates, thus contributing to identify which newborn could fail early continuous positive air pressure. SAT is also capable to detect

surfactant dysfunction in nBALs from MAS neonates. In this case, the impaired activity correlates with the neonatal lung aeration, the decrease in certain phospholipid species and the increase in secretory phospholipase A_2, an enzyme involved in surfactant phospholipid degradation. Moreover, an altered profile of SP-B and SP-C characterises the surface-active material of those MAS neonates, contributing to impair its capability to drastically reduce surface tension under compression. This was demonstrated in the Captive Bubble Surfactometer (CBS), a biophysical technique which emulates *in vitro* the dynamics of the alveolar breathing.

Once established that several compositional and structural alterations affect the interfacial properties of pulmonary surfactant in the early phases of a direct ARDS due to meconium aspiration, this Thesis has also suggested WBH as a possible candidate strategy to reduce lung inflammation and improve surfactant activity. WBH is applied in asphyxiated neonates with encephalopathy and consists of decreasing body temperature from 37 to 33.5 °C during 72 hours. Thus, testing pulmonary surfactant isolated from nBALs of those babies in CBS, a time-dependent improvement in the activity of the system was demonstrated when samples were analysed at 33.5 °C. This behaviour was associated to several compositional changes whose contribution was also explored by creating an *in vitro* model based on purified porcine surfactant and different surfactant lipid-protein mixtures. To do so, several biophysical and biochemical techniques were employed, among those Langmuir-Blodgett balances and Differential Scanning Calorimetry for the structural characterisation of surfactant complexes, lipidomic analysis to test composition and the innovative device Constrained Drop Surfactometer, which is the only method able to emulate an alveolus *in vitro* while studying simultaneously the effect of exogenous therapies during breathing-like dynamics. This has permitted to understand how the temperature-mediated improvement in lung surfactant activity is more evident when testing samples with high percentage of disaturated phospholipids with respect to unsaturated species. This occurs in endogenous and therapeutic surfactants under both physiological and oedema-like conditions. Starting from these evidences, the therapeutic combination of WBH and a disaturated phospholipid-enriched clinical surfactant (i.e. CHF 5633) was also proposed and explored in a piglet model of lung injury, with promising results.

Finally, the contribution of pulmonary surfactant inactivation upon fibrotic-like processes was also demonstrated in old wild type mice and young mice without a functional telomerase, which model may resemble some cases of idiopathic pulmonary fibrosis.

Overall, in this Thesis the possibility to test human and animal samples of different sources by basic biophysical techniques has made doable to study lung surfactant modifications in physiological processes and diseases, replacing simplified *in vitro* models that could not represent the *in vivo* complexity. This has allowed to demonstrate the crucial role of surfactant as a reliable indicator of the lung environment, introducing the new concept of translational research in surfactant biophysics.

Resumen

Las enfermedades respiratorias son una de las principales causas de muerte, discapacidad y gasto sanitario en todo el mundo. En este contexto, la falta o disfunción del surfactante pulmonar puede ser el desencadenante principal o un factor contribuyente de trastornos respiratorios graves, como el síndrome de dificultad respiratoria neonatal (RDS) y el síndrome de dificultad respiratoria aguda (ARDS). Gracias a su composición, estructura y actividad interfacial, el surfactante pulmonar cumple una función vital durante el proceso de la respiración, reduciendo la tensión superficial del fluido alveolar y minimizando la energía necesaria especialmente durante la exhalación. Aproximadamente el 90% del surfactante pulmonar son lípidos, principalmente fosfolípidos disaturados (~ 50%). El 10% restante lo componen fundamentalmente proteínas, dos hidrofílicas (SP-A y SP-D) y otras dos altamente hidrofóbicas (SP-B y SP-C). Para lograr esta función vital, los complejos lipoproteícos del surfactante se distribuyen como una densa red de membranas en la interfase aire-líquido generada entre la capa acuosa que recubre el epitelio pulmonar y el espacio aéreo alveolar. El resultado es una eficiente adsorción, propagación y reorganización del material tensoactivo que previene el colapso alveolar.

Dado que el surfactante pulmonar es esencial para el proceso respiratorio, explorar la naturaleza de sus alteraciones durante ciertas patologías pulmonares puede optimizar las estrategias diagnósticas y terapéuticas, así como las intervenciones clínicas. En esta línea, el principal objetivo de esta Tesis es investigar los aspectos relacionados con el surfactante en la patogenia y terapia de varios trastornos respiratorios. El empleo de técnicas biofísicas, utilizando muestras de pacientes, puede permitir explorar el papel fisiológico de este complejo como indicador crucial de cambios en el medio alveolar en diferentes condiciones patológicas. Para ello, se plantean los siguientes objetivos específicos:

1. Desarrollar métodos de diagnóstico rápido, no invasivos y sensibles para evaluar la calidad del surfactante en varias enfermedades pulmonares (SDR y SDRA debido a la aspiración de meconio), utilizando surfactantes obtenidos de diferentes fuentes (lavados broncoalveolares no broncoscópicos (nBAL) o líquidos amnióticos).

2. Comprender los principales mecanismos de la inactivación temprana del surfactante pulmonar durante una lesión pulmonar aguda pro-inflamatoria (SDRA neonatal debido a aspiración de meconio (MAS)).

3. Proponer nuevas estrategias terapéuticas para reducir la inflamación alveolar y la disfunción del surfactante ante un daño pulmonar agudo (tratamiento con hipotermia terapéutica de cuerpo entero (WBH) en neonatos con MAS).

4. Elaborar un modelo biofísico para explicar los efectos de la reducción de la temperatura sobre las propiedades del surfactante y utilizar este modelo para proponer enfoques terapéuticos novedosos (combinar WBH y terapia de reemplazo de surfactante para mejorar la restauración del surfactante).

5. Explorar la participación del surfactante pulmonar en enfermedades crónicas y relacionadas con la edad, que pueden parecerse a la fibrosis pulmonar idiopática debido a la disfunción de la telomerasa.

En la presente Tesis se mejoró una técnica biofísica, denominada prueba de adsorción del surfactante (SAT), que permite detectar la adsorción interfacial de material tensoactivo de manera sencilla, con el fin de crear un ensayo rápido y utilizable en clínica. Esta técnica se ha podido emplear para examinar la adsorción de los cuerpos lamelares presentes en los líquidos amnióticos de recién nacidos con SDR, contribuyendo así a seleccionar qué recién nacido puede necesitar una terapia de remplazo con surfactante exógeno. SAT también se ha demostrado capaz de detectar la disfunción del surfactante en nBAL de recién nacidos con MAS. En este caso, la actividad deteriorada del surfactante se ha podido correlacionar con la aireación pulmonar neonatal, la disminución de ciertas especies de fosfolípidos y el aumento de la fosfolípasa A_2 secretora, una enzima involucrada en la degradación del surfactante. Además, se ha encontrado un perfil alterado de SP-B y SP-C, lo que contribuye a perjudicar la capacidad del surfactante pulmonar para reducir drásticamente la tensión superficial bajo compresión durante el MAS. Esto se ha podido demostrar utilizando el Surfactómetro de Burbuja Cautiva (CBS), una técnica biofísica que simula el alveolo durante la dinámica respiratoria.

Una vez establecido que varias alteraciones composicionales y estructurales afectan a las propiedades interfaciales del surfactante en las primeras fases de SDRA debido a aspiración meconial, esta Tesis también ha sugerido la WBH como una posible estrategia para reducir la inflamación alveolar y mejorar la actividad del surfactante. La WBH se emplea en recién nacidos asfixiados con encefalopatía y consiste en disminuir la temperatura corporal de 37 a 33.5 °C. Así, se utilizó el surfactante pulmonar aislado desde el nBAL de esos bebés para ensayar su actividad en CBS, demostrando una mejora a 33.5 °C. Este comportamiento se asoció a varios cambios composicionales cuya contribución también se exploró mediante la creación de un modelo *in vitro*. Para ello, se emplearon diversas técnicas biofísicas y bioquímicas, entre las que destacan la balanza de Langmuir-Blodgett y calorimetría diferencial de barrido para la caracterización estructural de los complejos tensioactivos, análisis lipidómico para analizar la composición del sistema y el surfactómetro de gota sésil, un dispositivo innovador único, capaz de emular un alvéolo y posibilitar el estudio del efecto de terapias exógenas durante los ciclos respiratorios. Esto ha permitido comprender cómo la mejora mediada por la temperatura en la actividad tensoactiva del surfactante es más evidente cuando se analizan muestras con alto porcentaje de fosfolípidos disaturados con respecto a especies insaturadas. A partir de estas evidencias, también se exploró la combinación terapéutica de WBH y un surfactante clínico enriquecido en fosfolípidos disaturados en un modelo de lechones con lesión pulmonar.

Finalmente, también se ha podido demostrar la implicación de un surfactante pulmonar alterado durante procesos fibróticos tanto en ratones jóvenes sin una telomerasa funcional como en ratones senescentes.

En resumen, en esta Tesis se ha demostrado el papel crucial del surfactante pulmonar como un indicador fiable del entorno alveolar tanto en circunstancias fisiológicas como patológicas, introduciendo un nuevo concepto de investigación traslacional en biofísica.

Part of this text has been published in the following reviews:

Echaide M, Autilio C, et al., BBA Biomembr. 2017, 1859(9 Pt B):1725-1739

Autilio C & Perez-Gil J., Arch Dis Child Fetal Neonatal Ed. 2019, 104(4):F443-F451

Introduction

The economic burden of respiratory diseases

"A lot of people don't like the road, but it's as natural to me as breathing," Bob Dylan once told the New York Times (Gage, 2018). We take our pulmonary health and breathing for granted, but the lung is an organ as vital as vulnerable to direct and indirect injuries. Lung disease is a major cause of morbidity, disability and death worldwide mainly associated to low socioeconomic status (Wisnivesky & de-Torres, 2019). As a consequence, respiratory diseases pose a huge burden on worldwide society concerning premature mortality (four million people annually), disability and health service costs. The latter in Europe for chronic pulmonary conditions alone amounts to more than €380 billion every year (Soriano *et al*, 2020). Thus, the Global Alliance Against Chronic Respiratory Diseases (GARD) was launched by the World Health Organization (WHO) in 2006 as a non-profit alliance of national and international institutions, organisations and agencies to struggle against the global burden of lung disorders (Soriano *et al.*, 2020). GARD called "the big five" the most common respiratory conditions, among those chronic obstructive pulmonary disease, asthma, lung cancer and tuberculosis, affecting altogether more than 400 million people in the world (Ferkol & Schraufnagel, 2014).

Although less frequent, other diseases related to pulmonary surfactant lack or inactivation, such as neonatal Respiratory Distress Syndrome (RDS) or Acute Respiratory Distress Syndrome (ARDS) also contribute to the costs of care before and after hospital discharge. According to WHO, 15 million neonates are born preterm every year with the greatest number (around 7.4 million) in six countries – India, China, Nigeria, Pakistan, Indonesia and United States, corresponding to 50% of worldwide preterm births. Conversely, in Europe the percentage is lower (5-10%) and apparently independent from the healthcare infrastructure (Walani, 2020). Initial hospitalisation for an infant born at term in the United States costs around $930, reaching $576,972 per neonate born at 24 weeks' gestation (Petrou *et al*, 2019). Surfactant replacement therapy plays an important role since cost-effectiveness depend on clinical surfactant administration and the selected doses (Mugford, 2006).

ARDS is a life-threatening form of respiratory failure, accounting for 10% of intensive care unit admissions (Matthay *et al*, 2019) with a mortality ranging from 40 to 45 % (Papazian *et al*, 2019). Around 2 million patients are diagnosed annually in the United States, resulting in approximal 75,000 deaths each year (Fan *et al*, 2018). The incidence of the syndrome is about 17.9 per 100,000 person-years in Europe and 78.9 per 100,000 person-years in USA (Confalonieri *et al*, 2017; Rezoagli *et al*, 2017; Rubenfeld *et al*, 2005). The analysis of commercially-insured individuals from 2009 to 2013 in United States suggests that ARDS patients had longer stays (16.7 vs. 4.6 days), higher mortality (11.9% vs. 0.8%) and costs ($117,137 vs. $25,199) than non-ARDS hospitalised patients (Wu *et al*, 2015). Moreover, long-lasting effects beyond hospitalisation are also frequent, increasing the healthcare price (Mart & Ware, 2020).

Idiopathic Pulmonary Fibrosis (IPF) is generally considered a rare disease. However, it may contribute to the charge of respiratory disorders due to the high mortality rate and its expensive treatment options including lung transplantation (Raimundo *et al*, 2016).

Altogether these evidences indicate the importance to explore new strategies that can lower the costs and rise the health benefits. For this purpose, investigating the changes in the pulmonary surfactant system during lung injuries and exploring novel treatments to enhance its endogenous and therapeutic activities may contribute to alternative approaches to avoid serious complications as well as early and long-term costs of respiratory diseases.

Lung structure and respiratory mechanics

Lung morphology and physiology

The lungs are a complex organ, characterised by a pair of spongy and air-filled sacs placed into the chest (**Figure 1A**). Each sac is also divided into sections called lobes: three in the right lung, two in the left. The macro and microstructure of mammalian lungs define its functional capacity as a gas exchanger (Knudsen & Ochs, 2018). The lungs extend into the chest as an airway conducting tree, maximizing the diffusion of gases. The trachea serves to guide the inhaled air through the bronchi that are tubular branches. The bronchi are also divided into smaller and smaller branches, called bronchioles. These are connected, in turn, trough thin ducts to distal bunches of microscopic air sacs, known as alveoli with a radius of ~0.1 mm (Nkadi *et al*, 2009).

The respiratory bronchiole and all of its associated alveolar ducts and alveoli constitute the gas exchange unit, called alveolar acinus. The alveolar region, the most representative structure of parenchyma, has a huge surface in a small volume where air and blood are kept close to allow for gas exchange (Knudsen & Ochs, 2018). The oxygen from the air, necessary for cellular respiration, diffuses from the alveolar space to the de-oxygenated blood. The latter reaches the capillary beds that wrap each alveolar sac, flowing from the right ventricle of the heart through the pulmonary artery and arterioles (**Figure 1B**). At the same time of blood oxygenation, the waste product of cellular metabolism, carbon dioxide, moves up from the capillary blood to the alveoli to be exhaled, travelling bronchioles, bronchi and trachea backwards. This gases exchange is possible thanks to the difference in the partial pressure of oxygen (PaO_2) and carbon dioxide ($PaCO_2$) between the alveolar lumen and the pulmonary capillaries (64 mm Hg for oxygen, -6 mm Hg for carbon dioxide). Thus, the oxygenated blood (~100 mm Hg for oxygen, 40 mmHg for carbon dioxide) may flow again to the heart, reaching the left atrium through the pulmonary vein (Wagner, 2015).

To facilitate and optimise gas exchange, the interalveolar septum provides a large surface area (about 140 m^2 in humans) and a very thin diffusion barrier that is highly permeable to gases (2 μm in the human lung) (Knudsen & Ochs, 2018). The latter is characterised by three elements: 1) a mosaic of alveolar type I (AT-I) and more diffuse type II (AT-II) epithelial cells facing the alveolar lumen and residing on a basal membrane, 2) a continuous endothelium facing the capillary lumen and 3) the interstitium, i.e. the connective tissue layer in between (**Figure 1C**). Moreover, resident quiescent alveolar macrophages are also present close to pneumocytes as pathogen sensors, ready to promote the recruitment of immune cells when necessary and take part in lung surfactant catabolism (Agassandian & Mallampalli, 2013; Ikegami, 2006). AT-I cells cover 95% of lung surface area due to their thin and elongated shape, providing the barrier and permeability function to the alveolar membrane. Conversely, AT-II cells exhibit a cuboid shape, allowing for pulmonary surfactant secretion and both repair and renewal of alveolar epithelium.

The connective tissue backbone, made mostly of collagen and elastin fibres, is crucial to mechanically sustain the parenchyma, forming a self-stabilizing tensegrity (tension + integrity) structure (Knudsen & Ochs, 2018). Indeed, under the breathing-mediated changes in lung volume, the alveolar over-distention or collapse should be avoided and the thoracic movements should be accommodated by providing both stability and flexibility.

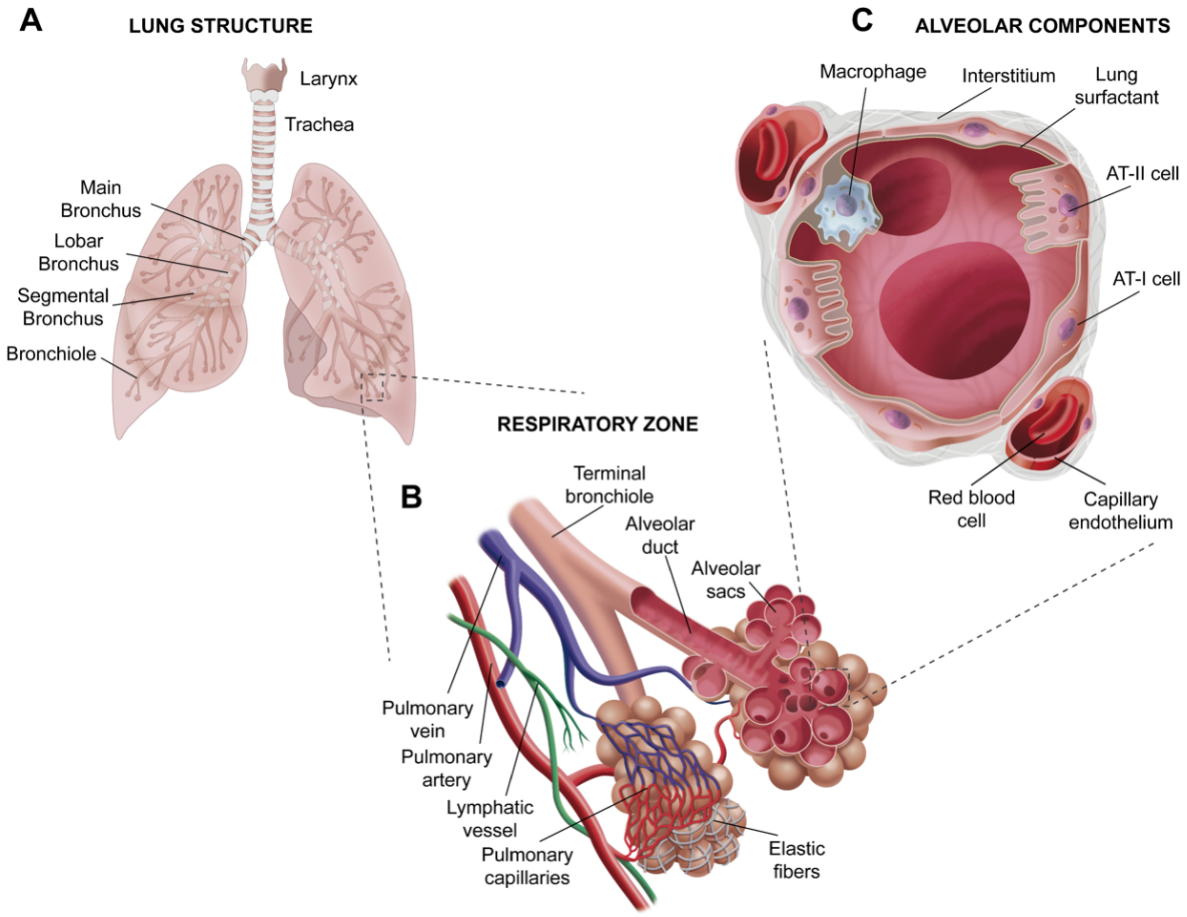

Figure 1. Lung structure and components. (A) The airway conducting tree of lungs and its complexity are shown. The alveolar sacs **(B)** as well as the crucial elements in alveoli **(C)** are also detailed. *Figure modified from https://www.mheducation.com/*.

Under each respiratory cycle, the changes in volume cause deformations in the structure size of ductal and alveolar airspaces as well as interalveolar septa when compared to the starting condition (Knudsen & Ochs, 2018). The tidal volume is the air volume inside the lungs displaced during a normal inhalation-exhalation cycle without applying extra effort. Thus, physiologically, deformation of the whole lung can be calculated using the tidal volume, whereas the functional residual volume (the volume remaining in the lungs after a passive exhalation) indicates the baseline situation. As for mechanical ventilation, the ventilator flow corresponds to the tidal volume, while the functional residual volume can be calculated as the lung volume at a given positive end-expiratory pressure (PEEP). The latter is the pressure applied by the ventilator at the end of patient's expiration to avoid alveolar collapse, maintaining the alveolar pressure higher than the atmospheric one.

In clinical setting, the elastic forces that counteract lung inflation are described by compliance measurements (the reciprocal of elastance), defining the lung capacity to expand and stretch (Cairo, 2019). The compliance can be quantitatively assessed by measuring the change (Δ) of volume (V) that takes place when pressure (P) is applied to the system, as follows:

$$\text{Compliance } (C) = \Delta V / \Delta P$$

As for the respiratory system, the total compliance is the sum of compliances of both thoracic structures and lung parenchyma. In a spontaneous breathing, it is defined by the change in lung volume "per unit change" in transmural pressure gradient (namely the difference between alveolar and pleural pressure). For mechanically ventilated patients, PEEP should be also considered when measuring static and dynamic compliances.

Under healthy conditions and not affected lungs, the volume differences during respiration occur under a minimal lung effort and an easy distensibility (high compliance), in part as a result of the elastic properties of fibres. In this line, elastin and collagen fibres have different mechanical contributions depending on the lung volume (Mason *et al*, 2010). Elastin fibres can be stretched by more than 130% of their length, being very compliant and having a low tensile strength. Conversely, collagen fibres are not compliant and show high tensile strength (the maximum stretching of their length is around 2%). Thus, elastin fibres bear much of the stress at low lung volume, whereas the collagen fibres remain coiled and inert. Increasing the volume, the collagen fibres become straight and give a major contribution to lung stiffening. In this way, lung overdistention is limited (collagen) and a high stability of the lung microstructure is provided, facilitating lung inflation (elastin) (Mason *et al.*, 2010).

However, the lung connective tissue is only responsible of one fourth to one third of the elastic resistance. As a consequence, the majority of lung elastance depends on pulmonary surfactant activity (Mason *et al.*, 2010). Alveoli have an innate tendency to collapse due to their intrinsic characteristics: small size, spherical shape, water vapor into the alveolar space and a watery layer lining the epithelium (Nkadi *et al.*, 2009). Nevertheless, this is avoided by lung surfactant that increases lung compliance through its capability to fall down alveolar surface tension, reducing the work required for lung expansion and preventing alveolar collapse at low volumes (end of expiration).

Lung surfactant, surface tension and oedema prevention

As aforementioned, while the epithelial cells are tightly attached to one another, the alveolar-capillary barrier is characterised by an interstitium that maintains the AT-I/AT-II cells and the endothelial cells more spaced. This allows for the exchange of waste and nutrients between bloodstream and tissues. This balance in liquid exchange is promoted by both the capillary structure and the fluid dynamics. According to Starling's equation, the rate of fluid exchange is governed by the hydrostatic pressure (P, the pressure of the liquid against the wall) and the oncotic pressure (π, the osmotic pressure resulting from the imbalance in protein concentration between the two sides of a semi-permeable membrane) (Wojciechowski, 2005). The first is higher in the pulmonary capillary than in the interstitium and promotes an overall movement of fluids to the interstitial space. However, this flow is counteracted by the capillary oncotic pressure of proteins that cannot cross the endothelial capillary membrane, mainly albumin. In physiological conditions, this results in a gradient that opposes the fluid transfer to the interstitial space, promoting a low filtration pressure (1mm Hg) (**Figure 2A**). Thus, there is a small net movement of fluids from the bloodstream to the interstitium that are continuously drained by lymphatic system, preventing liquid accumulation.

This process maintains the interstitial space and the alveolar epithelium relatively "dry". At the same time, sodium-pumps on AT-II cells also play a role to balance fluid exchanges between the alveolar space and the interstitium. Fluid pressure is large and negative in the alveolar corners (due to a very small radius of curvature), but slighter in the flatter alveolar

parts. This normally may attract fluids into the alveolar hypophase from the interstitial space via alveolar corners and fissures. However, sodium pumps in AT-II cells remove sodium from the hypophase and transport it into the interstitial space, causing a net passive fluid flow out of the alveolus, thereby preventing fluid build-up (Orgeig *et al*, 2010).

Therefore, the alveolar epithelium is only covered by a very thin liquid layer similar in composition to interstitial fluid (about 200 nm thin in the rat lung) that is the minimum necessary to create an aqueous milieu for cell survival. At the resulting air-liquid interface, water molecules in contact with air cohere more strongly, because the interactions with the water bulk phase are not compensated with interactions on the air side where water molecules in vapour phase are scarce (**Figure 2B**). This generates a net intermolecular cohesive force, which is defined as the surface tension (γ). When new surface exposed to air is opened (as necessary under each single inspiration), this cohesive superficial force needs to be overcome, providing the energy required for breaking the molecular interactions that the new molecules demand to break through the gas-liquid interface. As a consequence, at high surface tension, a proportion of metabolic energy would be dissipated by the work of breathing, namely opening the lungs 15-20 times/min, unavoidably ending in alveolar collapse (Autilio & Pérez-Gil, 2019).

This collapse of small alveoli also affects the surrounding bigger alveoli. According to Young-Laplace's law (**Figure 2B**), the inner pressure (ΔP) of an idealised spherical alveolus of radius r is calculated as follows:

$$\Delta P = 2\gamma/r$$

where γ is surface tension measured in mN/m and r is the radius of curvature measured in m. Therefore, alveoli with small radius are characterised by higher internal pressures compared to alveoli with larger radius. Accordingly, the small alveolus would tend to collapse and the air would move up to bigger ones. Moreover, because of the alveolar interdependence, any tendency for a group of alveoli to collapse generates great expanding forces on them due to the septal distortion of adjacent alveoli that are expanding to counterbalance (Sehlmeyer *et al*, 2020). This rises mechanical stresses, resulting in further damages to alveolar epithelium (Sehlmeyer *et al.*, 2020).

In this scenario, to permit alveolar size heterogeneity, prevent alveolar collapse and reduce the work of breathing, lung surfactant spontaneously generates a stable film at the air-liquid interface, displacing water molecules from exposure to air and therefore decreasing surface tension (**Figure 2B**). This reduction is drastic (to values < 2mN/m) especially at the end of expiration when the lung volume is decreased. At the same time, pulmonary surfactant contributes indirectly to maintain the alveoli "dry". High surface tension indeed ends in alveolar collapse lowering interstitial hydrostatic pressure, thus increasing the capillary filtration pressure and the transudation of fluids.

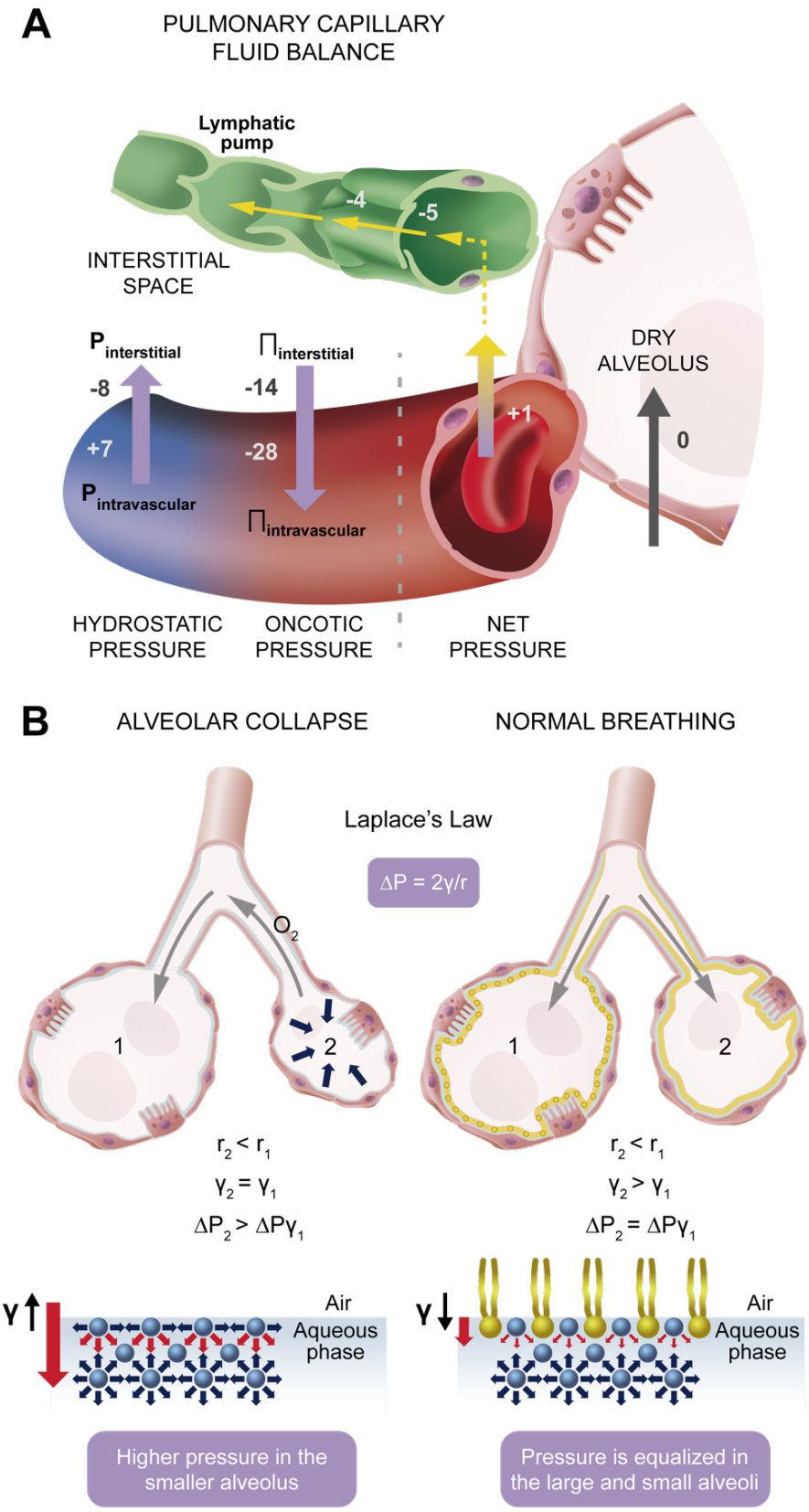

Figure 2. Pulmonary capillary fluid balance and surface tension. (A) Starling's equation principles applied to lung capillaries, interstitial space and lymphatic fluid. This occurs upon physiological condition, resulting in a relatively "dry" alveolus. **(B)** Synthetic representation of surfactant effects in alveoli according to Laplace's Law and illustration of surfactant-mediated surface tension reduction. *Figure modified from (Autilio & Pérez-Gil, 2019; Sehlmeyer et al., 2020; Van Vliet & Montani, 2005).*

Lung surfactant: from alveolar type II cells to the air-liquid interface

Surfactant composition

Lung surfactant, discovered in the 1950s by Richard Pattle, is a complex mixture of lipids and proteins synthetized by AT-II cells and secreted into the alveolar lining fluid from highly packed oblong organelles, called lamellar bodies. Once out of the cell, lung surfactant organises itself into a dense network of membranes, connecting the epithelial layer to the air-liquid interface. The resulting interconnected structures that extend into the liquid subphase are essential for surfactant elements to reach the air-liquid interface and play their surface-active role.

The major components of lung surfactant are lipids (~ 92% of the total mass), mostly phospholipids that represent the principal class with phosphatidylcholine (PC) being the most predominant species (70-80% of the total mass) (Autilio & Pérez-Gil, 2019). Phospholipids consist of a glycerol molecule, two fatty acids and a phosphate group that is modified by an alcohol (van Meer *et al*, 2008). This group is characterised by a negatively-charged polar head and represents the hydrophilic part of the lipid, whereas the fatty acids, that are uncharged, constitute the nonpolar hydrophobic tails (**Figure 3A**). As for PC, the lipid is a zwitterion (electrically neutral) at physiological pH, due to the presence of both a negative phosphate group and a positive choline group. Because of their amphipathic nature, all phospholipids distribute at the air-liquid alveolar interface as a monolayer with their hydrophilic heads facing the liquid epithelial layer and their hydrophobic tails facing outwards (**Figure 3B**).

Moreover, phospholipids and therefore PC, can be also classified as saturated or unsaturated depending on the absence or presence of double bonds between carbons in their fatty acid tails. Accordingly, saturated phospholipids have unkinked and straight tails, whereas unsaturated phospholipids have kinked and crooked tails (**Figure 3A**). This leads to a different area occupied by the lipid at the air-liquid interface and a different capacity to pack under the lateral compression depending on the saturation-unsaturation status. As a consequence, the surface tension is more reduced when saturated phospholipids are present since these species can be packed to a tighter extent at the air-liquid interface upon compression compared to the unsaturated ones. Thus, since the crucial function of surfactant is to drastically reduce surface tension, a saturated phospholipid, namely dipalmitoylphosphatidylcholine (DPPC, 16:0/16:0 PC), accounts for the majority of total lipid mass, from 40 to 50% depending on the species (Cañadas *et al*, 2020).

To increase lung surfactant fluidity, namely the lipid diffusion across the monolayer and the bilayers underneath, promoting the surfactant movement towards the air-liquid interface and its proper distribution, unsaturated phosphatidylcholine (unPC), the anionic phosphatidylglycerol (PG) and cholesterol are also important elements. They represent ~25%, ~10% and ~5–8% of the total mass, respectively. Finally, other lipid species (neutral lipids and other phospholipids) correspond to the remaining 8–10% (Autilio & Pérez-Gil, 2019).

The residual part of lung surfactant (~8-10% of the total mass) is constituted by four specific proteins, which can be classified into two families: the hydrophobic Surfactant Protein B (SP-B) and C (SP-C), and the hydrophilic SP-A and SP-D. SP-A, SP-B and SP-C are associated to surfactant membranes with preferential interactions with negative-charged phospholipids (SP-B, SP-C) and DPPC (SP-A), and are crucial for the formation of the lung

surfactant interfacial film, to organise and stabilise its structure, and warranting a correct recycling (**Figure 3B**). Moreover, SP-A and SP-D are members of the collectin (C-type collagen-containing lectins) protein family and are mostly required for the innate immune defence against potentially harmful inspired particles, allergens and lung pathogens (Autilio & Pérez-Gil, 2019).

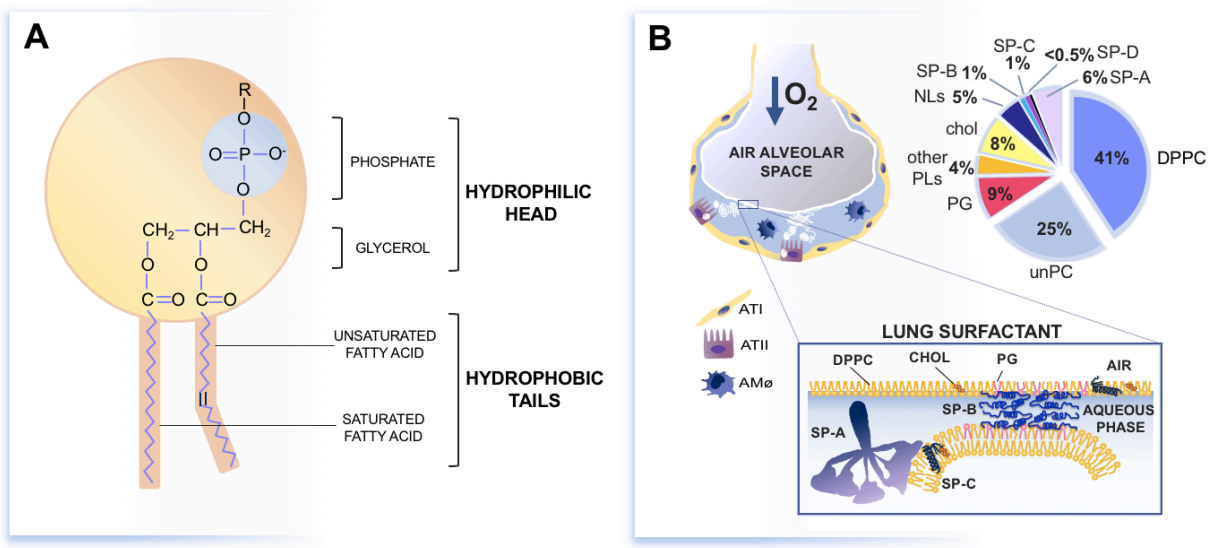

Figure 3. Major components of lung surfactant. (A) A phospholipid schematic representation, showing the hydrophilic and hydrophobic parts of the molecule and two different fatty acids, resulting in a kinked tail. **(B)** A schematic representation of a normal alveolus, with the lipid/protein composition of the surfactant system and the organisation of lung surfactant complexes at the air-liquid interface, showing the crucial elements. *Figure and caption adapted from (Autilio & Pérez-Gil, 2019) and lumen.learning.com.* Abbreviations: ATI, alveolar type I pneumocytes; ATII, alveolar type II pneumocytes; CHOL, cholesterol; DPPC, saturated dipalmitoylphosphatidylcholine; NLs, neutral lipids; PG, phosphatidylglycerol; PL, phospholipid; unPC, unsaturated phosphatidylcholine.

Surfactant lipid synthesis

Alveolarization is a process characterised by the simultaneous increase in the number of alveoli and the reduction in alveolar space, which takes place from 36 weeks preterm to 36 months postnatal period in human lungs (Copland & Post, 2004). This process is regulated by several factors, among those a precise balance between glucocorticoid and transforming growth factor β (TGF-β) signalling, which is essential for AT-II cells differentiation (McDevitt *et al*, 2007). The latter occurs among 24 and 34 weeks of gestation and is necessary for lung surfactant production (Nkadi *et al.*, 2009).

In differentiated AT-II cells, surfactant phospholipids synthesis occurs in the endoplasmic reticulum (ER) as a *de novo* synthesis or in lamellar bodies by secondary remodelling (Olmeda *et al*, 2017). These depends on the endogenous fatty acids availability that, in turn, is related to the activities and mRNA levels of key enzymes such as fatty acid synthase (FAS), acetyl CoA carboxylase and citrate lyase (Agassandian & Mallampalli, 2013). As expected and observed in cellular models, glucocorticoids can activate FAS activity in foetal lung, whereas TGF-β1 and thyroid hormone antagonise this effect (Lu *et al*, 2001b). Moreover, targeted disruption of mice genes codifying enzymes involved in PC synthesis such as cytidine triphosphate:phosphocholine cytidylyltransferase (CCT) alfa locus (*Pcytla*), results in

embryonic lethality, underlying the importance of PC during early embryogenesis (Wang *et al*, 2005b).

Around 45% of DPPC is synthetized by *de novo* synthesis and approximately 55-75% from the remodelling pathway (Agassandian & Mallampalli, 2013). The first process, also essential to synthetize other PC species, takes place via the Kennedy pathway, characterised by (1) the choline kinase-mediated phosphorylation of choline, (2) the conversion to cytidine diphosphate (CDP)-choline by CCT, and (3) the ultimate synthesis of PC promoted by choline phosphotransferase. For this final step, it is crucial the conversion of phosphatic acid into diacylglycerol intermediates by the action of phosphatidic acid phosphatase (Pol *et al*, 2014). At the same time, the remodelling pathway to generate disaturated PC (DSPC), namely Lands cycle, occurs by two steps: (1) de-acylation at the *sn*-2 position of unsaturated PC by cytosolic phospholipase A2 (PLA_2), mediated by a calcium-dependent phospholipase A2 (Filgueiras & Possmayer, 1990) or by the calcium-independent peroxiredoxin 6 activity (Fisher & Dodia, 2001; Olmeda *et al.*, 2017); (2) the re-acylation of the resulting lyso-PC with the corresponding saturated fatty acid (16:0 for DPPC) thanks to acyl-CoA:lysophosphatidylcholine acyltransferase (LPCAT1) action. The latter is indeed essential to maintain the correct amount of saturated-PC in AT-II cells and lamellar bodies in mice (Bridges *et al*, 2010) and seems to be involved in a cross-talk with the *de novo* pathway (Butler & Mallampalli, 2010).

As for PG, *de novo* synthesis occurs via CDP-diacylglycerol (Agassandian & Mallampalli, 2013) and the remodelling mechanism also takes place for generating disaturated species, mainly DPPG (17–38% of total PG (Olmeda *et al.*, 2017)), with LPCAT1 as the principal actor (Nakanishi *et al*, 2006).

Finally, the third crucial component of lung surfactant lipids, namely cholesterol, is provided to the lungs by 3 mechanisms (Olmeda *et al.*, 2017): 1) the circulating low and high-density lipoproteins (LDL and HDL) from blood plasma that supply the majority of the sterol (~80%), 2) the synthesis in the peroxisomes of AT-II cells and (Krisans, 1992) and 3) the action of cholesterol-binding proteins Niemann-Pick disease type C1 (NPC1) and C2 (NPC2) present in the limiting membrane of lamellar bodies (Roszell *et al*, 2012) involved in the trafficking in response to several environmental conditions, such as upon strenuous exercise or changes in body temperature (Doyle *et al*, 1994; Orgeig *et al*, 2003).

Hydrophobic surfactant proteins synthesis and function

SP-B is an essential protein of the lung surfactant system, involved both in its biogenesis and surface-active properties. It is required (1) to properly pack lipid membranes in lamellar bodies and stimulate their exocytosis (Clark *et al*, 1995; Martínez-Calle *et al*, 2018; Stahlman *et al*, 2000), (2) to correctly process SP-C, supporting its physiological proportion into the alveolar space, although which SP-B forms contribute to this process is still unknown (Clark *et al.*, 1995; Vorbroker *et al*, 1995), (3) to promote adsorption of surface active lipids from membranes into the air-liquid interface (Parra & Pérez-Gil, 2015; Ross *et al*, 2002; Rugonyi *et al*, 2008; Wang *et al*, 1996a; Wang *et al*, 1996b) and their lateral spreading during inspiration (Cruz *et al*, 2004; Schürch *et al*, 2010) and (4) to participate on a proper re-organisation and stability of surfactant membranes upon lateral compression (expiration) (Cabré *et al*, 2009; Diemel *et al*, 2002; Schürch *et al.*, 2010; Taneva & Keough, 1994b). Those biophysical properties are enhanced in the presence of SP-C. Moreover SP-B in surfactant films seems to accelerate the oxygen diffusion at the air-liquid interface (Olmeda *et al*, 2010) and exhibits a

putative anti-inflammatory role, which may protect the lung from oxidative stress (Miles *et al*, 1999; Tokieda *et al*, 1999; Um *et al*, 2013). Because of those crucial roles, the severe deficiency of SP-B causes lethal respiratory distress failure at birth in mice models and humans (Clark *et al.*, 1995; Nogee *et al*, 1994; Wilder, 2004).

SP-B is encoded by SFTPB, a single long gene (9.5 kb) on chromosome 2, composed of 11 exons and 10 introns, whose transcription is under thyroid transcription factor 1 (TTF-1) regulation (Nkadi *et al.*, 2009). RNA processing results in a 2.0 kb RNA which is polyadenylated and translated into a soluble preprotein of around 40 kDa. In the ER, the signal peptide at the N-terminal end is then cleaved, generating a shorter soluble pro-SP-B that is processed, in turn, by sequential proteolytic steps at both N- and C-terminals. This is associated to an increase in protein hydrophobicity and confinement in intracellular vesicles (**Figure 4**). Indeed, the processing of hydrophobic surfactant proteins occurs within different compartments from the ER through the Golgi apparatus and multivesicular bodies to lamellar bodies (Weaver, 1998). After the last cleavage that occurs in lamellar bodies, a mature hydrophobic form of around 8 kDa is generated (corresponding to exons 6-7) (García-Álvarez *et al*, 2019).

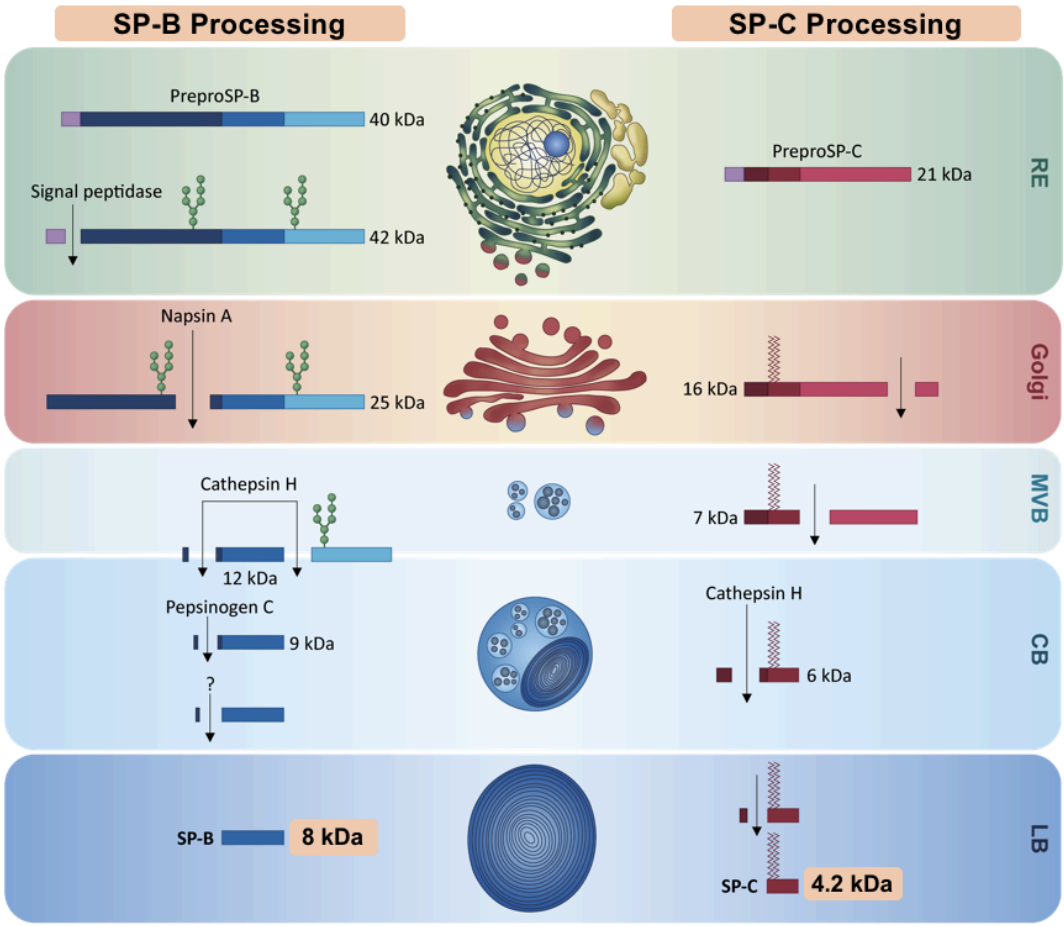

Figure 4. Processing of hydrophobic surfactant proteins. Schematic steps of SP-B and SP-C modifications involving several enzymes that cleave precursors to progressively more hydrophobic intermediates, moving from endoplasmic reticulum to lamellar bodies. *Figure adapted from (García-Álvarez et al., 2019).* Abbreviations: RE, endoplasmic reticulum; MVB, multivesicular bodies; CB, composite bodies; LB, lamellar bodies.

This mature SP-B is a hydrophobic 79 amino acid polypeptide that includes nine positive-charged residues, necessary for the interaction with anionic lipids of lung surfactant (Ross *et al.*, 2002; Walters *et al*, 2000), and two anionic residues.

SP-B belongs to the saposin-like protein family with approximately 40-50% of α-helix content (Olmeda *et al*, 2013) and is strictly associated to lipid membranes. Monomers of SP-B are characterised by five amphipathic α-helices in a folding clamp that resembles 2 leaves: one is composed of N-terminal α-helix 1, α-helix 4 and C-terminal α-helix 5. The other contains α-helices 2 and 3. Moreover, the protein also contains seven cysteines, six of them forming three intramolecular disulphide bridges (Johansson *et al*, 1991), whereas the seventh cysteine is involved in SP-B covalent dimerisation (**Figure 5A**).

A recent study has used the high-resolution structure obtained by crystallisation of a protein homologous of SP-B, called Saposin B, to build a model for SP-B supramolecular organisation (**Figure 5A**) (Olmeda *et al*, 2015). Monomers of SP-B may generate dodecamers that are structured in one ring of 12 subunits with a hydrophobic cavity inside. This organisation would assemble first by coiled-coil non-covalent interactions between the N-terminals of two monomers to create functional dimers. Six dimers could then associate laterally to form the ring-shaped oligomer, where the interactions between dimers would depend on salt bridges and the stabilisation of an intermolecular disulphide by Cys48 (**Figure 5A**).

The contact among lung surfactant membranes (Cabré *et al.*, 2009) necessary for lipid transfer (Liekkinen *et al*, 2020; Martinez-Calle *et al*, 2020), may occur by means of SP-B dodecamers (**Figure 5A**), simultaneously generating hydrophobic tunnels at the air-liquid interface and promoting film stability. Two ways of interaction between SP-B and the membrane lipids have been proposed: (1) membrane binding site: polar heads of lipids interact with the hydrophobic and positive-charged domains of N-terminal insertion α-helix 1 (SP-B 1-7), the amphipathic helix 1 (SP-B 8-22) and the C-terminal α-helix 5 (SP-B 63-79); (2) membrane perturbing site (SP-B 36-45): hydrophobic residues and positive charged amino acids in the loop between helices 2 and 3 penetrate to lipid membranes with a resulting perturbation. Moreover, the orientation of SP-B helices at the surface would promote the electrostatic interactions of positive residues (for instance arginine 36) with the anionic polar heads of PG. In support of this model, the presence of palmitoyloleoylphosphatidylglycerol (POPG), together with cholesterol, seems to be important for the correct parallel arrangement of the ring among the surfactant membranes (Liekkinen *et al.*, 2020).

SP-C is the most hydrophobic and small protein of the lung surfactant system and its expression is linked with the differentiation of pulmonary epithelium. In fact, SP-C is highly conserved among species (**Figure 5B**). SP-C is important to improve interfacial adsorption (Creuwels *et al*, 1993; Possmayer *et al*, 2001; Wang *et al*, 2005a) and generate 3D-stable structured films of lung surfactant upon compression (Amrein *et al*, 1997; Wang *et al.*, 2005b), providing a supporting function for SP-B (Sehlmeyer *et al.*, 2020).

SP-C activity seems to be somehow associated to cholesterol in models of surfactant membranes. The protein increases the sterol mobilisation which seems to be related to the fragmentation of lipid membranes (Parra *et al*, 2011; Roldan *et al*, 2016). Moreover, SP-C is not only involved in the stabilisation of cholesterol-containing surfactant films (Gómez-Gil *et al*, 2009a; Gómez-Gil *et al*, 2009b), but it may have an anti-inflammatory activity, interfering with macrophage Toll Like Receptor 4 (TLR-4) affinity for Lipopolysaccharide (LPS) by a

mechanism Cluster of Differentiation 14 dependent (Chaby *et al*, 2005) or independent (Garcia-Verdugo *et al*, 2009).

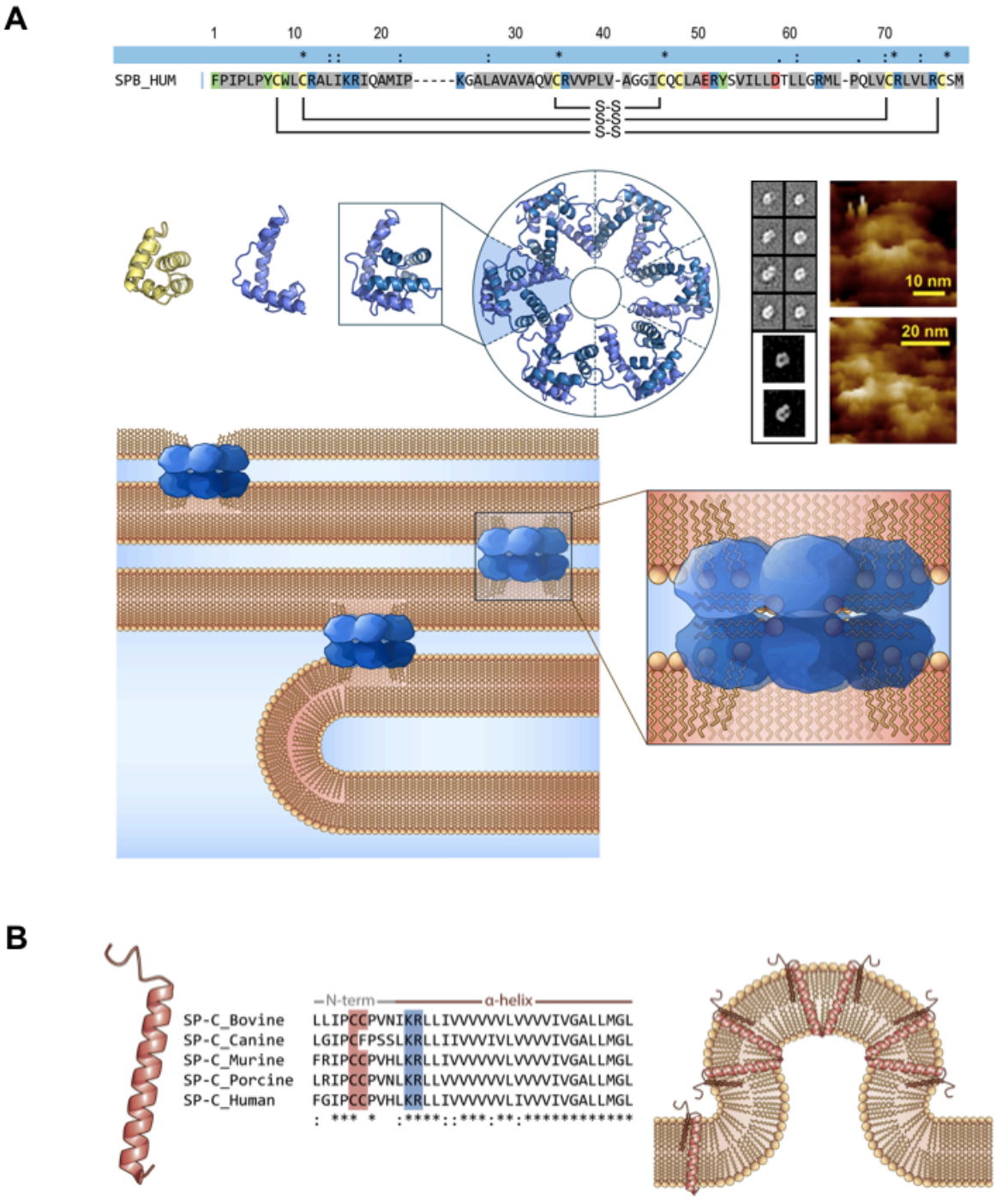

Figure 5. Structure of hydrophobic surfactant proteins. (A) Human SP-B amino acid sequence, showing aromatic residues in green, basic in blue, acidic in red, cysteine in yellow and hydrophobic in grey. The three intramolecular disulphide bonds are indicated as black bars. Monomeric structure along with a schematic illustration of SP-B dodecamers are also shown as resolved by electron microscopy and atomic force microscopy. The hypothetic organisation of SP-B in two rings interconnecting surfactant membranes is illustrated. **(B)** Amino acid sequence and structure of the highly conserved SP-C along with the proposed dimeric form potentially involved in creating membrane curvature. The cysteines, palmitoylation and positive residues are illustrated in red and light blue, respectively. *Figure adapted from (García-Álvarez et al., 2019).*

SP-C may also reduce the TLR-4 mediated pro-inflammatory effects of several danger-associated molecular patterns such as oxidised cholesterol and phospholipid species (Sehlmeyer *et al.*, 2020). Finally, a contribution of SP-C in lung surfactant recycling by alveolar cells has been also described (Poelma *et al*, 2004).

Because of its multiple roles, the severe deficiency of SP-C, although not lethal, may cause different deleterious modifications in lung tissues of mice models that are impaired further upon fibrotic conditions due to aging (Ruwisch *et al*, 2020). At the same time, mutations in SP-C gene are related to several lung dysfunction in humans, especially familial forms of pulmonary fibrosis, but also sporadic IPF (Lawson & Loyd, 2006; Sehlmeyer *et al.*, 2020). Moreover, a reduced expression of the protein seems to be associated to RDS in late pre-term infants and several variations of SP-C are related to interstitial lung diseases (Sehlmeyer *et al.*, 2020).

SP-C is encoded by SFTPC, a single locus gene (3.5 kb) on chromosome 8, composed of 6 exons and 5 introns, whose transcription is also under TTF-1 regulation (Nkadi *et al.*, 2009). As in the case of SP-B, SP-C is synthetised as a larger precursor of 21 kDa that is membrane associated and progressively processed in different steps until reaching its mature form (corresponding to exon 2) of around 4.2 kDa in lamellar bodies (**Figure 4**) (García-Álvarez *et al.*, 2019).

The mature SP-C is a small and very hydrophobic transmembrane α-helical peptide of 35 amino acids whose N-terminal residues are probably the only part of the protein that can be found outside the membrane (**Figure 5B**). Lys11 and Arg12 in the α-helix are very conserved basic residues that can promote the interaction with head groups of phospholipids, especially anionic lipids (Johansson, 1998). In the N-terminal region, two contiguous cysteines are located in positions 4 and 6 in a palindromic sequence motif and are covalently palmitoylated in most species by thioester bonds (Curstedt & Johansson, 2010). This post-translational modification is important for SP-C function, especially to stabilise the α-helical conformation. Palmitoylation is required for the ability of SP-C to reduce the deleterious effects of high cholesterol levels on surfactant membranes (Gómez-Gil *et al.*, 2009a; Gómez-Gil *et al.*, 2009b; Roldan *et al.*, 2016) and probably to maintain the connection of surfactant complexes with the most compressed interfacial films under maximal compressions at the end of expiration and thus promoting film stability (Baumgart *et al*, 2010; García-Álvarez *et al.*, 2019). The loss of palmitic chains can reduce its α-helical conformation, generating dimers with high content of β-sheet and resulting in amyloid fibrils, especially at increasing pH (Dluhy *et al*, 2003) and high lipid-protein content (Wüstneck *et al*, 2003).

A dimeric form for SP-C has been also described as possibly formed under physiological condition, involving helix-helix interactions at the C-terminal of the protein (Kairys *et al*, 2004). This interaction may generate a dimer with a conical shape, promoting curvature and ultimately fragmentation of surfactant membranes (**Figure 5B**) (Roldan *et al.*, 2016).

Synthesis and function of hydrophilic surfactant proteins

Hydrophilic surfactant proteins SP-A and SP-D belong to the collectin family and participate in host defence against pathogens and potential harmful particles entering the lung. In humans, they are encoded by three genes (SFTPA1: SP-A1, SFTPA2: SP-A2, and SFTPD: SP-D) on chromosome 10 (Silveyra & Floros, 2012).

Both their synthesis and post-translational processing, including their glycosylation and oligomerisation, take place in the ER (Crouch, 1998; Olmeda *et al.*, 2017; Weaver & Conkright, 2001). Monomeric SP-A (~35 kDa) and SP-D (43 kDa) can oligomerise, generating highly complex structures with higher immune response activity (Arroyo *et al*, 2020; Sánchez-Barbero *et al*, 2007). As for the highest immunoreactive oligomers, SP-A forms bouquet-like octadecamers (6 trimers) while SP-D forms dodecamers (4 trimers) and larger oligomers known as fuzzy-ball because of their shape (Arroyo *et al*, 2018). The basic trimerisation requires the N-terminal collagen-like domain, while binding to the surface of bacteria, virus or allergens occurs through the C-type lectin globular C-terminal carbohydrate-recognition domain (CRD) that is connected to the N-terminal by a neck helical region. In this way, the two proteins, SP-A and SP-D, can bind carbohydrates on pathogens with their CRD, with higher affinity for clustered oligosaccharides than for single monosaccharides (Hawgood & Poulain, 2001; Ochs *et al*, 2020).

Although SP-A is obtained associated with lung surfactant membranes upon centrifugation, the majority of the protein is probably secreted from AT-II cells by a pathway that does not involve lamellar bodies. It therefore would interact with lung surfactant complexes, once reaching the alveolar space (Ochs *et al*, 2002; Wissel *et al*, 2001). On this basis, SP-A is synthesised and processed along the ER and the Golgi apparatus as well as in multivesicular bodies and small vesicles associated to the apical cell membranes (Ochs *et al.*, 2002; Walker *et al*, 1986). Conversely, the fraction of the protein detected in lamellar bodies is very low and is present only in their periphery. It is still under discussion whether this peripheral SP-A may come from alveolar endocytosis (Osanai *et al*, 1998) or represents a minor portion of the protein that could be synthetized through the lamellar bodies rout (Fisher *et al*, 2010). In a similar way, SP-D secretion also seems to bypass lamellar body storage (Olmeda *et al.*, 2017; Schmiedl *et al*, 2005; Voorhout *et al*, 1992).

The protein variants SP-A2 and SP-A1, resulting from a gene duplication occurring in primates and humans, are related to different states of oligomerisation, with implications in protein function (García-Verdugo *et al*, 2002). SP-A2 may be involved in anti-inflammatory and immunomodulatory properties, whereas SP-A1 contributes more to lipid aggregation and helps in both adsorption and spreading of massive amounts of surfactant material at the air-liquid interface (Lopez-Rodriguez *et al*, 2016b). Moreover, apart from their immunomodulatory activity, SP-D seems to participate in lung surfactant catabolism by macrophages (Ikegami *et al*, 2001; Korfhagen *et al*, 1998; Postle *et al*, 2011) whereas SP-A may play an additional role facilitating the recycling of the most surface-active DPPC-enriched complexes into clathrin-coated vesicles by AT-II cells (Bates, 2010).

Cytoplasmic lipid trafficking, assembly in lamellar bodies and secretion

A proper maturation of lamellar bodies depends on the presence of CCT, SP-B and a correct SP-C biogenesis (Olmeda *et al.*, 2017; Ridsdale & Post, 2004; Tian *et al*, 2007). However, synthetized lipids and hydrophobic proteins seem to follow different traffic routes in AT-II cells before reaching lamellar bodies, assembling together and being secreted into the alveolar lining fluid. SP-B and SP-C complete their processing and integrate into lipids in multivesicular bodies as they are transferred into lamellar bodies. On the contrary, surfactant lipids previously reach the periphery of lamellar bodies by means of specific lipid transfer proteins, among those StAR Related Lipid Transfer Domain Containing 10 (StarD10), that is

involved in transport of saturated species of PC (Lin *et al*, 2015). Then, lipids are translocated into the lumen of the organelles by lipid transporters that belong to the ATP-Binding Cassette (ABC) family, using the energy of ATP hydrolysis. In detail, ABCA3 is essential for lamellar bodies biogenesis and is involved in PC, PG and cholesterol trafficking (Ban *et al*, 2007; Fitzgerald *et al*, 2007; Zarbock *et al*, 2015). As a result of this energy-dependent lipid-transfer and the simultaneous activity of vacuolar ATP-ases, lamellar bodies store highly packed lipids with a substantially dehydrated structure (Cerrada *et al*, 2015) and maintain an acidic internal pH (pH 6.1 or below (Chander *et al*, 1986)) that seems to be crucial for the last processing steps of SP-B and SP-C (Bañares-Hidalgo *et al*, 2014; Chintagari *et al*, 2010).

Once lamellar bodies are maturated, their proper secretion is regulated by the cytoplasmic levels of calcium in AT-II cells that promotes their fusion with the plasma membrane, the formation of a fusion pore and the final release by cytoskeleton activation (Olmeda *et al.*, 2017). The changes in Ca^{2+} levels and surfactant secretion depend on the exposure to air (Ramsingh *et al*, 2011) (the thinner the hypophase, the higher the lamellar bodies release) and the mechanical stretching of alveoli (Wirtz & Dobbs, 1990) as a direct signal on AT-II cells (Frick *et al*, 2004) or mediated by AT-I cells (Ashino *et al*, 2000). In this scenario, SP-B seems also to prompt the Ca^{2+}-dependent surfactant secretion by AT-II cells via ATP release (Martínez-Calle *et al.*, 2018). At the same time, SP-A inhibits lamellar bodies secretion stimulated by stretch without reducing the cytosolic calcium (Wirtz & Dobbs, 1990) and probably upon binding to AT-II cells (Mason & Voelker, 1998). Interestingly, DPPC also inhibits surfactant release *in vitro* (Suwabe *et al*, 1991), suggesting a possible feedback mechanism that may occur *in vivo* and regulates the alveolar presence of the main surface-active lipid.

Extracellular surfactant structure

After secretion, current models suggest that part of the dense lamellar bodies may transform in a tightly packed lattice-like structure called tubular myelin, which may represent a reservoir of surface-active material in connection with the air-liquid interface (Pérez-Gil, 2008). Four elements are essential to recreate tubular myelin *in vitro*: DPPC, PG, SP-B and SP-A, as well as the presence of calcium (Pérez-Gil, 2008). In this line, it has been suggested that SP-A may be involved in the formation of this structure since its soluble octodecamers could interact with selected lamellar bodies trough the globular domain, modifying the curvature of the membranes as they are unpacked. SP-A could therefore create the lattice organisation by establishing additional simultaneous protein-protein interactions via the collagen-like domains (Olmeda *et al.*, 2017). Moreover, SP-B may also have a role, orchestrating membrane-membrane adhesions and fusions (Cabré *et al.*, 2009; Martinez-Calle *et al.*, 2020). Interestingly, recent evidences suggest a direct interaction of glycocalyx, mainly present on AT-II cells surface, with both tubular myelin and the periphery of secreted lamellar bodies (Ochs *et al.*, 2020). The glycocalyx is a carbohydrate-rich cellular coat, characterised by proteoglycans with long glycosaminoglycan chains and glycoproteins with short carbohydrate chains (Reitsma *et al*, 2007). SP-A, as well as SP-D, could interact with these sugars by means of their CRD domains, whereas SP-B and SP-C could bind the hydrophobic regions in glycocalyx hyaluronans (Ochs *et al.*, 2020). These putative connections may somehow contribute to the conversion of lamellar bodies into tubular myelin *in vivo* and support the host-defence properties of tubular myelin.

Several models propose that a portion of freshly secreted lamellar bodies may directly reach the air-liquid interface in their original highly surface-active structure. Once there, SP-B and SP-C in the supramolecular complexes (Martínez-Calle *et al*, 2019), may promote the unfolding of lamellar bodies (Hobi *et al*, 2016) and the rapid transfer and distribution of new surfactant material (Haller *et al*, 2004) at the air-liquid interface.

Surfactant lipid-protein interactions and lipid organisation

The proper secretion of surfactant components, the correct balance in lung surfactant composition as well as the protein-lipid interaction and the organisation of surfactant membranes and derived structures, define the surface-active properties of lung surfactant, both in health and disease (Autilio & Pérez-Gil, 2019).

SP-A, SP-B and SP-C also establish homotopic and heterotopic protein-protein interactions, providing an additional complexity to their structure. In this way, they may play a cooperative role, for instance in tubular myelin formation or in packing and depacking lamellar bodies (Martínez-Calle *et al.*, 2019) and potentially to increase the cohesivity of the interfacial multilayer reservoir (Cañadas *et al.*, 2020). Once reaching the air-liquid interface, the hydrophobic proteins may then start their autonomous actions, orchestrating the biophysical activity of lung surfactant. For this purpose, SP-B and SP-C interact preferentially with PG to enhance interfacial adsorption and film stability (Ingenito *et al*, 2000; Liekkinen *et al.*, 2020; Parra *et al*, 2013), whereas SP-A and SP-D contact with DPPC (Bates *et al*, 2008) and phosphatidylinositol (PI) (Ikegami *et al*, 2009; Ikegami *et al*, 2005; Sano *et al*, 1998) respectively. Interactions between cholesterol and SP-C were also reported to refine the interfacial film (Baumgart *et al.*, 2010; Gómez-Gil *et al.*, 2009b; Roldan *et al.*, 2016) and suggested as part of the cross-talk between alveolar macrophages and AT-II cells (Ruwisch *et al.*, 2020). At the same time, SP-A seems to play a role in surfactant protection from cholesterol-mediated inhibition in ventilated-trauma patients (Hiansen *et al*, 2015) and potential selective interactions of SP-B with cholesterol were proposed as a result of molecular dynamic simulations (Liekkinen *et al.*, 2020).

Along with surfactant protein-protein and lipid-protein interactions, the organisation of surfactant lipids into membrane structures is also essential for the activity of the system. When exposed to a polar environment such as the alveolar aqueous subphase and depending on their molecular shapes, phospholipids can self-assemble and organise themselves into different supramolecular structures (**Figure 6A**). This ability to aggregate in a variety of ways according to the volume occupied by each lipid species defines the lipid polymorphism and contributes to the generation of membrane structures with negative, positive or zero curvatures (Jouhet, 2013). In detail, PC and PG are characterised by a constant cylindrical area from the headgroup to the acyl chains, promoting assembly into planar lamellar lipid organisations. On the contrary, molecules from lipid species with a small polar headgroup, such as phosphatidylethanolamine (PE), present a conical shape that promotes the formation of non-lamellar negatively-curved structures such as the hexagonal type II phase. At the same time, positive-curved structures as micelles or the hexagonal phase I, are generated by lipids with an inverted conical shape, such as lysophosphatidylcholine (LPC).

In the complexity of lung surfactant, this lipid organisation is modulated by several factors, including local lipid composition, surfactant proteins activity, pH, lateral pressure, hydration state and temperature. The latter plays a crucial role by varying the thermal energy

that affects the lipid mobility and order. Typically, membranes and interfacial films in lamellar phases show a high degree of order at low temperature, with limited translational and rotational molecular diffusion. Conversely, at temperatures above a defined threshold, the so-called melting temperature (T_m), lipid molecules gain mobility, becoming disordered (**Figure 6B**). This reversible transition and the energy associated to it, namely the enthalpy of the system, are determined by changes in Van der Waals forces which, in turn, depend on the degree of unsaturation and the length of the acyl chains in addition to the protein-lipid interactions (Autilio & Pérez-Gil, 2019). With increasing temperatures towards T_m and without sterols, the fluidity rises and phospholipid bilayers change from an ordered gel phase ($L\beta$) below the T_m to a disordered liquid-crystalline phase ($L\alpha$) above T_m. The two phases coexist in equilibrium at the T_m.

Additionally, sterols (such as cholesterol) influence the organisation of the system, inserting into phospholipid membranes in the gel phase, increasing their mobility, and packaging them tighter in the liquid phase (Sankaram & Thompson, 1991). This results in the so-called liquid-ordered (Lo) and liquid-disordered (Ld) phases, respectively, and the overall system fluidity: $L\beta < Lo < Ld < L\alpha$ (Zuo *et al*, 2008).

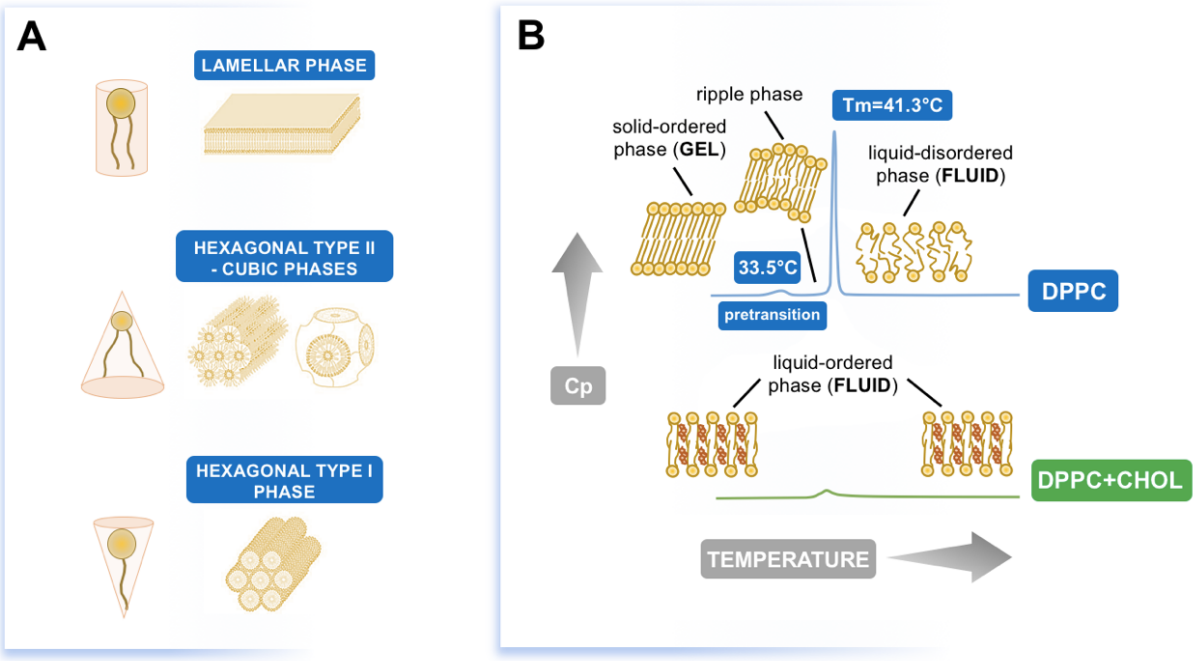

Figure 6. Structural phospholipid aggregation and membrane organisation. (A) Different lipid organisation according to the lipid polymorphism and the resulting membrane curvature. **(B)** Changes in DPPC lamellar phases depending on the temperature and the presence of cholesterol. The classic calorimetric thermograms of DPPC membranes with and without the sterol are illustrated. Upon normal conditions with rising in temperature, DPPC undergoes a pretransition (33.5°C) in which phospholipids progress from a highly ordered solid-like 'gel-phase' to an intermediate 'ripple phase' before reaching a disordered 'fluid phase' at a T_m of around 41°C. Conversely, when high amounts of cholesterol are present, a unique fluid phase is visible and the enthalpy associated to the ordered-to-disordered transitions (area under peak) is strongly decreased. *Figure and caption adapted from (Jouhet, 2013) and (Autilio & Pérez-Gil, 2019).* Abbreviations: Tm, melting temperature; CHOL, cholesterol; DPPC, saturated dipalmitoylphosphatidylcholine; Cp, specific heat capacity.

As for monolayers at the air-liquid interface, the lateral pressure should also be considered. The surface pressure (Π) of a film can be calculated from the difference between the surface tension of the pure subphase (72 mN/m for pure water at 25 °C) and that of the subphase covered with the surfactant film. This is around 22-25 mN/m for a surface-active material in equilibrium conditions, resulting in 50 mN/m of Π. The greater the lateral pressure, the lower the mobility of lipids, resulting in lower γ and higher Π. In this context, phospholipids with high lateral mobility and conformational freedom form a liquid-expanded (Le) phase, whereas the reduction in area per lipid molecule under increasing lateral compression (> surface pressures) packs those lipids in a liquid-condensed (Lc) state. As it happens for phospholipid bilayers, the presence of cholesterol may also change the phases of monolayers, varying their fluidity as follows: Le< Lo< Ld< Lc (Zuo *et al.*, 2008).

Since lipids with similar T_m and properties tend to assemble together, the effect of both temperature and cholesterol strictly depend on the system composition. As a result, lipids are heterogeneously organised in lung surfactant clusters, generating lipid domains and coexistence of segregated phases that may extend even to physiological temperature (37 °C) (Bagatolli *et al*, 2010; de la Serna *et al*, 2004; de la Serna *et al*, 2013). Interestingly, the two hydrophobic proteins, SP-B and SP-C, are strictly localised into liquid-disordered domains, very dynamic and prone to form membranes folds (de la Serna *et al.*, 2004), or accumulated at the ordered/disordered boundaries, and are also excluded from DPPC-enriched monolayers subjected to compression at the air-liquid interface (Nag *et al*, 1997).

Biophysical models of surfactant performance

As illustrated in **Figure 7**, three essential properties characterise the surface activity of lung surfactant during breathing (Autilio & Pérez-Gil, 2019; Parra & Pérez-Gil, 2015): (1) rapid movement towards the air-liquid interface (adsorption) and transfer of new lipid species to line the alveolar surface during inspiration; (2) proper packing (compressibility) of the interfacial film with a compression-driven reorganisation into surface-associated multilayered membrane structures on expiration, resulting in a drastic reduction of surface tension; and (3) lateral redistribution of packed lipids during periods of expansion of the air-liquid interface (respreading capability) at the subsequent inspiration and alveolar re-extension. These cycles of surfactant compression and re-extension constitute a partially reversible process in which the interaction of the lipids and proteins seems to play a key role.

To adsorb rapidly, first, lung surfactant needs to be assembled into large bilayer-based aggregates, with the potential to cooperatively transport and transfer a large mass of surfactant phospholipids to the interface. These surfactant membrane complexes, in many studies known as large surfactant aggregates or large aggregates, diffuse towards the air-liquid interface in a process facilitated by both calcium and protein SP-A (García-Verdugo *et al.*, 2002; Ruano *et al*, 1996; Sánchez-Barbero *et al.*, 2007). Once the interface is reached, the surfactant aggregates need to merge within the surface film. For this to happen, it has been proposed that a highly curved structural intermediate is generated between lung surfactant membranes and the interfacial film (Chernomordik & Kozlov, 2003).

SP-B has the major role by facilitating lipid exchange and stabilizing this transient structure, especially in the presence of anionic phospholipids (mainly PG) (Chavarha *et al*, 2013; Ross *et al.*, 2002; Walters *et al.*, 2000). As a matter of fact, it has been determined that SP-B forms supramolecular structures at the surface of freshly secreted surfactant complexes,

ready to open connections that facilitate rapid flows of phospholipids on making contact with the interface (Olmeda *et al.*, 2015; Parra *et al.*, 2013). It also seems that unsaturated phospholipids and cholesterol influence the insertion of surface-active species into the interfacial film (Walters *et al.*, 2000).

Overall, surfactant adsorption at the air-liquid interface reduces the surface tension from 70 mN/m (at 37°C) to values around 20 mN/m (equilibrium surface tension). Then, on expiration, the surface tension is further decreased, to reach values of less than 2 mN/m (**Figure 7**), as demonstrated by both *in vitro* and *in vivo* studies (Schürch *et al*, 2001). As mentioned above, this extremely low tension prevents the alveolar collapse through the selective reorganisation of the lung surfactant film into three-dimensional multilayered structure. This is characterised by highly packed domains in contact with air, thus avoiding fluid-air proximity. A so-called 'squeeze-out' model suggests that this reorganisation to fold part of the interfacial film towards the subphase would allow most of the DPPC molecules to remain at the surface with a multilayered surfactant reservoir associated to surface (Egberts *et al*, 1989; Pastrana-Rios *et al*, 1994; Pérez-Gil, 2008; Xu *et al*, 2020).

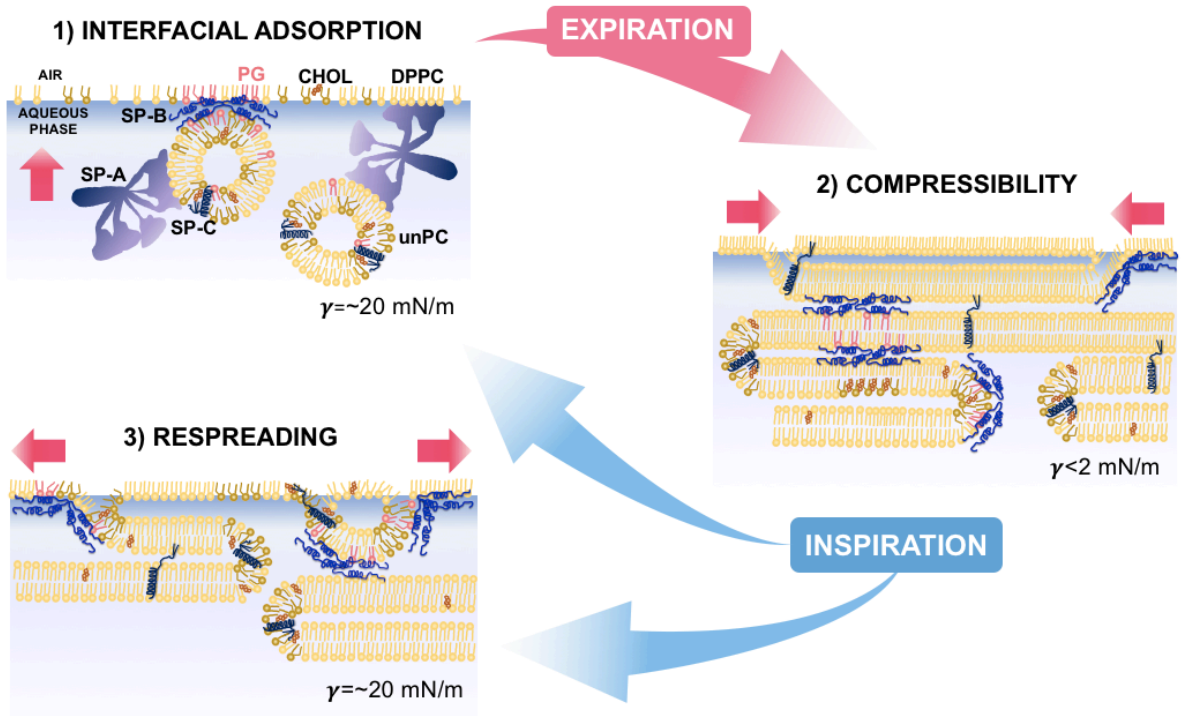

Figure 7. Essential biophysical properties of lung surfactant in healthy breathing. On expiration: According to the "squeeze-out" model, lung surfactant organises in multilayer structures characterised by the presence of DPPC at the air-liquid interface with the consequent drastic reduction in surface tension (<2 mN/m); during inspiration: re-extension of phospholipid membranes along with the initial adsorption of surfactant aggregates at the air-liquid interface, reaching the equilibrium surface tension of 20 mN/m. This process is mediated by SP-A and SP-B and facilitated by PG, cholesterol and unsaturated phospholipids. Abbreviations: CHOL, cholesterol; DPPC, dipalmitoylphosphatidylcholine; PG, phosphatidylglycerol; unPC, unsaturated phosphatidylcholine.

DPPC molecules would then act as a key component of highly-ordered domains with maximal packing and maximal surface tension reduction. Film reorganisation selectively

excludes unsaturated phospholipids and cholesterol from the interface as part of the more fluid and deformable film regions. However, several studies have demonstrated that some mammal/marsupial species can maintain proper respiratory mechanics with a surfactant containing relatively low amounts of DPPC and higher proportions of unsaturated PC (Bernhard *et al*, 2007; Lang *et al*, 2005).

During compression (at expiration), SP-B and SP-C are in principle also removed from the surface, since they are associated with the less compressible phospholipids by selective lipid-protein interactions (Taneva & Keough, 1994a). However, when the interfacial membranes are overcompressed, SP-B still has an important role in maintaining film stability against mechanical perturbations (Schürch *et al.*, 2010), possibly by providing a high intermembrane cohesivity to the multilamellar surfactant reservoir associated with the interfacial film (de la Serna *et al.*, 2013). With this in mind, SP-B and SP-C are essential to create and maintain the stable association of the multi-layered reservoir with the interface (Perez-Gil & Weaver, 2010). The two proteins also play a crucial role on inspiration, facilitating the respreading of lung surfactant and guiding the concerted reinsertion of excluded and new phospholipids into the interfacial surface (**Figure 7**).

Lung surfactant recycling and catabolism

Surfactant kinetics

As aforementioned above, a compositional and structural reorganisation of surfactant takes place upon breathing mechanics, promoting both recycling and catabolism of spent material by AT-II cells and macrophages. Labelled precursors of surfactant lipids, mainly of DSPC, can be used to calculate the rate of label incorporation into surfactant PC by mass spectrometry after intravenous administration. The rate of surfactant turnover depends on both age and lung conditions. Newborns are characterised by a slow surfactant clearance and catabolism, compensating the greater time needed for alveolar accumulation and secretion (Carnielli & Cogo, 2018). Moreover, surfactant turnover is even slower in preterm infants with RDS (17-75 hours (Bunt *et al*, 1998; Merchak *et al*, 2002)) compared to term infants without lung disease (9-44 hours (Bohlin *et al*, 2003; Cogo *et al*, 2002; Janssen *et al*, 2003)). At the same time, term neonates with respiratory failure show a turnover rate that resembles that of preterm infants with RDS (Bohlin *et al.*, 2003; Carnielli & Cogo, 2018).

Interestingly, surfactant hydrophobic proteins have a faster replacement kinetics than DSPC with a peak at ~20-30 hours in animal models (Baritussio *et al*, 1994; Ueda *et al*, 1995). This was also demonstrated for SP-B in both healthy subjects and ARDS patients (Simonato *et al*, 2011). This result may be explained by the crucial role of these proteins in biophysical properties, secretion and organisation of surfactant material at the air-liquid interface during respiratory dynamics.

The spent material resulting from breathing mechanics is mainly organised in small vesicles with light density and low interfacial activity that are probably generated by both SP-B and SP-C actions. These structures are called small aggregates and represents around 15% of surfactant subfraction phospholipids. The remaining part (about 85%) consists of surface-active large aggregates of heavy density (Günther *et al*, 1999; Veldhuizen *et al*, 1995) that can be isolated from tubular myelin, large lipid vesicles and secreted lamellar bodies.

AT-II cells and alveolar macrophages

De novo synthesis of surfactant components in AT-II cells is a slow process. Thus, to modulate the amount and composition of surfactant in the airways, its lipid content is mainly recycled, probably involving ABCA1 and ABCG1, two lipid transporters of the ABC family (Kennedy *et al*, 2005; Olmeda *et al.*, 2017; Wang *et al*, 2001). In this process, surfactant proteins may also play a role indirectly. SP-D and SP-C seem indeed to influence the structure and conversion of large aggregates into small aggregates, promoting membranes fragmentation (Ikegami *et al.*, 2009; Roldan *et al.*, 2016). At the same time, SP-A probably associated to small aggregates, stimulates the uptake of those surfactant structures by AT-II cells through a clathrin-dependent mechanism that involves cytoskeleton-associated protein 4 (P63/CKAP4) receptor (Bates, 2010). Once internalised, phospholipids organise themselves in early endosomes that are subsequently transferred to lamellar bodies in a calmodulin-dependent manner, whereas SP-A is re-secreted (Wissel *et al.*, 2001). This mechanism represents the main secretory pathway, although another non-clathrin actin-dependent endocytosis process was described without the contribution of SP-A. However, it accounts only for 3.5% of surfactant uptake (Bates *et al.*, 2008).

Excluding the portion of surfactant (15%) that is lost by diffusion toward the upper airways by means of the mucociliary escalator (Pettenazzo *et al*, 1988), AT-II cells provide about 65% of surfactant recycling, whereas macrophages account for the majority of its clearance (Rider *et al*, 1992). Upon this process, SP-D and SP-C seem also to play a role in surfactant and cholesterol clearance under both physiological conditions and aging (Botas *et al*, 1998; Ruwisch *et al.*, 2020). Moreover, pathways involving granulocyte-macrophage colony stimulating factor (GM-CSF) receptor and the lipid-sensitive nuclear receptor peroxisome proliferator-activated receptor gamma (PPARγ) seem to control, both directly and indirectly, the uptake, sorting and metabolism of surfactant components. Examples of proteins that have a role in this system are ABCA1/G1 (required for cholesterol efflux), scavenger receptor class B type I (SR-BI) (implicated in cholesterol metabolism) or cluster of differentiation 36 (related to the long-chain fatty acids metabolism), as well as several lysosomal enzymes (Lopez-Rodriguez *et al*, 2017).

Secretory phospholipase A_2

An intriguing question in physiological and pathological lipid homeostasis is undoubtedly the role played by secretory PLA_2 ($sPLA_2$) whose main alveolar source are macrophages and mast cells. $sPLA_2$ are a family of small enzymes (14 to 18 kDa) with multiple disulphide bonds (6-8) and His/Asp catalytic dyad that cleave fatty acid in position two of phospholipids (*sn*-2 position) (Murakami *et al*, 2011).

By means of this activity, $sPLA_2$s hydrolyse the bond between the second fatty acid and the glycerol molecule of phospholipids. This is a mM-order calcium-dependent mechanism that is primary extracellular and releases free fatty acids (FFAs) and lysophospholipids (LPLs). These molecules are involved in several cellular and extracellular processes including inhibition of pulmonary surfactant activity (Hite *et al*, 2005), generation of reactive species of oxygen (ROS) mainly mediated by the production of arachidonic acid (20:4) (Murakami *et al*, 1998; Sakata *et al*, 1987) and recruitment of inflammatory agents, such as eosinophils (Nishiyama *et al*, 2004).

The capacity to release arachidonic acid depends on the enzyme affinity to PC, the main component of surfactant and cellular membranes, with the following potency order for the different enzyme groups: X > V > III > IIF > IIA > IB > IID > IIE > XIIA (Bezzine *et al*, 2000; Murakami *et al*, 1999; Murakami *et al*, 2001; Murakami *et al*, 2003; Murakami *et al.*, 1998). In contrast to $sPLA_2$ X, V, III and IB that mainly bind PC, $sPLA_2$ II has a lower affinity for this zwitterionic lipid (Karray *et al*, 2020). This enzyme seems to bind preferentially PE, phosphatidylserine and PG (Seeds *et al*, 2012). In this context, the affinity for anionic lipids seems to depend on basic residues present in the part of protein surface involved in recognising lipid aggregates. Conversely, $sPLA_2$ subtypes with greater affinity for zwitterionic lipid species consist in lipid-contact surfaces reach in hydrophobic amino acids, mostly containing aromatic groups (Dennis *et al*, 2011). Together with arachidonic acids, $sPLA_2$s may also generate a variety of saturated, monosaturated and other polyunsaturated fatty acids which are precursors of anti-inflammatory lipid mediators (Murakami *et al.*, 2011).

It has been suggested that under physiological conditions, synthesis and secretion of $sPLA_2$s mediated by cytokines such as tumour necrosis factor-α (TNF-α) are finely controlled in alveolar macrophages, maintaining only the required extracellular enzyme levels necessary for pulmonary surfactant homeostasis (Touqui & Arbibe, 1999). This process is, at least in part, regulated by several components of the surfactant system. In endotoxin activated macrophages, SP-A and dioleoylphosphatidylglycerol (DOPG) seem to inhibit indirectly $sPLA_2$ IIA activity by reducing its expression probably by acting on TNF-α-mediated nuclear factor kappa B (NF-kB) signalling (Wu *et al*, 2003). At the same time, a direct inhibition of $sPLA_2$ IIA and X function by a putative interaction with SP-A was also suggested, but not confirmed for the pancreatic isoform IB and V (Arbibe *et al*, 1998; Chabot *et al*, 2003). Moreover, SP-B seems also decrease the lipid hydrolysis mediated by $sPLA_2$ IIA and IB in vesicles containing PC and PG (Hite *et al*, 2012).

Starting from these evidences, several pathological conditions that reduce lung surfactant amount and function presumably lead to the exacerbation of $sPLA_2$ II production. This event together with the increase in $sPLA_2$ -V and -X from airway bronchial epithelium and alveolar macrophages (Murakami *et al.*, 2011) result in a vicious cycle that may further impair the activity of the pulmonary surfactant system.

Lung surfactant alterations and respiratory disorders

Inactivation of lung surfactant activity

Traditionally, the inactivation of lung surfactant has been considered an impairment caused by exogenous agents that are not normally present in the alveolar region or whose levels are highly increased upon pathological conditions (Echaide *et al*, 2017). Moreover, the concentration of lung surfactant strongly influences the inactivation rate. This is probably due to the more efficient adsorption of surface-active aggregates when crossing a subphase characterised by high surfactant concentration (Eastoe & Dalton, 2000; Holm *et al*, 1999; Zuo *et al.*, 2008), and related to the structural complexity of surfactant aggregates (Gunasekara *et al*, 2008). In this regard, diluted surfactant seems to be characterised by unilamellar vesicles, while concentrated material forms larger packed and complex mesostructures (Gunasekara *et al.*, 2008).

The process of inactivation could be classified into four different mechanisms: (1) the competition of surface-active molecules for reaching the interface, (2) the direct insertion of membrane-perturbing molecules into lung surfactant layers, making contact with the lipid-protein complexes (Echaide *et al.*, 2017; Lopez-Rodriguez & Pérez-Gil, 2014), (3) the degradation of pulmonary surfactant phospholipids and (4) the oxidation of both lung surfactant lipids and proteins (Autilio & Pérez-Gil, 2019; Zuo *et al.*, 2008).

The first mechanism involves plasma proteins leaked into the airways during oedema formation such as albumin, fibrinogen, and hemoglobin and depends on their ratio with respect to lung surfactant (Holm *et al*, 1985; Holm *et al*, 1988; Tabak & Notter, 1977; Warriner *et al*, 2002). Those molecules are water-soluble, thus competing with surfactant membranes for the air-liquid interface by spontaneous adsorption. Then, once adsorbed, plasma proteins may create a steric and/or electrostatic energy barrier, reducing the portion of surfactant membranes that reaches the interface (Taeusch *et al*, 2005; Zasadzinski *et al*, 2005). For this reason, under breathing-like cycles, the decrease in surface tension occurs slowly when both surfactant and plasma proteins are present and compete (Zasadzinski *et al.*, 2005).

The second mechanism involves C-reactive protein (CRP), excess of cholesterol, bile acids, LPLs and free unsaturated fatty acids (Zuo *et al.*, 2008). These molecules may insert into surfactant membranes and drastically increase membrane fluidity, resulting in the impairment of surfactant surface-active properties (Gunasekara *et al*, 2005; Hite *et al.*, 2005; Malcharek *et al*, 2005; Sáenz *et al*, 2010). Moreover, bile acids could inactivate surfactant in several ways, as they could simultaneously promote film collapse directly due to its fluidizing action (Zuo *et al.*, 2008), act as mediators to mobilise and transfer cholesterol into surfactant complexes and enhance the hydrolysing activity of $sPLA_2$ (De Luca *et al*, 2011; Lopez-Rodriguez *et al*, 2011). The negative charge of bile acids seems indeed to assist the presentation of the phospholipid substrate to the catalytic site and, therefore, the consequent membrane hydrolysis (De Luca *et al.*, 2011).

The third mechanism of surfactant inactivation involves $sPLA_2$ activity that hydrolyses surfactant lipids and degrades surfactant membranes, whereas the fourth process takes place upon ROS environment. In this line, free radicals, such as hydroxyl and superoxide anion radicals, may steal electrons from the lipids, mostly polyunsaturated fatty acids. Indeed, the latter contain multiple double bonds with reactive hydrogen atoms (Stadtman & Levine, 2003). Moreover, several amino acids, especially those containing aromatic sidechains and sulfhydryl groups, can be directly modified by ROS, and polypeptide chains can be cleaved by oxidation of prolyl, glutamyl and aspartyl residues (Stadtman & Levine, 2003). Interestingly, in the case of SP-B, a considerable reduction of amino acids containing positive charges (Arginine, Lysine) after the oxidation of bovine lipid extract surfactant was described. These are essential for the interaction of the protein with the anionic phospholipid fraction and thus to mediate its physiological action on membranes (Echaide *et al.*, 2017; Rodríguez-Capote *et al*, 2006). At the same time, in the case of SP-C, oxidative stress may lead to the cleavage of the two thioester-linked palmitoyl groups, destabilising the protein structure and promoting the helix-to-beta transition (Rodríguez-Capote *et al.*, 2006).

Neonatal respiratory distress syndrome (RDS)

RDS is a common cause of morbidity in preterm neonates. It occurs in around 80% of babies born before the 28th week of pregnancy, when AT-II cells are still not fully differentiated. Thus, the syndrome is mostly due to lung immaturity and lack of lung surfactant that contains a low percentage of DSPC species and PG as well as a reduced content of surfactant proteins compared to a mature lung (Nkadi *et al.*, 2009). The resulting high surface tension impedes keeping the alveoli opened since the first breath, causing alveolar collapse and, in turn, starting a vicious circle of tissue damage, decreased oxygenation and further lung epithelial cell injury (**Figure 8A**). In the early 1980s, surfactant replacement therapy with an exogenous surfactant preparation contributed to decreasing mortality rates (Hentschel *et al*, 2020; Singh *et al*, 2015) from 50% to 30-10% (Halliday, 2017), as it facilitates respiratory mechanics, which stimulates the self-production of endogenous lung surfactant in newborns (Cavicchioli *et al*, 2001).

Nowadays, early continuous positive airway pressure (CPAP), sometimes followed by surfactant replacement therapy, has have become the standard of care in management of preterm infants with RDS, significantly decreasing incidence, severity and mortality of the syndrome (Hentschel *et al.*, 2020; Sweet *et al*, 2019). However, this improved survival of the preterm infant occurs along with an unacceptable rate of bronchopulmonary dysplasia (BPD), a chronic lung disease caused by prolonged mechanical ventilation that results in inflammation-mediated acute lung injury, disrupting alveolarization and leading to abnormal lung development (Thébaud *et al*, 2019). Moreover, the replacement therapy is not effective for respiratory failure due to severe genetic disorders, such as for instance SP-B deficiency due to mutations in the SFTPB gene or alterations in the ABCA3 gene (Lopez-Rodriguez *et al.*, 2017).

CPAP is the recommended non-invasive first line respiratory support, keeping the airways constantly opened upon spontaneous breathing (Subramaniam *et al*, 2016). Thus, by short soft nasal prongs or mask connected tightly to the baby's face, the set pressure (typically kept between 5 and 9 cmH_2O) is maintained during inspiration and expiration, delivering PEEP and avoiding alveolar collapse (Sweet *et al.*, 2019).

Treatments with antenatal steroids and early initiation of CPAP after birth have reduced the administration of surfactant therapy that is only reserved to neonates, failing CPAP. With this in mind, some neonates with mild prematurity manifest a spontaneous recovery without surfactant after 72-96 hours. Conversely, RDS babies that experience a disease worsening show increasing work of breathing and raised oxygen requirements to provide normal oxygen saturations (Sweet *et al.*, 2019).

Surfactant replacement therapy with exogenous surfactant preparations should be given as early as possible in CPAP-treated preterm babies (within the first 3 hours of life) in order to maximise its efficacy (Bahadue & Soll, 2012; Verder *et al*, 1999). This generates a dilemma for neonatologists since they need to predict, in a short timeframe, which neonate is going to fail CPAP and needs surfactant and which one can remain in CPAP.

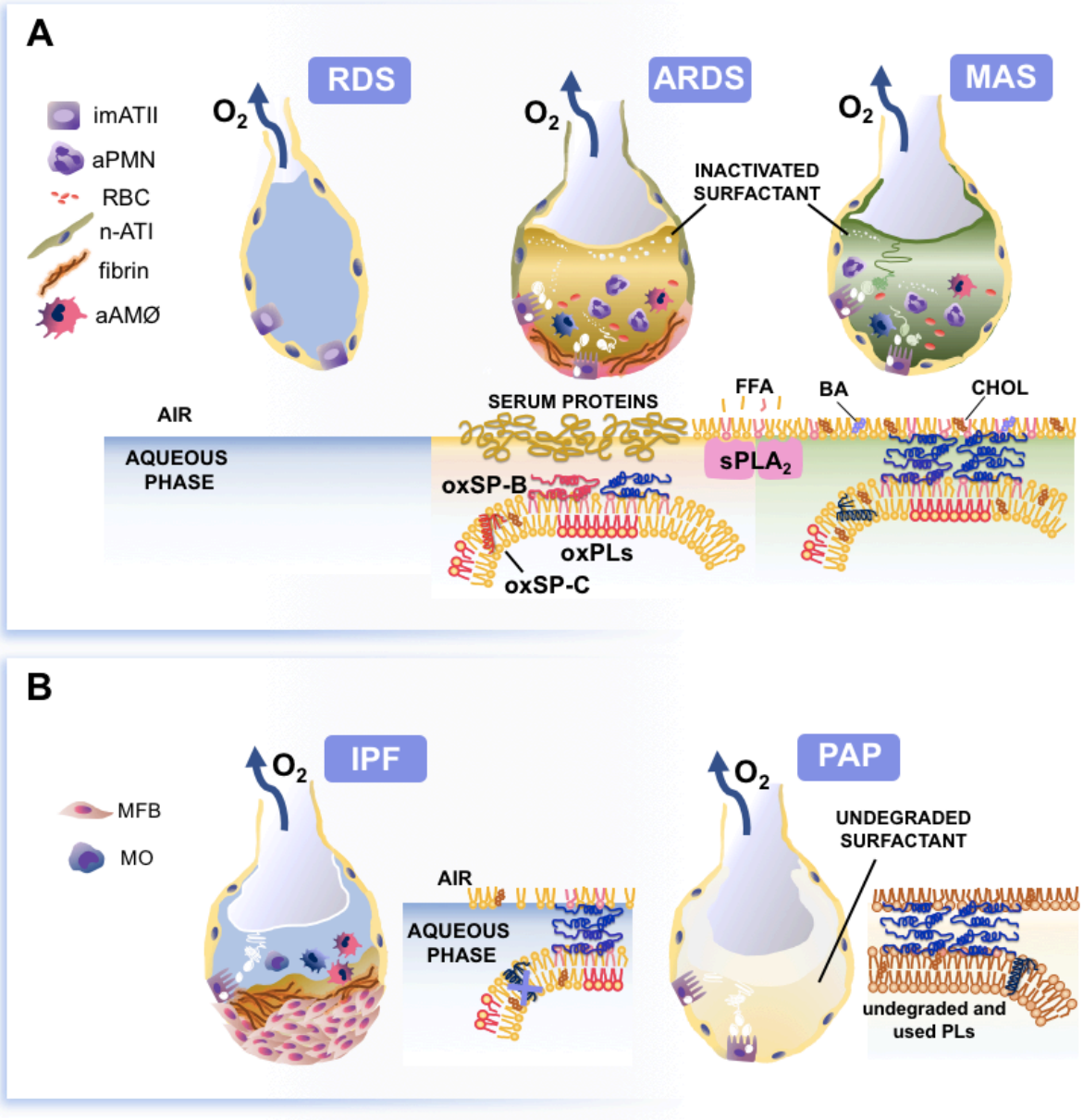

Figure 8. Lung surfactant in healthy and diseased human lung tissue. (A) Collapsed alveolus in RDS due to ATII cell immaturity and damaged alveoli both in ARDS and MAS. The resulting inhibition of lung surfactant complexes due to albumin exudate, ROS production, $sPLA_2$, cholesterol and bile acids is illustrated. **(B)** A schematic representation of an IPF alveolus (on the left) with changes in the available surfactant pool (SP-C reduction) and a PAP alveolus obstruction (on the right) due to the excessive production of lung surfactant, accumulating as already used material. Abbreviations: aAMφ, activated macrophages; aPMN, activated polymorphonucleated cells; ARDS, acute respiratory distress syndrome; BA, bile acid; CHOL, cholesterol; FFA, free fatty acids; imATII, immature alveolar type II pneumocytes; IPF, idiopathic pulmonary fibrosis; MAS, meconium aspiration syndrome; MFB, myofibroblasts; MO, monocytes; n-ATI, necrotic alveolar type I pneumocytes; ox-PLs, oxidised phospholipids; ox-SP-B, oxidised SP-B; ox-SP-C, oxidised SP-C; PAP, pulmonary alveolar proteinosis; PL, phospholipid; RBC, red blood cell; RDS, respiratory distress syndrome; $sPLA_2$, secretory phospholipase A2.

Adult and neonatal acute respiratory distress syndrome (ARDS)

Surfactant replacement therapy is debated in conditions where both endogenous and therapeutic surfactant are directly or indirectly inactivated (Autilio & Pérez-Gil, 2019). Among those, ARDS is a quickly progressive severe respiratory failure characterised by widespread acute inflammation into the lungs (**Figure 8A**).

The Berlin definition is the most recent definition of the syndrome in adult patients: it is based on acute hypoxemia (with a ratio of arterial oxygen partial pressure to fractional inspired oxygen (PaO_2/FiO_2) ≤ 300 mmHg) in a ventilated patient within one week of a known or suspected trigger, whose PEEP is 5 mmHg at least, presenting bilateral lung opacities not totally explained by heart failure or volume overload (Papazian *et al.*, 2019; Ranieri *et al*, 2012). In this way, adult ARDS can be divided in mild, moderate and severe according to PaO_2/FiO_2 levels.

The Montreux definition is the definition of neonatal ARDS (De Luca *et al*, 2017) whereas the Paediatric Acute Lung Injury Consensus Conference (PALICC) definition illustrates paediatric ARDS (Khemani *et al*, 2015). The first refers to neonates from birth until 44 weeks, or until 4 weeks postnatal age, while the second to children beyond the period covered by Montreux definition and until adolescence. In the two cases, the definition is based on an acute onset within 7 days from a known or suspected clinical insult. The neonatal ARDS is due to diffuse, bilateral, and irregular opacities or infiltrates, or complete opacification of the lungs, which have no causes in local effusions, atelectasis, transient tachypnoea, congenital lung anomalies as well as hyaline membrane disease or primary surfactant deficiency. Moreover, the clinical onset should be not fully explained by congenital heart disease. The paediatric ARDS is characterised by new infiltrates consistent with acute parenchymal process where a bilateral lung opacity is not always present. The clinical signs should be not totally explained by fluid overload or heart failure. The severity of paediatric and neonatal ARDS can be classified according to oxygenation index classes (De Luca, 2019).

ARDS accounts for 10% of all cases in intensive care units worldwide. Mortality is age-dependent and remains around 40-50% in adults and 25% in children and neonates (De Luca *et al.*, 2017; Matthay *et al.*, 2019; Riviello *et al*, 2016). Up to now, no causal therapies are available for the syndrome. Primary ARDS occurs after a direct insult to the lung such as pneumonia and aspiration of gastric, oral and oesophageal contents (Matthay *et al.*, 2019). Conversely, the secondary syndrome is caused by the effects in the lung of a systemic inflammatory response due to sepsis, transfusion, cancer, bone fractures and pancreatitis, among others. Thus, the primary and the secondary forms of ARDS differ because they are associated with epithelial and endothelial injury, respectively (Calfee *et al*, 2015; Matthay *et al.*, 2019; Sinha & Calfee, 2019).

A co-primary factor for direct ARDS may be considered surfactant inactivation by the actions of early-produced local inflammatory mediators such as cytokines, ROS and $sPLA_2$ (Calfee *et al.*, 2015; Nakos *et al*, 2005). Moreover, the injury in vascular endothelium and the subsequent leakage of protein-rich oedema fluid leaking into alveoli further impair surfactant function in the late stages of direct ARDS or during the secondary syndrome (Autilio & Pérez-Gil, 2019; Günther *et al*, 2001; Gunther *et al*, 1996; Schmidt *et al*, 2007; Schmidt *et al*, 2001). Thus, the inactivation of both endogenous and therapeutic surfactant may partially explain the failure of surfactant replacement in clinical trials to date (Meng *et al*, 2019; Raghavendran *et al*, 2011). In this line, the identification of which patients with ARDS can benefit the most, the

timing, the dose, the administration modality and the best composition for exogenous surfactant preparations that could resist to inactivation, are an important challenge in clinical research.

Among the various possible types of neonatal ARDS, a particular one is the meconium aspiration syndrome (MAS) that is triggered by the inhalation of meconium into the lungs. In spite of its relative rarity, meconium-induces neonatal ARDS may have a relevant mortality (around 40%)(Autilio & Pérez-Gil, 2019; De Luca *et al.*, 2017; Gouyon *et al*, 2008; Singh *et al*, 2009; Wiswell *et al*, 2002). Meconium is a sterile, black-green, odorless complex mixture that starts to accumulate in the foetal intestine during the third month of gestation. It consists of numerous substances of host origin which are mainly derived from the digestive tract (Echaide *et al.*, 2017; Salvesen *et al*, 2014). It is composed of 72–80% water and contains cholesterol and its precursors, lipids, enzymes including $sPLA_2$, mucopolysaccharides, bile acids and proteins such as cytokines IL-1,-6,-8 and TNF-α. The main sterols present in meconium are cholesterol and bile salts, including cholic, taurocholic and glycocholic acids (Echaide *et al.*, 2017). Thus, after meconium inhalation, MAS may affect surfactant activity by means of the same compounds described above, which may be found in the meconium mixture (De Luca *et al.*, 2011; Echaide *et al.*, 2017; Kopincova & Calkovska, 2016). Moreover, a simultaneous action is mediated by meconial cholesterol and bile acids, drastically increasing surfactant fluidity and contributing further to its inactivation (**Figure 8A**). Besides, bile acids act as a cofactor of $sPLA_2$, increasing the enzyme activity and contributing to lung injury (Autilio & Pérez-Gil, 2019; Kopincova & Calkovska, 2016).

Although several *in vitro* evidences (Bae *et al*, 1998; Herting *et al*, 2001; Lopez-Rodriguez *et al.*, 2011; López-Rodríguez *et al*, 2012; Moses *et al*, 1991; Ochs *et al*, 2006; Oh & Bae, 2000; Sun *et al*, 1993) and experiments using animal models (Cleary *et al*, 1997; Hilgendorff *et al*, 2003; Lyra *et al*, 2009; Mikolka *et al*, 2016; Natarajan *et al*, 2016; Salvesen *et al.*, 2014) contributed to understand the effects of meconium on surfactant activity, no *in vivo* studies have been performed to clarify the inflammation-mediated surfactant damages in the early phases of MAS in neonates. This is an open question and a crucial point since it may help to understand which surfactant modification may cause the severity of the syndrome soon after birth, promoting early surfactant therapies.

Other diseases

Lung surfactant dysfunction could be also behind IPF, a chronic and progressive epithelial injury which still nowadays remains unsolved. Specifically, a reduction in SP-C and the implication of cholesterol were described as possible triggering and contributing events to the fibrotic process of this lung disease (Autilio & Pérez-Gil, 2019; Sehlmeyer *et al.*, 2020). Moreover, the plasticity of alveolar macrophages seems to play a critical role in the pathogenesis of IPF (Desai *et al*, 2018) which may lead, in turn, to a resulting unbalance between surfactant degradation and recycling (**Figure 8B**).

The insufficient uptake and catabolism of lung surfactant or an abnormal surfactant production could also be due to primary, secondary and congenital pulmonary alveolar proteinosis (PAP). The primary PAP is caused by an autoimmune or hereditary disfunction in GM-CSF signalling. This is due to GM-CSF and its receptor autoantibodies or mutations in CSF2RA or CSF2RB genes that encode for the receptor α- and β-chains. The secondary PAP is related to different conditions, from haematological disorders to pharmacological

immunosuppression, that can affect the number and function of alveolar macrophages. Finally, the congenital PAP is due to mutations in genes encoding surfactant proteins or proteins related to surfactant production (Salvaterra & Campo, 2020). All these diseases can be associated to an abnormal accumulation of old and less functional surfactant in the alveoli with a decrease in the pulmonary diffusion capacity and an increase in lung surfactant oxidation (Autilio & Pérez-Gil, 2019) (**Figure 8B**).

Restoration of lung surfactant activity

Animal-derived and synthetic surfactant preparations

Currently, three animal-derived surfactants from porcine or bovine sources are commercialised in Europe (Beractant, Bovactant and Poractant alfa), whereas in the USA market the commercialised natural preparations are three: Beractant, Calfactant and Poractant alfa (Halliday, 2017). BLES is commercialised mainly in Canada, while Kelisu, Butantan, Surfacen, Newfactan and Surfactant-TA are marketed in China, Brazil, Cuba, Korea and Japan respectively (Tridente *et al*, 2019). Lucinactant is the only synthetic preparation commercially available to date since CHF 5633, a synthetic surfactant containing SP-C and SP-B analogues, is still under clinical evaluation (Ramanathan *et al*, 2020; Sweet *et al*, 2017). The composition and source of all the therapeutic surfactants available today is summarised in **Table 1**.

The main difference is related to the protein-phospholipid content and the concentration (Hentschel *et al.*, 2020). Among all preparations, Poractant alfa extracted by liquid gel chromatography of minced porcine lung tissues, is only characterised by polar lipids and contains the highest SP-B and phospholipids amount. Thus, compared to other animal-derived commercialised surfactants, Poractant alfa can be administered by using a lower volume and higher doses (up to 200 mg/kg, 2.5 mL/Kg).

Since the size of the first dose is important for clinical responses (Sweet *et al.*, 2019), this may partially explain the significantly lower infant mortality and better respiratory outcomes observed for Poractant alfa at 200 mg/kg in several studies (Ramanathan *et al*, 2013; Tridente *et al.*, 2019). However, a recent meta-analysis also suggests similar outcomes in premature neonates for Beractant and Poractant alfa, taking real-world evidences into account (Sánchez Luna *et al*, 2020). On this basis, when similar surfactant doses are compared (100 mg/kg), no differences in survival advantage was noticed among porcine and bovine preparations (Hentschel *et al.*, 2020).

Compared to the first-generation protein-free synthetic surfactants, inable to properly adsorb at the air-liquid interface, the second-generation synthetic preparations contained additives to facilitate lipid spreading and adsorption (Ardell *et al*, 2015). Among those, Exosurf® (DPPC, tyloxapol, hexadecanol) was a synthetic mixture available worldwide until 2003. Although more efficacious for RDS treatments than the first-generation surfactants, the second-generation preparations were withdrawn from the market because they were clearly inferior compared to the animal-derived surfactants in clinical trials (Phibbs *et al*, 1991).

Subsequently, two third-generation synthetic surfactants were proposed, consisting of lipids, recombinant SP-C and SP-B-like peptides. Lusupultide (Venticute®) containing a recombinant SP-C was only used for adult ARDS with disappointed results and never commercialised (Hentschel *et al.*, 2020; Spragg *et al*, 2004). On the contrary, Lucinactant is characterised by a DPPC-enriched phospholipid mixture (DPPC/POPG in a 3:1 ratio) and KL4

acetate that should act as a surrogate of positively charged helical segments of SP-B. This is a short amphipathic peptide characterised by leucine amino acids with a lysine moiety inserted at each fifth residue (Zuo *et al.*, 2008).

Lucinactant was approved and commercialised since it shows *in vitro* and *in vivo* results similar to porcine and bovine animal-derived surfactants (Moya *et al*, 2005; Sinha *et al*, 2005). However, its handling was complicated (Hentschel *et al.*, 2020) and its volume dose (175 mg/Kg, 5.8 mL/Kg) was 2.5 times higher than that of Poractant alfa (200 mg/Kg, 2.5 mL/Kg). Thus, in spite of its good resistance to inactivation, Lucinactant, commercialised as Surfaxin®, was withdrawn from the market in Europe in 2006. Currently it is under clinical evaluation as aerosolised surfactant (Aerosurf®) (Finer *et al*, 2010; Hentschel *et al.*, 2020).

Recently, a novel third-generation synthetic surfactant, CHF 5633, was developed by Chiesi Farmaceutici S.p.A., and consists of the main surface-active agent of surfactant, namely DPPC combined with POPG in a 1:1 ratio by mass. This synthetic mixture also contains synthetic analogues of the two hydrophobic proteins involved in surfactant biophysical activity (**Figure 9**): (1) a recombinant SP-C33Leu (1.5% with respect to phospholipids by mass) similar to native SP-C with a N-terminal phenylalanine-glycine truncation, palmitoyl-cysteines substituted by serines as well as leucines instead of valines and the methionine in the hydrophobic C-terminal helical segment, and lysine instead of the leucine in position 12, (2) a short-cut version of SP-B (Mini-B, 0.2% with respect to phospholipids by mass) characterised by 34 residues of the N-terminal (8-25 aa) and C-terminal (63-78 aa) helical regions of SP-B, two internal disulphide linkages between them and a net charge of +7 as the human mature form (**Figure 9**) (Glaser *et al*, 2016; Johansson & Curstedt, 2019; Sarker *et al*, 2007; Sato & Ikegami, 2012).

Generic name	Trade name	Producer/Country	Source	PLs concentration (mg/mL)	PLs dose (mg/Kg)
Beractant	Survanta®	Ross Labs (USA)	Minced bovine lung extract, plus DPPC, TPG and PA	25	100
Bovactant	Alveofact®	Thomae (Germany)	Bovine lung lavage extract	40	50
Poractant alfa	**Curosurf®**	**Chiesi Farmaceutici (Italy)**	**Minced porcine lung extract, plus concentration by LGC**	**80**	**200 - 100**
Calfactant	Infasurf®	ONY Inc. (USA)	Calf lung lavage extract	35	105
BLES	Neosurf® or Liposurf®	BLES Biochemicals Inc. (Canada)	Bovine lung lavage extract	27	135
Calsurf	Kelisu®	CR Double-Crane (China)	Calf lung lavage extract	30	100
Korean bovine surfactant	Newfactan®	Not known (Korea)	Minced bovine lung extract	25	120
Surfactant-TA	Surfacten®	Tokyo Tanabe (Japan)	Minced bovine lung extract, plus DPPC, TPG and PA	25	120
Butantan	Not known	Butantan group (Brasil)	Minced porcine lung extract	25	100
Surfacen	Not known	Not known (Cuba)	Porcine lung lavage extract	25	100
Lucinactant	Surfaxin® / Aerosurf®	Discovery Labs (USA)	Synthetic	30	175
CHF 5633	**Elifactant®**	**Chiesi Farmaceutici (Italy)**	**Synthetic**	**80**	**200 - 100**

Generic name	Clinical dose (mL/Kg)	SP-B (mg/mmol)	SP-C (mg/mmol)	Main PLs (total mass %)	Chol (total mass %)
Beractant	4	0 - 1.3	1 - 20	DPPC (70) and PS (4)	0
Bovactant	1.25	2 - 5.6		DPPC (39) and PG (8.5)	3.2
Poractant alfa	**2.5 - 1.25**	**2 - 3.7**	**5 - 11.6**	**DPPC (46) and PE (6)**	**0**
Calfactant	3	5.4	8.1	DPPC (41) and PG (6)	5
BLES	5	0.17	0.49	DPPC (42) and PG (11)	0
Calsurf	3.3	0.2	0.25	DPPC (50) and PI (3)	3.6
Korean bovine surfactant	4.8	1.1 ± 0.17 % of total mass		DPPC (60) and PG (6)	Not known
Surfactant-TA	4.8	Not known		DPPC (65)	0
Butantan	4	5-10 % of total mass		DPPC (76) and PE (7)	Not known
Surfacen	4	1% of total mass		DPPC (45) and PI (12)	0
Lucinactant	5.8	KL-4 (19.8)	None	DPPC (75) and POPG (25)	0
CHF 5633	**2.5 - 1.25**	**Mini-B (0.2)**	**SP-C33Leu (1.5)**	**DPPC (50) and POPG (50)**	**0**

Table 1. Biochemical and pharmacological data of all current animal-derived and synthetic surfactant preparations. Therapeutic surfactants used in the present Thesis (Poractant alfa and CHF 5633) are in bold type and highlighted in blue. *Table adapted from (Echaide et al., 2017), (Tridente et al., 2019) and (Guo et al, 2020).* Abbreviations: CHOL, cholesterol; DPPC, dipalmitoylphosphatidylcholine; PG, phosphatidylglycerol; TPG, tripalmitoylglycerol; PA, palmitic acid; LGC, liquid gel chromatography; PE, phosphatidylethanolamine; PS, phosphatidylserine; PI, phosphatidylinositol; POPG, palmitoyloleoyl phosphatidylglycerol; PLs, phospholipids.

CHF 5633 was evaluated in a phase I clinical trial on 40 infants with 27–34 weeks gestational age (GA), demonstrating a rapid improvement in oxygen requirement, no unexpected adverse events and a good tolerability (Sweet *et al.*, 2017). This synthetic surfactant was compared with Poractant alfa in a multicenter double-blinded phase II clinical trial (Clinical-Trials.gov NCT02452476) and resulted as effective as Poractant alfa in both moderate and severe RDS (Hentschel *et al.*, 2020; Ramanathan *et al.*, 2020).

Figure 9. Sequence comparison between native human SP-B/SP-C and the corresponding proteins contained in CHF 5633 and Poractant alfa. Cysteines involved in intramolecular and intermolecular disulphide bonds are indicated in violet**.** Charged amino acids are highlighted and the resulting protein net charge shown. Amino acid differences from the human native proteins are indicated in red. *Table adapted from (Johansson & Curstedt, 2019).*

As for ARDS treatment, compared to Lusupultide, CHF 5633 contains both SP-C and SP-B analogues, probably making this preparation more efficacious. Moreover, it allows for longer *in vivo* residence time in the lung compared to Poractant alfa (Madsen *et al*, 2018) and seems to reduce the *in vitro* synthesis of proinflammatory cytokines by macrophages (Glaser *et al*, 2017). CHF 5633 was also found to be more resistant to *in vitro* and *in vivo* injury (Seehase *et al*, 2012). However, the exact biophysical mechanism under this resistance still remains unknown.

Surfactant additives

Surfactant hydrophobic nature as well as its capability to quickly adsorb at the air-liquid interface and efficiently spread along the alveolar surface make it a good candidate to vehiculise hydrophobic drugs into the lungs. Among those, budesonide, a synthetic glucocorticoid, may be added to Poractant alfa and CHF 5633 without altering their biophysical and surface-active properties (Hidalgo *et al*, 2017). An efficient anti-inflammatory effect for this drug when administrated together with therapeutic surfactants was demonstrated in animal models (using Curosurf 100 mg/Kg) (Kothe *et al*, 2018) and in RDS neonates (using Beractant 100 mg/Kg) (Yeh *et al*, 2016; Yeh *et al*, 2008), showing a great reduction of BPD. This has paved the way to a current clinical trial using budesonide-supplemented surfactant for prevention of BPD: SASSIE trial:ClinicalTrials.gov NCT02907593 (Hentschel *et al.*, 2020).

At the same time, hydrophilic additives, including non-ionic (polyethylene glycol and dextran (Kobayashi *et al*, 1999; Taeusch *et al*, 1999)), anionic (hyaluronan (Lu *et al*, 2005a)) and cationic (chitosans (Zuo *et al*, 2006)) polymers, when added to therapeutic preparations seem to enhance surfactant resistance to inhibition in both *in vitro* and *in vivo* animal studies (Calkovska *et al*, 2008; Kobayashi *et al.*, 1999; Lu *et al*, 2005b; Lu *et al*, 2005c; Lu *et al*, 2001a). The mechanism of action of those polymers is related to their chemical properties (Zuo *et al.*, 2008). Polyethylene glycol has a great capability to bind water, probably increasing the lamellar-body like dehydration of surfactant complexes. Moreover, non-ionic polymers may enhance the adsorption and aggregation of surfactant, inducing the conversion of small to large aggregates in the bulk phase by depletion forces. As for ionic polymers, the mechanism

by which they increase surfactant activity is still unclear and, although preliminary positive *in vitro* data, several negative results were reported when administered with surfactant in animal studies (Zuo *et al.*, 2008).

Objectives

Lung diseases constitute a huge charge on worldwide society concerning premature mortality and health service costs. Lung surfactant is a membrane-based system composed by lipids and proteins that covers the alveolar lining fluid. It is essential to drastically lower surface tension during expiration, preventing alveolar collapse. Both, prematurity-related lack of lung surfactant, which causes RDS, and the acute lung inflammation whose side-effects may be drastically exacerbated by the impairment of lung surfactant during ARDS, contribute to the mortality and global costs of care. Thus, studying the role of this system in both health and disease is decisive to propose new strategies that can rise the health benefits and the efficacy of clinical intervention. Therefore, this PhD Thesis is focused on translational research in surfactant biophysics, with the main goal of exploring surfactant-related factors in the pathogenesis and therapies of several respiratory diseases. To accomplish these objectives, the following specific aims are proposed:

1. Developing quick non-invasive and sensitive diagnostic methods to assay surfactant quality in RDS neonates and the need for therapeutic surfactant administration. In this line, the specific aim is to optimise a biophysical method based on lung surfactant adsorption that could be used as screening for CPAP failure in pre-term neonates.

2. Understanding the main mechanisms of early lung surfactant inactivation in neonatal ARDS. For this purpose, another goal is to study the composition of lung surfactant as well as its structural and biophysical properties within the first 3 hours of life in neonates with severe MAS.

3. Proposing new therapeutic strategies in ARDS patients after a direct lung injury. On this basis, the specific aim is to investigate the potential beneficial effects of therapeutic hypothermia on neonatal lung physiology and surfactant activity under both healthy and pathological conditions. Also, to elaborate a biophysical model to explain the effects of reducing temperatures on surfactant surface-active properties by *in vitro* studying the behaviour of animal and synthetic surfactant mixtures.

4. Optimising therapeutic strategies to improve lung surfactant activity under acute lung injury. For this purpose, another goal is to analyse the synergistic effects of therapeutic hypothermia together with the administration of synthetic (CHF 5633) or animal-derived (Poractant alfa) surfactant preparations both *in vitro* and in animal models.

5. Exploring the involvement of lung surfactant in chronic and age-related diseases. In this line, the specific aim is to investigate the connection between short telomeres, AT-II cell damage and lung surfactant activity in age-related murine model of lung fibrosis in the presence or absence of a telomerase therapy.

Part of this text has been published in the following paper:
Autilio C, Echaide M, et al., J Pediatr. 2017, 182:66-73.e1

Chapter I

"Surfactant activity in RDS neonates:
when both time and place are important"

Introduction

A therapeutic prophylaxis, only administrating surfactant preparations, is less effective than coupling early CPAP and selective surfactant therapy in decreasing both death and BPD of preterm neonates (Schmölzer *et al*, 2013). Confirming these evidences, latest American and European guidelines strongly recommend to administer selective surfactant treatments after early CPAP (Fetus & Newborn, 2014; Sweet *et al.*, 2019). In detail, surfactant replacement in preterm infants treated with CPAP should be started only when the oxygen requirements are increasing (Sweet *et al.*, 2019). However, the ideal time for surfactant administration and how to predict which neonates will require the replacement therapy still remain unclear. When the threshold of FiO_2 is exceeding 0.30 for all babies with a clinical diagnosis of RDS, the latest European guidelines suggest to start surfactant administration as early as possible (Sweet *et al.*, 2019). However, the true oxygenation status and the lung biology during RDS are not properly reflected by these arbitrary thresholds.

Since the amniotic fluid (AF) is in direct contact with the foetus lung, maintaining opened the air sacs and stimulating their growth, this material has been proposed as a good candidate to assay lung maturity and surfactant production by several tests that could predict the occurrence of RDS. Among those, the lecithin/sphingomyelin ratio, the stable microbubble test, the lamellar body count (LBC) and the percentage of PG grew in importance for antenatal RDS prediction, the need for intubation and postnatal early surfactant therapy prediction as well as for the diagnosis of secondary surfactant deficiency (Bhatia *et al*, 2013; Hentschel *et al.*, 2020; Stichtenoth *et al*, 2014; Vieira *et al*, 2012).

However, none of the current lung maturity assays are used in clinical practice or have been previously tested to predict CPAP failure in patients with RDS. Moreover, these techniques detect the amount of lung surfactant, but do not give information about its functional activity. They are also difficult to standardise, time-consuming and require a technical expertise.

The lecithin/sphingomyelin ratio was the first test of lung immaturity, considered as the gold standard, and serves to detect the ratio in AF between lecithin (PC), the major lung surfactant component whose amount increases during gestation, and sphingomyelin, a minor surfactant lipid that does not tend to vary throughout pregnancy (Roux *et al*, 1972). After amniocentesis, the sample is centrifuged and commonly measured by Thin Layer Chromatography. In normal pregnancy, the value should be 2.5 or higher at 35 weeks' gestation, whereas inferior ratios are related to lung immaturity. Contamination of the samples by urine, blood, meconium or vaginal secretions strongly interfere with testing, resulting in false values. PG is considered a crucial component in lung surfactant and appears at around the 35-36 gestation week, soon after PC, thus its presence in AF is an indicator of pulmonary maturity. PG is assayed by a qualitative rapid agglutination test (positive results ≥ 2 μg/mL) that uses antibodies to detect PG as visible agglutinates and is not subjected to interference by contaminants (Benoit *et al*, 1986). As expected, those two methods are invasive, complex or coarse and are no longer available (McGinnis *et al*, 2008; Neerhof *et al*, 2001).

Once agitated, surfactant contained in AFs forms small stable microbubbles (<15 μm in diameter), which are reduced or absent in RDS. This is the principle of the stable microbubble test (Pattle *et al*, 1979), which seems to be a rapid (5–7 minutes to perform) and effective method (Bhatia *et al.*, 2013) to predict RDS. However, this technique is (1) too cumbersome and coarse for routine use (Vieira *et al.*, 2012) and (2) influenced by sample dilution, since the quality of material is not typically tested under comparable surfactant phospholipid amount.

Finally, LBC seems to be superior to the lecithin/sphingomyelin ratio for RDS prediction (< 20,000/30,000 count/μL) and is a quick technique (Besnard *et al*, 2013). The higher the lamellar bodies-like in AF, the more mature are the foetal lungs. This method uses automated platelets counters to detect the amount of lamellar bodies due to their similar size to platelets (1-5 μm) (Szallasi *et al*, 2003). However, the viscosity of amniotic and tracheal fluids makes LBC technically impossible in same cases.

According to a recent meta-analysis on available reports, preterm neonatal outcomes seem to improve following early surfactant replacement when the administration occurs within 2-3 hours after birth (Bahadue & Soll, 2012). However, a reliable tool to predict the need for surfactant therapy at an early stage in preterm infants is still missing to date. For this purpose, this ideal test should be easy to use at the bedside, providing quickly available results for rapid and timely decision making.

Around ten years ago, Ravasio *et al*. developed a rapid, sensitive and high-throughput fluorescent method to indirectly test both adsorption and stable accumulation of surfactant at the air-liquid interface, defined as Surfactant Adsorption Test (SAT) (Autilio & Pérez-Gil, 2019; Ravasio *et al*, 2008). This technique was largely used to test *in vitro* surfactant activity (Cerrada *et al.*, 2015; Lopez-Rodriguez *et al.*, 2011; Ravasio *et al.*, 2008) or therapeutic surfactant preparations (Danhaive *et al*, 2015) and, more recently, to assay *ex vivo* non-bronchoscopic bronchoalveolar lavages (nBALs) from human term and preterm neonates (De Luca *et al*, 2020; De Luca *et al*, 2014). Interestingly, because the SAT can be considered a semi-quantitative functional test, it may describe both lung surfactant activity and the neonatal lung physiopathology, being a potential tool for guiding surfactant replacement therapy. Starting from these considerations, in the present chapter the feasibility of performing SAT in AFs of preterm neonates' mothers will be explored. By increasing SAT analytical sensitivity and its turn around time, the usefulness of this technique as a screening tool for early surfactant administration will be investigated.

Key techniques and patients

Enrolled patients and clinical parameters

The clinical part of the present study (patients' enrolment, collection of clinical parameters, surfactant administration, lung ultrasonography and LBC) was performed by the Neonatal Intensive Care Unit (NICU) team at the Division of Pediatrics and Neonatal Critical Care directed by Prof. Daniele De Luca at "A.Béclère" Medical Center of Paris. The study protocol was approved by the local ethical committee of the South Paris University Hospitals (n. PP13-046) and parental consent was obtained upon NICU admission.

The prospective pilot study was designed following Standards for Reporting of Diagnostic Accuracy guidelines (Bossuyt *et al*, 2003). The eligible population consisted of neonates admitted to "A Beclérè" Hospital NICU in Paris between February and June 2015 fulfilling the following criteria: GA <37 weeks and the need for nasal CPAP. Nasal CPAP was started early in the delivery room immediately after stabilisation in neonates of ≤32 weeks GA or at NICU admission for RDS in neonates of >32 weeks GA.

Eligible neonates underwent lung ultrasound in the first 2 hours after NICU admission and before eventual surfactant administration, in accordance with the hospital internal policy.

The lung ultrasound score (LUS) is a score obtained from lung patterns observed by ultrasonography. The latter is a safe and non-invasive technique based on high-frequency sound waves to create images of lungs. By using a transducer, the electrical current is converted into sound waves that cross body's tissues, bouncing back from the body's structure and reflecting back to the transducer. Thus, the transducer converts the waves into electrical signals whose pattern is used to create a digital image by a computer. LUS can be employed to estimate lung aeration (the higher the LUS, the higher the Oxygenation Index (OI)) and define the total spectrum of possible lung conditions: a normal aerated lung, an interstitial pattern, an alveolar pattern, and consolidation (dense material instead of air into alveoli) (Brat *et al*, 2015).

As described previously (Brat *et al.*, 2015), each lung was divided into 3 zones (upper anterior, lower anterior, and lateral) and examined transversely and longitudinally (**Figure 10**). For each lung area, a score from 0 to 3 points was assigned, resulting in a total score for the two lungs from 0 to 18. Citing Brat *et al*. (Brat *et al.*, 2015): "0 indicates A-pattern (defined by the presence of the only A-lines (lateral white arrowheads in (**Figure 10**)); 1, B-pattern (defined as the presence of ≥3 well-spaced B-lines (white arrows in (**Figure 10**)); 2, severe B-pattern (defined as the presence of crowded and coalescent B-lines with or without consolidations limited to the subpleural space); and 3, extended consolidations (white box in **Figure 10**). A-lines represent reflection of pleura due to ultrasound diffusing through an air-filled lung; B-lines are due to fluid filling the interstitium (and the alveolar space if they become confluent)".

The oxygenation index was calculated at neonate admission (OI_{adm}) as follows: OI_{adm} = CPAP (mmHg) x FiO_2 x 100/PaO_2. Transcutaneous PO_2 was measured for 15 minutes using a transcutaneous monitor appropriately calibrated at 44°C according to American Association of Respiratory Care guidelines (Restrepo *et al*, 2012). Surfactant administration protocol followed 2013 European Guidelines (Sweet *et al*, 2013). Poractant alfa was administered when the FiO_2 requirement reached 0.3 within the first 24 hours of life in infants <28 weeks GA or 0.4 within the first 24 hours of life in infants >28 weeks GA (Sweet *et al.*, 2013). Late respiratory failures requiring surfactant therapy were not considered for the study.

A control group of full-term healthy neonates was enrolled with no maternal history of diabetes, cholestasis, or hypothyroidism. These infants had an uncomplicated perinatal transition and early postnatal period, and were cared for in the well-baby nursery.

Exclusion criteria for both groups were the following: (1) need for delivery room intubation, according to international guidelines for neonatal resuscitation (Wyllie *et al*, 2015); (2) meconium aspiration syndrome, defined as the presence of meconium-stained AFs and typical chest radiographs or lung ultrasound images (Piastra *et al*, 2014); (3) pulmonary haemorrhage, defined as respiratory distress with increasing oxygen requirements, white lung on chest radiographs, and the presence of bloody airway secretions; (4) maternal blood aspiration, defined with the same criteria of pulmonary haemorrhage with the addition of bloodstained AFs; (5) antenatal suspicion of any lung malformation; (6) oligohydramnios or anhydramnios; (7) absence of clear AFs; and (8) major congenital malformation or known chromosomal abnormalities.

All data were collected prospectively in real time from the NICU electronic database and subsequently analysed.

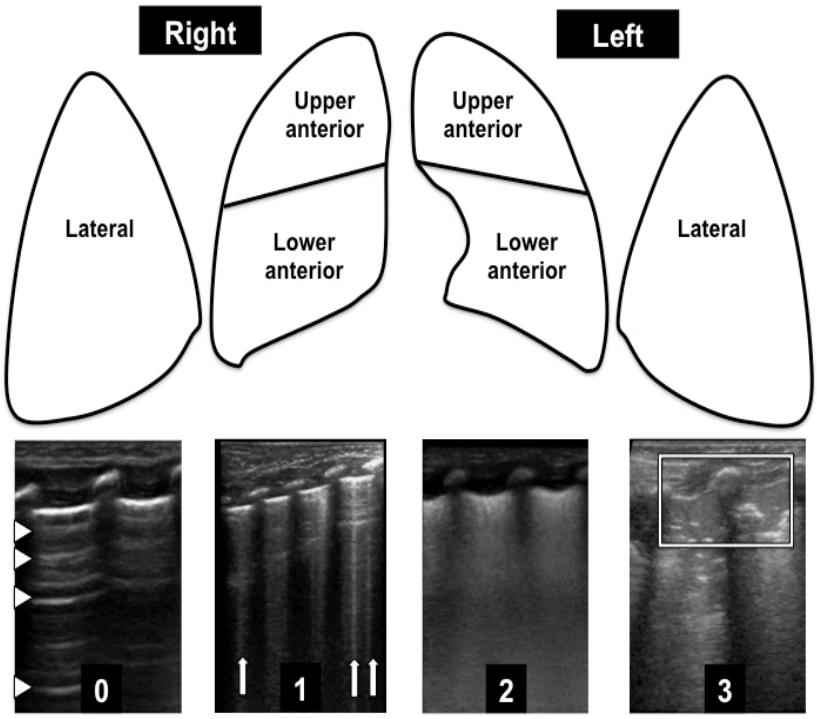

Figure 10. Lung Ultrasound Score (LUS) illustration. The 3 lung areas in which the lung is divided are shown as well as the score assigned to each zone according to the lung ultrasonography pattern. Score details are described in the text. *Figure adapted from (Brat et al., 2015).*

Sample collection and handling

At the time of vaginal or caesarean delivery, a sample of clear AFs ranging from 500 μL to 2 mL was collected and immediately divided into 2 aliquots. The first aliquot was used to count lamellar bodies in the platelet window of an automatic blood cell counter, after gently mixing the specimen five times (LH780, Beckman Coulter, Brea, CA, USA). The second aliquot was centrifuged at 700 g for 10 minutes in order to discard the cellular components. The supernatant was immediately frozen at -80°C and thawed only once for the analysis.

Porcine surfactant was collected from total bronchoscopic bronchoalveolar lavages (BALs) of fresh lungs of slaughtered adult pigs and purified by Sodium Bromide (NaBr) density-gradient centrifugation (Taeusch *et al.*, 2005). The pool of AFs from the control groups (term neonates) were purified using the same procedure, after removing the excess of mucus by passing the samples through a gauze. Levels of phospholipids of purified porcine surfactant (PS) used for the serial dilution experiments were measured through the lipid phosphorus mineralisation (Rouser *et al*, 1966). Conversely, since the majority of surfactant phospholipids is characterised by PC (~90%), surfactant content of AFs and PS used as internal reference was calculated through PC quantification by a quick enzymatic and colorimetric assay. Further details of the techniques are described in Materials and Methods chapter.

Modified Surfactant Adsorption Test (SAT)

As introduced above, SAT is a biophysical method that measures the kinetics of adsorption of surface-active materials and its accumulations at the air-liquid interface, developed by Ravasio *et al.* (**Figure 11**) (Ravasio *et al.*, 2008).

This is possible by labelling surfactant with a fluorescent analogue of PC (BODIPY-PC, Molecular Probes, Life Technologies, CA, USA) at a final molar ratio of 1-4% (fluorescent PC/surfactant), incubating the suspension for 1 hour at 37 °C with intermittent shaking (1400 rpm) every 10 minutes. In this way, fluorescent PC species can be incorporated into surfactant membrane aggregates. After incubation, the fluorescent PC/surfactant mixture is diluted with a saline buffer solution (5 mM Tris and 150 mM NaCl at pH 7.4) until reaching 3 μg of surfactant in a volume of 20 μL. This volume is injected at the bottom of the wells of a microtiter plate, containing 80 μL of a quenching solution of Brilliant Black dye (Sigma Aldrich, St. Louis, Missouri, USA) at a final dye concentration of 13 μg/μL in the same buffer.

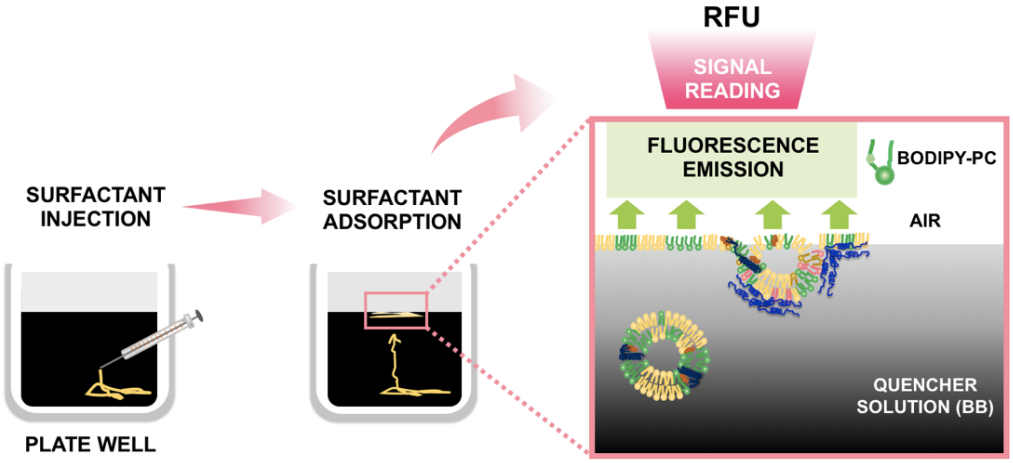

Figure 11. Schematic representation of SAT. The principle and crucial steps of the technique are illustrated. *Figure modified from (Autilio & Pérez-Gil, 2019).* Abbreviations: relative fluorescence units, RFU; BB, brilliant black.

Brilliant Black presents a high molar extinction coefficient for both the emission and excitation wavelengths used for the fluorescence reading of BODIPY-PC (emission: 540 nm, excitation: 485 nm) (Ravasio *et al.*, 2008). Moreover, this dye has no affinity for the interface and do not show surface-active properties. Fluorescent PC/surfactant suspensions are dispensed in triplicate by using a multichannel pipette in the Brilliant Black solution previously heated to 37 °C. This is done by touching the bottom of the wells with the tips and releasing slowly 20 μL of the sample.

Subsequently, the reading of fluorescence is quickly initiated and monitoring for 2 hours at 37 °C with intermittent shaking of the plate. Since the BODIPY-PC probe is masked by the Brilliant Black light adsorption in the bulk phase, no fluorescence is detected until surfactant adsorbs at the air-liquid interface and escapes from the quenching bulk environment. Thus, the method allows for the detection of both lung surfactant capability to move up towards the air-liquid interface crossing the subphase volume and the kinetics of its accumulation over time at the interface.

Although the resulting data are not surface tension values, they are indirectly related to the adsorption properties and expressed as relative fluorescence units (RFU) after subtracting the fluorescence units detected when the brilliant black is assayed alone. The latter are obtained by subtracting from each sample value, the fluorescent background of Brilliant Black without sample (**Figure 11**).

Since the aim of the study was to enhance SAT analytical detection in order to analyse lung surfactant in AFs of preterm neonates with poor surface-active properties, the classic protocol used in previous *in vitro* studies for PS/lamellar body-like particles/synthetic lipid mixtures (Cerrada *et al.*, 2015; Lopez-Rodriguez *et al.*, 2011; Ravasio *et al.*, 2008) was changed as follows: (1) using a BODIPY-PC molar percentage with respect to surfactant phospholipids of 2% and (2) reducing the volume of the bulk phase contained in each well (from 80 to 50 μL). BODIPY-PC molecules contain a fluorescent dye in one of the two acyl chains, resulting in a bulky hydrophobic moiety. This increases the space occupied by the molecule as it occurs for unsaturated phospholipids, influencing the fluidity of the membranes and films. Fluid components seems to rise the adsorption of surfactant to a clean surface (Veldhuizen *et al*, 1998; Walters *et al.*, 2000). Thus, it can be speculated that higher amount of BODIPY-PC could presumably help to increase the fluorescent signal and the analytical SAT detection by enhancing surfactant adsorption rate and the emission of BODIPY-PC/surfactant mixture once at the air-liquid interface. Moreover, the experimental procedure consists in pipetting the sample at the bottom of a well previously filled with a certain volume of quenching solution. As a result, BODIPY-PC/surfactant suspension needs to pass thought the subphase to reach the air-liquid interface. Starting from these considerations, it is reasonable to speculate that the rate of this process is related to the Brilliant Black volume contained in the well and when such volume is reduced, the adsorption of surfactant material with poor surface-active properties could become early visible and measurable within 2 hours.

To confirm the increased sensitivity in SAT detection with the proposed protocol modifications, PS suspension was serially diluted to reach different total phospholipid content in 20 μL of buffer: 3, 1.5, 0.75, 0.38, 0.19, 0.094, 0.047 μg. Buffer alone mixed with the BODIPY-PC amount used for doping 3 μg of PS was also included. Subsequently, the volume of 20 μL containing the different amounts of PS and BODIPY-PC was used to perform the classic and modified SAT methods. Results are shown in **Figure 12**.

The modified SAT showed promising results, increasing the analytical detection of PS accumulation at the interface until the fifth serial dilution (0.094 μg), whereas the classic method did not differentiate the third dilution (0.38 μg) from buffer.

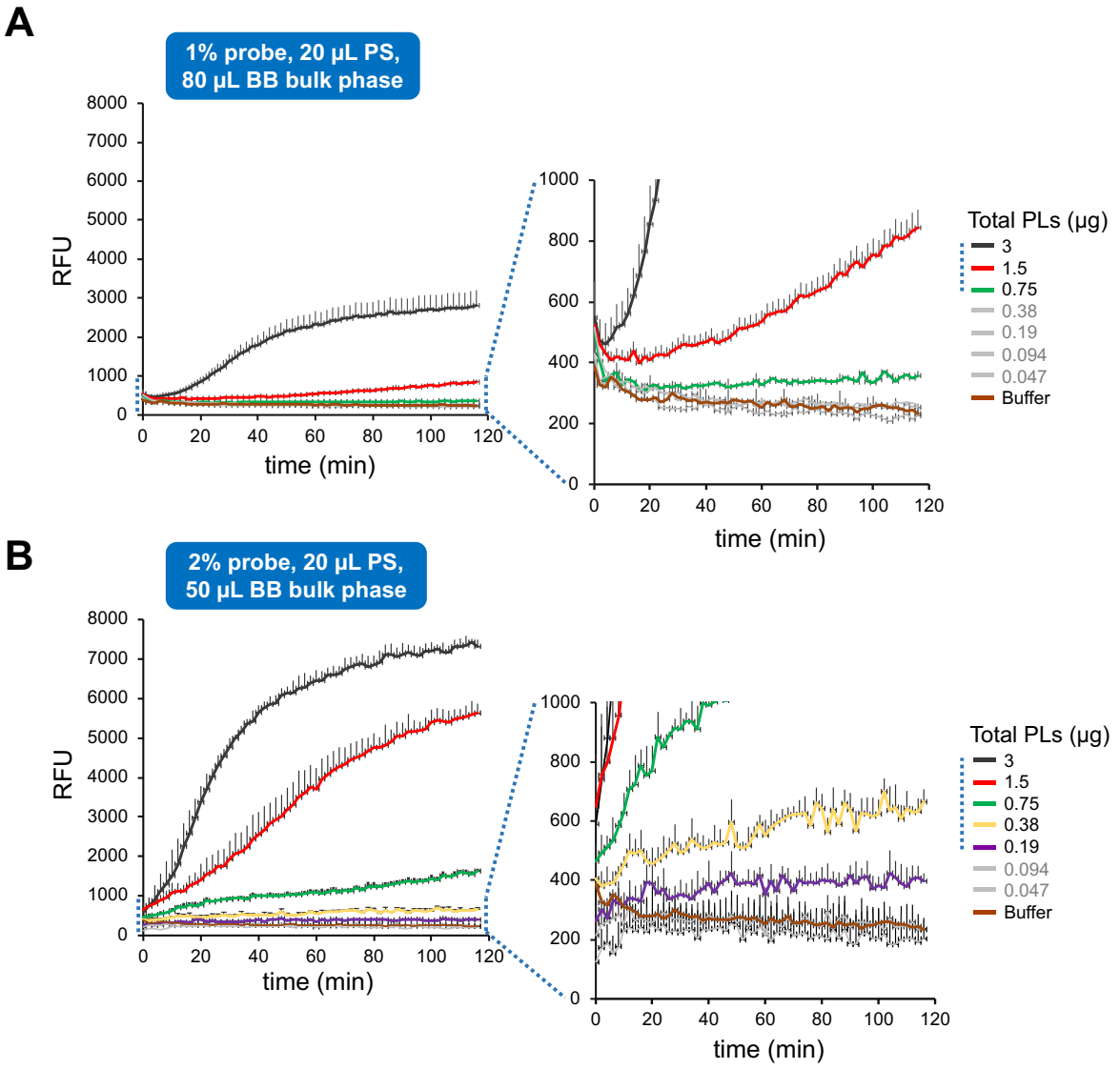

Figure 12. Differences in analytical detection between the classic SAT and the modified SAT procedures. PS suspension was serially diluted to reach the following total phospholipid content in 20 µL of buffer: 3, 1.5, 0.75, 0.38, 0.19, 0.094 and 0.047 µg. Subsequently, the volume of 20 µL containing the different amounts of PS and BODIPY-PC was used to perform **(A)** the classic SAT procedure (1% BODIPY-PC/surfactant in 80 µL bulk phase) or **(B)** the proposed modified SAT (2% BODIPY-PC/surfactant in 50 µL bulk phase). Mean of three inter-assay replicates and the corresponding SD are shown for each condition. The experiment was performed three times in different days with similar results. RFU obtained for only buffer and probe are included. Abbreviations: PLs, phospholipids; PS, purified porcine surfactant; BB, Brilliant Black; RFU, relative fluorescence units.

Considering the positive data, we cannot exclude that the volume reduction and the increase in probe percentage are not a synergistic effect and similar results could be obtained by (1) maintaining the bulk phase volume (80 µL) with increased BODIPY-PC amount (2 %) or (2) rising both the volume of the injected sample (from 20 to 50 µL) and the bulk phase (from 80 to 50 µL) using 2% of probe. To investigate this aspect, serially diluted PS (3 to 0.38 µg of phospholipids) was assayed (**Figure 13**) with disappointing results as indicated by the blue arrows. Maintaining the same volume with increased BODIPY-PC (2%), the fluorescent signal only rises for material that reaches the air-liquid interface, being impossible to detect diluted PS (no differences between buffer and 0.38 µg of PS). On the contrary, injecting PS in a

volume of 50 μL and using a reduced bulk phase (50 μL), the SAT analytical sensitivity seems to increase. However, the different dilutions are characterised by RFU overlapping both at the beginning and at the end of the assay. This is probably due to the volume-related movement of the injected sample, making difficult to maintain material at the bottom of the well at the start of the test.

Starting from these results, AFs samples of enrolled neonates were tested, using a final molar ratio of 2% (BODIPY-PC/surfactant) and a bulk volume of 50 μL. Analysis was performed using a FLUOstar OPTIMA Microplate Reader (BMG Labtech, Offenburg, Germany). The fluorescence intensity reaching the surface was followed at 37°C for 118 minutes, namely for 60 readings. Fluorescence kinetic cycles were characterised by a measurement start time of 0.2 second, a cycle time of 120 seconds, a shaking time of 3 seconds, double orbital shaking, and a fluorescence gain of 2000.

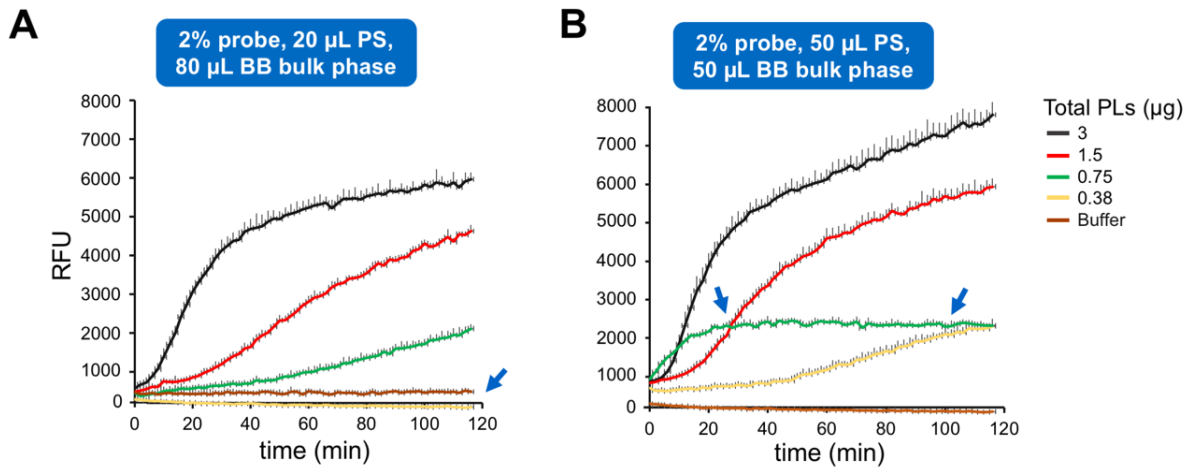

Figure 13. Alternative modifications of the SAT protocol. PS suspension was serially diluted to reach total phospholipid content in 20 or 50 μL of buffer: 3, 1.5, 0.75, 0.38 μg. Subsequently, the volume containing different amounts of PS and BODIPY-PC was used to perform **(A)** 2% BODIPY-PC/surfactant in 80 μL bulk phase or **(B)** 2% BODIPY-PC/surfactant in 50 μL bulk phase, respectively. Mean of three inter-assay replicates and the corresponding SD are shown for each condition. RFU obtained for only buffer and probe are included. Abbreviations: PLs, phospholipids; PS, purified porcine surfactant; BB, Brilliant Black; RFU, relative fluorescence units.

Experiments were performed in triplicate, and results are reported as RFU. All data were corrected by subtraction of the measured background and labelled buffer of each run. Intra-assay (repeatability) and inter-assay (reproducibility) coefficients of variation were calculated at minute 30 for PS specimens (mean (SD):10 (5.7)%; 5.36%, respectively).

Moreover, to increase the feasibility of the assay and maintain its turn around time within 3 hours, surfactant was tested using directly AFs without precipitating materials (1 hour at 22.000-44.000 g) as performed for neonatal BALs in the past (De Luca *et al.*, 2014). At the same time, the quantification of PC in both AFs and PS (used as internal reference), was carried out by the rapid enzymatic and colorimetric method (5 minutes) instead of the time-consuming and less sensible phosphorous assay. Finally, the incubation time for surfactant staining was reduced to 45 min.

All AFs and PS were diluted to a final concentration in the bulk phase of 0.043 μg/μL (corresponding to a total of 3 μg of PC in a volume of 70 μL) by using the buffer solution.

Moreover, as a further internal control and to verify whether the SAT results were altered by surfactant purification, the remaining volume of AFs obtained from healthy neonates were pooled, purified and re-assayed by the SAT in triplicate. This was done after completing the assay on non-purified AFs.

Statistical Analyses

Data are expressed as mean ± standard deviation (SD) or median (interquartile range (IQR)), as appropriate. After a preliminary Kolmogorov-Smirnov test to assay the sample distribution, comparison among the groups of PS, healthy controls (AFs from term neonates) and RDS (AFs from preterm neonates) was carried out by Kruskal-Wallis ANOVA, followed by the Conover-Iman post hoc test. These two statistical analyses are the equivalent of ANOVA when the sample distribution is non-parametric. Mann Whitney U test was performed to compare AFs of preterm neonates who failed CPAP needing surfactant administration with those of preterm neonates who only needed CPAP. Spearman coefficient (ρ) was used for correlation analysis. To study the diagnostic accuracy of the SAT for predicting which preterm neonates would not fail CPAP (namely the patients who did not need surfactant replacement therapy), a receiver operator characteristic curve analysis was carried out. Area under the curve (AUC) was calculated for fluorescence results at different time points and compared using the DeLong method. Diagnostic sensitivity and specificity, likelihood ratios, and predictive values were calculated with 95% confidence interval (CI). Analyses were carried out using SPSS 15.0 (SPSS, Chicago, Illinois, USA). $p < 0.05$ was considered significant.

The adsorption of amniotic surfactant is more compromised in RDS neonates who needed both C-PAP and surfactant therapy compared with RDS neonates who only needed C-PAP

15 term neonates and 41 preterm neonates were enrolled as control and RDS group, respectively. Demographic characteristics are shown in **Table 2**, among which the 5-minute Apgar score and the Critical Risk Index for Babies II (CRIB-II) are listed. The Apgar score is a rapid method to score the clinical status of a neonate at 1 and 5 minutes of age to promptly intervene and initiate breathing. Five components are considered: heart rate, reflexes, colour, muscle tone and respiration, giving a score from 0 to 2 for such of these characteristics (Watterberg *et al*, 2015). CRIB-II score calculates the illness severity and the initial risk of mortality within one hour at admission, considering several components: GA and sex of the neonate, body temperature, birth weight and the base excess (Parry *et al*, 2003).

As emerged in **Table 2**, neonates in the RDS group were critically ill, according to CRIB-II score and OI on admission.

Demographic characteristics	RDS group n=41	Control group n=15
GA (weeks), mean (SD)	30.7 (2.6)	40 (0.8)
Birth weight, g, mean (SD)	1,523 (517)	3,890 (750)
Male sex, %	51.2	53
Antenatal steroid use, %	70.7	0
Cesarean delivery, %	61	13.3
5-minute Apgar score, median (IQR)	9 (8-10)	9 (9-10)
Surfactant administration, %	43.9	0
CRIB-II score, mean (SD)	4.5 (2.9)	-
OIadm, median (IQR)	3 (2-4)	-

Table 2. Demographic characteristics of the study population. OI_{adm} and CRIB-II score related to the clinical illness were not calculated for the control group of healthy term neonate. Abbreviations: OI_{adm}, oxygenation index at admission; CRIB-II, Critical Risk Index for Babies II; GA, gestational age; SD, standard deviation; IQR, interquartile range.

No significant differences were observed in total PC amount among AFs of term neonates [198 (64) μg/mL], RDS neonates who only needed CPAP [336 (323) μg/mL] or failed CPAP [978 (2210) μg/mL] by Kruskal-Wallis test (p= 0.486). This result is probably due to the huge PC variability in preterm neonates' samples, observing from the high SD values.

Figure 14A shows the surface accumulation of fluorescently labelled surfactant from 6 PS (internal run references, red lines), 15 term neonate AFs (control group, yellow lines) and 41 preterm neonate AFs (RDS group, black lines). Although injecting the same amount of PC, the 3 groups were characterised by different kinetics of interface adsorption and accumulation. A sigmoid-like curve was observed for PS and the control group. The first showed a very rapid adsorption at SAT beginning, reaching 1500-3500 RFU after 10 minutes with comparable results among samples prepared and stained in different days. Conversely, term neonate AFs displayed a slower and broader adsorption, maintaining values in the range of 800-3000 RFU after 10 minutes. Moreover, following the surface accumulation over 120 minutes, RFU values continued to rise for all PS materials, reaching 5500-8000 at the end of SAT, whereas the kinetics of AFs was slower, going up to 5000 RFU at most. The adsorption of those samples showed a tendency to decrease in most cases, once reaching the plateau. The purified pool of control AFs (blue line, **Figure 14B**) was characterised by a quicker adsorption than the non-purified surfactant. However, a similar accumulation at the interface was evident once reaching the plateau with a stable surface activity (4000 RFU) that did not tend to increase.

In contrast to PS and term AFs, the majority of preterm AFs showed a different trend for the adsorption/accumulation kinetics, more similar to a square root function (black lines, **Figure 14A**). This can be probably considered similar to the initial part of SAT kinetics for term AFs before reaching the plateau. Specifically, after 10 minutes surfactant accumulation reached only 1000 RFU at most. Moreover, the kinetics of adsorption was very slow overtime, maintaining values <1000 RFU for most of the samples and doubling only in few cases.

In this regard, SAT can be considered a robust method to differentiate surface-active properties of different materials upon the same PC amount. In detail, differences in the fluorescence trend between the 3 groups began after approximately 15 minutes of reading.

Moreover, taking only into account the RDS group (**Figure 14C**), a partial overlap in adsorption/accumulation kinetics was observed between preterm neonates treated with only

CPAP (CPAP group, yellow lines) and RDS infants receiving both CPAP and surfactant administration (CPAP + surfactant, black lines). Apart from a single outlier, this last group presented an overall lower fluorescence accumulation especially in the first 30 minutes of the assay (grey vertical bar). Moreover, no detectable activity (< buffer signal) was observed in 5 out of 18 RDS neonates.

With this in mind, the time point after 30 minutes was used to compare the different studied groups (**Figure 14D**). Surfactant adsorption was higher in the PS samples (4877 (261) RFU) compared with healthy neonates (2532 (713) RFU) and neonates with RDS (478 (423) RFU; overall p< 0.0001, Kruskal-Wallis test with post-doc comparisons showed in the figure).

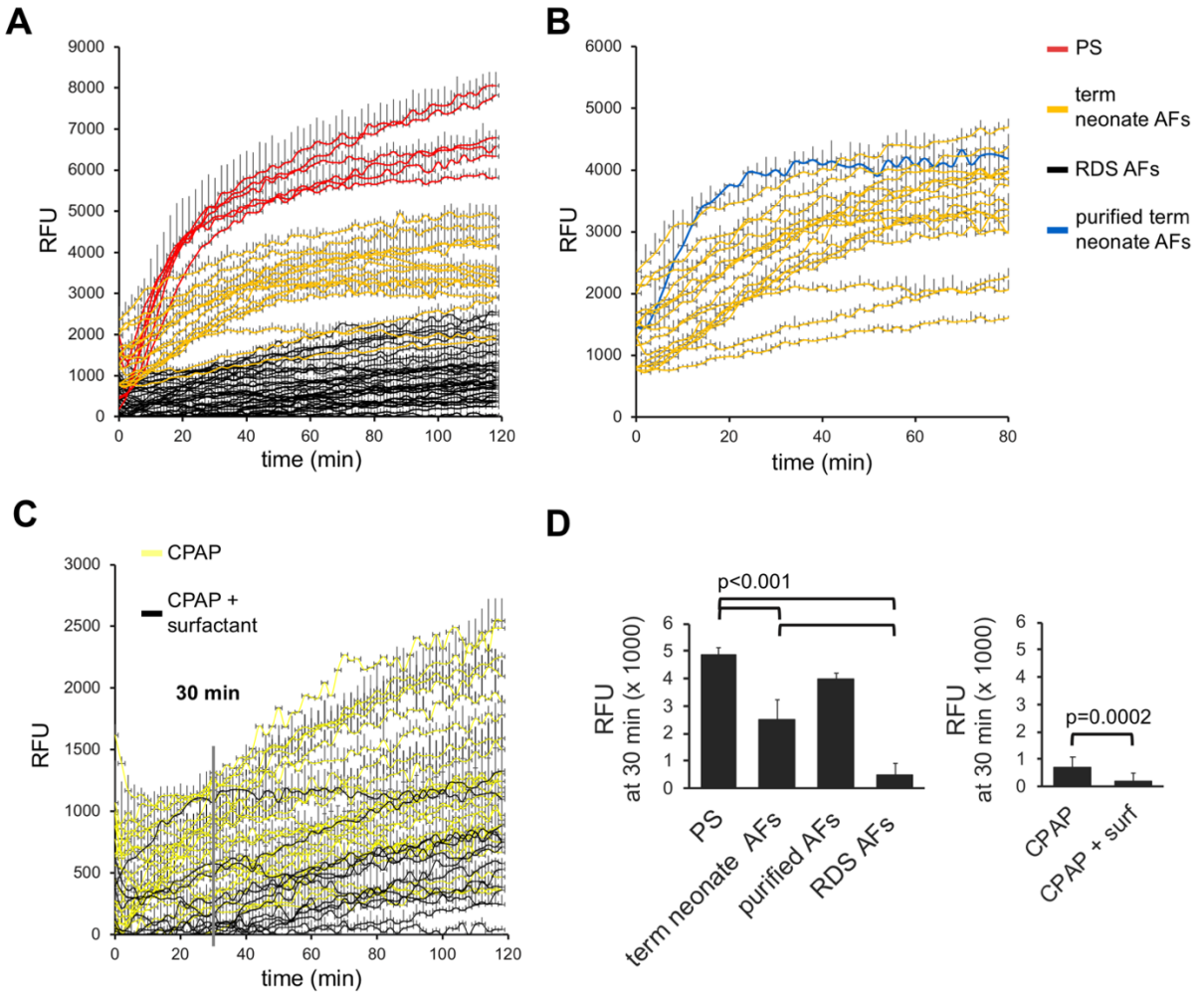

Figure 14. Surface accumulation of fluorescently labelled surfactant during the whole experiment. (A) Results from the whole dataset are shown. The red lines represent PS from 6 pigs, whereas yellow and black lines represent AFs from 15 healthy normal neonates (control group) and from 41 preterm neonates with RDS treated with CPAP (RDS group), respectively. **(B)** Results from AF surfactant of the control group (yellow lines) and its purified pool (blue line) are depicted. **(C)** Data from the RDS group. The black lines represent AFs from RDS neonates who received surfactant replacement (18 neonates), and the yellow lines represent AFs from preterm neonates who did not fail CPAP (23 neonates). The grey vertical bar indicates the minute 30. **(D)** Histograms showing data for all group at the 30-minute fluorescence reading. p< 0.001 indicates the post-doc comparisons among the different groups after a Kruskal-Wallis test (Conover-Iman test). p= 0.0002 (Mann-Whitney U test). Columns and T-bars represent mean and SD. Abbreviations: PS, purified porcine surfactant; AFs, amniotic fluids; RDS, respiratory distress syndrome; CPAP, early continuous positive airway pressure; surf, surfactant administration; RFU, relative fluorescence unit.

Moreover, a significantly higher mean surfactant adsorption was observed in neonates treated with CPAP when compared with neonates who also received surfactant (714 (376) RFU vs 177 (288) RFU; p= 0.0002, Mann-Whitney U test).

Surfactant adsorption correlates with amniotic lamellar bodies count and lung ultrasound score in RDS neonates

As a second step, considering the significant difference in surfactant activity at minute 30 between CPAP treated neonates (n= 23) and preterm infants who failed CPAP and needed surfactant administration (n= 18), a correlation analysis was performed between RFU values from the 30' of SAT analysis and LUS or LBC (**Figure 15**). Due to the technical difficulties (viscosity of the sample), LBC was only performed in 28 neonates, but it was enough to obtain positive results. In this regard, the fluorescence accumulation of AF surfactant at the air-liquid interface correlated directly to the amount of lamellar bodies like, with a Spearman coefficient (ρ) of 0.51 (p= 0.006), whereas there was an inverse correlation with LUS (ρ= -0.39; p= 0.013). These results are expected since lung surfactant reaches the air-liquid interface through lamellar bodies and great LUS values defines a low lung aeration which, in turn, depends on the amount and activity of the system. A correlation between SAT results and GA was also obtained, although less significant (ρ= 0.34; p= 0.03).

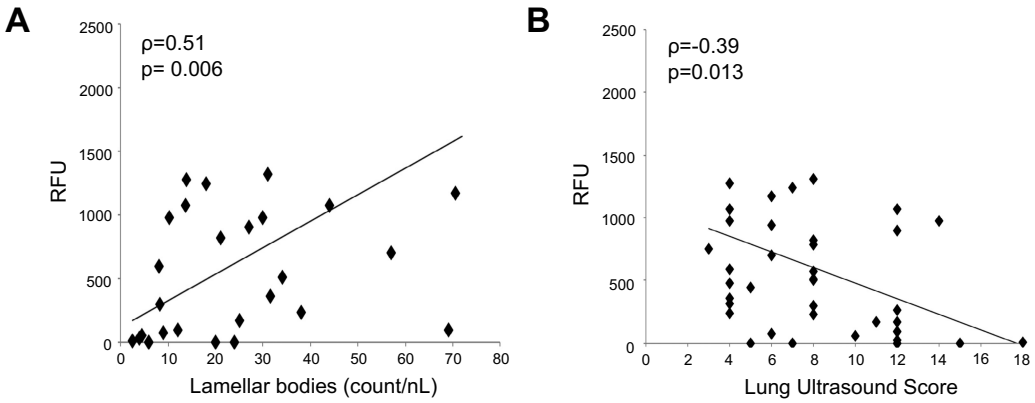

Figure 15. Correlation plots. Correlation between surfactant adsorption/accumulation at the air-liquid interface at minute 30 expressed as RFU and values obtained from LBC **(A)** or LUS **(B).** The correlation tendency line (black bar) and (ρ) coefficients are also indicated. The analyses were performed using a Spearman correlation (ρ). Abbreviations: RFU, relative fluorescence unit.

Receiver operating characteristic curves for the prediction of RDS neonates successfully treated with CPAP without surfactant therapy

Once demonstrated that the fluorescence reading after 30 minutes was a good time point to significantly differentiate preterm babies who needed CPAP (n= 23) from RDS neonates who needed both CPAP and replacement therapy (n= 18), the second step was to define a cut-off value for the adsorption/accumulation of AF surfactant.

In this regard, the diagnostic accuracy to predict neonates who did not fail CPAP was tested, using several time points of SAT: 15, 20, 30, 60 and 118 min. In **Figure 16A**, the ROC curve analysis and the statistical comparisons are shown, while in **Table 3**, the corresponding AUCs and details about standard error (SE) and CI (95 %) were reported.

No significant differences were observed analysing all time points, although the readings at 30 minutes had the highest AUCs, with a best cut off level of 170 RFU (sensitivity, 96% [78%-100%]; specificity, 72% [47%-90%]; positive likelihood ratio, 3.44 [1.6-7.3]; negative likelihood ratio, 0.060 [0.009-0.400]; positive predictive value, 82% [62%-94%]; negative predictive value, 93% [66%-100%]).

This means that, considering the group of 23 preterm neonates who did not fail CPAP, surfactant from 22 of them showed values higher than 170 RFU by SAT. However, within the group of 18 RDS neonates who failed CPAP and needed replacement therapy, surfactant from 5 preterm babies also exhibited the same activity (> 170 RFU), being false negatives. This suggests that SAT can be considered a robust test to exclude neonates who do not need surfactant administration, but has a lower power to directly identify RDS babies who failed CPAP.

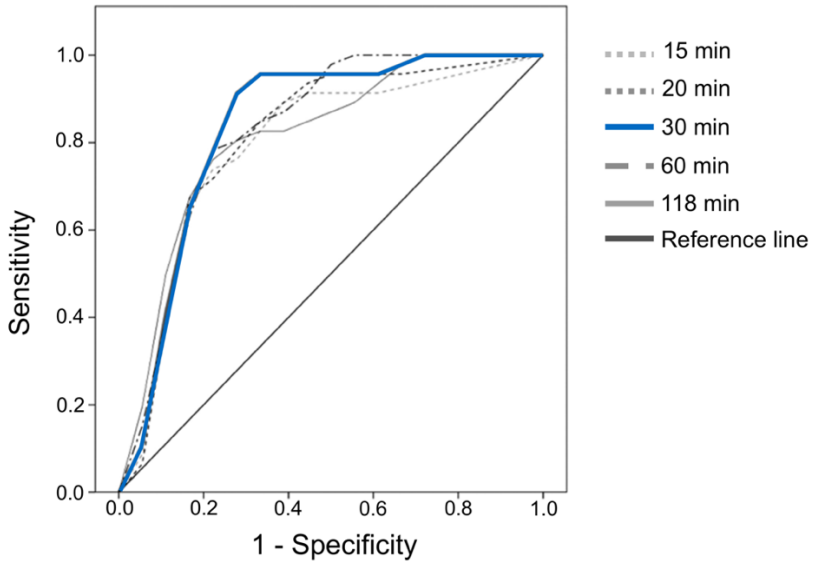

Figure 16. ROC curves for several time points of fluorescence reading by SAT. Curves show a similar trend with comparable area and no significant differences, being 30 min (blue line) the best time point in predicting CPAP success. 15 min vs 30 min, p= 0.180; 15 min vs 60 min, p= 0.501; 15 min vs 118 min, p= 0.755; 30 min vs 60 min, p= 0.735; 30 min vs 118 min, p = 0.632; 60 min vs 118 min, p= 0.627 (DeLong method).

SAT fluorescence reading (min)	AUC	SE	CI (95%)
15	0.790, p= 0.002	0.066	0.723 - 0.984
20	0.810, p= 0.001	0.064	0.734 - 0.986
30	0.840, p< 0.001	0.059	0.059 - 0.999
60	0.826, p< 0.001	0.060	0.750 - 0.984
118	0.812, p= 0.001	0.061	0.731 - 0.970

Table 3. AUCs, SE and IC (95%) for several time points of fluorescence reading. Abbreviations: AUC, area under the curve; SE, standard error; CI, confidence interval.

Discussion

In this chapter, the use of SAT as a screening tool to guide therapeutic surfactant administration in preterm neonates treated with CPAP has been investigated. This method shows a good diagnostic accuracy and correlates with other indirect important indices of surfactant physiopathology, such as LBC or LUS. SAT has therefore the potential to be developed into a clinically relevant point-of-care technique. In this regard, the method allows for the early identification of patients needing surfactant and can be employed to avoid delays in surfactant administration until the time when alveolar collapse appears and FiO_2 requirements increase. Although the strategy may have the cost of several false positives (identifying some CPAP failures as successes), the method is capable to rule out most of babies (96%) who did not need the therapy.

Since the clinical efficiency of surfactant replacement therapy is maximal when administrated within the first 2-3 hours of life (Bahadue & Soll, 2012), SAT may be a good candidate method to guide the treatment, potentially optimising the therapeutic benefits. On this basis, an important characteristic of SAT is its analytical precision and reproducibility (5-10% intra- and inter-assay CV%) along with its quickness that provides readily interpretable data. Moreover, to perform the assay, no invasive procedures are needed, using low amounts of AFs collected directly at delivery.

LBC seems to have similar sensitivity and specificity of SAT for the diagnosis of RDS according to a recent analysis on diagnostic data (Besnard *et al.*, 2013). However, no evidences are available on its capability to differentiate between clinical RDS diagnoses and the need for surfactant replacement therapy. Conversely, according to the present data, SAT is able to discriminate neonates who will need CPAP and/or surfactant therapy from those with no lung disease. On this basis, LBC is a quantitative technique for assaying the amount of lamellar bodies, but does not contribute to assess the real surface-active properties of the available surfactant. Conversely, the SAT indirectly measures one of the biophysical characteristic of the system (Ravasio *et al.*, 2008), namely its capability to adsorb at the air-liquid interface, although without providing quantitative information. Indeed, a standardised dilution with a normalised choline content is employed for SAT, meaning that surfactant adsorption is measured at the same PC amount (almost the same phospholipid concentration) in each sample. Therefore, the SAT might qualitatively evaluate surfactant activity and be coupled to LBC in the clinical setting of RDS neonates, providing both quantitative and functional information. In this line, several studies using SAT have already demonstrated the surface-active properties of various commercially available surfactants and human surfactant samples from non-bronchoscopic BALs of term and preterm infants (Danhaive *et al.*, 2015; De Luca *et al.*, 2020; De Luca *et al.*, 2014). As expected, SP-B content emerged critical for the adsorption of material in a pool of preterm infant tracheal aspirates (Danhaive *et al.*, 2015). In the present study, the amount of SP-B in AFs from each enrolled neonate could not be measured due to the very low available volume/PC content (AFs are more diluted than BALs) and the need to perform a simultaneous LBC analysis.

The difference in the adsorption of AF surfactant among term and RDS neonates is not surprising since this property can be influenced by multiple variables in the neonatal and foetal lung, due to either altered amount of lamellar bodies or their quality, under the same PC content. Indeed, several conditions can influence surfactant adsorption properties: (1) the amount of SP-B, SP-C and/or SP-A (Lopez-Rodriguez *et al.*, 2016b; Ross *et al.*, 2002; Ruano

et al., 1996; Sánchez-Barbero *et al.*, 2007; Walters *et al.*, 2000), (2) the rate of anionic phospholipids, such as PG (Chavarha *et al.*, 2013), (3) the oxidation status of lipids and proteins due to ROS-mediated modifications (Rodríguez-Capote *et al.*, 2006; Stadtman & Levine, 2003) (4) the structural properties of surfactant membranes and, especially for lamellar bodies, their hydration status (Cerrada *et al.*, 2015), (5) the amount of $sPLA_2$ with respect to total phospholipids and (6) the presence of substances able to inhibit surfactant activity that can be found in AFs such as meconium (Cerrada *et al.*, 2015; Lopez-Rodriguez *et al.*, 2011). This latter point can be ruled out considering the exclusion criteria defined for the study. Still changes in $sPLA_2$ activity, surfactant structure and lipid-protein composition could be factors occurring under RDS when AT-II cell immaturity can alter the proper development of lamellar bodies. As a result, the product of secretion of these organelles are lower in RDS neonates than in term infants, as corroborated by LBC. However, at the same time, they are probably abnormal and less functional when detectable, due to changes in SPs, lipid composition or their dehydrated status.

The correlation between lung aeration measured by LUS and the SAT values confirms the idea that alveolar expansion is proportional to the amount of functionally active surfactant. On this basis, the more active is surfactant available in AFs, the greater the lung aeration and availability for gas exchange at birth. Moreover, the correlation between LBC and GA and the SAT results was also confirmed. This corroborates that alveolar surfactant films are generated from secreted lamellar bodies, whose secretion is the crucial and primary step, increasing proportionally with GA (Fakhoury *et al*, 1994).

The complex and time-consuming preliminary procedure to purify surfactant (Taeusch *et al.*, 2005) is not necessary for running the SAT, since no important difference in fluorescence readings was noticed when testing AFs from control neonates subjected or not to purification. Interestingly, surfactant adsorption and accumulation at the air-liquid interface was significantly higher for PS compared to AFs of control term neonates before and after surfactant purification. This result is probably due to the different material (porcine BALs and human AFs) which is also related to the different collection procedure. In this regard, PS derived from a whole lavage of porcine lungs, likely containing most of the material from the distal airways, including the most active surfactant complexes. Conversely, AFs, collected at the delivery, likely represent only the fraction of surfactant that is easily mobilised out from the lung by the amniotic fluid flows.

As schematised in **Figure 17**, results from SAT are obtained after overall 90 minutes (10 minutes for the PC assay, 45 minutes for probe staining, 10 minutes for background reading and 30 minutes to complete fluorescence readings). This time could be shortened by reducing the time for probe staining and background reading and/or creating a dedicated hand-held fluorometer to carry out the test at the bedside. However, even without reducing the turn around time, SAT produces results within the first 3 hours of life, opening access to the optimal time window for therapeutic surfactant administration (Bahadue & Soll, 2012; Yost & Soll, 2000).

In spite of the promising results, several limitations should be considered: (1) the relatively small sample size, (2) due to the exclusion criteria, the lack of a detailed analysis about SAT reliability for AFs potentially contaminated with mucus or meconium and/or with high viscosity, (3) the small volume/PC amount, making impossible to complement the study by determining the SPs content or analysing surfactant structure, (4) the use of PS as internal control, instead of purified human surfactant. The latter is not available in large amounts from

healthy human lungs. Human surfactant can be obtained from the therapeutic lavages performed in PAP patients, but PAP surfactant is impaired by oxidation due to the accumulation of undegraded surfactant and improper recycling of its components (Autilio & Pérez-Gil, 2019). However, relevant similarities between porcine and human surfactants are well known (Blanco *et al*, 2012; Curstedt *et al*, 2015). Theoretically, it would be also of interest to study a group of spontaneously breathing preterm neonates with RDS, but this would be unethical, because all neonates of ≤ 32 weeks GA receive CPAP according to current European guidelines (Sweet *et al.*, 2019).

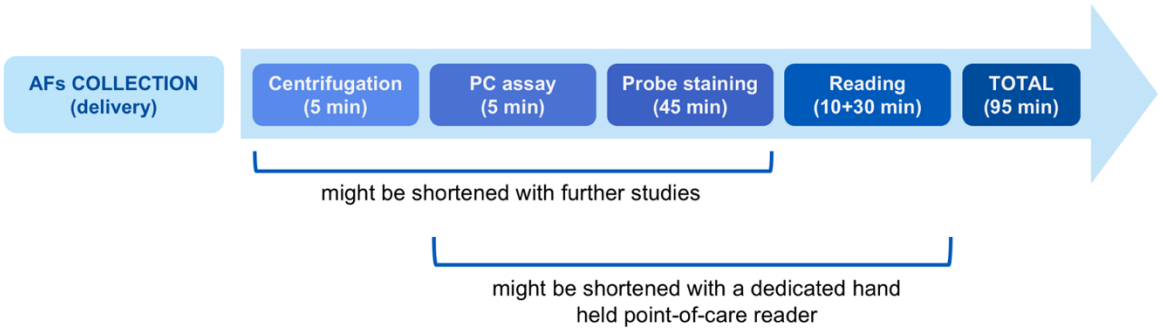

Figure 17. SAT turn around time. The different steps to perform SAT procedure are illustrated with the corresponding time along with the possible interventions to reduce the turn around time.

Finally, further multicenter and industrial research are necessary for the optimisation and miniaturisation of SAT in order to use this technique at the bedside into the routine clinical care. Still, according to the latest European guidelines the need to accurately identify RDS patients treated with CPAP who will need surfactant administration is real (Sweet *et al.*, 2019). SAT emerges in this sense as a very promising technique compared to the other tests for lung immaturity in AFs, producing data about surfactant adsorption at the air-liquid interface and complementing both LUS and LBC as a valuable asset for clinicians caring for preterm neonates.

The present work received the
"Bengt Robertson Award for Research
of the Neonatal Lung 2018" *from* ***ESPR***

Part of this text has been published in the following paper:
Autilio C, Echaide M, et al., Am J Respir Cell Mol Biol. 2020, 63(3):327-337

Chapter II

"Surfactant injury in the early phase of neonatal ARDS due to meconium aspiration"

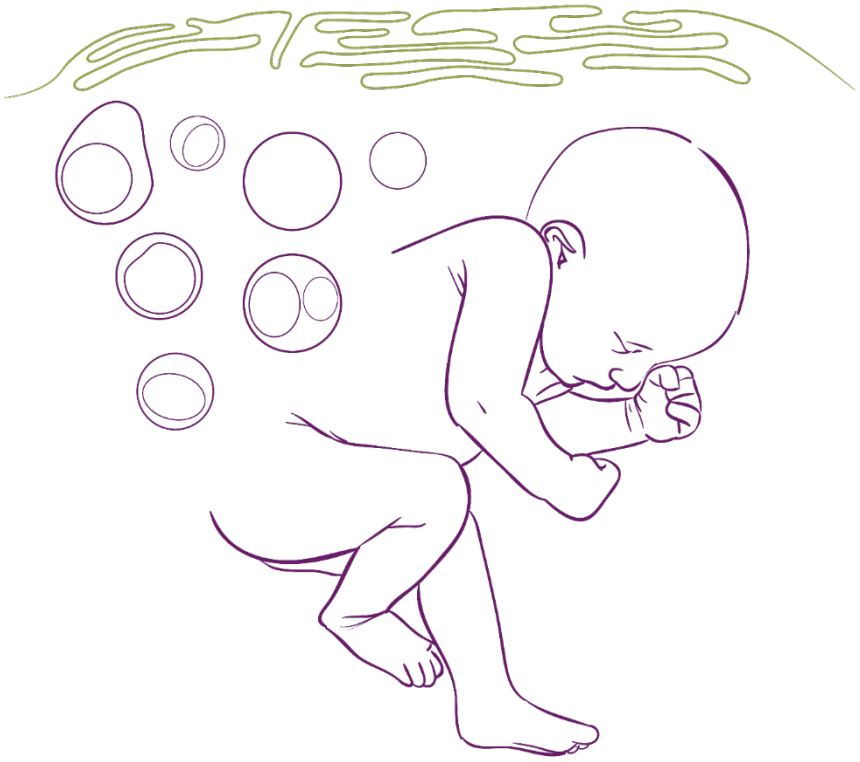

Introduction

Surfactant is a cornerstone of neonatal critical care for RDS neonates, improving respiratory outcome of those babies who failed CPAP. However, as for neonatal ARDS and, in particular, severe MAS, the situation is more complex. This syndrome is characterised by a multifactorial physiopathology that includes the inactivation of the lung surfactant system. Thus, the therapeutic approach that has been proposed is represented by lavages with diluted surfactant or administration of surfactant in bolus. The first strategy has demonstrated a reduction in mortality in most studies, but needs an experienced neonatologist due to the high risk of the procedure (Dargaville *et al*, 2011). Conversely, therapy with surfactant in bolus is safer, but not superior, showing only improvement for minor outcomes (Choi *et al*, 2012; Cochrane *et al*, 1998; Dargaville & Mills, 2005; Hahn *et al*, 2013; Hentschel *et al.*, 2020; Natarajan *et al.*, 2016). Interestingly, positive results were obtained in newborn pigs, using lavages with diluted surfactant followed by administration of Poractant alfa (125 mg/kg) (Henn *et al*, 2016). However, further research is needed to validate the benefits in severe MAS, before recommending surfactant treatment in routine clinical practice (Natarajan *et al.*, 2016). For this reason, replacement therapy with animal-derived surfactant is still not approved by the Food and Drug Administration and is reserved to personal clinical decisions.

Since MAS is characterised by a progressive inflammation-mediated damage of lung tissues, resulting in surfactant impairment, the timing of the dose administration is essential. This probably explains the lack of benefits in key outcomes for some cases with late intervention (Dargaville & Mills, 2005; Natarajan *et al.*, 2016). In this scenario, understanding which lung surfactant components are damaged during the early phase of severe MAS is essential for developing new surfactant protection strategies.

As extensively described in the introduction, several animal or *in vitro* studies explored the detrimental effects of meconium on the lung surfactant complex and these effects are brought about by various agents, such as proteases, cholesterol, $sPLA_2$, bile acids, FFAs, several proteins and cytokines (Autilio & Pérez-Gil, 2019; Kopincova & Calkovska, 2016). $sPLA_2$ has a dual role, as it hydrolyses surfactant phospholipids, degrading surfactant complexes, and also participates in the first step of the arachidonic acid (20:4) cascade that generates several thrombogenic and inflammatory molecules. This occurs when $sPLA_2$ hydrolysing activity involves PC containing arachidonic acid (Lambeau & Gelb, 2008). Arachidonic acid translocates through lung epithelial cell membranes by a “flip-flop” mechanism and may activate Rac1-mediated NADPH oxidases that generate ROS (Takemura *et al*, 2010). The latter can damage both alveolar cellular membranes and extracellular surfactant structures when released by the destroyed cells.

Interestingly, $sPLA_2$ is significantly increased in BALs from neonates with MAS, as well as in older children and adults with ARDS (De Luca *et al*, 2013; De Luca *et al.*, 2011; Nakos *et al.*, 2005). However, important gaps in the current knowledge emerge. Meconium is rich in the pancreatic isoform of $sPLA_2$ ($sPLA_2$-IB) and alveolar macrophages of MAS patients also produce $sPLA_2$-IIA as a response to meconium insult (De Luca *et al.*, 2011). Nonetheless, other $sPLA_2$ isoforms may be actually produced during MAS, playing additional roles in meconium-induced surfactant and cellular injury.

Moreover, scanty data are available about the effect of meconium on human lung surfactant *in vivo* during the first phases of MAS. Meconium seems to reduce PC and SP-A

synthesis at the height of clinical severity in patients finally needing extra-corporeal life support (Janssen *et al*, 2006; Lotze *et al*, 1990). However, those evidences are related to lung responses after at least one day. Thus, the meconium-induced changes in lung surfactant composition, structure and function in the early phase of MAS have not been characterised in detail. This is a crucial point, since the previous *in vitro* experiments do not consider the physiological lung milieu and all possible surfactant inhibiting agents associated to it during the inflammation-mediated injury of MAS.

Starting from these evidences, in this second chapter, a translational prospective cohort study was proposed to explore and clarify the changes in lipids, proteins, and structure of lung surfactant of neonates with severe MAS, as well as the impact on surfactant biophysical properties and lung aeration during the early phase of the syndrome.

Key techniques and patients

Enrolled patients and clinical parameters

The clinical part of the present study (patients' enrolment, collection of clinical parameters, lung ultrasonography, lavages collection and microbiological testing) was performed by the NICU team from the Division of Pediatrics and Neonatal Critical Care directed by Prof. Daniele De Luca at "A.Béclère" Medical Center of Paris. The study protocol was approved by the local ethical committee of the South Paris University Hospitals (n. PP13-046) and parental consent was obtained upon NICU admission.

Due to the rarity of MAS, a convenient sample size of 14 patients was chosen and considered feasible. Those diagnosed patients fulfilled the criteria of the Montreux definition for neonatal ARDS (De Luca *et al.*, 2017), identifying meconium aspiration as the trigger event leading to respiratory failure on the following bases: (1) presence of both meconium stained amniotic fluid and airway secretions, (2) respiratory distress starting soon after birth and requiring invasive ventilation, (3) typical chest imaging (Piastra *et al.*, 2014). The control group was characterised by 18 neonates with no lung disease (NLD) who were mechanically ventilated for extrapulmonary reasons. Those newborns accomplished the following criteria: (1) GA greater than 37 weeks, (2) clear amniotic fluid and airway secretions, (3) no sign of respiratory distress, (4) normal results of chest imaging and clinical examination, and (5) peripheral O_2 saturation > 95% in room air. The exclusion criteria for the two groups were (1) chromosomal abnormalities or congenital malformations, (2) any sign of early-onset sepsis or congenital pneumonia and (3) any lung disorder other than MAS.

Neonates were ventilated as follows. NLD were ventilated using a time-cycled, pressure-regulated, assisted-controlled ventilation with 4 ± 6 mL/Kg tidal volume, pH between 7.4 and 7.2, $PaCO_2$ between 35 and 65 mmHg, PEEP of 4-6 cmH_2O, FiO_2 as low as possible to keep saturation between 90% and 95% and PaO2 between 50 and 70 mmHg. MAS patients were treated with high frequency oscillatory ventilation (HFOV) within the first hour of life at a mean airway pressure (Paw) of 2 cmH_2O higher than Paw provided in conventional ventilation and anyway not less than 15 cmH_2O. Optimum lung volume strategy was applied and alveolar recruitment was performed, as needed. Frequency was 12 ± 9 Hz and oscillation amplitude was adjusted to obtain visible chest oscillation; both frequency and amplitude were titrated according to blood gas values and targeted to deliver volume of ≤ 2.5 mL/Kg.

In all patients the arterial blood gases values (indwelling arterial line) were used to follow the respiratory status and calculate the oxygenation index (OI = FiO_2 x Paw/PaO_2) and the PaO_2/FiO_2 ratio. Before any surfactant administration, lung aeration was carried out in MAS patients by LUS (Brat *et al.*, 2015).

Sample collection and handling

nBAL was performed within the 3 hours of life and before surfactant administration, according to the advice of the European Respiratory Society (de Blic *et al*, 2000) and using a well-standardised technique, detailed in Materials and Methods chapter. Meconium samples were collected from 7 enrolled MAS neonates within the first 24 hours of life. Around 200 μL of nBALs were sent for microbiological testing of sterility resulting negative. The remaining lavage was immediately centrifuged to discard cell pellets at 800 g for 10 minutes, frozen at –80°C and carefully thawed before the start of each analysis.

Total PC was preliminarily measured using an enzymatic and colorimetric method, directly from nBALs. Subsequently, a sample volume corresponding to around 50 μg of the resulting PC was dried and resuspended in chloroform/methanol (2:1). At the same time, an organic extraction was performed for the meconium collected from MAS patients. The obtained samples were used for lipidomic analysis. This characterisation was carried out at the Research Unit on BioActive Molecules (RUBAM) at the Department of Biomedicinal Chemistry (IQAC-CSIC) in Barcelona under the supervision of Dr. Josefina Casas. The liquid chromatography–high-resolution mass spectrometry (LC-HRMS) was performed using an Acquity ultra-HPLC system connected to a time-of-flight detector (Waters). Each lipid class was expressed as the molar percentage of the total lipids. The subclasses of lipids were expressed as the percentage of the corresponding lipid class. LPC species (16:0, 18:0) released by the $sPLA_2$ hydrolysis (Lambeau & Gelb, 2008) of several reduced or increased PC subclasses were also measured.

The amount of $sPLA_2$ subtypes IB, V, and X were tested using specific Enzyme-Linked ImmunoSorbent Assay (ELISA) kits and normalised with respect to PC levels previously assayed by the enzymatic method. Total proteins were measured using a bicinchoninic acid assay. SP-A was assayed by ELISA and normalised with respect to PC amount. SP-B and SP-C were analysed by polyacrylamide gel electrophoresis (PAGE) and Western blotting followed by band densitometry. Because total proteins changed, whereas PC amount did not change between the two cohorts, PAGE was performed under non-reducing conditions, loading 4 μg of PC from surfactant large aggregates previously obtained by ultracentrifuging nBAL supernatants (~22,000 g for 1 hour at 4 °C). Less hydrophobic SP-B precursors and monomeric SP-B were detected by PAGE and Western blotting under reducing conditions (4% β-mercaptoethanol), loading 11 μg of PC from lyophilised nBAL supernatants. Stripping of membranes was performed using guanidine thiocyanate (4 M) and both anti-SP-A and anti-pro-SP-B antibodies were used for the second detection. Purified porcine SP-B, synthetic PC and PG and reduced glutathione (GSH) were employed for the *in vitro* experiment illustrating glutathione-promoted protein deoligomerisation. In detail, the volume corresponding to 400 ng of purified porcine SP-B and 4 μg of PC/PG (7/3, w/w) in chloroform:methanol (2:1) was dried under a nitrogen flux and resuspended for 1 hour at 37 °C in 20 μL of saline buffer (5 mM Tris and 150 mM NaCl at pH 7.4), containing increasing amount of GSH. Purified porcine SP-B with and without lipids was used as internal control. Subsequently, after protein denaturisation,

10 μL (corresponding to 200 ng of SP-B in 2 μg of lipids) were loaded in PAGE for western blotting. Only the two internal controls were treated with 4% β-mercaptoethanol. The amount of GSH and oxidised glutathione (GSSG) in cell- and surfactant-free nBALs of patients (MAS, NLD and proteinosis) were determined by a Glutathione Colorimetric Detection Kit.

Surfactant adsorption was assayed by modified SAT in all patients, directly diluting nBALs. Conversely, large aggregates at 12 mg/mL PC obtained from nBALs of five patients (two NLD and three MAS) were used to perform a full biophysical analysis by Captive Bubble Surfactometry (CBS) at a frequency of 20 cycles/min at 37 °C. As experimental control, PS was incubated (1 hour at 37°C) with and without a pool of meconium (10% with respect to total PS phospholipid weight) that contained double of the amount of cholesterol present in PS. Finally, the nanostructure of surfactant large aggregates of seven neonates with NLD and six with MAS was analysed upon dilution at 10 mg/mL by Cryogenic Electron Microscopy (cryo-EM). Further details of the aforementioned techniques and materials are described in Materials and Methods chapter.

Purified human hydrophobic surfactant proteins

To get samples of human surfactant proteins to be used as a reference, surfactant was isolated from the therapeutic BAL of a primary PAP adult patient after obtaining the consent. After cell-free BAL ultracentrifugation (100,000 g for 1h), material was subjected to a NaBr density gradient and subsequently to an organic extraction. The resulting organic fraction was separated into lipids and proteins by size exclusion chromatography with a Sephadex LH20 column. Subsequently, a Sephadex LH60 column was used to isolate SP-B and SP-C, and the protein amount was quantified by amino acids analysis. Technical details are described in the Materials and Methods chapter. Five elution fractions were collected (F1, F2, F3, F4, F5) from the Sephadex LH60 column. As shown in **Figure 18**, the presence of hydrophobic human proteins as well as the lack of cross contaminations were verified through a non-reducing and reducing PAGE followed by silver staining and Western Blot analysis, respectively. Further methodological aspects are detailed in the Materials and Methods chapter.

Around 50 ng of the purified human SP-B and SP-C were run in each PAGE as internal standards to normalise samples values across gels. With this purpose, loading the same PC levels of neonatal samples (4 μg), the amount of SP-C as well as the quantity of dimeric and monomeric forms of SP-B were calculated by bands densitometry (ImageJ for Mac OS X) and expressed as percentage of the purified human surfactant proteins. This was possible since a portion of monomeric SP-B was detectable under non-reducing condition in the BAL of the PAP adult patient.

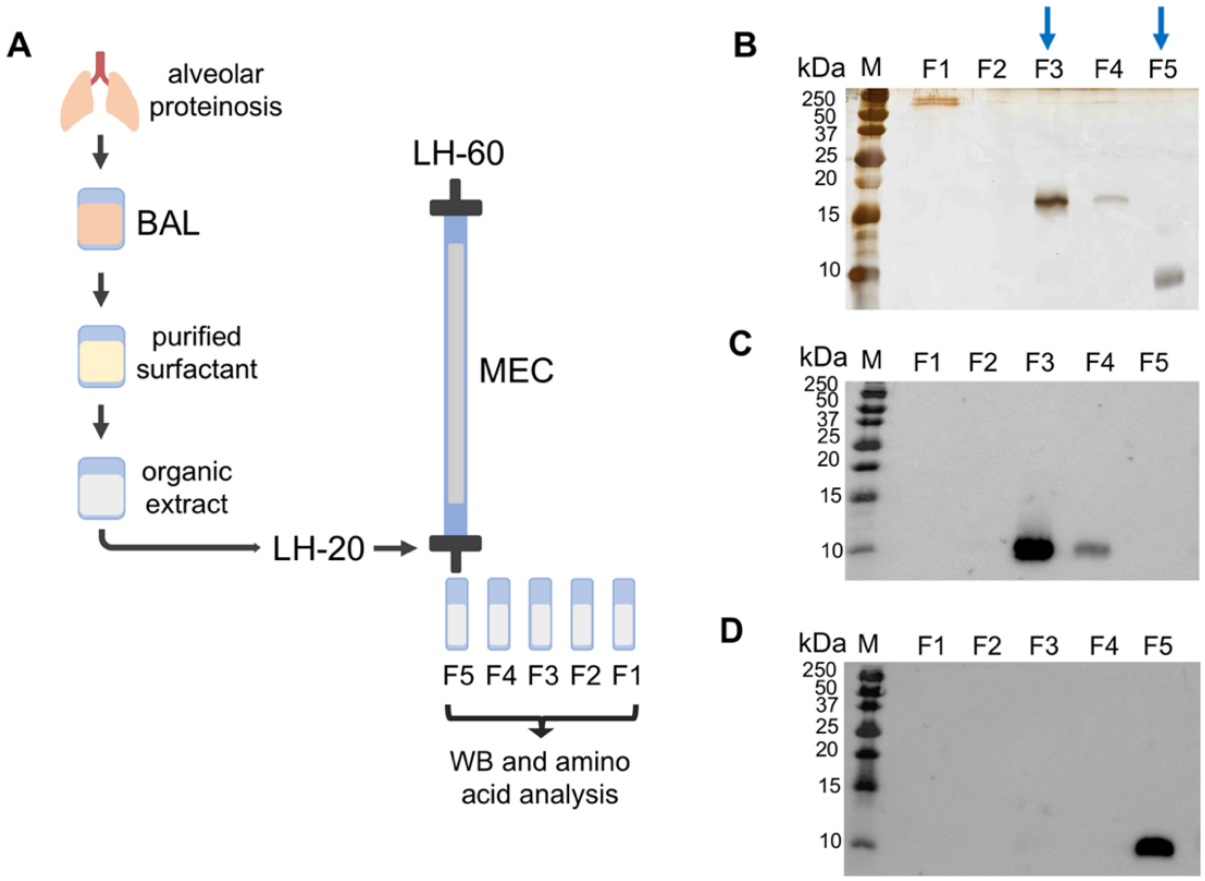

Figure 18. Purification of human SP-B and SP-C. (A) Schematic illustration of the different experimental steps to obtain Sephadex LH-60 elution fractions containing purified human hydrophobic surfactant proteins. Briefly, (1) BAL from the PAP patient was used to purify surfactant, (2) the purified material was subjected to organic extraction, (3) the extract was passed through Sephadex LH-20 and LH-60 columns, (4) the 5 elution fractions obtained from the LH-60 column were used for Western Blot and amino acid analyses. Silver staining **(B)** and Western blot anti-SP-B **(C)** and SP-C **(D)** are shown. Around 50 μL of organic extract were dried out, resuspended in electrophoresis Laemmli buffer and run under non-reducing condition **(B)** or adding 4% of β-mercaptoethanol **(C-D)**. No cross-contamination is visible among the purified fractions. As indicated by blue arrows, proteins in F3 and F5 were selected as internal standards. Abbreviations: BAL, bronchoalveolar lavage, MEC, molecular exclusion chromatography; F(1-5), fractions eluted from the column; kDa, kilodalton; M, protein molecular weight marker.

Statistical Analyses

Data were assayed for normality with the Shapiro-Wilk test and expressed as mean (SD) or median [interquartile range] when appropriate. Comparisons of results were conducted with the χ^2, Fisher's exact, Student t, or Mann-Whitney U test when appropriate. Correlations were performed using Spearman's ρ-coefficient. Analyses were carried out using SPSS 15.0 (SPSS, Chicago, Illinois, USA). A p value <0.05 was considered significant.

Meconium aspiration leads to early changes in surfactant composition and microstructure along with increased levels of secretory phospholipase A_2

The enrolled population was composed by 14 neonates with MAS and 18 babies with NLD ventilated for non-pulmonary reasons (12 for perinatal asphyxia, 1 for Ondine syndrome and 5 for congenital heart defects). **Table 4** shows the basic demographic details among which there is the Score for Neonatal Acute Physiology with Perinatal extension II (SNAPPE-II). This is characterised by physiology-based indicators to predict risk mortality and outcomes of neonates within the first 12 hours of NICU admission (Richardson *et al*, 2001). Since NLD neonates are hospitalised patients and not completely healthy newborns, they present a SNAPPE-II score, although significantly lower than that observed for MAS patients.

Demographic characteristics	MAS group (n=14)	NLD group (n=18)	P value
GA (weeks), mean (SD)	40.5 (2.1)	39.6 (1.9)	0.214
Birth weight, g, mean (SD)	3,300 (310)	3,420 (322)	0.296
Male sex, %	7 (50%)	8 (44.4%)	0.754
SGA neonates, %	1 (7%)	1 (5.5%)	0.854
Cesarean section, %	3 (21.4%)	4 (22.2%)	0.957
5-minute Apgar score, mean (SD)	4 (1.4)	4.5 (1.5)	0.343
SNAPPE-II, mean (SD)	61 (5)	50 (3.2)	> 0.0001
OI, mean (SD)	25 (1.8)	2 (1)	> 0.0001
LUS, mean (SD)	13.5 (2)	3 (1)	> 0.0001
Postnatal age at nBAL, h, mean (SD)	1.6 (0.8)	2 (0.6)	0.116

Table 4. Demographic characteristics of the study population. Abbreviations: nBAL, nonbronchoscopic bronchoalveolar lavage; LUS, lung ultrasound score upon neonatal ICU admission; MAS, neonates with meconium aspiration syndrome; NICU, neonatal ICU; NLD, neonates with no lung disease; OI, oxygenation index upon NICU admission; SGA, small for gestational age; SNAPPE-II, Score for Neonatal Acute Physiology with Perinatal extension II. Data are expressed as mean (SD) or count (percent).

Surfactant lipid-protein profile and $sPLA_2$ levels

As a first step, the lipid-protein content of surfactant along with the levels of $sPLA_2$ enzymes, which may influence the degradation of surfactant membranes were assayed. When the amount of lipids was tested by lipidomic analysis, lipid classes and subclasses were all detectable in MAS and NLD samples. In detail, to avoid misinterpretations of results due to errors in the starting PC amount, data were expressed as percentage with respect to the total moles of lipids instead of absolute values.

No differences were observed among the two cohorts of patients when lipid classes were taken into account (**Table 5**). Interestingly, when the percentage of lipid subclasses within each lipid class was considered, several significant differences emerged (**Table 6** and **Figure 19**).

DPPC (PC 32:0) did not vary, but an increase in free cholesterol and the disappearance of cholesterol esters were observed (**Figure 19A**). Two polyunsaturated PC (PuPC) species (**Figure 19B**) containing arachidonic acid were increased (PC 36:4 and PC 38:4), together with 32:1 PG, PI and PE levels (**Figure 19C**). At the same time, several other phospholipid species

decreased (**Figure 19D**): palmitoyloleoylphosphatidylcholine, (POPC (PC 34:1)), PC 32:2, PC 34:2, phosphatidylcholine plasmalogen (plPC) 34:0, and DOPG (PG 36:2).

Lipid	MAS group (n=14)	NLD group (n=18)	P value
PC (molar %)	93.3 [89.9-94.5]	91.5 [89.8-93.1]	0.133
plPC (molar %)	3.2 [2.7-3.9]	3.3 [2.4-3.6]	0.447
PG (molar %)	1.2 [0.7-2.3]	1.8 [1.3-3.2]	0.898
PI (molar %)	1.5 [1.1-2.5]	1.9 [1.2-2.0]	0.596
PE (molar %)	0.6 [0.4-0.9]	0.5 [0.3-0.9]	0.268
t-CHOL (molar %)	1.1 [0.4-1.6]	1.3 [0.7-1.6]	0.810

Table 5. Profile of main lipid classes for the two patients' cohorts. The content in lipid classes has been analysed by LC-HRMS and indicated as molar percentage (%) with respect to total lipids. Data are expressed as medians and interquartile range. Abbreviations: LC-HRMS, liquid chromatography-high resolution mass spectrometry; MAS, meconium aspiration syndrome neonates; NLD, no lung disease neonates; PC, phosphatidylcholine; PE, phosphatidylethanolamine; PG, phosphatidylglycerol; PI, phosphatidylinositol; plPC, phosphatidylcholine plasmalogen; t-CHOL, total cholesterol.

Lipid	MAS group (n=14)	NLD group (n=18)	P value
PC 32:0, DPPC (molar % PC)	42 [41.7-43.8]	41.9 [39.1-42.9]	0.101
free CHOL (molar % total chol)	20.7 [17.9-22.5]	11.1 [3.4-19.9]	0.027
CHOL esters (molar % total lipids)	0.009 [0.003-0.013]	1.1 [0.7-1.4]	<0.001
PC 36:4 (molar % PC)	4.7 [4.5-5.3]	3.2 [2.5-3.9]	0.004
PC 38:4 (molar % PC)	2.7 [2.1-3.2]	1.9 [1.5-2.2]	0.03
PG 32:1 (molar % PG)	13.4 [12.2-16.5]	7.9 [5.0-9.9]	0.03
PI 32:1 (molar % PI)	7.6 [6.2-11.5]	4.6 [3.7-6-4]	0.03
PE 32:1 (molar % PE)	3.2 [2.1-4.6]	1.8 [0.4-2.7]	0.005
PC 34:1, POPC, (molar % PC)	8.2 [7.9-8.7]	10.6 [8.9-11.9]	0.004
PC 32:2 (molar % PC)	1.2 [0.7-1.6]	2.4 [1.3-3.5]	0.045
PC 34:2 (molar % PC)	5.9 [5.5-6.2]	9.0 [6.8-9.8]	0.001
plPC 34:0 (molar % plPC)	6.4 [5.1-7.2]	8.2 [7.0-9.0]	0.009
PG 36:2 (molar % PG)	12.4 [2.0-16.4]	15.3 [7.0-25.1]	0.003
LPC 16:0 (molar % substrates)	2.0 [1.9-2.5]	1.4 [1.2-2.1]	0.04
LPC 18:0 (molar % substrates)	1.6 [1.3-1.9]	1.0 [0.9-1.2]	0.004

Table 6. Lipid molecular species significantly changing between the two cohorts of babies. The content for each lipid subtype is normalised with respect to the total lipids of that class and expressed as percentage (%). LPC 16:0 and 18:0 were normalised for the total amount of PC 34:1, PC 34:2 and plPC 34:0, which represent the substrates of $sPLA_2$ hydrolysis and expressed as percentage (%) of the substrates in the $sPLA_2$ reaction. Lipid subclasses that are significantly increased and reduced in MAS compared to NLD are shown in salmon and light blue, respectively. All lipid subclasses were analysed by LC-HRMS. Data are expressed as medians and interquartile range. Abbreviations: LPC, lysophosphatidylcholine.

Since the changes in lipid subclasses could be influenced by the presence of meconium in lungs of MAS patients, only lipids significantly increased in MAS samples were determined in the meconium collected from 7 MAS patients. As shown in **Table 7**, apart from free cholesterol, all other lipids were very low or undetectable in meconium.

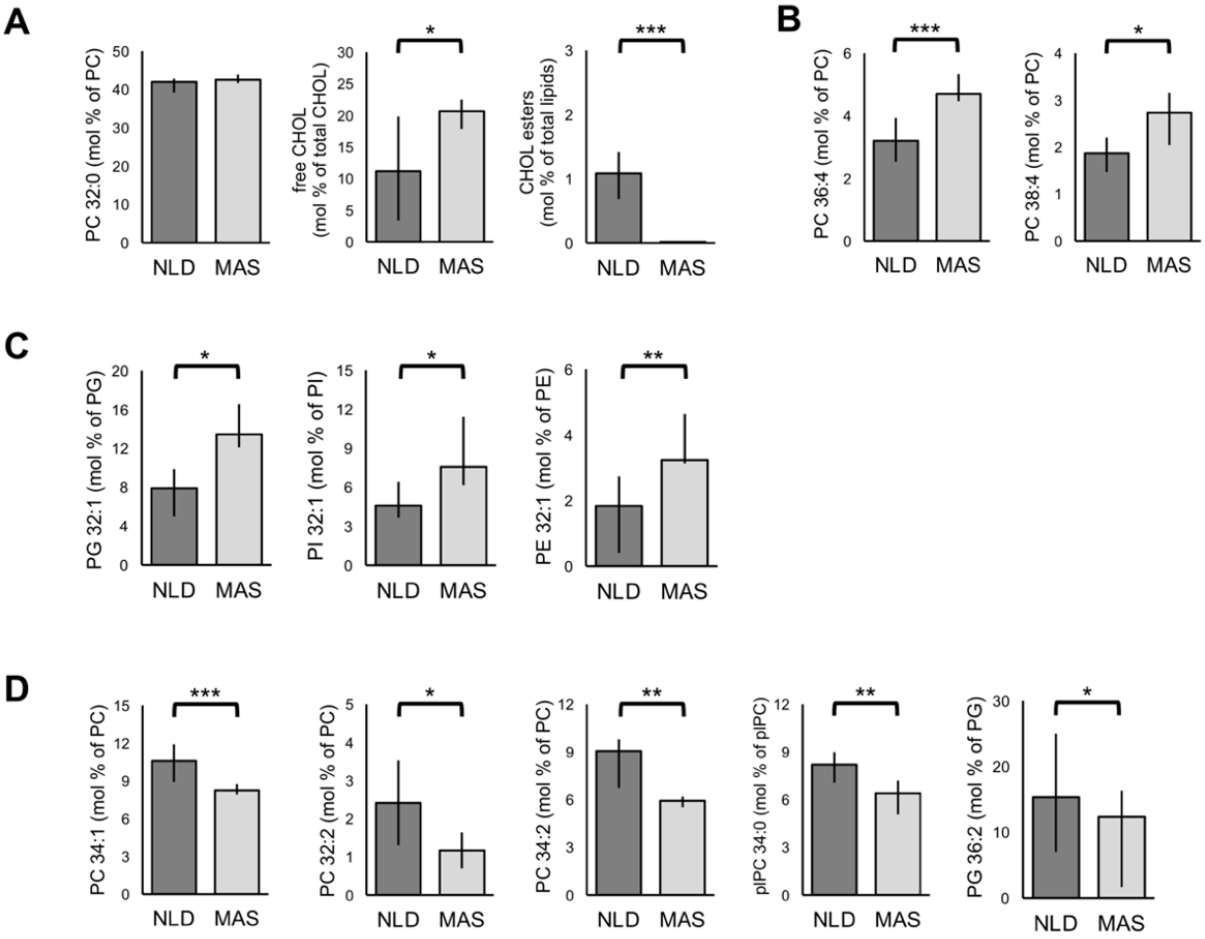

Figure 19. Lipid subclasses in the two cohorts of babies. The content of each lipid subtype is normalised to the total lipids of that class and expressed as a percentage. Lipid subclasses were analysed by LC-HRMS. **(A)** PC 32:0 (i.e., DPPC) content and changes in CHOL species. **(B)** Increment of polyunsaturated PC, probably containing arachidonic acid (20:4). **(C)** Increment of 32:1 anionic and zwitterionic species. **(D)** Reduction of levels of PC 34:1 (i.e., POPC), di-unsaturated PC 34:2 and 32:2, plPC 34:0, and PG 36:2 (i.e., DOPG). Bars represent medians; black lines represent interquartile ranges. Horizontal lines represent statistical comparisons. Mann-Whitney U test: *p< 0.05, **p< 0.01, and ***p< 0.005. Abbreviations as in **Table 5**.

When the levels of LPC species released by $sPLA_2$ hydrolysis of POPC, PC 34:2 and plPC 34:0 were analysed with respect to the substrates, a significant difference was detected (**Figure 20A** and **Table 6**).

Consistently, as shown in **Figure 20B**, $sPLA_2$-IB (NLD, 2.2 [0–9.7] ng/mg; MAS, 25.1 [3.2–47.8] ng/mg; p= 0.049) and $sPLA_2$-X (NLD, 0.03 [0.02–0.16] ng/mg; MAS, 0.22 [0.18–0.39] ng/mg; p= 0.004) were significantly increased in neonates with MAS. Simultaneously, there was a tendency to increase for $sPLA_2$-V (NLD, 2.04 [0.00–5.63] ng/mg; MAS, 9.42 [0.73–18.4] ng/mg, p= 0.16) that probably does not reach the significance due to the small number of samples tested (6 NLD and 4 MAS).

Lipid	meconium (n=7)
free CHOL (molar %)	58.9 [50.2 - 61.6]
PC 36:4 (molar %)	0.009 [0.004 - 0.035]
PC 38:4 (molar %)	0.009 [0.004 - 0.028]
PG 32:1 (molar %)	n.d.
PI 32:1 (molar %)	n.d.
PE 32:1 (molar %)	n.d.
LPC 16:0 (molar %)	0.17 [0.11 - 0.27]
LPC 18:0 (molar %)	0.043 [0.039 - 0.092]

Table 7. Profile of main lipid molecular species in meconium. Only lipids significantly increased in BAL samples of MAS neonates were determined. The content in lipid species were analysed by LCHRMS, after organic extraction and indicated as molar percentage (%) of total lipids in meconium (mainly ceramides, dihydroceramides, sphingomyelin, dihydrosphingomyelin, hexosylceramide, ceramide dihexoside, PC, triacylglycerol and cholesterol). Data are expressed as medians and interquartile ranges. PG, PI and PE are undetectable. Abbreviations: n.d., not detectable: for others see **Table 5**.

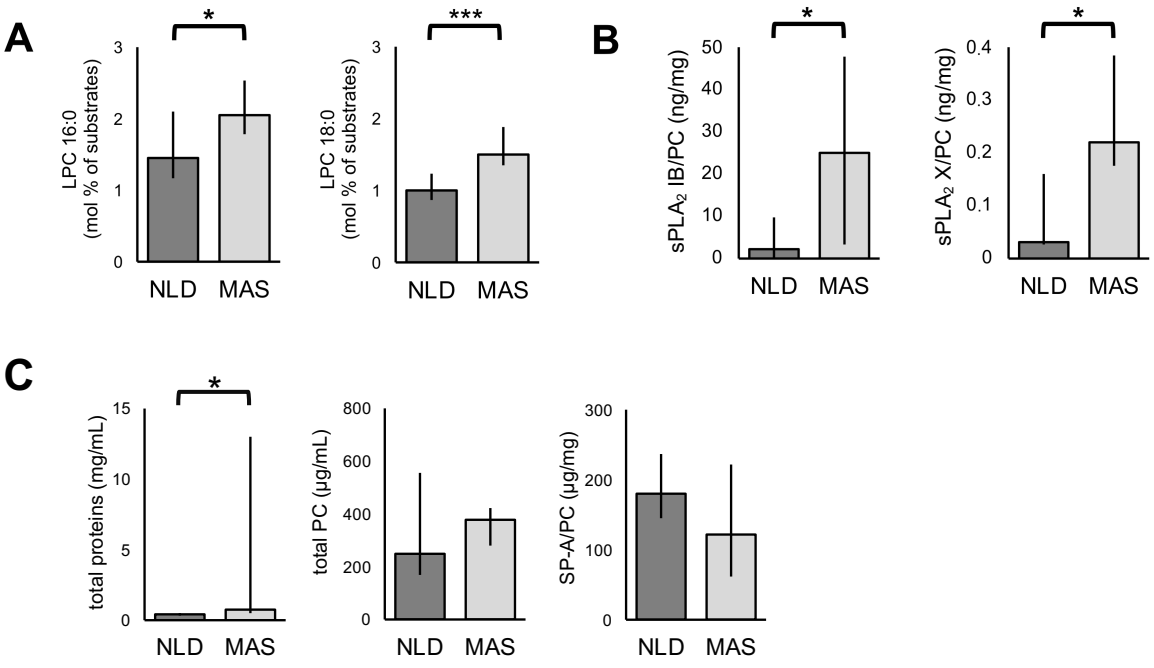

Figure 20. LPC, sPLA$_2$ and SP-A levels. (A) Amount of LPC 16:0 and 18:0 and the concentrations of sPLA$_2$-IB and -X **(B)**, normalised with respect to PC content. **(C)** Levels of total proteins and PC along with the concentration of SP-A, normalised for PC content. Bars represent medians; black lines represent interquartile ranges. Horizontal lines represent statistical comparisons**.** Mann-Whitney U test: *p< 0.05 and ***p< 0.005. Abbreviations: PC, phosphatidylcholine.

Total protein levels significantly increased in MAS, as described previously (De Luca *et al.*, 2011) (NLD, 0.45 [0.3-0.53] mg/mL; MAS, 0.74 [0.54-13.49] mg/mL; p= 0.028, **Figure 20C**). Conversely, no differences were observed for total PC amount (**Figure 20C**, **Table 5**). The level of the three surfactant proteins involved in the biophysical activity of lung surfactant (SP-A, SP-B and SP-C) were also calculated, normalising data to PC (SP-A, **Figure 20C**) or loading the same amount of PC per sample in PAGE (SP-B/C, **Figure 21**).

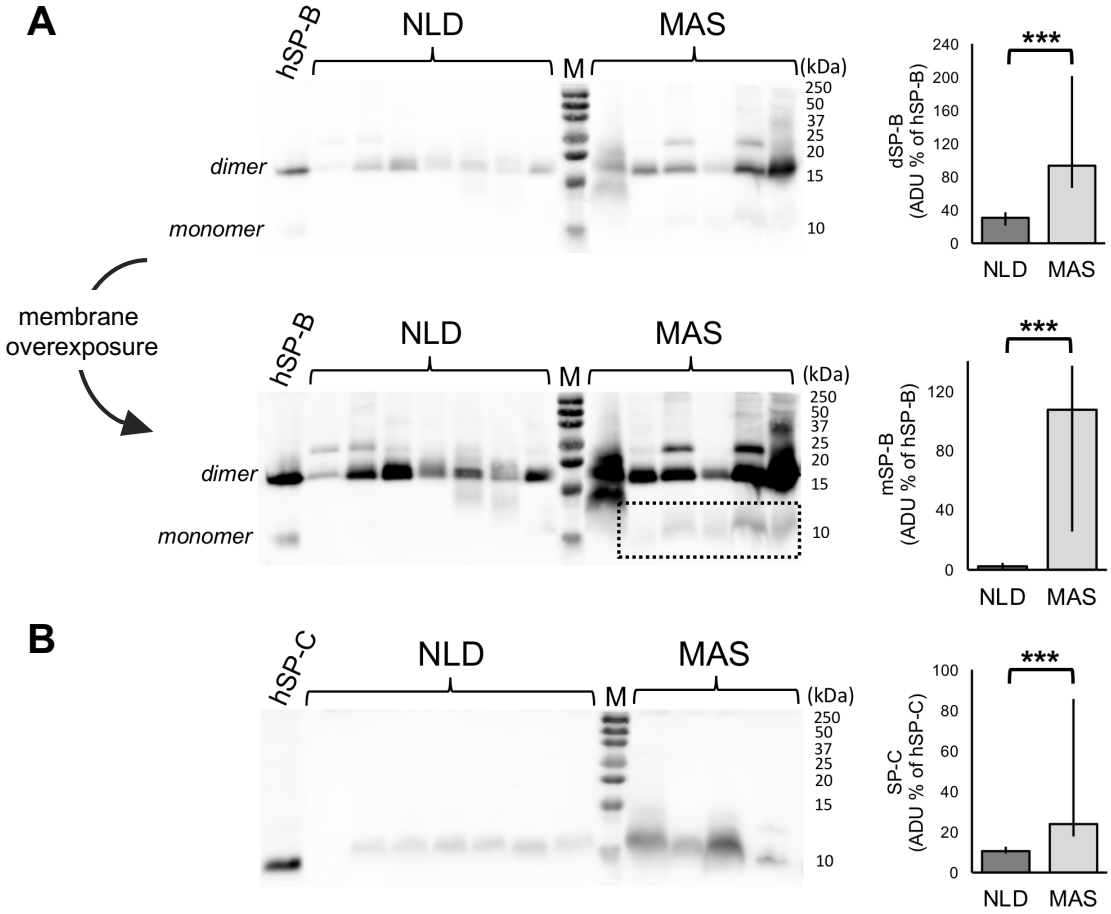

Figure 21. Levels of hydrophobic surfactant proteins. Western blotting of hydrophobic surfactant protein SP-B **(A)** and SP-C **(B)** under non-reducing conditions. One illustrative membrane, comparing samples from 13 patients is shown. A quantity of 4 μg of PC for each sample was loaded into the gel, and 50 ng of isolated human SP-B and SP-C were used as internal controls. Higher concentrations of dimeric SP-B and SP-C were found in neonates with MAS than in neonates with NLD. After membrane overexposure **(A)**, monomeric SP-B is present only in MAS (hatched frame, second row). Bars represent medians; black lines represent interquartile ranges. Horizontal lines represent statistical comparisons**.** Mann-Whitney U test: ***p< 0.005. Abbreviations: ADU, arbitrary densitometry units; dSP-B, dimeric surfactant protein B; hSP-B, purified human surfactant protein B; hSP-C, purified human surfactant protein C; M, protein molecular weight marker; mSP-B, monomeric surfactant protein B.

As shown in **Figure 20C**, no significant differences among the two cohorts were detected with respect to SP-A levels, although a tendency to decrease was revealed. Conversely, a significant increase in both mature SP-B and SP-C amounts in large aggregates of PS of neonates with MAS (**Figure 21**) was detected. In this line, both the dimeric (~16 kDa) and the monomeric (~8 kDa) forms of mature SP-B were observed in nBALs of patients with MAS and in the protein of reference (obtained from a PAP patient) even under non-reducing conditions. As expected, the apparent molecular masses of the two surfactant proteins, especially for the highly hydrophobic SP-C, are generally higher in neonatal samples than in purified human surfactant as a consequence of reduced electrophoretic mobility in the presence of lipids.

When overexposing the blotting membrane, the presence of monomeric SP-B was also more evident, remaining absent in neonates with NLD. Since the appearance of a monomeric form could be related to the increased amount of SP-B/PC in nBALs of MAS patients, 13 μg

instead of 4 μg of PC from large aggregates of 2 NLD babies were loaded into the gel (**Figure 22A**). Moreover, to investigate the mass of those forms as well as the possible appearance of several less hydrophobic SP-B precursors, a volume of nBALs corresponding to 11 μg of PC was lyophilised to keep the hydrophilic proteins in the samples and loaded into the gel (**Figure 22B**). In this way, the presence of hydrophobic mature SP-B forms (mainly present in surfactant large aggregates) and the more hydrophilic SP-B precursors (soluble in nBAL supernatants) were simultaneously analysed under reducing conditions. In spite of loading a higher amount of PC from nBAL of NLD neonates, no monomeric SP-B bands were detected, suggesting that the presence of such forms are strictly associated to the lung inflammation-mediated milieu of MAS patients.

Under reducing conditions, an increase of SP-B in patients with MAS was confirmed and bands with lower electrophoretic mobility were also observed (**Figure 22B**). These bands probably correspond to different forms of the last steps of pro-SP-B maturation whose expected theoretical masses (9-12 kDa) are distorted by the presence of lipids. However, it is important to underline that those SP-B forms could also result from an incomplete reduction of dimers. Nonetheless, as highlighted by the arrows, it is striking that several bands with different masses are present in the same sample electrophoretic run. This probably indicate that these more hydrophilic SP-B forms are physiologically enclosed into lamellar bodies of AT-II cells and released into nBALs after MAS-induced epithelial injury.

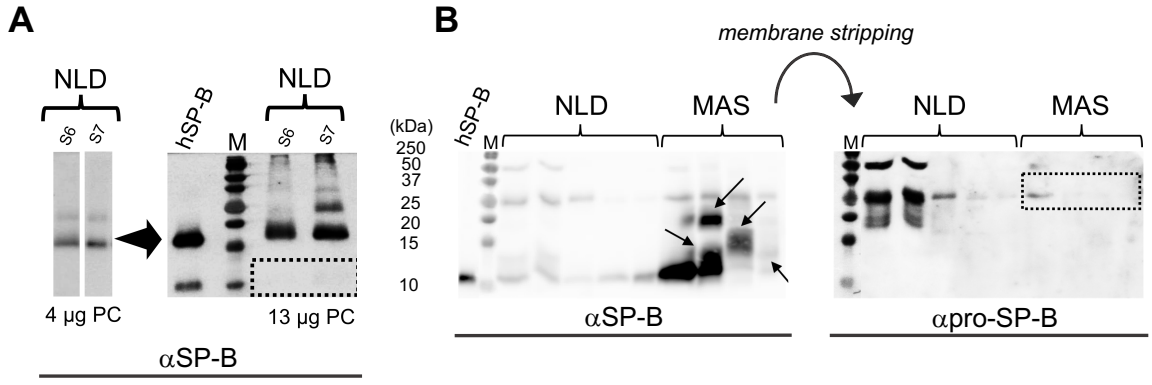

Figure 22. Western blotting of SP-B films. (A) Comparison between western blotting under non-reducing conditions of the same two NLD neonates, but loading increasing amount of PC. No bands corresponding to monomeric SP-B appeared (in the area marked by the black dotted line rectangle). **(B)** On the left, higher levels of monomeric SP-B and several bands with higher molecular mass together with mature SP-B are visible in MAS neonates (black arrows) under reducing conditions. On the right, after membrane stripping, pro-SP-B bands are revealed in both NLD and MAS neonates, although reduced levels of the precursor are detectable in MAS neonates (black dotted line rectangle). Abbreviations: hSP-B, human surfactant protein B; αSP-B, anti SP-B antibody; αpro-SP-B, anti pro-SP-B antibody.

After membrane stripping with guanidine thiocyanate and using a polyclonal anti-pro-SP-B antibody, only bands of 20-25 kDa or higher mass were detected. In this regard, SP-B precursors were more evident in NLD babies compared to MAS patients, confirming the higher amount of mature SP-B and/or almost mature SP-B forms after meconium injury.

Since the presence of monomeric SP-B could be related to the particular redox context in MAS samples, an additional experiment was carried out. A stripping of the membrane corresponding to the PAGE analysed under non-reducing conditions was performed. Subsequently, a polyclonal anti-SP-A antibody was used to investigate the presence of

monomeric SP-A isoforms (~26/38 KDa) and increased dimeric forms of ~60 kDa in MAS samples. As shown in **Figure 23**, together with monomeric SP-B, the presence of the 2 monomeric SP-A isoforms could be detected along with higher levels of SP-A dimers with respect to trimers in some nBALs from MAS patients.

Starting from these intriguing results, it is tempting to speculate that the redox milieu upon meconium injury could be related to a defence mechanism against ROS production. GSH is an antioxidant tripeptide (cysteine, glycine, glutamate) that together with GSH peroxidase counteracts the effects of ROS in mitochondria and nucleus (Green *et al*, 2006). However, upon the MAS-induced inflammation-related epithelial injury and the $sPLA_2$-mediated arachidonic acids production, increased levels of intracellular GSH could be released and detected in nBALs.

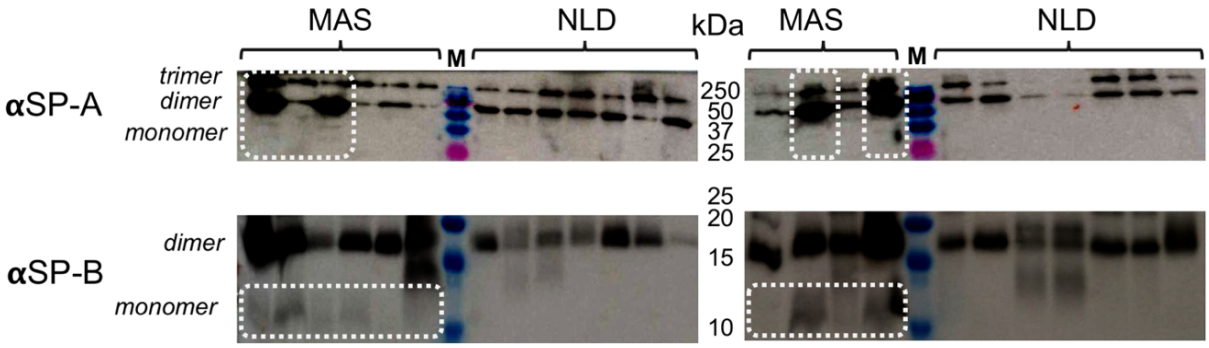

Figure 23. Western blotting of SP-A and SP-B. The two membranes obtained from non-reducing PAGE were stripped (guanidine thiocyanate) and incubated with a polyclonal anti-SP-A antibody. After membrane overexposure, together with monomeric SP-B, the 2 monomeric isoforms of SP-A and an increased amount of SP-A dimeric forms are visible in several nBALs from MAS patients (white dotted line rectangle). Abbreviations: αSP-A, anti SP-A antibody; αSP-B, anti SP-B antibody.

In this line, an increased level of GSH was already demonstrated in lung lavages of smokers and COPD patients (Drost *et al*, 2005). Once in the alveolar space, GSH might reduce the intermolecular disulphide bonds of accessible proteins (GSH cannot cross lipid membranes) such as soluble SP-A dimers and trimers, or the dimers contained within SP-B rings involved in the contact between different surfactant membranes. This may further contribute to the inactivation of the system, influencing its biophysical activity and recycling during MAS. To confirm this hypothesis, the amount of GSH and GSSG in nBALs of MAS and NLD babies (n= 6) as well as in nBAL of the proteinosis patient (n= 1) were tested (**Figure 24A**). Unlike NLD babies, there was an increase in GSSG levels compared to GSH amount in both MAS neonates and in the proteinosis patient. In detail, there was a significant decrease in GSH after meconium aspiration compared to NLD group with a simultaneous significant rise in its oxidised form (**Figure 24A**).

The capability of GSH to reduce the sulfide bonds of SP-B in the presence of lipids was confirmed *in vitro*, adding an increasing percentage amount of the reducing agent (0.0025, 0.065, 0.125, 0.25, 0.5, 1.25, 2.5, 5, 10, 20, 25 and 50% with respect to SP-B amount by weight) to PC/PG membranes containing 1% by weight of purified porcine SP-B (**Figure 24B**). Porcine SP-B was used rather than the PAP human protein since the latter also presents a monomeric form, observable under non-reducing condition (h-SP-B, **Figure 21**).

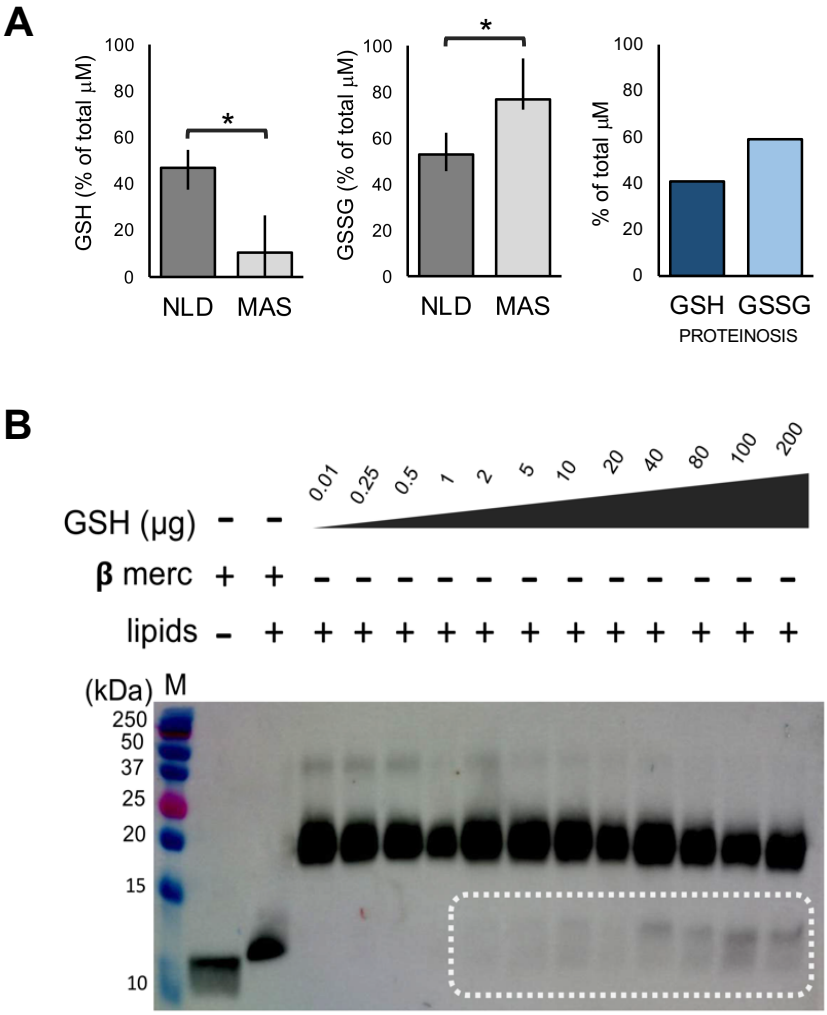

Figure 24. GSH/GSSG levels in MAS and NLD neonates and GSH effect on purified porcine SP-B. (A) GSH and GSSG contents were measured in NLD (n=6), MAS (n=6) and proteinosis (n=1) patients and expressed as percentage of total glutathione. **(B)** The reducing activity of GSH was tested at increasing percentage of the tripeptide with respect to SP-B by weight. The monomeric form of the protein after incubation with β-mercaptoethanol was used as internal control in presence or absence of lipids. Mann-Whitney U test: *p< 0.05. Abbreviations: GSH, reduced gluthatione; β merc, β-mercaptoethanol.

Interestingly, 2% of GSH is already able to generate a reduced form of the protein (monomeric SP-B of ~8 kDa) as indicated in the area of the gel within the white dotted line rectangle. At the same time, it is necessary 20% of GSH for tetrameric SP-B (~36 kDa) to disappear and 40% of the reducing agent to observe a clear decrease in the dimeric form (~16 kDa). Thus, the reducing action of GSH on surfactant proteins upon MAS was confirmed. The release of GSH to the alveolar spaces after meconium injury may probably reduce the oligomeric forms of surfactant protein SP-B and SP-A.

Surfactant nanostructure

Considering that the amount of surfactant proteins as well as the lipid composition of surfactant complexes (with both defying the structure and the biophysical activity of surfactant) are altered in babies with MAS, the nanostructure of large aggregates from 13 neonates, 7 with NLD and 6 with MAS, was investigated by Cryo-EM. Samples were prepared, using the same PC concentration (around 10 mg/mL) to avoid misinterpretations due to differences in membranes dilution. In **Figure 25A** and **B**, a representative image from each NLD and MAS sample is shown.

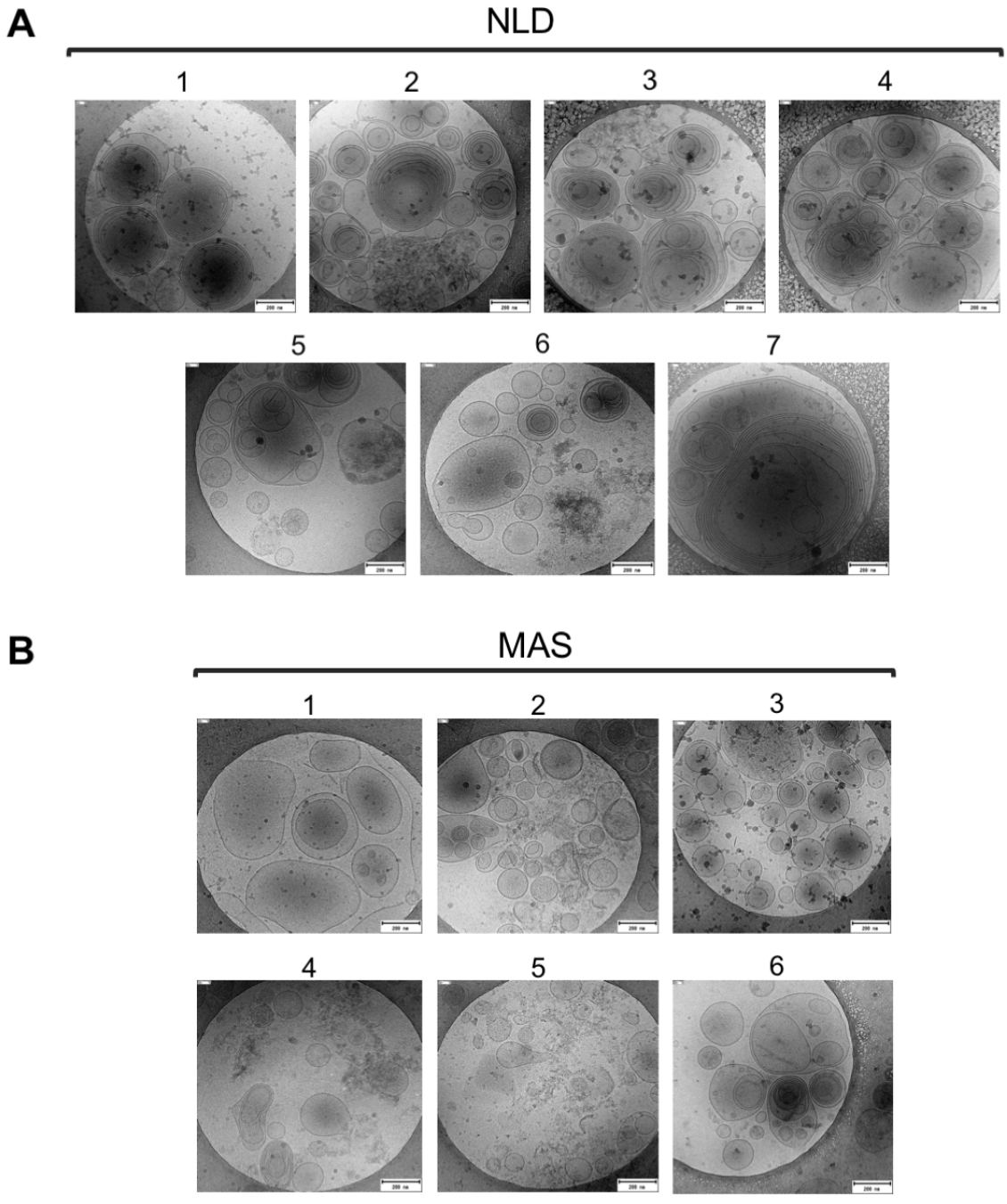

Figure 25. Cryo-EM of surfactant large aggregates of NLD (n=7) and MAS (n=6) neonates. One out of four images used for the analysis per NLD **(A)** and MAS **(B)** neonate is shown.

At the same time, data from 4 images per sample were analysed to define the size and the complexity of large aggregates. Results are summarised in **Figure 26**.

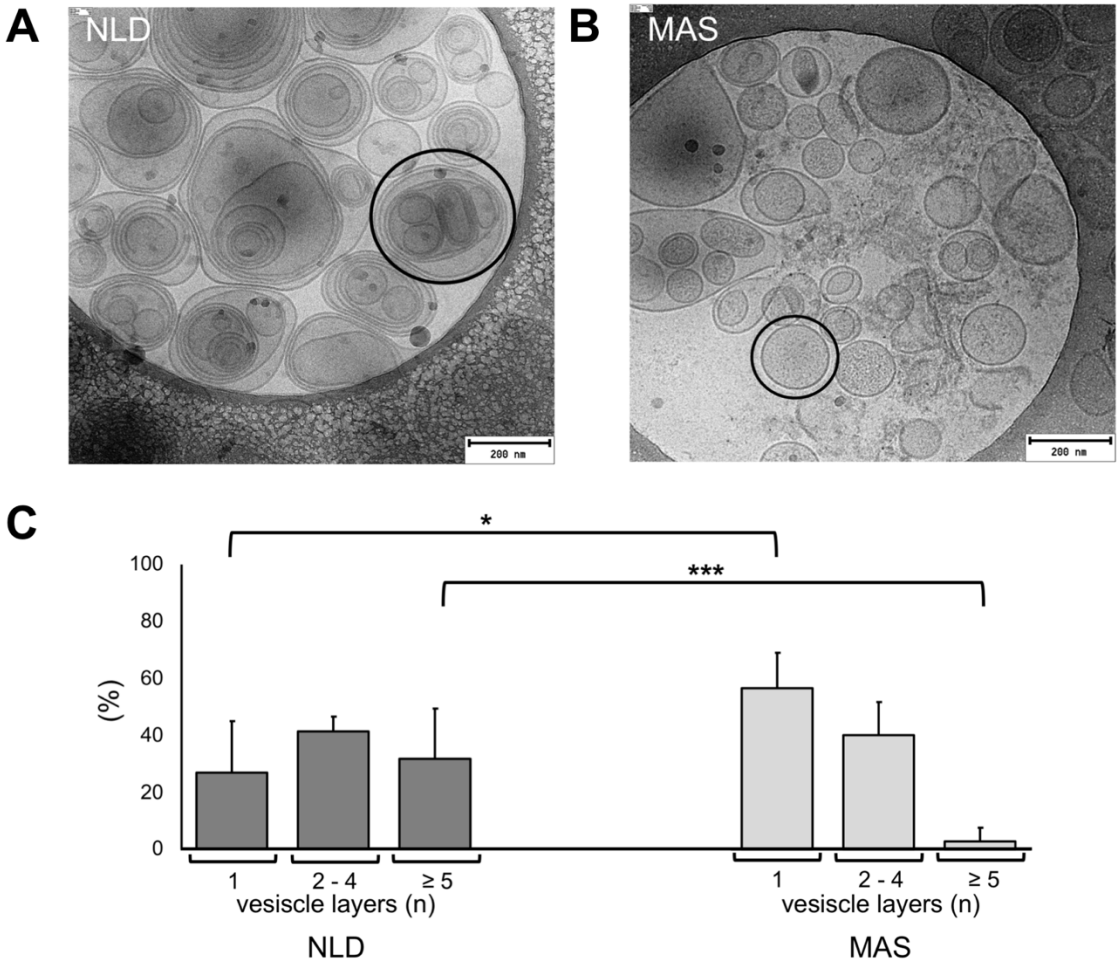

Figure 26. Surfactant nanostructure in NLD and MAS neonates as studied by cryo-EM. (A and B) Cryo-EM was performed with surfactant from seven neonates with NLD and six neonates with MAS. Two illustrative images of surfactant from one neonate with NLD (A) and one neonate with MAS (B) are shown. Black circles indicate representative surfactant assemblies that appear smaller and have a structure with fewer layers in patients with MAS. Scale bars, 200 nm. **(C)** The mean layer count (averaged from four distinct images in each of the seven NLD and six MAS samples) is shown; columns and T-bars represent mean and SD, respectively. *p = 0.006 and ***p = 0.003.

Surfactant structure upon MAS appeared considerably damaged and characterised by:

(1) vesicles with smaller size in neonates with MAS [mean (SD), 187 (123)] nm than in neonates with NLD [249 (162)] nm, p< 0.0001;

(2) less complex appearance (at the same PC amount) with fewer vesicles having a multilayer structure in neonates with MAS [2.9 (4.9)%] than in neonates with NLD [31.7 (17.8)%], p= 0.003;

(3) more vesicles with only a single layer in infants with MAS [56.8 (12.5)%] than in infants with NLD [27 (18.1)%], p= 0.006.

Changes in surfactant composition and structure are related to reduced surfactant activity and lung aeration in neonates with meconial ARDS

The impaired lipid-protein composition and the less complex membrane structure of surfactant from MAS could be also related with altered biophysical properties.

When nBALs were used to test surfactant adsorption and accumulation at the interface overtime by modified SAT, the samples from neonates with MAS showed a significant reduction in surfactant activity similar to that of PS incubated with the amount of meconium necessary to double PS cholesterol (**Figure 27A**). This was performed to reproduce *in vitro* the increase in free sterol observed in MAS patients *in vivo* (**Figure 19A**).

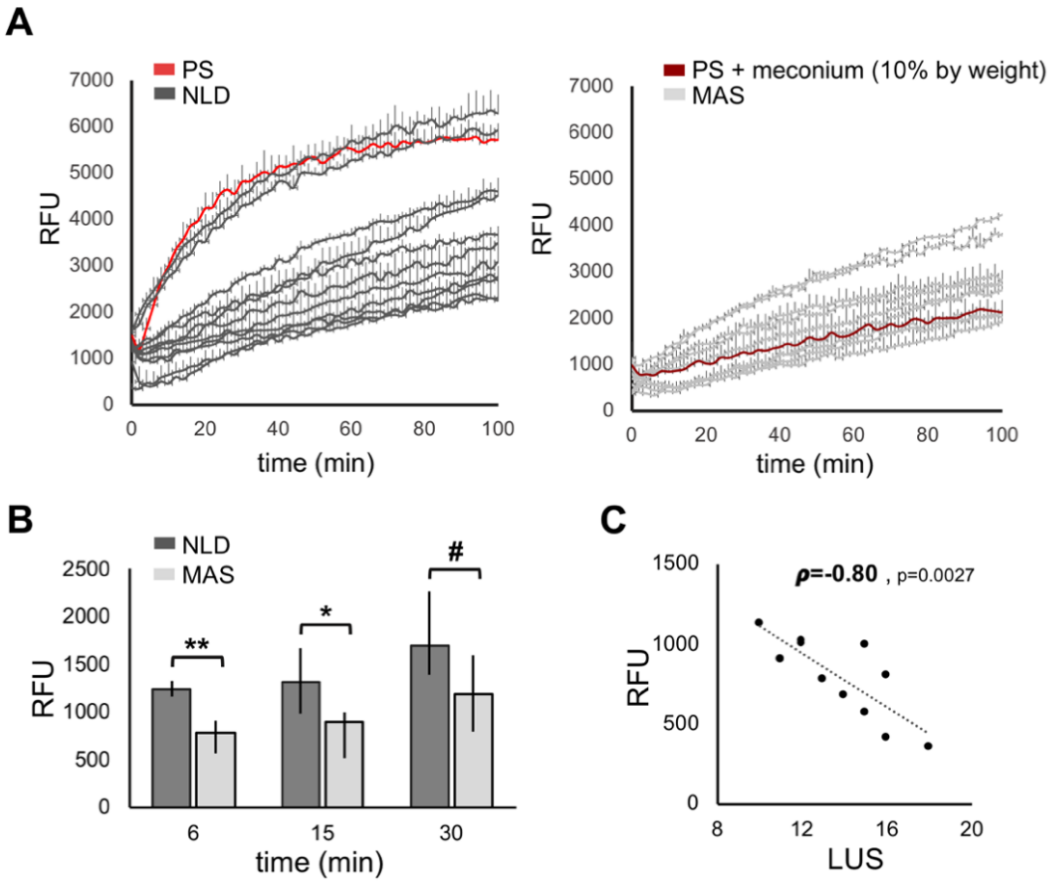

Figure 27. Surfactant adsorption and lung aeration. (A) Surfactant adsorption and accumulation curves of all samples from NLD babies (on the left) and MAS neonates (on the right). PS tested before and after *in vitro* meconium exposition is also shown in light and dark red, respectively. **(B)** Surfactant adsorption over time read at 6 minutes, 15 minutes, and 30 minutes of fluorescence. Bars represent medians. Black lines represent interquartile ranges. Horizontal lines represent statistical comparisons. **(C)** Relationships between surfactant adsorption (read at 6 min of fluorescence) and ultrasound-assessed lung aeration in neonates with MAS. Surfactant adsorption is expressed as RFU; aeration is semi-quantitatively expressed as dimensionless LUS. Mann-Whitney U test: *p< 0.05, **p< 0.01, and #p= 0.05. Hatched correlation line is shown together with correlation coefficient. Abbreviations: LUS, lung ultrasound score; RFU, relative fluorescence units; PS, purified porcine surfactant.

The observed meconium-induced inhibition of surfactant activity confirms the previous results obtained by testing PS and its organic extract in SAT (Lopez-Rodriguez *et al.*, 2011). At the same time, surfactant from NLD babies showed a relatively good adsorption that resembles the PS trend for the majority of samples (6 min, NLD, 1,242 [1,167–1,326] RFU; MAS, 786 [575–908] RFU; 15 min, NLD, 1,324 [988–1,672] RFU; MAS, 905 [520–1,006] RFU; 30 min, NLD, 1,700 [1,388–2,264] RFU; MAS, 1,187 [795–1,592] RFU) (**Figure 27A-B**). In detail, if a cut-off of 2500 RFU was considered, the last points of the adsorption kinetics curves (100 min) fell above that threshold for the majority of NLD samples. Conversely, this occurred in only three out of eleven nBALs from MAS neonates. Moreover, taking the trend of the curve into account, the plateau was only reached for surfactant of several NLD babies.

Interestingly, there was a highly significant inverse correlation between early surfactant adsorption (6 min) and ultrasound assessed lung aeration of neonates with MAS (ρ= -0.80; p= 0.0027) (**Figure 27C**). Consistently, the LUS and the oxygenation index were significantly higher in neonates with MAS than in neonates with NLD (**Table 4**). A correlation analysis was performed between the adsorption at 6 minute and the quantitative values available for surfactant components known to be important for surfactant adsorption (**Figure 28**). In this regard, there were significant correlations between early adsorption and the levels of SP-A (ρ= 0.52; p= 0.0075), or the amount of PC 34:1 (POPC) (ρ= 0.73; p<0.0001), and an inverse correlation of adsorption and the presence of $sPLA_2$-IB (ρ= 20.74; p= 0.0097).

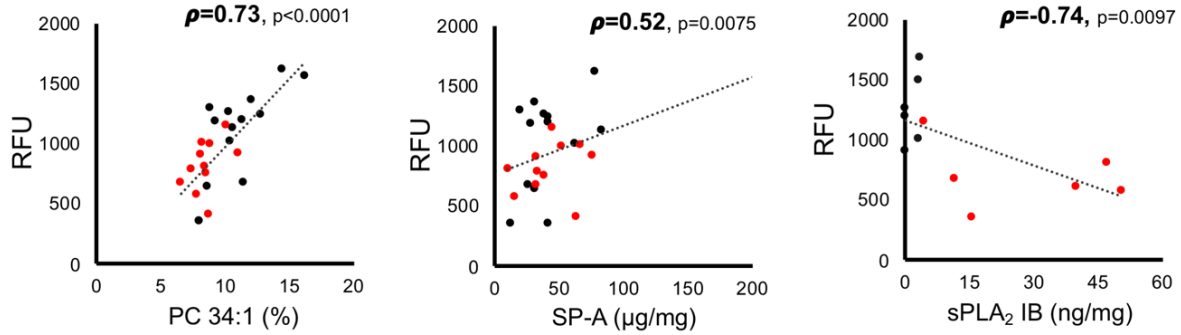

Figure 28. Relationships between surfactant adsorption (fluorescence read at 6 minute) and A) SP-A/PC, B) PC 34:1 (POPC) and C) $sPLA_2$-IB. SP-A (n=25) is expressed as µg per mg of PC, POPC (n=25) is expressed as molar % of total PC by LC-HRMS analysis, $sPLA_2$-IB (n=12) is expressed as ng per mg of PC. Red and black points represent MAS and NLD patients, respectively. Hatched correlation lines are shown together with correlation coefficients.

Although promising, modified SAT data provides only information about the capability of lung surfactant to adsorb and accumulate at the air-liquid interface without testing the dynamic properties of the system once subjected to breathing-like dynamics. Fluidification of material (e.g. due to the presence of high cholesterol levels) may affect the drastic reduction in surface tension under compression without influencing surfactant initial adsorption. On this basis, to investigate in detail how the spreading and dynamic properties of lung surfactant are altered after meconium aspiration, a complete biophysical study was performed by CBS. These functional experiments were carried out using large aggregates at 12 mg/mL of 5 selected samples (two neonates with NLD and three babies with MAS). At the same time, PS at 10 mg/mL with and without meconium (10% by weight) was tested as control for optimal biophysical activity or meconium-induced inhibition.

As shown in **Figure 29A**, once spread at the air-liquid interface of the bubble, PS was able to reduce the surface tension of buffer (~70 mN/m) to values around 20 mN/m in 1-5 seconds. At the same time, this equilibrium surface tension was maintained at 20 mN/m from the beginning of bubble post-expansion. Moreover, during four slow compression-expansion quasi-static cycles and ten breathing-like dynamic cycles, the material was able to drastically reduce surface tension to ~1 mN/m upon compression, maintaining values of ~30 mN/m during each expansion. This confirms the optimal re-adsorption properties of PS to stably maintain highly surface active films.

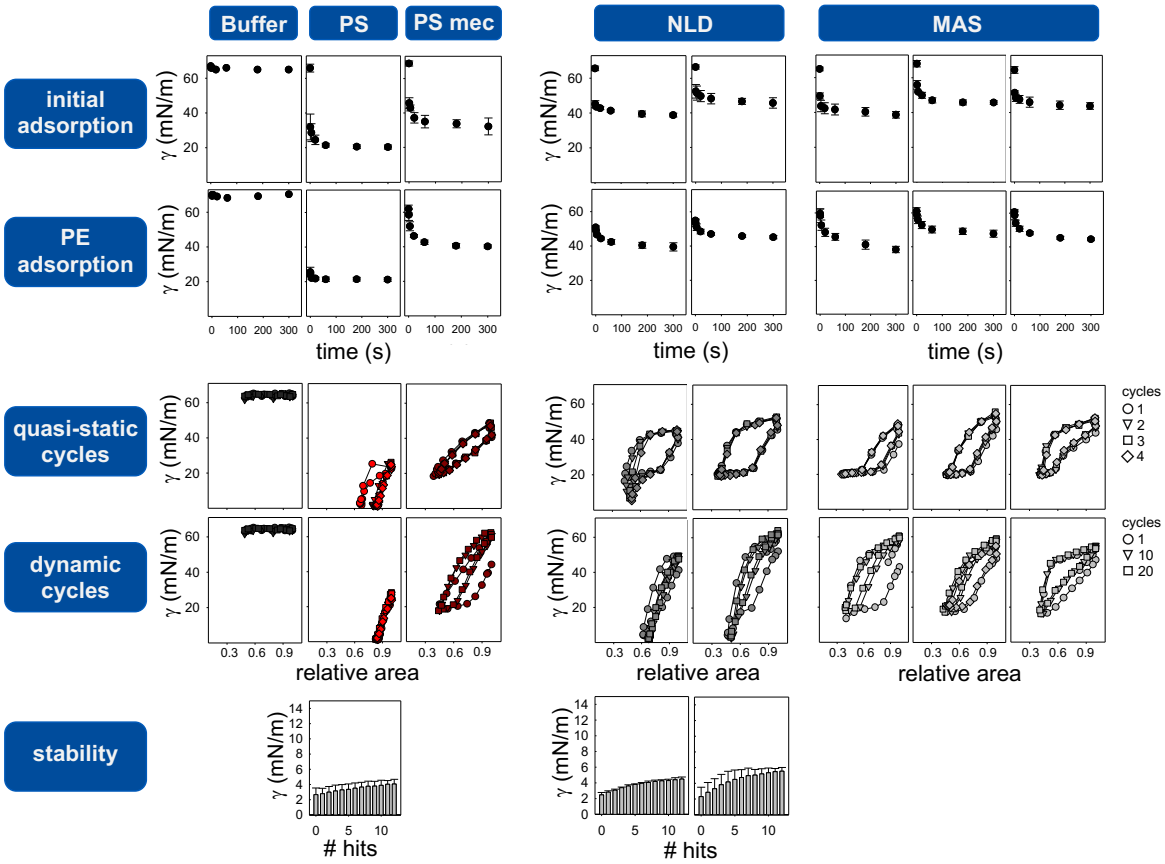

Figure 29. Analysis by CBS of the performance of PS exposed to meconium or obtained from NLD or MAS neonates. (A) Initial and PE adsorption and, quasi-static and breathing-like dynamics of PS with and without meconium (10% w/w). **(B)** Surface activity in the CBS of surfactants from NLD and MAS neonates. Mean and SD of three replicates are shown for initial and PE adsorption. A representative isotherm is shown for the 4 quasi-static and the first, 10th and 20th dynamic cycles. Mean and SD of surface tensions in the stability experiments is also depicted as a grey-bar histogram. This was performed, discharging the indicated number of hits with a pendulum hammer onto the bubble. PS with and without meconium is shown in light and dark red, respectively. Surfactant from NLD and MAS neonates are represented in dark and light grey, respectively. Buffer alone is used as negative control and shown in black. Abbreviations: γ, surface tension; PE, post expansion; PS, purified porcine surfactant; PS mec, purified porcine surfactant incubated with meconium.

Hysteresis defines the difference in the rate of surface tension variation between the compression and the expansion of the interfacial area. Thus, this parameter measures indirectly the work associated with the reorganisation of surfactant at the air-liquid interface upon cycling. On this basis, it can be calculated as the enclosed area between the compression and expansion segments of the isotherms. As emerges in **Figure 29A**, PS only showed hysteresis in the first slow cycle which required a 40% reduction in surface area to

reach the minimum surface tension. In this line, materials working properly can quickly decrease surface tension with a minimum reduction of bubble interfacial area. The increased hysteresis and larger relative area of compression for PS are due to the reorganisation of material upon the first compression cycle. Indeed, highly surface-active components are maintained at the bubble surface, while most lipids with lower interfacial properties are excluded and not more re-adsorbed. This mechanism is mainly mediated by proteins SP-B and SP-C and leads to minimal hysteresis and reduced area variation in the following slow and dynamic cycles. Finally, PS stability, namely its capability to sustain low surface tensions upon subsequent mechanical perturbations, was also high.

Conversely, the presence of meconium affected both the spreading and post-expansion adsorption of PS, which only reached surface tensions of 30 and 40 mN/m, respectively, after 5 minutes from the spreading of material. At the same time, the dynamic properties were also inhibited since PS exposed to meconium was still not able to reduce surface tensions to values lower than 18 mN/m both upon slow and quick cycles. Moreover, a moderate hysteresis and an area variation of ~60% were observed during each compression-expansion cycle. This suggests that meconium at this percentage of cholesterol (about twice of that of PS) is able to alter surfactant interfacial properties and its capability to exclude the less active material from the interface, even upon high compression rates of the surface bubble area. This result was expected since it is well known that the presence of high cholesterol amounts, well above the physiological proportion, fluidify excessively surfactant films. The latter lose their capability to tightly pack at the air-liquid interface under compression and to drastically reduce surface tension. Moreover, the insertion of meconial cholesterol into surfactant membranes seems to be facilitated, as observed *in vitro*, by the bile acids present in meconium (Lopez-Rodriguez *et al.*, 2011).

When moving from *in vitro* to *ex vivo* experiments (**Figure 29B**), we obtained similar, but not identical results when comparing surfactant from MAS patients with PS pre-exposed to meconium. Moreover, several differences were observed between PS and the control group (surfactant from NLD babies). In this line, both spreading and post-expansion adsorption were similar between NLD and MAS neonates and comparable to those of meconium-treated PS. This result may be explained by the different source of surfactant materials. Compared to PS, obtained from porcine excised lungs, nBAL likely collects surfactant components preferentially from the upper airways, with a lower content in surfactant hydrophobic proteins. Moreover, unlike PS, this material is not purified to remove blood and other non-surfactant components. These two differences are crucial for the resulting interfacial properties. Surfactant from MAS patients were not able to reduce surface tension upon the four quasi-static cycles, even after a surface area variation between 56 and 60% under compression (**Table 8**), and exhibited high maximum surface tensions under expansion (50-60 mN/m) and high hysteresis. Consistently, this trend was also evident upon dynamic cycles. The trend is similar in behaviour to that of meconium-treated PS, but the hysteresis area and shape were different (**Figure 29**). At the same time, during the slow compression-expansion cycles surfactant from NLD babies presented a higher hysteresis, although maintaining the same maximum surface tension compared to MAS neonates. This higher work to re-organise material at the air-liquid interface promoted a subsequent decrease in the minimum surface tension to values <2.2 mN/m upon dynamic cycles. This occurred with a reduction in hysteresis and surface area variation (42-53%, **Table 8**), but still maintaining high maximum surface tension values (50-65 mN/m).

On this basis, unlike PS, surfactant from NLD and MAS neonates showed a reduced capability to spread and re-adsorb, and exclude less surface-active lipids from the air-liquid interface upon quasi-static cycles. This is probably due to (1) the low content in SP-B and SP-C with respect to PC, when compared with PS, (2) the presence of less active-already used material in surfactant collected from the upper airways (nBAL) and (3) the slow reduction of interfacial area (0.5 cycle/min). However, in the case of surfactant isolated from NLD neonates, the rapid dynamic (20 cycles/min) seems to assist surfactant proteins to promote the exclusion of the less surface-active lipids during the first compression. These interfering materials have relatively poor surface properties and have no time to re-adsorb at the air liquid interface upon expansion.

The presence of a relatively normal SP-B profile (as shown in **Figure 21**) and a modest amount of cholesterol and PuPC (as shown in **Figure 19**) in NLD samples, probably leads to a more effective surfactant depuration (**Figure 29**) during compression and an optimal film stability, still maintaining 4-6 mN/m after 12 hits of the material. To confirm these results, the lipid composition and the interfacial dynamic properties of surfactant were compared in the samples from MAS and NLD neonates previously tested by CBS. With this purpose, changes in certain lipid species were compared to several biophysical parameters calculated from the 20th breathing-like dynamic cycle: hysteresis (J/m^2), relative area of compression (%), minimum surface tension and compressibility ($\Delta\Pi/\Delta A$). Compressibility measures the changes in relative volume of a substance under stress. Lipids able to highly pack at the interface, with areas rich in saturated species such as DPPC, being less deformable than those containing unsaturated lipids that occupy higher surface area. As a consequence, low compressibility indicates a tight packing of surfactant components at the interface, favouring a quick surface tension reduction upon compression. Compressibility can be indirectly calculated as the slope value of the line passing through the minimum and maximum points of compression (minimum and maximum areas of the bubble) in the dynamic cycling curve. The steeper the slope, the lower the compressibility of the surfactant film.

Lipid % and biophysical parameters	NLD		MAS		
DPPC/PC (%)	44.5	39.0	45.9	39.9	42.4
POPC/PC (%)	11.0	11.5	6.5	10.4	8.4
PuPC/PC (%)	1.2	3.5	5.6	8.9	10.9
POPC/DPPC (%)	25.0	29.8	14.2	26.1	19.7
PuPC/DPPC (%)	9.1	2.6	12.1	22.3	25.7
free CHOL (%)	8.2	8.3	20.6	17.8	20.8
γmin (mN/m)	1 .5 (1.2)	2.1 (0.5)	19.1 (1.3)	18.5 (0.5)	19.5 (1.4)
relative area (%)	52.3 (0.8)	41.7 (1.2)	55.8 (0.2)	58.7 (0.5)	59.8 (2.1)
hysteresis (J/m2)	10.5 (1.2)	7.1 (2.1)	10.4 (2.1)	11.6 (0.8)	14.7 (1.3)
compressibility ($\Delta\Pi/\Delta$A)	137 (2)	120 (4)	103 (5)	79 (3)	70 (5)

Table 8. Lipid composition and interfacial properties of surfactant films from NLD and MAS babies. The main surfactant lipid species analysed by LC-HRMS present in surfactants from the 5 neonates tested by CBS. The minimum surface tensions, relative area of compression, compression–expansion hysteresis, and compressibility of the first dynamic cycle are shown. As for biophysical parameters the mean and SD of three replicates are shown. Increased and reduced values among the two cohorts are highlighted in salmon and light blue, respectively. Abbreviations: γ, surface tension; Π, pression; A, area; PuPC, polyunsaturated phosphatidylcholine.

As shown in **Table 8**, the four biophysical parameters were compared with the levels of those lipid species that changed in MAS neonates with respect to DPPC: free cholesterol, POPC and PuPC (PC 36:4, PC 38:4). Interestingly, patients with MAS showed high levels of

PuPC/PC and PuPC/DPPC ratios as well as free cholesterol, with higher minimum surface tension, compressibility, relative area of compression and hysteresis compared to surfactant from NLD neonates (**Table 8**). Moreover, as for patients with MAS, PuPC/PC ratio was higher, and compressibility, relative area of compression and hysteresis tended to be proportionally greater as well.

Discussion

In this second chapter, the *in vivo* effect of meconium on the composition, structure and interfacial properties of lung surfactant was investigated in the early phase of MAS, soon after birth. In detail, the following interesting changes emerged: (1) the surfactant phospholipid profile is significantly altered, and, notably, LPC species presumably released by the $sPLA_2$ hydrolysis are increased; (2) the content of SP-B and SP-C is apparently increased; (3) reduced forms of SP-B and SP-A are visible due to GSH release upon epithelial injury; (4) as a consequence of the aforementioned alterations, surfactant nanostructure appears to be damaged; (5) these compositional and structural changes also drastically impair the biophysical properties of surfactant. Surfactant capability to adsorb and form surface-active films at the interface is substantially impaired and this correlates with lung aeration (i.e., with the estimated lung volume available for gas exchange); (6) surfactant capability to reduce surface tension under interfacial compression is also compromised. These results are novel since the subject has never been comprehensively investigated *in vivo*.

Meconium is known to inhibit surfactant biophysical activity *in vitro*, affecting the adsorption as well as the dynamic interfacial properties of PS and clinical surfactants tested by SAT, CBS or the Pulsating Sessile Drop (Lopez-Rodriguez *et al.*, 2011; Moses *et al.*, 1991; Sun *et al.*, 1993). It has been suggested that the main mechanism of inactivation is the fluidification of surfactant membranes mediated by meconial cholesterol. The latter intercalates into surfactant films, and bile acids in meconium seem to enhance this process (Lopez-Rodriguez *et al.*, 2011). However, there is a world of difference between the *in vitro* and *in vivo* conditions and, so far, it is unclear which lung surfactant modifications entail surfactant impairment and how surfactant lipids and proteins are affected in the early phase of severe MAS *in vivo*.

The lipid profile in early MAS is characterised by several peculiarities. Unexpectedly, 32:0 (DPPC) levels did not change much during MAS, but an increase in PuPC species and in DPPC/PuPC ratios arose. Moreover, as described for adult ARDS (Markart *et al*, 2007), we also observed high levels of free cholesterol at the expense of sterol esters (**Figure 19A** and **B**). These surfactant lipid modifications may be associated with a response to the oxidation caused by meconium-induced inflammation (Fessler & Summer, 2016) or by incorporation of free cholesterol present in meconium. On this basis, the increased amount of PuPC (PC 36:4, PC 38:4), probably containing the 20:4 fatty acid, could be related to an unbalance of the intracellular control of free arachidonic acid levels. This machinery is physiologically mediated by the simultaneous action of PLA_2 and lysophospholipid acyltransferases activity. Thus, the increased levels of arachidonic acid through $sPLA_2$ hydrolysis of injured plasma membranes during meconium-induced inflammation may promote the incorporation of 20:4 acyl chains in PC by Kennedy Pathway in AT-II cells (Pérez-Chacón *et al*, 2009). As a result, the amount of PuPC species in surfactant from MAS babies increases compared to NLD neonates. This may be a physiological response, being the double bonds of PC acyl chains a scavenger for ROS.

However, at the same time, high PuPC/DPPC ratios seem to affect surfactant dynamic interfacial properties as observed in CBS experiments (**Figure 29** and **Table 8**). Interestingly, similar results were recently obtained *in vitro*. The polyunsaturation of 1,2-dilinoleoyl-sn-glycero-3-phosphocholine (36:4, 18:2/18:2) compromises the interfacial behaviour of DPPC monolayers in a Langmuir Blodgett trough with a fluidification effect (Zhang *et al*, 2019). At high molar fractions, the presence of this compound completely abrogates the Lc-Le co-existence plateau of DPPC. Moreover, under high compression of the interface, the surface pressure of DPPC films decreases from 65 to 40 mN/m and the area per molecule increases from 30 to 50 $Å^2$.

In addition, patients with MAS had reduced PC 34:1 (POPC), plPC, and di-unsaturated PC, whereas corresponding LPC species increased. LPC is a product of $sPLA_2$ hydrolysis; thus, these results may be a consequence of the increased levels of these enzymes. Meconium is known to be rich in pancreatic $sPLA_2$ (i.e., $sPLA_2$-IB (Sippola *et al*, 2006)) but, once the insult commences in the lung, $sPLA_2$-IIA is also produced locally by alveolar macrophages (De Luca *et al.*, 2011). The main lipid substrate for $sPLA_2$-IIA is PG, whereas $sPLA_2$ IB preferentially degrades PC (Hite *et al.*, 2005). However, total PG is not reduced in MAS patients, but a significant decrease in PG 36:2 (DOPG) subclass was observed. This is a natural inhibitor of $sPLA_2$-IIA production (Wu *et al.*, 2003), and its reduction may facilitate the "inflammation–surfactant injury–inflammation" vicious cycle typical of ARDS. In this scenario, the interaction of the enzyme with its specific macrophage receptors (Saegusa *et al*, 2008) and the subsequent pro-inflammatory action, should also nourish the ROS-induced oxidation milieu.

Simultaneously, the hydrolysis of surfactant PC in MAS may be mainly mediated by the activity of $sPLA_2$-IB and the other airway epithelial isoforms: $sPLA_2$-X and $sPLA_2$-V (**Figure 20**) (Seeds *et al.*, 2012). These findings suggest that other phospholipases may be produced once the meconium has triggered the lung injury, and these enzymes may contribute at different levels to the changes in surfactant composition and activity. However, $sPLA_2$-IB remains the most abundant subtype with the most evident effect on surfactant hydrolysis, since there is a negative correlation between surfactant adsorption and its amount (**Figure 28**). Interestingly, since the hydration state of $sPLA_2$ is crucial for the enzymatic hydrolysis, the high PuPC/DPPC ratios and the subsequent higher fluidity may enhance further the activity of the enzyme on surfactant membranes *in vivo*. At the same time, the increase in certain anionic and zwitterionic phospholipids, such as PI, PG, or PE 32:1, may be related to a possible physiological compensation for the reduction of the other PC species: POPC, PC 32:2, and PC 34:2.

Overall, these data support the development of surfactant protection strategies such as the use of $sPLA_2$ inhibitors, as a clinically interesting strategy for patients with MAS (De Luca *et al*, 2012). Intriguingly, besides the development of new molecules protecting surfactants, budesonide has proven to be clinically effective for severe MAS (Basu *et al*, 2007), which is consistent with its inhibitory role in the $sPLA_2$-induced inflammatory cascade (Triggiani *et al*, 2009).

DPPC and SP-A did not change when comparing MAS and NLD babies. Reduced levels of DPPC have previously been observed at the peak of MAS clinical severity (Janssen *et al.*, 2006) whereas SP-A has been found to increase over time in patients recovering from MAS during extracorporeal life support (Bui *et al*, 1992; Lotze *et al.*, 1990). Therefore, it is likely that surfactant injury would worsen over time and finally lead to a reduction in SP-A and DPPC in the severest cases. Moderately lower DPPC amounts have also been found in some adults

with ARDS (Günther *et al.*, 2001), and this may also be due to the timing of sampling during the natural course of the syndrome or to the different ARDS triggers. In fact, enrolled MAS patients had no infection, whereas other cases of ARDS may be triggered by an infectious process, and this may lead to a decrease in total PC (Günther *et al*, 2002). In this line, the reduction in DPPC synthesis seems to be driven by pathogens and pathogen-associated molecules that induce the ubiquitin-mediated degradation of LPCAT1 (Zou *et al*, 2011). Finally, a crucial point is that the increase in certain phospholipids observed in MAS seems to be due to a response confined to the neonatal lung and not related to meconial cellular debris. In fact, those lipid species were almost undetectable in meconium (**Table 7**).

Hydrophobic surfactant proteins are also affected in MAS. The apparent content in SP-B and SP-C was increased compared with controls. Interestingly, SP-B increased both in the dimeric (~16 kDa) and monomeric (~8 kDa) forms (**Figure 21)**. At the same time, reduced forms of SP-A were also observed in MAS neonates (**Figure 23**). One reason could be the reduction of disulphide bridges in the presence of extracellular GSH. This tripeptide tends to increase upon inflammation and promotes the reduction of hydrogen peroxide assisted by glutathione peroxidases. As a matter of fact, during the epithelial injury resulting from meconium insult, GSH might be released from epithelial cells and act as a reductive agent in the alveolar spaces. On this basis, irrespective to PC concentration, the monomeric form of SP-B is only present in MAS and in the proteinosis control. The levels of oxidised GSH seem to increase at the expense of its reduced form in ARDS and alveolar proteinosis (Bunnell & Pacht, 1993; Ghio *et al*, 2008; Schmidt *et al*, 2004). Consistently, increased levels of GSSG were also detected in nBALs of MAS neonates compared to NLD babies as well as in the patient of alveolar proteinosis (**Figure 24A**). It could be argued that extracellular GSH levels transiently increase as an inflammation response or after epithelial damages due to meconium injury. This promotes a reduction in the extracellular oxidative environment, leading to GSSG formation. At the same time, such high GSH content also reduces the disulphide bonds of surfactant proteins, especially the most accessible ones, resulting in monomeric forms. Since the characterisation of neonatal nBALs was performed 3 hours after meconium aspiration, the increase in GSSG and monomeric surfactant proteins can be interpreted as a consequence of this mechanism. In support of this, the capability of GSH to reduce purified porcine SP-B dimers and oligomeric forms were also demonstrated *in vitro* (**Figure 24B**). The tripeptide cannot cross the lipid membranes; thus, the *in vivo* action of extracellular GSH is probably confined to the SP-B oligomers accessible at the surface of large surfactant aggregates. This may perturb the essential connection between SP-B rings involved in adsorption and re-adsorption of surfactant lipids and the stability of the system.

Furthermore, patients with MAS also showed larger forms of SP-B, which may correspond to the last steps of pro-SP-B processing during the formation of lamellar bodies (Brasch *et al*, 2004). Monomeric SP-B_{1-25} peptide, but not its disulphide linked homodimer, has shown to enhance the uptake of small aggregates by alveolar rat macrophages *in vivo*. This suggests a possible role of the monomeric form of SP-B in the catabolism of injured lipids and proteins (Poelma *et al*, 2007). However, the larger forms of SP-B may also result from a boost in the lamellar body secretion to replace the injured surfactant, or be due to the inflammation-induced necrosis of AT-II cells with a concomitant release of cellular debris. The first hypothesis seems corroborated by the damaged nanostructure of surfactant (**Figures 25** and **26**) and by animal data showing increased SP-B expression in experimental MAS after ~6 hours from the injury (Hilgendorff *et al*, 2006). The second hypothesis is consistent with some data in the literature showing that cultured alveolar epithelial cells (A549 cells) may undergo

necrosis or caspase-dependent apoptosis soon after meconium exposure (Jeng *et al*, 2010). Interestingly, nBALs were analysed in the early phase of respiratory failure after meconium aspiration, suggesting how early epithelial cells sense a harmful environment also *in vivo*. Moreover, this mechanism is consistent with the increase in both extracellular SP-B immature forms and GSH after epithelial injury. In this line, dimers of no-fully processed SP-B can contribute to increase the overall amount of the protein and be also subjected to the same reduction activity on cysteine 48.

Alternatively, the increments in both SP-B and SP-C might represent a defensive mechanism during acute inflammation, as described in neonates with pneumonia (D'Aronco *et al*, 2015) or chorioamnionitis (Verlato *et al*, 2018). Consistently, SP-B reduces the *in vitro* activity of both $sPLA_2$-IB and -IIA in lipid mixtures (Hite *et al.*, 2012) and this mechanism may be even more relevant in MAS because there is no increment of SP-A and there is even a reduction in DOPG, the other two surfactant components inhibiting $sPLA_2$ IIA and X expression and/or activity (Karray *et al.*, 2020; Wu *et al.*, 2003). At the same time, SP-C seems to contribute to lung surfactant recycling by alveolar macrophages (Poelma *et al.*, 2004) and it is essential for the *in vitro* stabilisation of cholesterol-containing surfactant films under physiological conditions (Gómez-Gil *et al.*, 2009a; Gómez-Gil *et al.*, 2009b). Thus, its increment could be an intent to compensate the deleterious effect of high free cholesterol levels on surfactant interfacial properties upon MAS. At the same time, SP-C seems to reduce the pro-inflammatory effects of several danger-associated molecular patterns, such as oxidised cholesterol and phospholipid species on TLR-4 (Sehlmeyer *et al.*, 2020). These mechanisms should be related to an increase in SP-C expression, but, unlike SP-B, the content of SP-C messenger RNA was found to be reduced 6 hours after meconium injury in an animal model (Hilgendorff *et al.*, 2006).

Starting from these considerations, the most likely process occurring in the early phase of MAS seems to be the raise in surfactant proteins after AT-II injury due to the ROS burnt or as a direct effect of meconium. As demonstrated *in vitro*, meconium may promote caspase-dependent cell death and necrosis of AT-II cells within the first 6 hours (Jeng *et al.*, 2010). Moreover, this material can attract and activate neutrophils and macrophages that generate large amounts of ROS, also stimulating further production of TNF-α from alveolar macrophages (Kopincova & Calkovska, 2016). As a result of the epithelial injury, the release of the intracellular content more proximal to the alveolar space of AT-II cells (e.g. lamellar bodies, which are rich in hydrophobic surfactant proteins (Oosterlaken-Dijksterhuis *et al*, 1991)) cannot be excluded. SP-A and the hydrophobic proteins follow two different pathways of exocytosis. Thus, quasi-mature lamellar bodies (multivesicular and composite bodies) with mature SP-C and different forms of SP-B, but not SP-A, may be released after epithelial damage. The short SP-B immature forms are indeed similar to the mature protein and may still contribute to correctly processing SP-C in lamellar bodies. However, although increased in the alveolar space of MAS neonates, those surfactant proteins could be subjected to ROS-mediated oxidation with a subsequent reduction of their interfacial properties.

Overall (**Figure 30**), the simultaneous increase of SP-C and SP-B in a highly oxidative environment, the reduction in POPC and other PC species as well as the increase in free cholesterol and PuPC/DPPC ratios influence the nanostructure of surfactant large aggregates. The latter show a decrease in both size and multi-layer complexity compared to NLD neonates. These compositional and structural changes affect surfactant function in terms of interfacial adsorption, surface tension reduction, and eventually lung aeration. This is confirmed by the

correlations found between surfactant adsorption/accumulation after 6 minutes, POPC, and sPLA$_2$-IB (**Figure 28**). Interestingly, this impaired surfactant adsorption strongly correlates with the estimated amount of lung volume available for gas exchange. The latter is the lung aeration assessed by semiquantitative lung ultrasound that, together with oxygenation, are significantly worse in neonates with MAS than in neonates with NLD (**Table 4**).

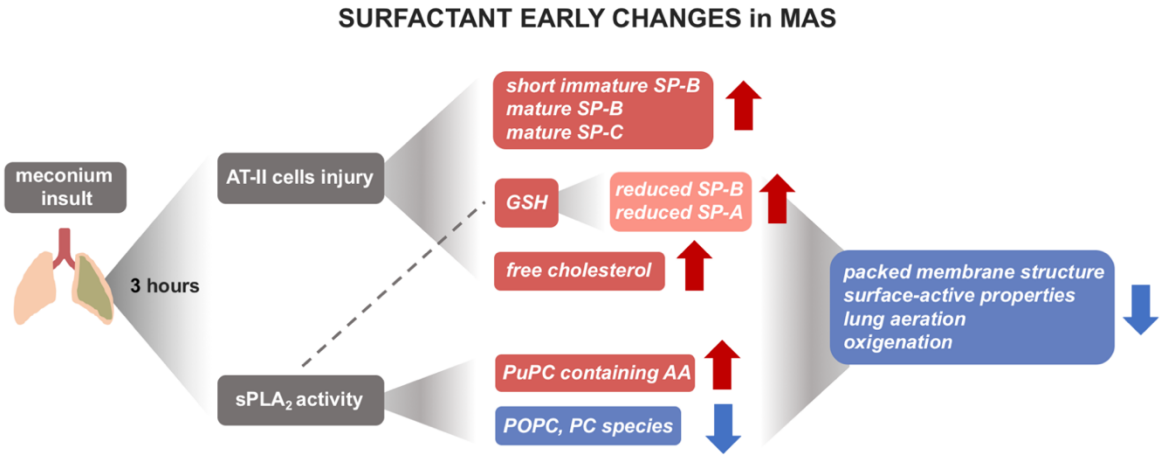

Figure 30. Schematic representation of the early surfactant changes during severe MAS, 3 hours after birth. The different increased (salmon colour) and reduced (light blue colour) components in nBALs of neonates along with biophysical and respiratory parameters are summarised. Abbreviations: AA, arachidonic acid; GSH, reduced glutathione; PuPC, polyunsaturated phospholipids.

This is a crucial point since the correlation between lung aeration and the early adsorption provides the link between biophysical processes and MAS physiopathology. Moreover, we demonstrate the effectiveness of modified SAT to detect impairment of surfactant status/quality also in nBALs, confirming its feasibility as rapid screening test for surfactant activity. The surfactant function seemed worse when free cholesterol and PuPC/DPPC ratios tend to increase (**Figure 29** and **Table 8**). The relative increase of these lipids alters a fair proportion between unpackable lipids and DPPC, increasing surface tension under compression as well as surfactant hysteresis during breathing-like dynamic cycles (Verlato *et al.*, 2018; Zhang *et al.*, 2019). Differences in hysteresis and relative area of compression seem less evident than the change in minimum surface tension and compressibility, but this is interesting because it occurs regardless of cholesterol concentration and is probably related to the PuPC amount.

In spite of the promising results, several limitations should be considered: (1) because of the rarity of MAS and the complexity of the analysis, a relatively small sample size was enrolled; (2) nBALs instead of BAL were performed and this lavage also collects material from the larger intrathoracic airways like trachea and larger bronchi. However, this is the only doable and non-invasive technique feasible in neonates; (3) because of the small volume recovered from each lavage and the need to carry out different techniques, not all of them were performed for all samples. This was the case of methods for which high volume of specimens (ELISA) or relatively high concentrated surfactant (CBS and Cryo-EM) are necessary. (4) for the same reason, SP-D levels were not analysed. This would help to better understand if the increase in hydrophobic surfactant proteins was related to a surfactant recycling response. (5) PC is

typically described to account for 60–70% of surfactant lipids, but higher amounts in both neonates with NLD and MAS were detected (~90%). However, these results are in accordance with recent data obtained from healthy children (Griese *et al*, 2015). (6) The different ventilatory strategies needed to support patients in the two groups could have theoretically influenced some results.

To conclude, in this second chapter the surfactant status in the early phase of acute lung injury due to severe MAS was extensively investigated. The changes in surfactant composition that affect its structure and function are related to the early pro-inflammatory response triggered by meconium and can be summarised in three points (**Figure 30**): (1) raise in the levels of several $sPLA_2$ isoforms (IB from meconium and X-V in the neonatal lung) and subsequent PC degradation; (2) epithelial injury and release of immature lamellar bodies and GSH with the subsequent increase in hydrophobic surfactant SP-C, dimers and immature forms of SP-B as well as reduced forms of SP-B and SP-A; (3) increase in PuPC species with respect to DPPC and other PC components, probably as a result of arachidonic acid production related to $sPLA_2$ activity.

These novel evidences should be added to the well-known increase in free cholesterol upon MAS. Moreover, since meconium is only a trigger agent, this study can be used as a model to describe the effects of *in vivo* early inflammation on lung surfactant activity. Other processes also triggering inflammation could share similar patterns if analysed early enough.

Overall, these findings support early surfactant protection strategies as a possible treatment for severe MAS, suggesting the importance of the timing of the dose as well as the composition of surfactant preparations in adult primary ARDS.

Part of this text has been published in the following paper:
Echaide M, Autilio C, et al., Sci Rep. 2020, 10(1):1385

Chapter III

"CHF5633 as an effective clinical surfactant in oedema-like inhibiting contexts"

Introduction

In the first chapter, the analytical sensitivity of SAT was improved to test surfactant in samples with poor amount of material, making possible testing directly AFs. This modified technique was then used in the second chapter, together with other biophysical and biochemical methods, to identify the early changes in composition, structure and function of lung surfactant in neonates with a severe type of ARDS due to meconium aspiration. Apart from the well-known *in vitro* cholesterol-mediated inactivation of surfactant by meconium, the effects of the early inflammatory response in the lungs bring about other effects regardless of the meconium presence: changes in the levels of SP-B and SP-C, modification in the PC profile with an increase in PuPC, a physiological reduction of disulphide bridges in surfactant proteins and increased levels of lungs-derived $sPLA_2$ enzymes. Interestingly, irrespective of cholesterol levels, the greater the PuPC/PC ratios in tested samples, the worse are surfactant dynamic properties in terms of compressibility and hysteresis. Since these surfactant alterations are not directly related to meconium composition, but likely due to the pro-inflammatory response triggered by meconium in the lung, they can be used as potential markers for other forms of direct ARDS. Most direct ARDS are characterised by a quick production of local inflammatory mediators such as cytokines and $sPLA_2$ that may affect surfactant activity (Nakos *et al.*, 2005). Starting from these evidences, early exogenous surfactant replacement with clinical preparations resistant to inhibition and available in larger amounts than animal-derived surfactants, should be considered for possible future clinical trials in MAS and other forms of direct ARDS.

On this basis, CHF 5633 is a synthetic surfactant that has shown promising results in a phase II clinical trial (Ramanathan *et al.*, 2020) and proven to be more resistant than Poractant alfa to inactivation by serum proteins in preterm lambs (Seehase *et al.*, 2012). It is characterised by a simple mixture containing 98.3% lipids by mass in a 1:1 ratio of DPPC and POPG and 1.7% by mass of peptides analogues of both SP-B and SP-C (Glaser *et al.*, 2016; Sato & Ikegami, 2012). Nowadays, surfactants from natural origin, typically organic extracts of either calf or porcine BALs as well as from minced lung lavages, are used to treat RDS and emerged effective in some cases of neonatal and adult ARDS (Blanco & Pérez-Gil, 2007). However, several issues concern the obtainment of surfactant preparations from animal-derived sources: (1) the high cost of production due to the large number of animals needed to obtain the product, (2) the impossibility to have a constant and repetitive formula, (3) the hazard of potential immunogenic response if many repeated doses are required, (4) a non-negligible risk of exposure to animal-derived pathogens. Moreover, the future development of surfactant-assisted drug delivery will require production of large amounts of materials with a simple composition, good interfacial properties and relative resistance to inactivation.

After previous disappointing efforts to create synthetic surfactants based on lipids with or without peptides mimicking hydrophobic surfactant proteins, the story highlights the crucial role of both SP-B and SP-C to provide an optimal interfacial performance comparable to that of animal-derived preparations (Hentschel *et al.*, 2020). With this purpose, the SP-B analogue in CHF 5633 is a 34-amino acid peptide obtained by analogy with the two halves (Mini-B, residues 8-25 and 63-78) of the human SP-B, with two intramolecular disulphide bridges mimicking those in the native protein. The SP-C analogue (SP-C33Leu) is a 33-amino acid peptide resembling native SP-C, where valines have been substituted by leucines giving rise to a more conformationally stable protein.

Starting from this basis, in the present chapter the interfacial properties of CHF 5633 have been compared with PS and Poractant alfa, the most used clinical surfactant from porcine origin, in physiological-like and inhibiting contexts. In this line, the use of meconium as a model for surfactant inactivation would give a reductive information, describing a condition nor extendible to different types of direct ARDS, neither properly identifiable with early stages of severe MAS. Conversely, plasma/serum contains several components found in the lung upon early inflammation, such as $sPLA_2$ IIA liberated from leucocytes as well as oedema-related molecules like total serum proteins that increase in later stages when also endothelial damages occur. Thus, plasma inhibition was chosen as a model to *in vitro* test and compare the biophysical performance of the three materials, resembling pulmonary inflammation-like and acute injury contexts.

Key techniques

PS was purified from BAL of porcine excised lungs and subjected to a sodium bromide gradient centrifugation to remove potential blood contaminants after discarding cells. Phospholipid concentration was determined by phosphorus mineralisation. Clinical surfactants, Poractant alfa and CHF 5633, were provided by Chiesi Farmaceutici S.p.A. (Parma, Italy). Porcine serum was obtained by pooling samples from different pigs and centrifuging them at 500 g for 10 minutes at 4 °C to remove cell components. Total proteins in serum were assayed by the Lowry method. The dilution of materials was performed with 5 mM Tris buffer, containing 150 mM NaCl at pH 7.4.

The spreading capability of surfactants was assayed by using a Wilhelmy balance at 25 °C, where a drop of 10 µL of surfactant suspensions containing 50, 100 or 150 µg of phospholipids were spread at the air-liquid interface while monitoring surface pressure. The interfacial adsorption and accumulation of materials were also tested at 37 °C by SAT in the absence or presence of different amount of total serum proteins per well (1, 0.75, 0.5 or 0.25 µg). At the same time surfactants at 10 mg/mL were assayed in CBS at 37 °C, using a clean bubble interface or previously saturated with serum proteins. Thus, the adsorption, re-adsorption, stability and surfactant capability to reduce surface tension under slow and quick compression-expansion cycles were also analysed.

The lateral structure of interfacial surfactant films regarding the compression-driven segregation of liquid-condensed domains was observed by epifluorescence microscopy at 25 °C. Briefly, 2.5 µg/µL of PS or Poractant alfa or 50 µg/µL of CHF were labelled with NBD-PC for 1 hour at 37 °C to obtain a final molar ratio of 1% (dye/surfactant). In the case of PS and Poractant alfa, 15 µL of dye/surfactant suspension were spread at the air-liquid interface of a Langmuir-Blodgett trough. As for CHF, 3 µL of dye/surfactant suspension were applied with the barrier totally closed before opening it at a constant speed of 5 cm^2/min. After 10 minutes equilibration, each surfactant film was subjected to compression at a constant speed of 25 cm^2/min, while transferring the interface onto a glass coverslip that had been previously immersed into the subphase. The resulting supported film, captured at different surface pressures was observed under an epifluorescence microscope (Echaide *et al*, 2020).

The thermotropic transitions between different phases in surfactant membranes and complexes were analysed by Differential Scanning Calorimetry (DSC). Each surfactant was diluted to reach a concentration of 3 µg/µL and measured within a temperature range from 10

to 55 °C along 15 consecutive scans. Further details of these techniques and materials are described in the Materials and Methods chapter.

CHF 5633 adsorbs and spreads slower than Poractant alfa, but sustains optimal dynamic interfacial properties

As shown in **Figure 31 A-C**, when testing the kinetics of interfacial spreading at limiting conditions due to the low temperature (25 °C) and surfactant amount, PS and Poractant alfa were able to rapidly spread over and adsorb to the interface even at 50 μg (5 mg/mL). However, CHF 5633 needed three times higher lipid concentration (150 μg, 15 mg/mL) to reach a surface pressure close to that of equilibrium.

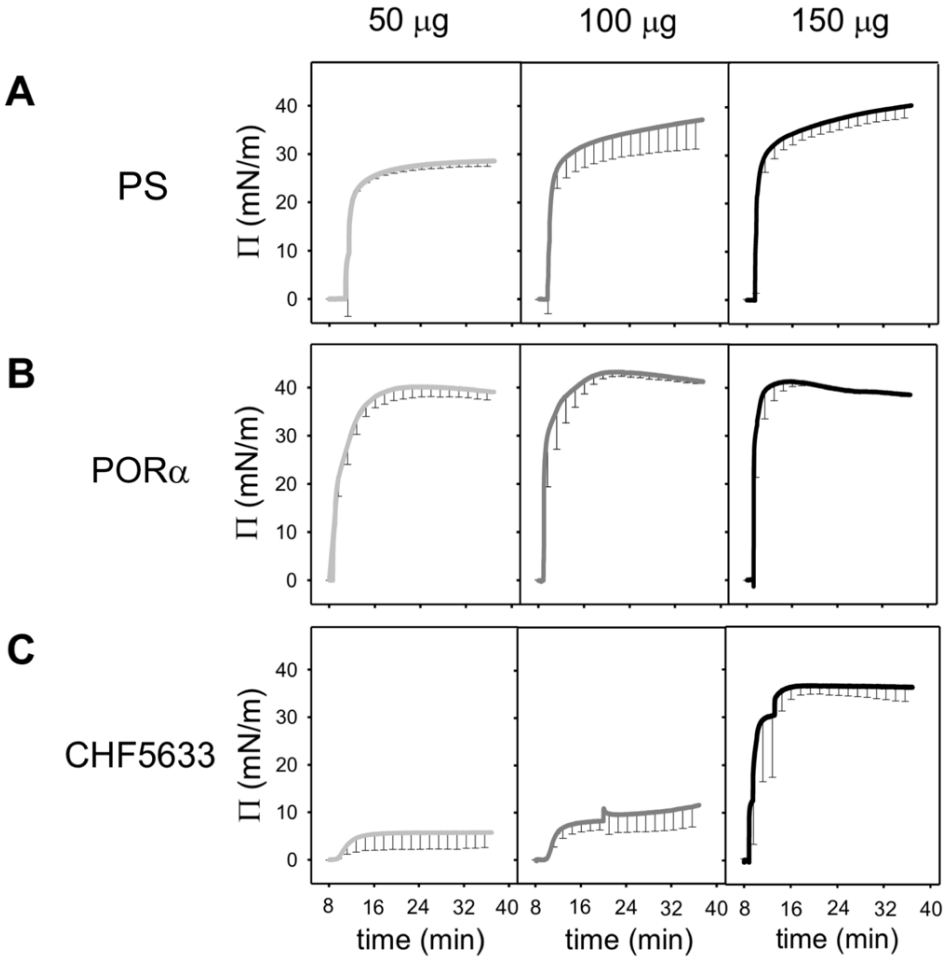

Figure 31. Interfacial adsorption isotherms of surfactants in a Wilhelmy balance. Spreading isotherms of 50 (light grey), 100 (dark grey) and 150 μg (black) of (**A**) PS, (**B**) Poractant alfa (PORα) and (**C**) CHF 5633 are shown. Each surfactant was applied as a single drop at the air-liquid interface, before monitoring surface pressure along 40 minutes. The mean of three replicates is depicted. Black vertical lines represent standard deviations. Abbreviations: PS, purified porcine surfactant; PORα, Poractant alfa; Π, surface pressure.

This is probably due to a slower adsorption rate of this material. Due to the simple lipid composition of CHF 5633 (DPPC:POPG, 1:1 w/w), and the low temperature the lipid-peptides complexes may not form stable surface-associated structures from which surface-active phospholipids could be transferred into the interface. However, increasing surfactant concentration to a level still far from that used for clinical replacement therapy (15 mg/mL vs 80 mg/mL), once a critical concentration was reached, surfactant may probably condense from dispersed structures to extended membrane networks with optimal adsorption (Gunasekara *et al.*, 2008). This may explain the improvement in CHF 5633 adsorption at the air-liquid interface regardless of the testing temperature. This hypothesis is corroborated by the clearly better interfacial performance of the same material when both concentration and temperature increase in the CBS experiments. In this regard, when the formation and performance of surface films were assessed at 37 °C and 10 mg/mL, all samples reached the equilibrium surface tension, although with a somehow slower rate in the case of CHF 5633 (**Figure 32**).

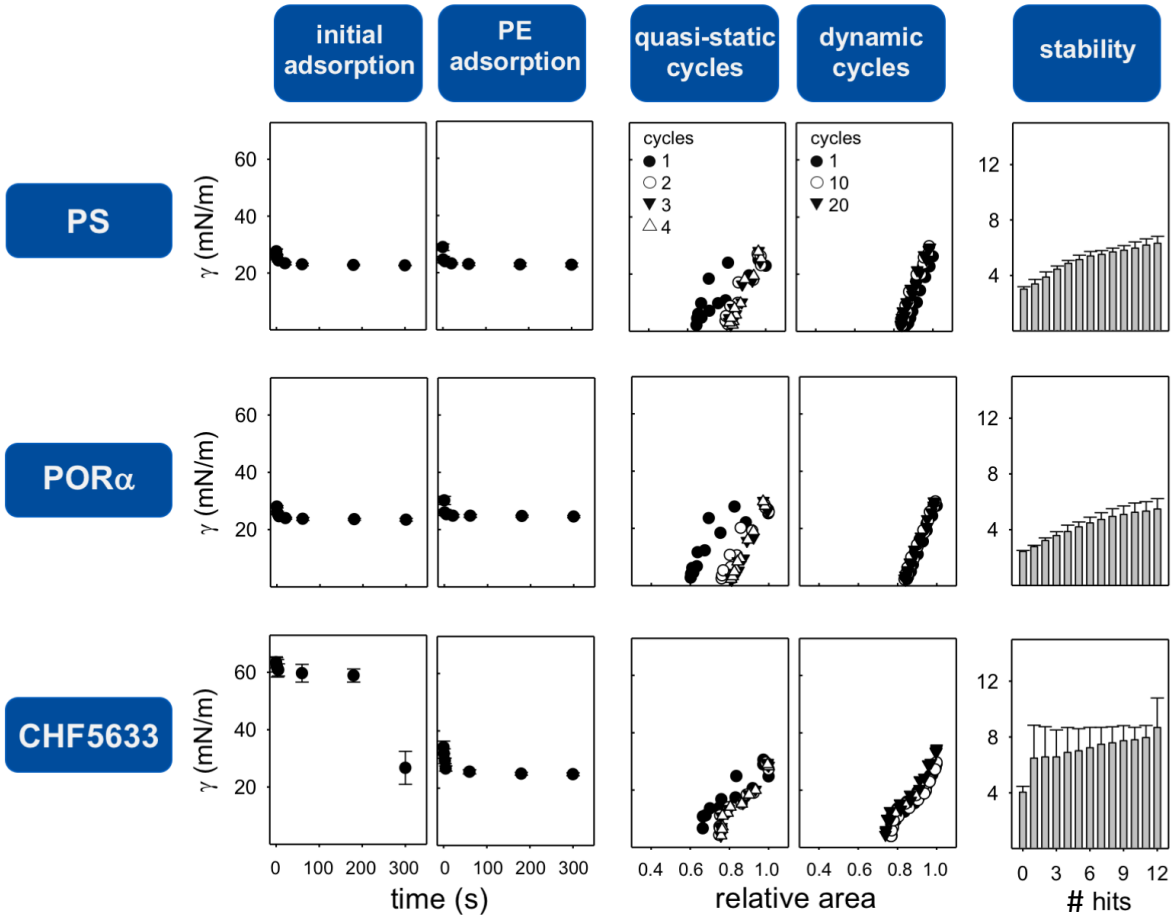

Figure 32. Interfacial behaviour of surfactants as assessed in CBS. Initial and post-expansion adsorption and slow quasi-static and fast dynamic compression-expansion isotherms are compared for PS, Poractant alfa (PORα) and CHF 5633. Around 300 nL of surfactant at 10 mg/mL were injected onto the bubble in each experiment. The mean of three replicates is depicted for initial adsorption, post expansion adsorption and stability. A representative isotherm is shown for quasi-static and dynamic cycles. Black vertical lines represent standard deviations. Abbreviations: PS, purified porcine surfactant; PORα, Poractant alfa; γ, surface tension.

PS and Poractant alfa reduced the surface tension to values around 23 mN/m after 1 second from the injection of material (**Figure 32**, first column). Conversely, CHF 5633 needed around 3 minutes to reduce surface tension to values around 26 mN/m. However, once the air-liquid interface was reached and a proper reservoir was formed below, CH5633 generated a stable structure that reduced surface tension to equilibrium values in few seconds after bubble expansion when a new interface was open. Thus, as it happens for PS and Poractant alfa, protein analogues in CHF 5633 efficiently help lipid films to reorganise and quickly spread at the bubble surface, transferring surface active species into a newly open interface.

When slow quasi-static and subsequent rapid compression-expansion cycling of the interface was applied, PS and Poractant alfa showed similar behaviour. As discussed in chapter II, under the first slow cycle, materials reorganise in the first compression, requiring a larger reduction of interface area to reduce surface tension to a minimum with higher hysteresis, compared to those of the following slow or quick compression-expansion cycles. However, at the end of the second slow compression cycle, both materials were competent to reduce surface tension to values less than 2 mN/m, with a minimal compression of the interfacial area (20%). At the same time, maximal surface tension at the end of the expansion steps was slightly lower than 30 mN/m.

Under rapid breathing-like compression expansion cycles with a frequency of 20 cycles/min both PS and Poractant alfa exhibited practically no hysteresis and extreme stability, producing the lowest surface tensions (≤3 mN/m) along all the cycles with less than 20% area reduction. Maximal surface tension under dynamic conditions is slightly higher than in the slow cycle regime, but still not much higher than 30 mN/m. CHF5633 films also worked properly under both slow and quick cycling, although they showed an interesting behaviour different from the typical exhibited by Poractant alfa and PS. In detail, material was already able to sustain minimal surface tension during the slow compression cycles, but this minimal value was slightly higher (~4 mN/m) compared with those of the other tested surfactants (~2 mN/m). Moreover, CHF 5633 films needed slightly more than 20% area reduction to reach the lowest surface tension values with an evident plateau, both in the compression and the expansion moieties of the isotherms. However, once arriving at the plateau, the reduction in surface tension occurred quickly with very low compressibility, suggesting that only lipids that can maintain high packing remain at the air-liquid interface (DPPC). Thus, it is likely that CHF 5633 films undergo a structural transition before reaching the less compressible stages. This probably occurred by the exclusion upon compression of POPG from the air-liquid interface, with a subsequent reincorporation when enough space is opened again between packed DPPC condensed domains during the following interface expansion.

Finally, once compression leads to formation of a packed lipid status at the air-liquid interface, CHF 5633 was less stable to mechanical perturbations than the other tested surfactants with a rise in surface tension values of around 3-4 mN/m after a single hit with the pendulum hammer.

CHF 5633 is more resistant to serum inhibition than Poractant alfa

The resistance to inactivation of PS, Poractant alfa and CHF 5633 was assayed in CBS as previously described (López-Rodríguez *et al.*, 2012). An excess of serum (3 μL) was applied close to the bubble in order to saturate the bubble interface with serum surface-active

components, mostly proteins, but also lipoproteins containing cholesteryl esters, triglycerides and phospholipids. After injecting serum at the interface, the surface tension decreased from 70 mN/m to values around 45 mN/m, confirming the saturation of the interface with surface-active components. Then, surfactant materials were applied without touching the bubble surface. This avoids the destabilisation of the steric barrier created by the surface-active serum proteins.

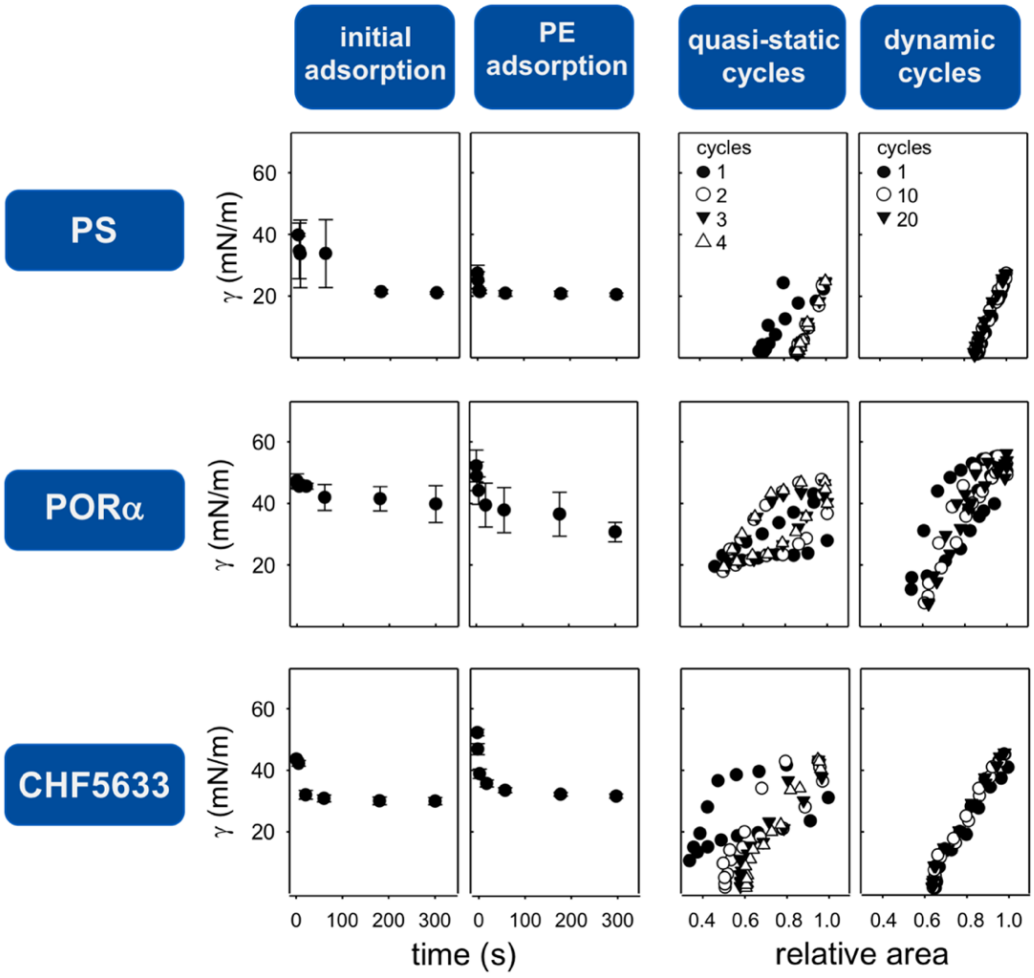

Figure 33. Interfacial resistance to inactivation by serum of surfactants as assessed in the CBS. Initial and post-expansion adsorption and slow quasi-static and fast dynamic compression-expansion isotherms are compared for PS, Poractant alfa (PORα) and CHF 5633. Bubble air-liquid interface was previously saturated by injecting 3 μl of serum, reaching around 45 mN/m of surface tension**.** Around 300 nL of surfactant at 10 mg/mL were then left close the bubble in each experiment. The mean of three replicates is depicted for initial and post expansion adsorption. A representative isotherm is shown for quasi-static and dynamic cycles. Black vertical lines represent standard deviations. Abbreviations: PS, purified porcine surfactant; PORα, Poractant alfa; γ, surface tension.

Interestingly, synthetic CHF 5633 was more resistant to serum inactivation than Poractant alfa as it can be observed in **Figure 33**, where it shows a dynamic behaviour similar to that of PS. Though it requires a higher compression of the interface compared with the native material, CHF 5633 films could reach the lowest surface tension already at the second

slow cycle, showing no hysteresis upon rapid breathing-like compression of the bubble interface.

However, an evident increase in maximum surface tension could be observed compared to PS in both dynamic and quasi-static cycles. Conversely, Poractant alfa was not able to reduce surface tension upon compressions of the bubble surface during slow dynamics. The minimum surface tension during quick cycles was around 6 mN/m with an evident hysteresis until reaching cycle 20. These results are in accordance to previous *ex vivo* evidences of BALs from RDS lambs treated either with Poractant alfa or CHF 5633 (Seehase *et al.*, 2012). The importance of both SP-A and a preserved native membrane structure emerge essential for reducing the serum-mediated inhibition as observed by the optimum behaviour of PS.

To confirm the apparent resistance of CHF 5633 to inactivation and investigate on the influence of material concentration on this mechanism, its accumulation at the interface compared with those of PS and Poractant alfa were tested by SAT, in the presence of different amounts of total serum proteins to the subphase as previously described (Cerrada *et al.*, 2015). Results from this experiment are shown in **Figure 34A**. Though CHF 5633 adsorbed and accumulated at slower rate at a clean surface, it is surprisingly less altered by serum proteins than the other surfactants tested. Interestingly, the accumulation of surfactant after 60 minutes was similar in the presence or absence of serum in the case of CHF 5633 (**Figure 34B**), suggesting that serum components in the subphase have almost no effect in the adsorption kinetics of this material.

Conversely, Poractant alfa was quite affected even at the lowest amount of total serum proteins tested. PS showed a similar behaviour to Poractant alfa, although starting from an optimal interfacial adsorption and accumulation at a clean interface, probably due to the presence of SP-A that facilitates the massive transfer of surfactant aggregates towards the air-liquid interface (Lopez-Rodriguez *et al.*, 2016b).

When considering the sample activity calculated as the percentage of the difference in RFU between the same material in presence and absence of 1 μg of total serum proteins, CHF 5633 maintained almost the same activity of its control compared with PS and Poractant alfa (**Figure 34C**). This suggests that at very limiting amount and low concentration, as it happens in the SAT experiment (3 μg of total phospholipids at 0.15 mg/mL), serum components tend to inhibit at greater extent surfactants characterised by heterogenous lipid-protein mixtures like those of PS or Poractant alfa. This is probably due to additional time- and concentration-dependent mechanisms that may enhance the competition with serum proteins to reach the air liquid interface. In this line, it is necessary to consider the different experimental conditions. Materials are dispensed close to the bubble surface in CBS, promoting a quick interface saturation (1 minute). Conversely, surfactants are dispensed at the bottom of the well in SAT experiments, reaching the interface slowly (5-10 minutes) as less-compact aggregates. As a result, the plateau of surface saturation is observed after around 60 minutes in the control condition of both PS and Poractant alfa, but never reached in the case of CHF 5633 in this experimental condition (**Figure 34A**).

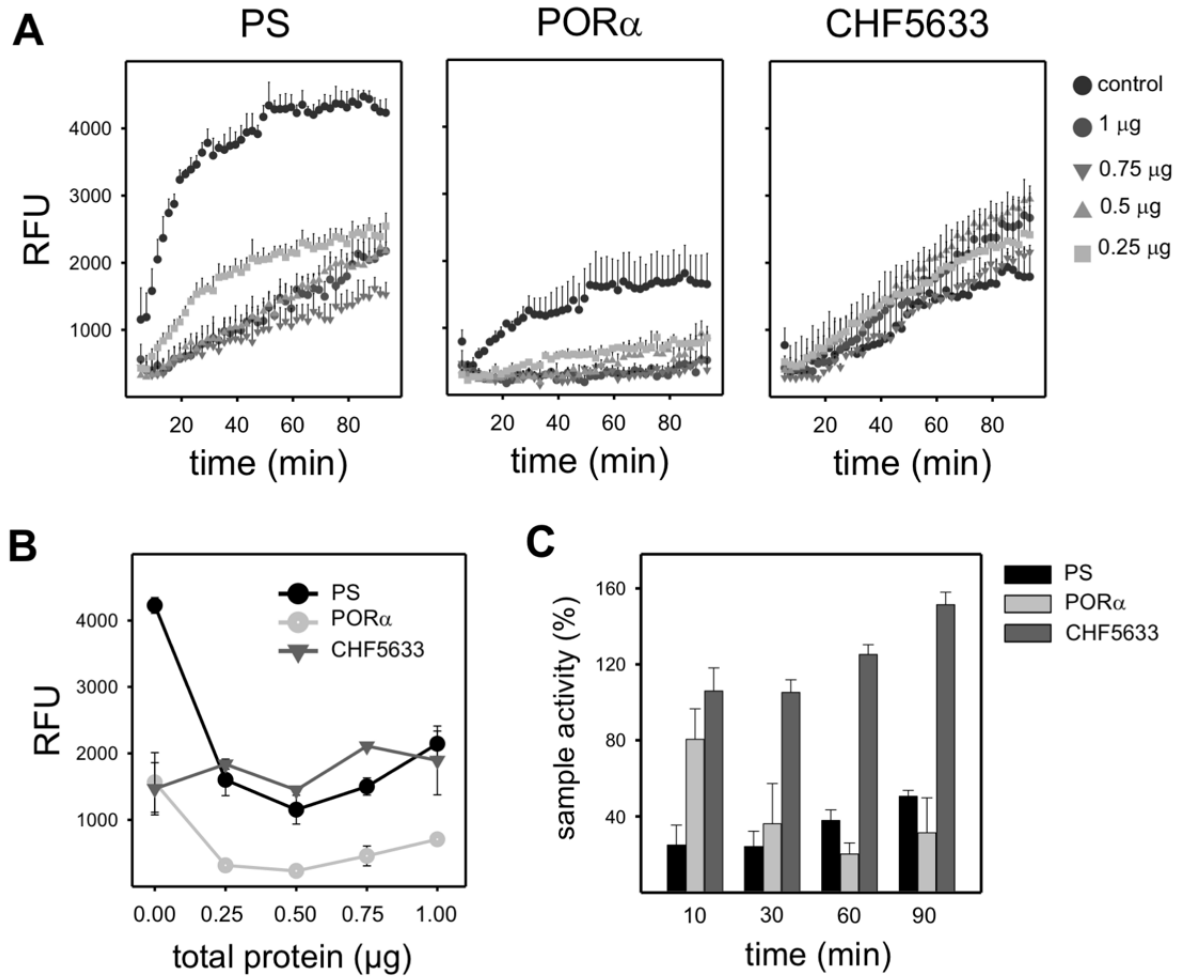

Figure 34. Interfacial adsorption and accumulation of surfactants. (A) Overtime kinetics of surfactant adsorption and accumulation in the absence or presence of several amounts of total serum proteins. **(B)** Surfactant interfacial performance after 60 minutes when different serum protein quantities are added to the well. **(C)** Overtime interfacial activity of surfactants when 1 μg of total serum proteins is added to the well. Circles and bars represent the mean of three replicates. Black vertical lines represent standard deviations. Abbreviations: PS, purified porcine surfactant; PORα, Poractant alfa; RFU, relative fluorescence units.

The thermotropic properties and lateral structure of CHF 5633 defines its biophysical activity

The compression-driven segregation of different phases or domains in interfacial films made of the three materials was studied at 25 °C in a Langmuir-Blodgett surface balance by epifluorescence microscopy. Moreover, lipid-protein phase segregation was only studied in a clean surface since the presence of serum/plasma makes samples very heterogenous and difficult to study. To reveal the presence of condensed areas of highly packed lipids forming at the interface, a fluorescent lipid (NBD-PC) was included, which resembles those lipids that distribute into more fluid and disordered phases under compression such as it occurs with unsaturated lipids. Interestingly, in other studies plasma fibrinogen was also found to associate with the liquid-expanded phases of interfacial films (Williams *et al*, 2019).

Again, to obtain an efficient adsorption and spreading of CHF 5633 at 25 °C, it required three times the lipid amount required in the case of Poractant alfa or PS. Thus, while for the animal-derived materials, 50 μg of suspension were dispensed at the air-liquid interface of the Langmuir-Blodgett trough, 150 μg was applied in the case of CHF 5633. This protocol allowed starting the experiments from the same surface pressures (2 mN/m), ensuring to have a similar amount of surface-active material associated to the air-liquid interface. Since at surface pressure close to 40 mN/m, the interface starts to be saturated by condensed black material, making difficult to observe the shape and quality of domains, the epifluorescence analysis was performed, choosing a lateral compression in the range of 25 - 35 mN/m.

As shown in **Figure 35A**, when compared with Poractant alfa and PS, films of the synthetic mixture were characterised by a very conspicuous phase segregation at 25 °C once compressed to 25 mN/m. This was characterised by a larger number of small condensed domains that aggregated in clusters in some cases. Moreover, at this surface pressure, the appearance of three phases was conspicuous in the case of CHF 5633 (see red squares). These are probably characterised by highly-packed DPPC-rich regions (dark spots), a mixture of DPPC and POPG (dark green background) and fluorescent brilliant green spots where an accumulation of the label with or without POPG has been produced. Interestingly, the latter disappeared at higher surface pressure (> 27 mN/m), suggesting the loss of that material during interfacial compression.

Increasing the compression of the interface, a similar distribution of condensed domains was observed regardless of the material tested, although with larger and more polymorphic shapes of the domains in the case of CHF 5633 and Poractant alfa, due to the absence of cholesterol. Interestingly, when comparing surfactants at the highest analysed surface pressure (32 mN/m), CHF 5633 showed the largest and darkest domains with the clearest fluid background, indicating a very efficient phase segregation. The synthetic material was also able to reach higher surface pressure under high compression status (63 mN/m compared to 50 mN/m), than the other surfactants.

As shown in **Figure 35B**, PS membranes confirmed a melting temperature at around 32 °C (de la Serna *et al.*, 2004), with its main calorimetric peak ending close to 37 °C. Total enthalpy associated with the melting of ordered phases in PS was around 3 kcal/mol. Poractant alfa and CHF 5633 melted at significantly lower temperatures than PS, 28 °C and 27 °C respectively. Moreover, while Poractant alfa showed a relatively lower associated enthalpy, in the order of 2 Kcal/mol, the thermotropic transitions occurring in CHF 5633 complexes liberated twice as much enthalpy than PS or Poractant alfa (~4 Kcal/mol). The enthalpy associated with the phase transition depends on the lipid structure, especially on the packing and order reached by lipids with saturated or unsaturated bonds and the length of the acyl chain (Chiu & Prenner, 2011). The higher enthalpy in CHF 5633 may be related with a particularly efficient segregation of DPPC-enriched ordered phases. Pure DPPC membranes, for instance, have an enthalpy for their order-to-disorder phase transition of about 8-9 Kcal/mol (Mabrey & Sturtevant, 1976).

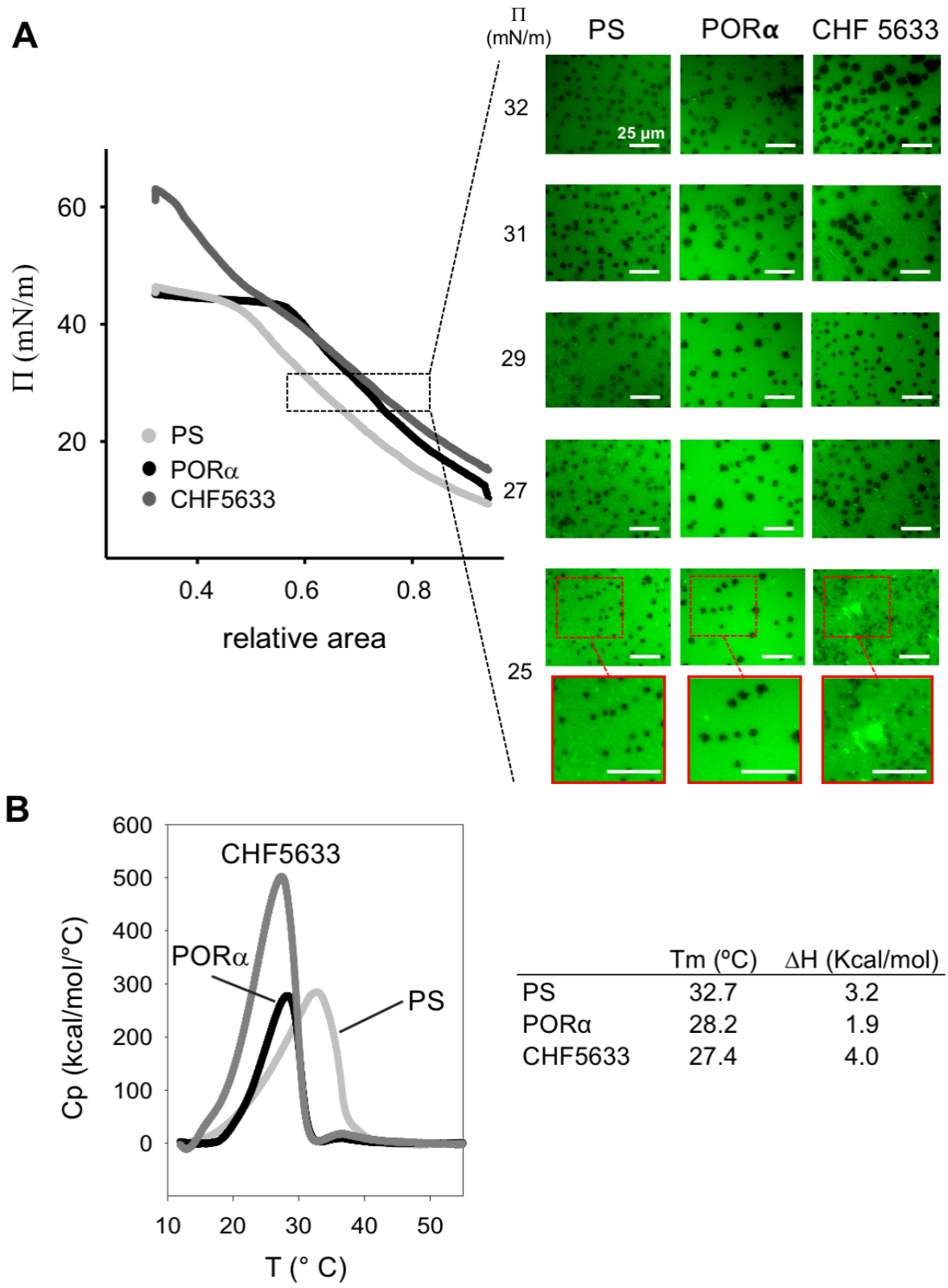

	Tm (ºC)	ΔH (Kcal/mol)
PS	32.7	3.2
PORα	28.2	1.9
CHF5633	27.4	4.0

Figure 35. Phase segregation under compression and thermotropic behaviour of surfactants. (A) On the left a representative compression isotherm of films formed by Poractant alfa, PS or CHF 5633 are compared. On the right, lateral micro-structure of surfactant films (doped with 1% of NBD-PC) compressed to different surface pressures and observed under a epifluorescence microscope**. (B)** Thermotropic properties of surfactant suspensions as analysed by DSC. A representative peak from three replicates is shown. Abbreviations: PS, purified porcine surfactant; PORα, Poractant alfa, Π, surface pressure; Cp, Specific heat capacity; T_m, melting temperature; ΔH, enthalpy associated to the system.

Discussion

In this third chapter, the functional and structural properties of CHF 5633, a new synthetic clinical surfactant, were investigated in comparison with PS and the clinical surfactant Poractant alfa. The latter is a widely available surfactant obtained by minced porcine lungs, which effectiveness in neonatal critical care was suggested by European guidelines and evidence-based data (Foligno & De Luca, 2020; Sweet *et al.*, 2019).

The lipid-protein content and the structure of lung surfactant determine its three crucial biophysical properties: (1) a rapid adsorption towards the air-liquid interface, (2) an optimal reorganisation under breathing-like interfacial compression and expansion, producing a minimal surface tension < 5 mN/m at the end of exhalation, and (3) a proper re-adsorption and re-spreading of material excluded from the interface during compression at the subsequent expansion (inhalation) (Autilio & Pérez-Gil, 2019). On this basis, the high percentage of DPPC and POPG in CHF 5633, along with the only presence of the two hydrophobic peptides define its particular biophysical performance. For surfactant to fulfil an optimal interfacial adsorption, along with the two hydrophobic proteins SP-B and SP-C, SP-A seems also to play a role. In detail, the collectin isoform SP-A1 is important to sustain a packed reservoir interconnected to the interface, thus contributing to adsorption and expansion of new material during each compression cycle (Lopez-Rodriguez *et al.*, 2016b). In this regard, the presence of SP-A may explain the best rates of both adsorption and accumulation at the interface of PS, when compared with the other two collectin-free clinical materials. Poractant alfa is obtained by an organic extract of porcine lung surfactant and during this procedure all hydrophilic proteins are depleted. This explains its slower adsorption and accumulation rate at very limiting lipid concentration (0.15 mg/mL) in the SAT experiments. However, when compared to CHF 5633, this material adsorbed quicker. This is likely due to the presence of the full SP-B protein that can organise itself in oligomeric forms, originating rings connecting contiguous surfactant membranes to enhance lipid transfer into the air-liquid interface (Olmeda *et al.*, 2015). Conversely, Mini-B lacks the central sequence of the mature SP-B, whose residues are involved in the structural and functional dimerisation that generate dodecamers as suggested by the current model (Liekkinen *et al.*, 2020).

Moreover, as it happens for the adsorption, during spreading experiments, the application of low amounts of CHF 5633 at the interface was related with a worse initial performance of this material in the Wilhelmy balance. This is probably due to: (1) the higher content of DPPC, that is around 50% by mass compared to PS and PORα (in which DPPC accounts for around 40% (Sato & Ikegami, 2012)) which makes the system less dynamic due to its saturated acyl chains, particularly when tested at 25 °C; (2) the nature (synthetic fragment vs native) and content (0.2% vs 1% in PS/Poractant alfa) of the SP-B analogue. However, this worse performance of the synthetic surfactant only emerged under limiting conditions and was absent when higher concentration and doses of material were applied at 37 °C, as confirmed in both *in vivo* and *in vitro* previous results (Ricci *et al*, 2017). In this line, when testing CHF 5633 at 10 mg/mL in the CBS, an optimal performance was observed during post-expansion and dynamic cycles, reaching low surface tension values with no hysteresis and low relative area reduction. Interestingly, the particular shape of the isotherm under interfacial compression suggests that once a critical lateral pressure is reached, POPG could be excluded, maintaining highly packed DPPC at the interface with very low compressibility. This preferential exclusion

of POPG was confirmed by the bright spots at the structure of the film observed under the epifluorescence microscope.

Thus, cooperative exclusion of POPG would leave a film mainly composed of DPPC at the air-liquid interface, thus contributing to a quick fall in surface tension to extremely low values. Excluded POPG would remain connected to the interface, presumably through the participation of surfactant peptides, contributing to a reversible reinsertion when the interface is re-opened during expansion. Typically, plateaus in the compression isotherms of surfactant films are associated with lateral or three-dimensional structural transitions preceding the acquisition of the non-compressible states required to reach the minimal surface tension (maximal lateral pressures). Such plateaus exhibit a variable degree of hysteresis in animal-derived surfactants, which is indicative of the work necessary to promote the film transformation upon compression (Wang *et al*, 2007). However, the plateau in the CHF 5633 isotherm was clearly non-hysteretic, suggesting that the structural transition producing the plateau is perfectly reversible. This means that the reorganisation of material under compression is not related to a significant loss of energy and POPG remains associated to the interface. This is probably mediated by the two hydrophobic peptides, competent to establish ionic interactions among the basic amino acids (with the same net charge of native porcine proteins, see **Figure 9**) of the proteins and the anionic head of POPG, providing optimal activity during the following re-extension.

The lateral structure of the CHF 5633 films was also similar to those of animal-derived surfactants, confirming the importance of the two peptides for counteracting the negative charge of POPG and facilitating both lipid clustering and domain condensation (Cruz *et al*, 2000). Interestingly, the bright spots revealed during the interfacial compression of CHF 5633 may be due to light scattering under the epifluorescence microscope. This may suggest the presence of three-dimensional protruding surfactant structures attached to the surface film, probably enriched in the less surface-active species POPG. These structures may serve as a source of material for lipid re-adsorption during expansion and help for more effective exclusion of lipids difficult to pack during compression. The low melting temperature of CHF 5633, around 27 °C, is probably due to the high amount of POPG characterised by a T_m of -2°C. Moreover, the higher cooperativity (less broaden) of the thermogram of both Poractant alfa and the synthetic mixture compared to PS may be due to the absence of cholesterol that affect lipid populations by segregating them with different packing and melting properties (de la Serna *et al.*, 2013).

When the three materials were compared in the presence of serum, CHF 5633 showed higher resistance to inhibition than Poractant alfa under very limiting concentrations (0.15 mg/mL). PS was more inhibited by serum components only in static conditions when the adsorption and accumulation of very diluted material was assayed by SAT. Conversely, at higher concentration (10 mg/mL) in CBS experiments, PS showed the best adsorption and dynamic activity in the presence of serum. Interestingly, Poractant alfa seemed to exhibit the worst performance amongst the materials tested in agreement with previous *ex vivo* results (Seehase *et al.*, 2012). In detail, both adsorption and accumulation as well as the dynamic properties of Poractant alfa were strongly impaired in the presence of serum regardless of the material concentration. Surfacen, another natural clinical surfactant preparation, derived from BAL of porcine lungs, shows the same kind of dynamic isotherms as Poractant alfa in presence of serum (Lugones *et al*, 2018). Conversely, CHF 5633 films, though needing a larger compression extent, have still no hysteretic isotherms when subjected to dynamic cycles in the presence of serum.

It can be argued that, due to the high percentage of POPG (50%) in CHF 5633, a higher reduction of the interface is needed to exclude those lipid species likely with the assistance of the positively charged peptides. However, in spite of the higher work, this process may also facilitate the exclusion of negatively charged proteins, such as albumin that represent the most abundant protein in serum (55%). These components may be more easily swept along from the interface due to the charge repulsion with the excluded POPG. For the same reason, the high content of negative charges in CHF 5633 compared to Poractant alfa and PS (50 vs ~10%) may also promote a better adsorption and accumulation at the interface of this material. This probably occurs by displacing more easily serum albumin from the surface or by inhibiting albumin adsorption when POPG covers the interface. In support of this, the adsorption of bovine albumin to microcapsules is lowest on surfaces characterised by the same isoelectric point (Muramatsu & Kondo, 1992).

In spite of these interesting results, several limitations should be considered: (1) whether the two protein analogues have similar or distinct contribution to CHF 5633 film structure and interfacial performance is still to be established, (2) further experiments exchanging POPG by zwitterionic lipid species may also help to identify the contribution of negative charges in the resistance of CHF 5633 to serum, (3) the use of single serum inhibiting molecules (e.g. albumin or $sPLA_2$ IIA) may provide deeper understanding on which is the most important inhibiting agent involved in PS and Poractant alfa inactivation, and (4) incubating the clinical surfactants directly with BALs from ARDS patients may help to better recreate a physiological-like inhibitory context.

In summary, CHF 5633 is a synthetic surfactant with great potential to be used in clinical practice. The higher percentage of POPG (50%) contained in the mixture may fulfil an anti-inflammatory effect (Cañadas *et al.*, 2020) as well as create an electrostatic repulsion against negatively charged serum proteins. At the same time, its synthetic and reproducible composition makes it a good candidate for future clinical trials in the treatment of adult ARDS when high and multiple doses are needed, especially upon indirect ARDS when the injury in the vascular endothelium causes a protein-rich oedema fluid leaking into alveoli. Moreover, CHF 5633 resistance to inactivation may also suggest its potential utility in the early stages of MAS when lung surfactant is early impaired by the pro-inflammatory challenge.

Part of this text has been published in the following papers:

Autilio C, Echaide M, et al., PLoS One, 2018, 13(2):e0192295

Autilio C, Shankar-Aguilera S, et al., AJP Lung. 2019, 316(3):L498-L505

Autilio C, Echaide M, et al., Ther Hypothermia Temp Manag. 2020, 10(3):186-189

Chapter IV

"Therapeutic hypothermia improves surfactant activity in neonates with and without ARDS"

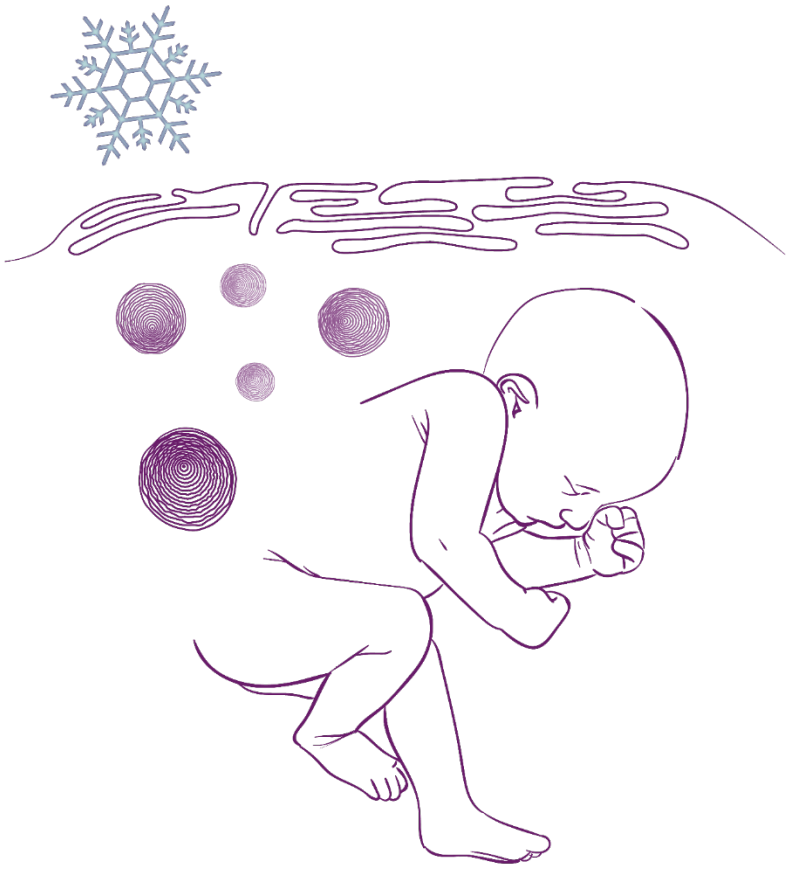

Introduction

In the third chapter the biophysical performance of CHF 5633, a novel synthetic surfactant preparation launched by Chiesi Farmaceutici S.p.A., was analysed in the presence and absence of serum as inhibiting agent. This therapeutic surfactant shows optimal interfacial properties comparable to those of PS and Poractant alfa. Moreover, the synthetic lipid-protein composition of CHF 5633 endorses a higher resistance to serum inhibition in terms of interfacial saturation and dynamic proprieties, compared to those of animal-derived clinical surfactants. Those results confirm previous studies performed in animal models (Seehase *et al.*, 2012) and support the use of CHF 5633 as a promising replacement therapy for lung disorders characterised by a high inflammatory status. In this regard, as demonstrated for severe MAS, several components found in plasma and serum such as total proteins and $sPLA_2$ tend to early increase after a direct lung injury. Those compounds may inactivate surfactant properties, partially explaining the failure of surfactant replacement in ARDS clinical trials to date (Meng *et al.*, 2019; Raghavendran *et al.*, 2011). Conversely, unlike animal-derived preparations, CHF 5633 interfacial properties are significantly less affected by serum, probably due to its lipid composition characterised by high proportion of the negatively charged POPG and the surface-active DPPC.

In this scenario, and together with early administration of exogenous therapeutic surfactants more or less resistant to inhibition, other treatments able to promptly reduce lung inflammation may be considered in both MAS and direct ARDS. On this basis, therapeutic hypothermia can be proposed as a good therapeutic option. This treatment is used as an effective method to limit brain injury after certain types of cardiac arrest and perinatal asphyxia, by decreasing patient body temperature from 37 °C to 33.5 °C (Arrich *et al*, 2016; Pietrini *et al*, 2012). Cooling in neonates with encephalopathy due to perinatal asphyxia is usually applied as whole-body hypothermia (WBH), starting early from birth and continuing for the following three days (Jacobs *et al*, 2013). Although the beneficial effect of this treatment on the neonatal brain is well known, few data are available about the effect of hypothermia in other organs.

As for the lung, preliminary studies suggest possible benefits in cooled patients suffering of ARDS (Hayek *et al*, 2017; Karnatovskaia *et al*, 2014; Slack *et al*, 2017; White *et al*, 2017) or necrotising enterocolitis (Hall *et al*, 2010). Moreover, a reduction in both IL-6 and IL-8, mainly after 72 hours of WBH, was demonstrated in asphyxiated neonates (De Luca *et al.*, 2014). At the same time, cooling seems to exert a protecting effect against lung injury in preterm lambs. This treatment also ameliorates respiratory mechanics and decreases lung tissue inflammation in other animal models (Ball *et al*, 2010; Cruces *et al*, 2013; Hong *et al*, 2005). Moreover, recent evidences demonstrate an improvement in several clinical outcomes such as reduction of respiratory support and hospital stay in cooled neonates with MAS (De Luca *et al*, 2016).

Thus, controlled hypothermia may be theoretically effective in those respiratory conditions characterised by high lung tissue inflammation with a putative protective role also for the lung surfactant system. In this line, previous human and animal data sustain the following evidences: (1) an increase in neonatal surfactant adsorption/accumulation at the air-liquid interface that occurs after 48h of WBH with a reduced surface saturation at 72 hours (De Luca *et al.*, 2014); (2) the *in vivo* DPPC replacement is not altered during therapeutic hypothermia of neonates (Nespeca *et al*, 2016); (3) during torpor, warm-active dunnarts show a rapid increase in both cholesterol (4 hours) and disaturated (8 hours) species of lung surfactant (Langman *et al*, 1996); (4) an increase in total surfactant phospholipid content and

certain unsaturated lipid species occurs during hibernation of summer-active ground squirrels, promoting optimal interfacial properties (Suri *et al*, 2012); (5) the surface activity of rabbit lung extracts tends to improve upon decreasing temperature from 40 to 15° C (Lempert & Macklem, 1971).

However, considering these previous evidences, apart from the data on adsorption kinetics by SAT (De Luca *et al.*, 2014), no detailed studies have been reported on the biophysical performance and composition of lung surfactant in neonates during WBH. In this line, surfactant initial adsorption can be increased by certain lipids, such as cholesterol, but simultaneously impairing its capability to reduce surface tension under compression (Yu & Possmayer, 1993) at excessive fluidification levels (Lopez-Rodriguez *et al.*, 2011). Thus, in this fourth chapter both adsorption and breathing-like dynamic properties of lung surfactant of asphyxiated neonates were investigated under WBH. Samples were tested before cooling, each 24 hours during cooling and 3 hours after rewarming. The therapeutic hypothermia-mediated effects on surfactant activity were also studied per se in a baby with meconium-stained amniotic fluid (MSAF) who did not develop MAS and in two neonates with severe MAS receiving replacement therapy with clinical surfactant. Moreover, the changes in surfactant lipid species and proteins as well as the activity of $sPLA_2$ were analysed at the peak of hypothermia effect in healthy neonates.

Key techniques and patients

Enrolled patients and clinical parameters

The clinical part of the present study (patients' enrolment, collection of clinical parameters, lavages collection and microbiological testing) was performed by the NICU team from the Division of Pediatrics and Neonatal Critical Care directed by Prof. Daniele De Luca at "A.Béclère" Medical Center of Paris. The study protocol was approved by the local ethical committee of the South Paris University Hospitals (n. PP13-046) and parental consent was obtained upon NICU admission.

Eleven and twelve asphyxiated neonates were enrolled to perform biophysical and compositional studies, respectively. Those babies were admitted to NICU and required WBH. Exclusion criteria were congenital lung disease, complex malformations and blood-staining of nBAL samples. WBH has been provided at 3 hours of life following TOBY trial criteria (Azzopardi *et al*, 2009) using whole body, core temperature servo-controlled, water-filled mattresses set at 33.5 °C. The asphyxiated neonates needing WBH were kept intubated and ventilated until complete rewarming (at 37 °C), even though they did not need that for pulmonary reason (De Luca *et al.*, 2014), in order to reduce the metabolic demand. Extubating always takes place 6 hours after rewarming.

Twenty patients did not show any lung disease (NLD group). They had normal amniotic fluid and no signs of infection; chest imaging and clinical examination were always normal and they never needed any supplemental oxygen. One cooled asphyxiated patient showed MSAF, but did not develop MAS.

Two patients were diagnosed with meconium aspiration (MAS group), as they had meconium-stained amniotic fluid and secretions upon tracheal suctioning; they developed respiratory distress early from birth and had chest X-rays or lung ultrasound (Piastra *et al.*,

2014) typical for MAS. As a therapeutic intervention, these patients received BAL (Dargaville *et al.*, 2011) with diluted Poractant alfa (Curosurf, Chiesi Farmaceutici, Parma, Italy; 75 mg/kg in 15 mL/kg 0.9% saline), immediately followed by 200 mg/kg Poractant alfa within the first 24 hours of life. For these patients the first BAL was performed before the onset of WBH and before any surfactant therapy. All patients were ventilated as described in chapter II.

Sample collection and handling

All patients were subjected to a nBAL before the onset of WBH and then every 24 hours to perform microbiological surveillance or secretions removal. The last nBAL was performed just before extubation. nBALs were done only when neonates needed to be suctioned for clinical reasons: no procedure was performed solely for the study purposes and no change was provided to the routine clinical assistance. The first nBAL was considered as control measurement under normothermia. Lavages were performed with a well-standardised procedure according to the European Respiratory Society advices (de Blic *et al.*, 2000) and detailed in Materials and Methods chapter.

Around 200 μL of nBALs were sent for microbiological testing of sterility, resulting negative. The remaining lavage was immediately centrifuged at 800 g for 10 minutes to discard cell pellets, frozen at -80°C and carefully thawed before the start of each analysis.

As for the biophysical study, both surfactant large and small aggregates of 11 neonates (8 NLD, 2 MAS, 1 MSAF) were used as collected together. With this purpose, nBAL supernatants were ultracentrifuged at 100,000 g for 1 hour at 4 °C. The resulting pellet was diluted to reach a total PC concentration of 8 mg/mL that was employed for the analysis. The dilution was performed with 5 mM Tris buffer, containing 150 mM NaCl at pH 7.4. This limiting concentration of material was used to enhance differences among the two experimental temperatures (37±0.5 and 33±0.5 °C) within each sample. PC and cholesterol were assayed in triplicate using enzymatic colorimetric methods. After surfactant precipitation, around 50 μg of PC was recovered from each sample. The biophysical activity was evaluated applying ~200 nL of surfactant suspension (8 mg/mL) in the CBS operated at a frequency of 20 cycles/min at 37 °C. Previous results using human surfactant samples from nBALs revealed main differences in biophysical activity during initial adsorption and dynamic cycles; the interfacial study was then focused on these two parameters.

As for the compositional study of lung surfactant and $sPLA_2$ profile under therapeutic hypothermia, nBALs were used as follows. nBALs collected pre and after 72 hours of WBH from 4 neonates were precipitated at ~22,000 g for 1 hour at 4 °C to perform a lipidomic analysis by LC-HRMS and to assess the content of SP-B and SP-C by PAGE. The latter experiment was performed as described in chapter II, loading 4 μg of PC per sample and 50 ng of purified human SP-B and SP-C from a patient with alveolar proteinosis, as a reference. LC-HRMS was carried out at RUBAM at the the Department of Biomedicinal Chemistry (IQAC-CSIC) in Barcelona under the supervision of Dr. Josefina Casas.

In other experiments, nBALs collected pre and after 72 hours of WBH from 8 neonates were used to assay the content of SP-A and the global activity of $sPLA_2$. PC was assayed in triplicate, directly in nBALs using an enzymatic colorimetric method. SP-A and $sPLA_2$ activity were normalised for total PC content. Further details of these techniques and materials are described in the Materials and Methods chapter.

Statistical Analyses

Data were assayed for normality with the Shapiro-Wilk test and expressed as mean (SD) or median [interquartile range] when appropriate. As for the CBS analysis, comparisons among different temperatures and time points were carried out by Two-way ANOVA, followed by paired- or unpaired- t test as appropriate. As for the compositional study, paired t test or Mann-Whitney U test were used according to data distribution to compare pre and 72 hours results during hypothermia treatment. Correlations were performed using Pearson's r-coefficient. Analyses were carried out using SPSS 15.0 (SPSS, Chicago, Illinois, USA). A p value < 0.05 was considered significant.

Whole body hypothermia enhances lung surfactant activity in neonates with and without meconial ARDS in a time-dependent manner

The demographic characteristics of the ten patients (8 NLD and 2 MAS) and 1 MSAF baby enrolled for the CBS study are detailed in **Table 9**.

Figure 35 shows the initial adsorption of surfactant material isolated from nBALs of NLD babies with clean amniotic fluids (NLD group), the MSAF neonate and the two MAS babies along with the content of cholesterol normalised for total PC.

Demographic characteristics	n=10	n=1
GA (weeks), mean (SD)	39 (1.5)	41
Birth weight, g, mean (SD)	3,138 (251)	3,840
Sex	4 females/6 males	1 female
Cesarean section, %	7 (70%)	yes
5-minute Apgar score, mean (SD)	5 (1.9)	4
SNAPPE-II, mean (SD)	52 (10.5)	50
Diagnosis	8 NLD, 2 MAS	NLD (MSAF)

Table 9. Basic characteristics of all enrolled neonates. Data are expressed as mean (standard deviation) or numbers (%). NLD neonates were intubated for delivery room resuscitation and kept ventilated to reduce their metabolic demand during hypothermia. Abbreviations: GA, gestational age; SNAPPE-II, Score for Neonatal Acute Physiology-Perinatal Extension-II; NLD, no lung disease; MAS, meconium aspiration syndrome.

When material of NLD babies was tested at the 2 experimental temperatures, an overall significant impairment was detected at 33 °C regardless of the time point analysed ($p< 0.001$). The equilibrium surface tension after 5 minutes from the injection of material was around 38-42 mN/m at 37 °C and 40-45 mN/m at 33 °C with a delay of ~5 mN/m assessing samples under hypothermia condition. Interestingly, a significant impairment in the initial adsorption after 48 hours of WBH ($p= 0.002$, orange line) emerged regardless of the experimental temperature when comparing the different time points (pre, 24, 48, 74 hours and post). At the same time, cholesterol/PC ratios were around 20-25% and did not significantly change during WBH, but showed a tendency to rise at 24 hours (in 5 out of 8 neonates) and then decreasing after 48 hours (**Figure 35**, first row).

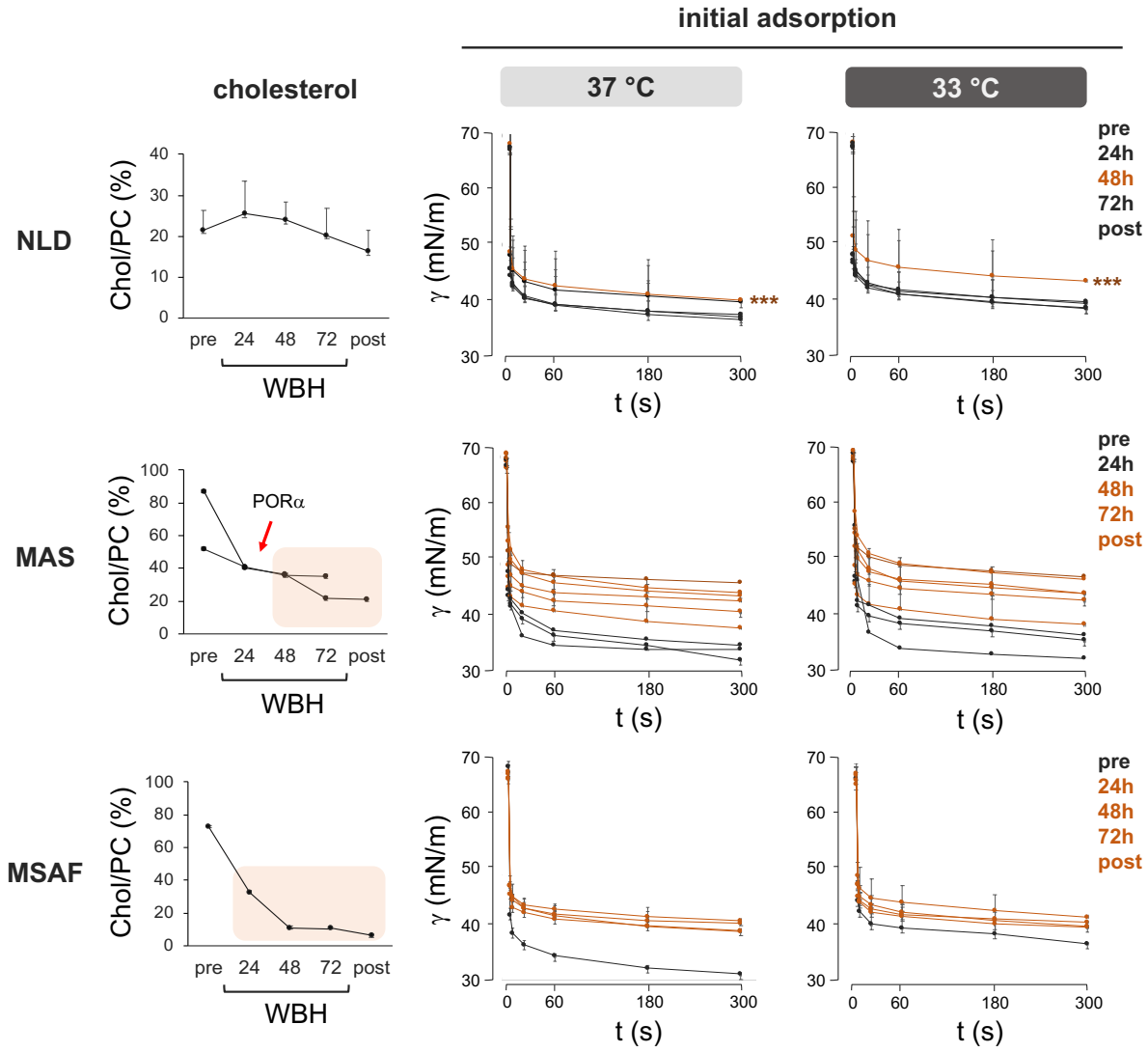

Figure 35. Initial adsorption and cholesterol content of surfactants from NLD, MAS and MSAF neonates upon WBH. Cholesterol content: data were normalised for the content in PC and expressed as weight percentage with respect to total PC. As for NLD babies, a tendency to increase cholesterol after one day was observed: paired t test (pre vs 24 hours), p= 0.1. Initial adsorption: around 200 μL of material at 8 mg/mL was injecting onto the bubble. In the first row, the mean and SD of results from 8 NLD neonates is shown for each time point and temperature condition. In the second and third rows, the means and SD of the three experimental replicates per neonate are shown. Orange line represent low-performance adsorption. The red arrow shows the moment of the replacement therapy with Poractant alfa. Two-way ANOVA test: temperature, p< 0.001; time: ***p= 0.002, orange asterisk. Abbreviations: NLD, no lung disease; MAS, meconium aspiration syndrome; MSAF, meconium stained amniotic fluid; WBH, whole body hypothermia, Chol, cholesterol; PC, phosphatidylcholine; PORα, Poractant alfa, γ, surface tension.

When samples from the two MAS neonates were analysed, the adsorption was also reduced when materials were tested at 33 °C compared with 37 °C. However, a better performance (30-35 mN/m) was observed pre and after 24 hours of WBH compared to the other time points (40-47 mN/m) especially when material was tested at 37 °C. At the same time, cholesterol levels were very high and tended to decrease only at 48 hours, reaching values lower than 40%. Thus, before MAS neonates were subjecting to therapeutic hypothermia, and in the first day of cooling immediately after Poractant alfa therapy, the

content of the sterol in surfactant films was more than double the amount detected in NLD neonates, starting to decrease after the second day of cooling. This is probably due to the presence of cholesterol from meconium and may explain the better adsorption of surfactant at increased fluidity of the system (de la Serna *et al.*, 2004). Moreover, this also makes clear why this better adsorption is not so evident at 33 °C due to the counterbalancing action on fluidity at low temperatures (Neidleman, 1987). This hypothesis is corroborated by the similar results obtained for the MSAF baby. As for this neonate, who presented meconium in her amniotic fluid, but nor developed the syndrome, neither received Poractant alfa, surfactant pre-hypothermia was characterised by high cholesterol/PC ratios with an evident improvement in initial adsorption, especially at 37 °C. This neonate showed cholesterol levels as well as an adsorption profile similar to those of NLD babies after the first 24 hours. Conversely, surfactants from the two MAS neonates reached comparable values only after 72 hours of hypothermia (20% cholesterol/PC and 37 and 43 mN/m).

Moving to the dynamic interfacial properties, the overall activity of NLD neonates at 37 °C was worse than that observed for similar babies in chapter II. This result is due to the different concentration of surfactant tested (12 vs 8 mg/mL). However, this experimental condition was deliberately chosen to investigate on subtle differences in the interfacial activity between 33 and 37 °C. This was only possible by using a very diluted material to avoid the saturation of the air-liquid interface. The minimum surface tension reached under the 20 dynamic cycles are shown for the different WBH time points (pre, 24, 48, 74 hours and post) and experimental temperatures (37 and 33 °C) in **Figure 36**. When subjecting materials from the 8 NLD neonates (s1-s8) to breathing-like compression expansion cycles (20 cycles/min), apart from one neonate (s8), the remaining surfactants show a similar behaviour. Material tested at 37 °C mostly did not change its dynamic properties, maintaining minimum surface tensions around 20 mN/m regardless of the time point and the experimental temperature. Conversely, apart from sample 6 for which the dynamic properties improved at both 33 and 37 °C, there was always a tendency for the dynamic interfacial activity to improve when reducing the experimental temperature. Moreover, this temperature-mediated improvement started to be very clear after at least 72 hours of WBH and remained during rewarming, namely in the first 6 hours post WBH treatment. These results are highlighted in orange in **Figure 36**.

The same behaviour was observed for the MSAF baby and in the two MAS neonates, showing an early effect at 48 hours for one of the two babies with severe meconium aspiration syndrome. Moreover, as observed in the picture (**Figure 36**, on the lower right), surfactants collected overtime from the MSAF baby underwent an evident change in colour after 48 hours. This suggests a normalisation of surfactant and its depuration from meconium components after at least two days of hypothermia treatment.

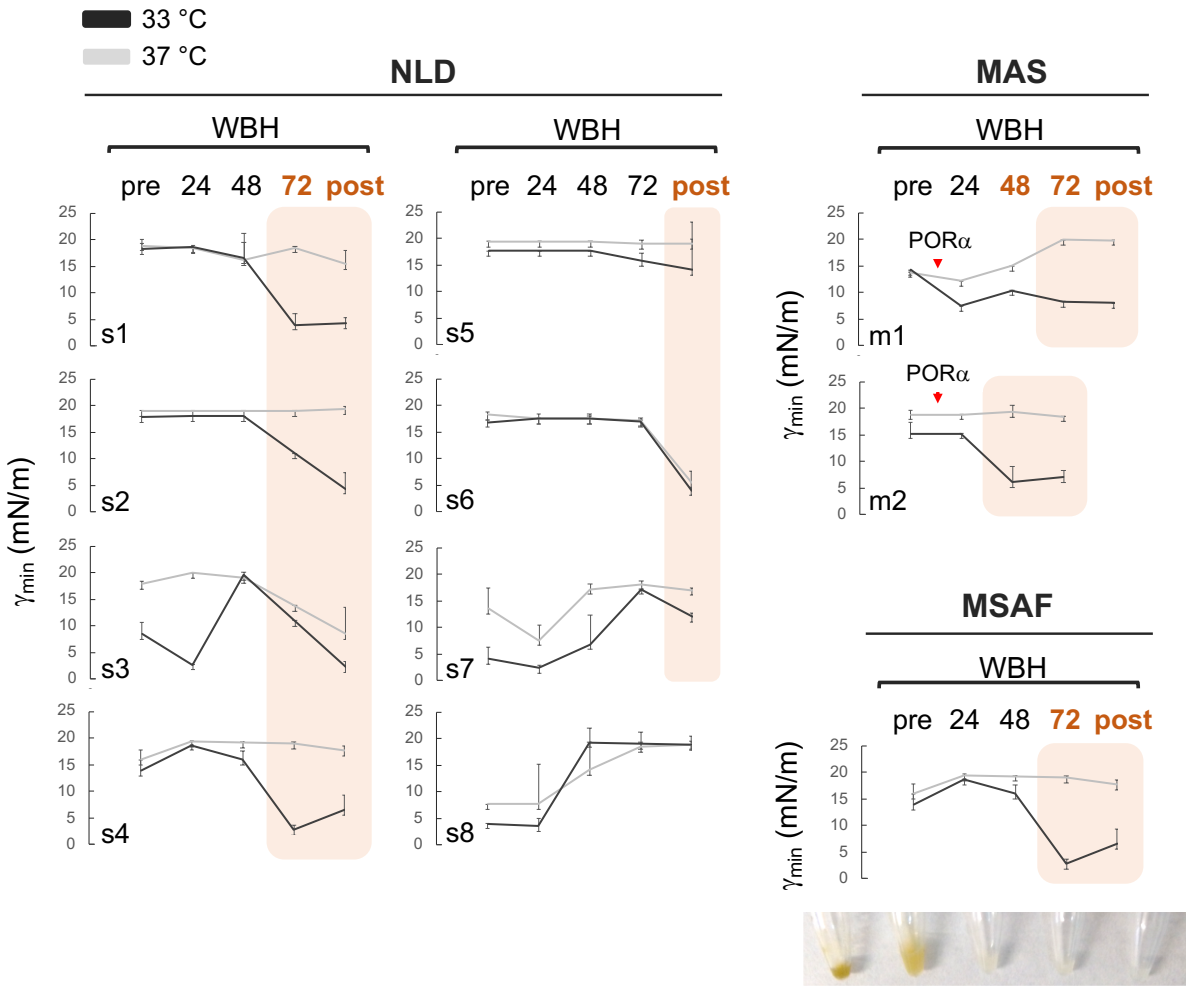

Figure 36. Minimum surface tensions under breathing-like compression expansion cycles reached by surfactants from NLD, MAS and MSAF neonates upon WBH. Light-grey and dark grey colours represent values obtained at 37 and 33 °C, respectively. Black vertical lines represent the mean and SD after averaging three experimental replicates. The red arrow shows the moment of the replacement therapy with Poractant alfa. The time points with a temperature-mediated improvement in dynamic properties of surfactant are highlighted in orange. The changes in colour from green to white of surfactant from MSAF neonate under WBH were also shown. Abbreviations: NLD, no lung disease; MAS, meconium aspiration syndrome; MSAF, meconium stained amniotic fluid; WBH, whole body hypothermia; PORα, Poractant alfa, γ_{min}, minimum surface tension; s, samples from NLD neonates; m, samples from MAS neonates.

As extensively discussed in the previous chapters, the minimum surface tension values give reductive information about the reorganisation of material undergoing interfacial compression as well as its depuration from less active lipid species. Thus, the isotherm behaviours of the different samples were compared in more detail, focusing on the compressibility of the materials.

Figure 37 shows the γ-area relationship of representative replicates from one MAS and the MSAF baby tested pre and after 72 hours of WBH at the two experimental conditions, 33 and 37 °C. These two neonates were selected since in the two cases surfactant was stained by meconium pre-hypothermia, although MSAF patient did not develop MAS. However, the first baby (first row) developed MAS and received Poractant alfa within the first 24 hours, whereas the second one (second row) maintained the clinical parameters similar to NLD neonates and

did not develop MAS. In this way, the *in vivo* effect of hypothermia treatment on meconium-rich surfactant could be compared, regardless of the MAS-related inflammation and the replacement therapy.

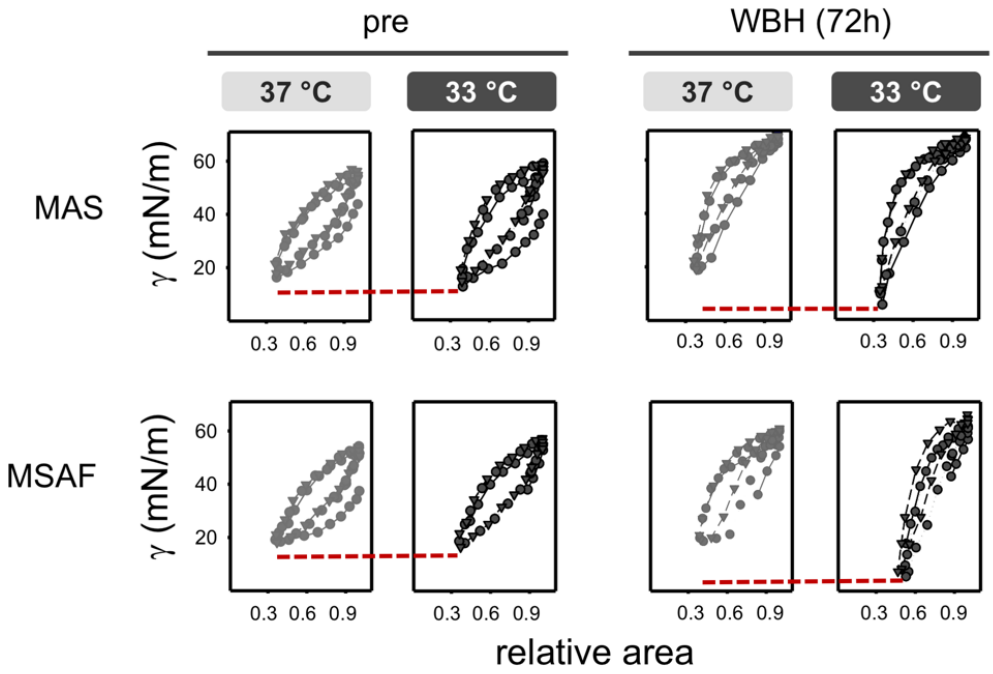

Figure 37. Representative dynamic γ-area isotherms from one MAS and one MSAF neonates pre and after 72 hours of WBH. Grey and dark-grey colours represent the sample tested at 37 and 33 °C, respectively. Circles depict the first and 10th cycles, whereas inverted triangle shows the 20th cycle. Dashed red lines highlight the differences in minimum surface tension among the two experimental temperatures. Abbreviations: MAS, meconium aspiration syndrome; MSAF, meconium stained amniotic fluid; WBH, whole body hypothermia; PORα, Poractant alfa, γ, surface tension.

The activity of samples tested pre WBH treatment showed a subtle tendency to improve when assayed at hypothermia temperature (33 °C) compared with 37 °C. This occurred without evident changes in compressibility, maintaining an evident hysteresis that resembles surfactants from severe MAS babies as tested in chapter II. Interestingly, as shown by dashed red lines, this temperature-mediated improvement in dynamic interfacial properties became very evident after 72 hours of WBH with a drastic reduction in compressibility upon all cycles, especially during the 20th one. This suggests that surfactant cooled *in vivo* for three days undergoes a particular compositional change that favours the exclusion of less active lipid species from the interface at 33 °C, but not at 37 °C. Essentially, it could be argued that the WBH-mediated compositional changes and the operation of a reduced temperature have a synergistic effect on the dynamic activity of material, promoting this temperature-mediated result. Moreover, since this mechanism was still evident after rewarming of the neonates, it is probably related to both rapid changes in cholesterol and variations in other surfactant components that need more than 48 hours to occur.

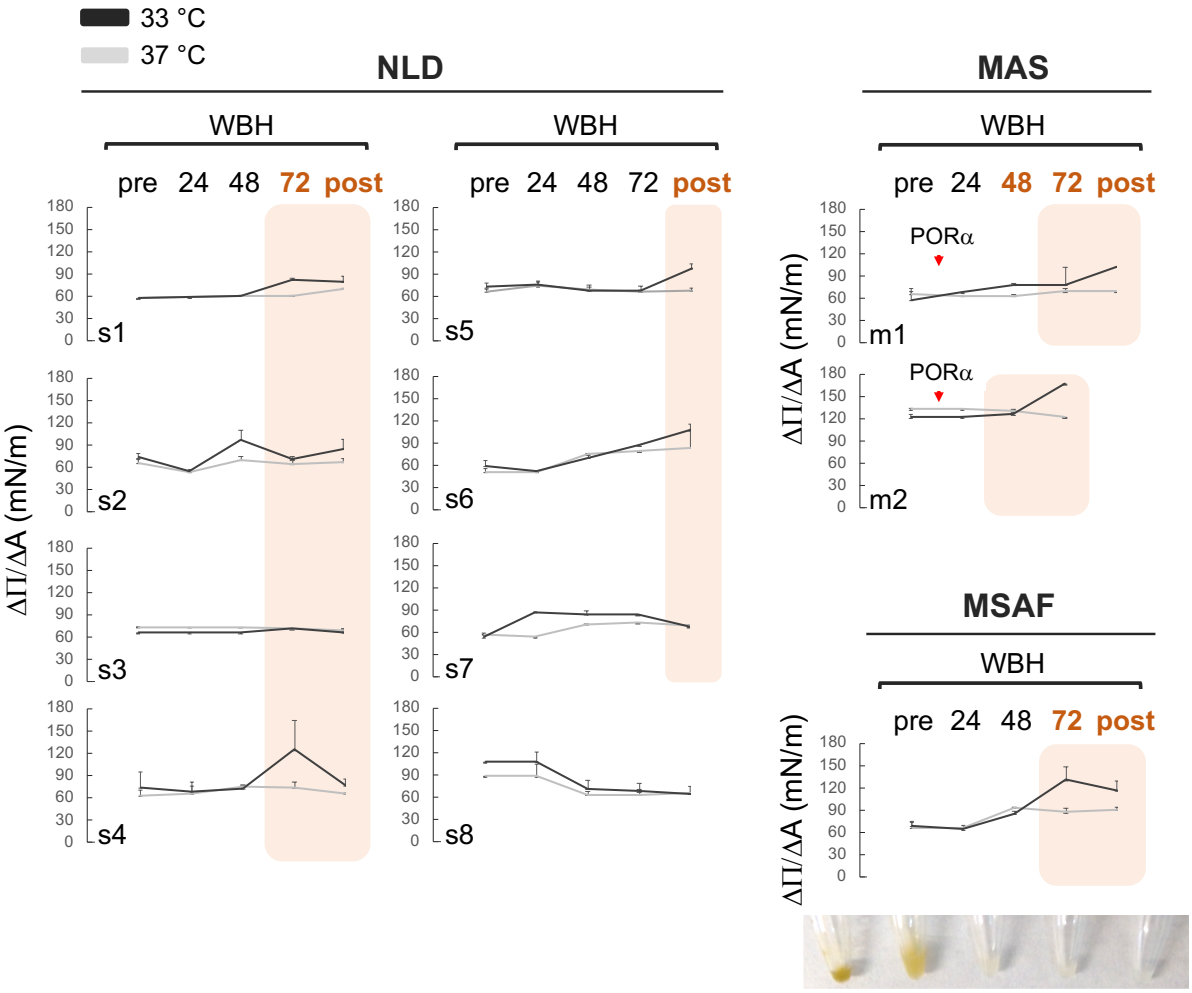

Figure 38. Compressibility of surfactants from NLD, MAS and MSAF neonates. Compressibility was indirectly calculated as the slope value of the line passing through the minimum and maximum points of compression during the 20th dynamic cycle. Light-grey and dark grey colours represent values obtained at 37 and 33 °C, respectively. Black vertical lines represent the mean and SD of three experimental replicates. The red arrow shows the moment of the replacement therapy with Poractant alfa. The time points with a temperature-mediated improvement in compressibility of surfactant are highlighted in orange. The changes in colour from green to white of surfactant from MSAF neonate under WBH were also shown. Abbreviations: NLD, no lung disease; MAS, meconium aspiration syndrome; MSAF, meconium stained amniotic fluid; WBH, whole body hypothermia; PORα, Poractant alfa, Π, pression; A, area s, samples from NLD neonates; m, samples from MAS neonates.

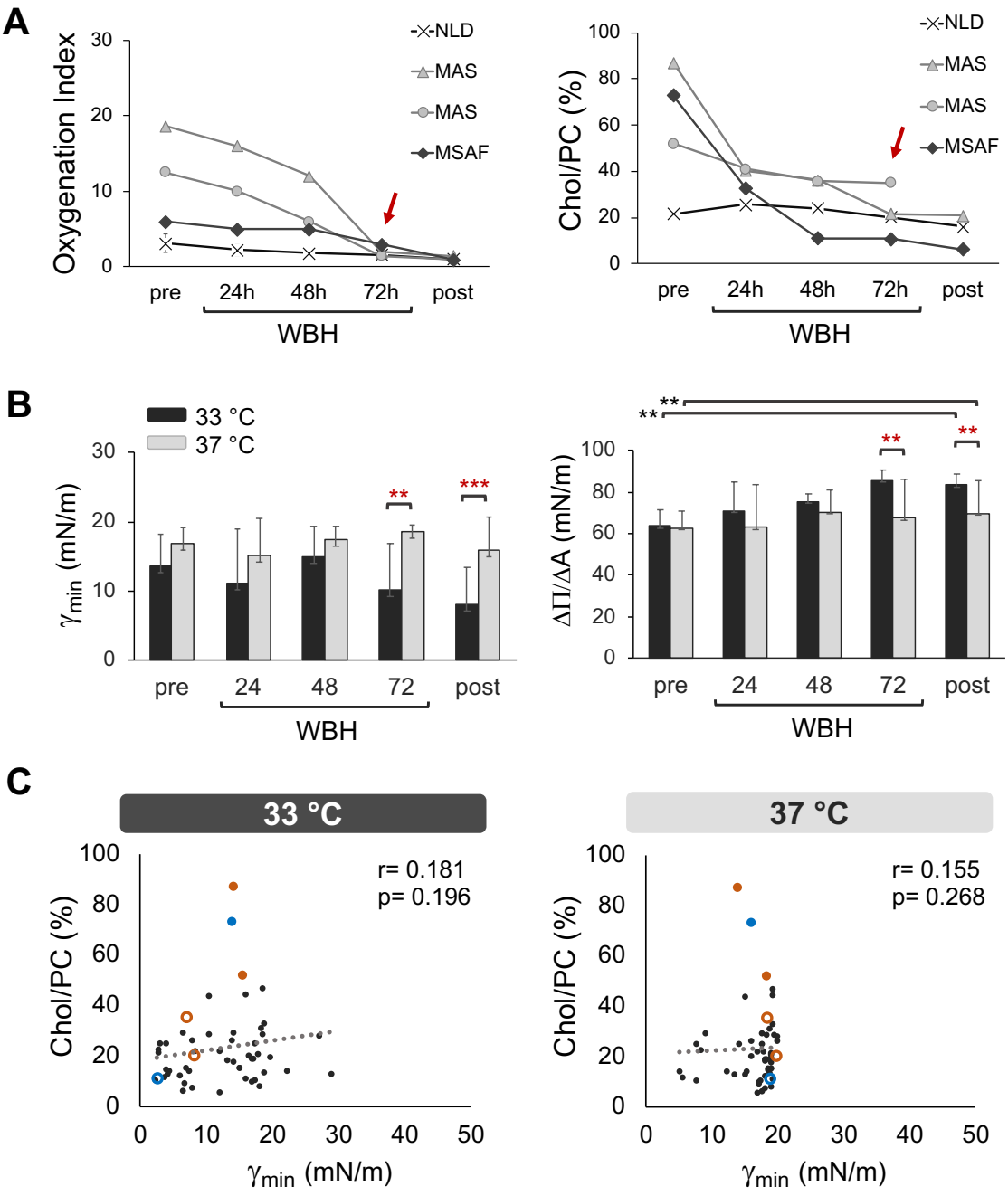

Figure 39. Dynamic properties, cholesterol levels and oxygenation index in all cooled neonates. **(A)** Cholesterol data were normalised for the content in PC and expressed as weight percentage with respect to total PC. Red arrows show the time point of 72 hours of WBH, corresponding to the simultaneous reduction in oxygenation index and cholesterol levels. **(B)** Overtime minimum surface tension and compressibility values at 20th dynamic cycle from all enrolled neonates (8 NLD, 2 MAS and 1 MSAF). Data are expressed as mean and SD. Red asterisks mark significant comparisons between experimental temperatures, whereas black asterisks correspond to comparisons between different time points of WBH. **(C)** Correlation analysis between Cholesterol/PC ratios and minimum surface tension. Full and open orange circles correspond to MAS neonates pre and 72 hours of hypothermia treatment, respectively. Full and open light-blue circles correspond to the MSAF baby pre and 72 hours of hypothermia treatment, respectively. Two-way ANOVA test: temperature, $p< 0.001$; time: $p< 0.001$; post-hoc paired t-test comparisons: ***$p< 0.001$, **$p< 0.01$. The correlation tendency line (black bar) and (ρ) coefficients are also indicated. Abbreviations: NLD, no lung disease; MAS, meconium aspiration syndrome; MSAF, meconium stained amniotic fluid; WBH, whole body hypothermia; γ_{min}, minimum surface tension; Π, pression; A, area; Chol, cholesterol; PC, phosphatidylcholine.

The reduction in compressibility (namely the increase in the slope values of the line passing through the minimum and maximum variations of the area compression) at 33 °C after at least 72 hours of WBH could be detected in the majority of samples tested (**Figure 38**) regardless of the clinical conditions.

Since in the majority of the samples tested, the temperature-mediated improvement of surfactant activity was always observed after at least 72 hours of WBH, regardless of the lung injury, results from all neonates were pooled to perform a statistical analysis. Interestingly, as shown in **Figure 39A**, the oxygenation index of MAS neonates tended to reduce to normal values after 72 hours, reaching the same levels than that of NLD and MSAF babies. Moreover, Cholesterol/PC ratios also decreased at this time point, falling down to levels below 40%. At the same time, after three days of therapeutic hypothermia, the dynamic properties significantly improved in terms of minimum surface tension and compressibility when samples were tested at 33 °C compared to 37 °C (**Figure 39B**). Moreover, there was a significant reduction in compressibility (i.e., increase in the slope value) post hypothermia treatment compared to the pre-WBH situation. This occurred regardless of the experimental temperature.

Although in the case of meconium-rich surfactant (MAS, MSAF) there was an evident decrease in the sterol content at the same time of a better oxygenation index and a lower minimum surface tension, this result was less evident when considering all the enrolled neonates (**Figure 39C**). On this basis, the levels of cholesterol did not correlate with the minimum surface tension regardless of the experimental temperatures. Similar results were obtained when the cholesterol/PC ratios were compared to the compressibility of material expressed as slope values (37 °C, r= -0.140, p= 0.366; 33 °C, r= -0.250, p= 0.09). One reason for the lack of a strong significance could be the low analytical sensitivity of the two colorimetric kits used for assaying the lipids, which best detection method is the lipidomic analysis. However, a tendency to an inverse correlation (p= 0.09) was present for compressibility at 33 °C. This suggests that the reduction in the slope of the isotherm could be related to both the absence of the sterol and the lower temperature.

In vivo changes in surfactant composition and $sPLA_2$ activity after 72 hours of moderate hypothermia suggest a protective role for ARDS

Overall, the aforementioned results rise two open questions: (1) which is the reason for the tendency of surfactant to work better at 33 °C compared with 37 °C, (2) why this tendency becomes significant after 72 hours of WBH and remains significant after rewarming (6 hours) in neonates with and without lung injury. This last point strongly suggests that some slow compositional and/or structural changes take place in surfactant after three days apart from the cholesterol reduction. Starting from these evidences, twelve NLD neonates were enrolled to perform surfactant compositional analysis and investigate on the $sPLA_2$ activity before and after 72 hours of WBH (**Table 10**).

As first step, a lipidomic analysis of lipid classes and subclasses was carried out in 50 μg of PC of isolated large aggregates from nBALs of four babies (4 pre and 4 WBH).

Demographic characteristics	n=12
GA (weeks), mean (SD)	37.5 (1.8)
Birth weight, g, mean (SD)	3,131 (375)
Sex	6 females/6 males
Cesarean section, %	8 (66.7 %)
5-minute Apgar score, mean (SD)	4 (1.9)
SNAPPE-II, mean (SD)	30 (19 - 34)
Diagnosis	NLD

Table 10. Basic characteristics of enrolled NLD neonates. Data are expressed as mean (standard deviation) or numbers (%). NLD neonates were intubated for delivery room resuscitation and kept ventilated to reduce their metabolic demand during hypothermia. Abbreviations: GA, gestational age; SNAPPE-II, Score for Neonatal Acute Physiology-Perinatal Extension-II; NLD, no lung disease.

All species were detectable in the eight samples tested. In detail, to avoid misinterpretations of results due to errors in the starting PC amount, data were expressed as percentage with respect to the total moles of phospholipids instead of absolute values. Similarly, total cholesterol was expressed as percentage with respect to the total moles of phospholipids.

Lipid	NLD pre (n=4)	NLD WBH (n=4)	P value
PC (molar %)	92.6 (3.7)	77.5 (32.6)	0.392
LPC (molar %)	0.19 (0.05)	0.89 (1.44)	0.391
PE (molar %)	0.97 (0.69)	1.65 (1.96)	0.599
LPE (molar %)	0.012 (0.016)	0.026 (0.03)	0.548
PI (molar %)	2.05 (1.39)	10.6 (16.4)	0.358
PG (molar %)	3.0 (2.84)	7.5 (10.8)	0.407
LPG (molar %)	0.21 (0.14)	1.18 (1.08)	0.338
t-CHOL (molar %)	**0.9 (0.5)**	**0.6 (0.5)**	**0.03**

Table 11. Main lipid profile for the two patients' cohorts. The content in lipid classes has been analysed by LC-HRMS and indicated as molar percentage (%) with respect to total lipids. Data are expressed as mean (SD). One neonate shows an increase in PG, PI and PE with respect to PC under hypothermia (neonate n4), rising SD for those four parameters. The increased values among the two time points are highlighted in salmon. Abbreviations: LC-HRMS, liquid chromatography-high resolution mass spectrometry; NLD, no lung disease neonates; WBH, whole body hypothermia; PC, phosphatidylcholine; PE, phosphatidylethanolamine; PG, phosphatidylglycerol; PI, phosphatidylinositol; LPC, lysophosphatidylcholine; LPE, lysophosphatidylethanolamine; LPG, lysophosphatidylglycerol; t-CHOL, total cholesterol.

Apart from the total amount of the sterol that significantly decreased after 72 hours of hypothermia (p =0.03), no significant changes in other lipid classes were detected (**Table 11**, **Figure 40A**). In detail, this cholesterol reduction was even more evident when comparing the amount of total sterol before and after 72 hours of WBH within the same cooled neonate. In this regard, as shown in **Figure 40A**, the values during hypothermia were expressed as percentage with respect to the pre-hypothermia time point for each baby (orange arrowheads). However, no differences were detected when esterified and free cholesterol forms were taken into account (p= 0.231).

At the same time, as shown in **Figure 40B**, no variation in PC 32:0 (DPPC) and other PC subclasses as well as changes in the content of saturated and unsaturated PC species were noticed. A tendency to increase the levels of saturated species (included DPPC) can be observed, but it was not significant (p= 0.1). As for the other lipid subclasses, a significant rise was only detected for the following PG species: PG 34:0 [pre= 2.6 (3.1), WBH= 4.9 (2.7), p= 0.048] and PG 36:1 [pre= 8.4 (3.9), WBH= 1.8 (5.1), p= 0.023]. As it was demonstrated for MAS neonates, the reduction in cholesterol amount after 72 hours of WBH was also confirmed in these four NLD babies. This suggests that after an apparent rise of the sterol at 24 hours (**Figure 35**, first row), it is clear that cholesterol tends to decrease upon hypothermia.

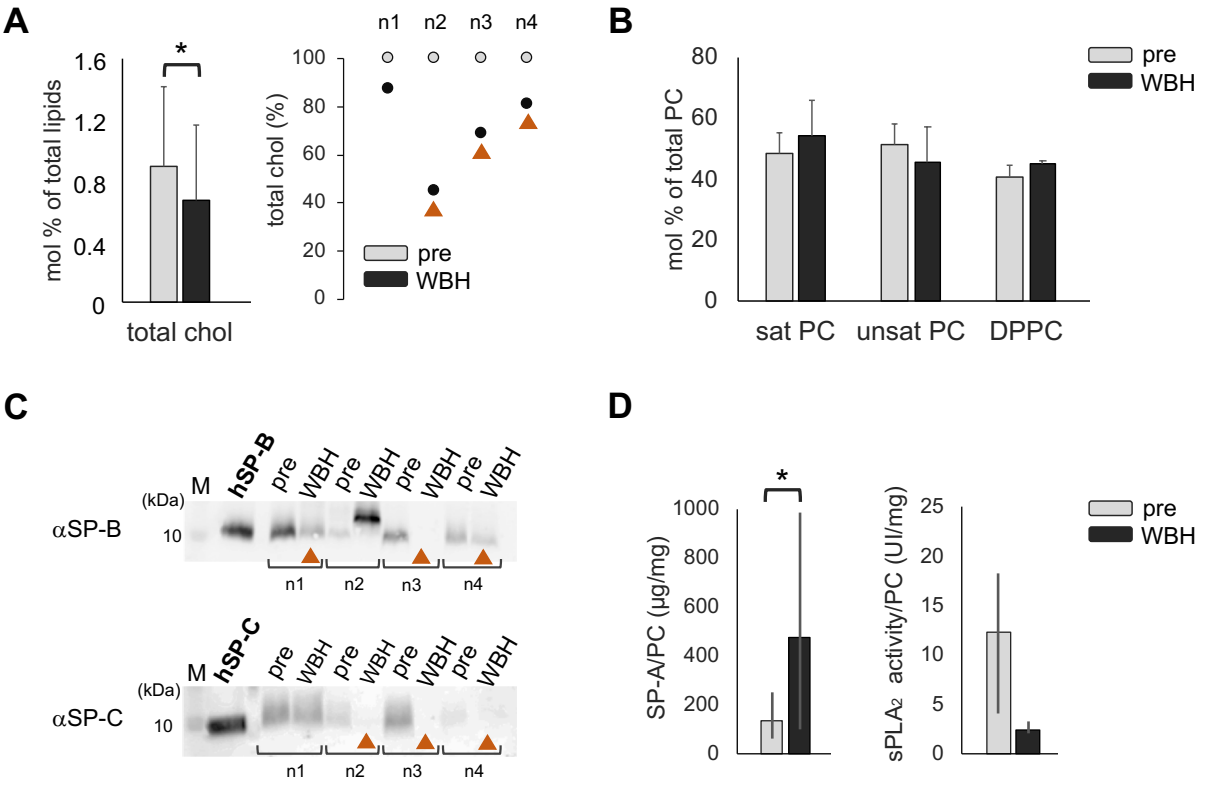

Figure 40. Changes in main surfactant components and activity of sPLA$_2$ under WBH. (A) The amount of total cholesterol was expressed as percentage of total phospholipids. Data are expressed as mean and SD of 4 neonates. Moreover, within each patient the percentage if variation at 72 hours with respect to pre-WBH is also shown. Orange arrowheads illustrate the reduction in cholesterol upon cooling. Paired t-test: *p< 0.05. **(B)** Percentage of DPPC, and saturated and unsaturated PC molecular species expressed as mean and SD. **(C)** Western blotting of hydrophobic surfactant proteins under nonreducing conditions. A quantity of 4 µg of PC from each sample was loaded into the gel, and 50 ng of isolated human SP-B and SP-C were used as internal controls. Orange arrowheads illustrate the reduction in hydrophobic proteins upon cooling. **(D)** Levels of SP-A and sPLA$_2$ activity of 8 neonates normalised for total PC and expressed as median and interquartile range. Mann Whitney U test: *p< 0.05. Abbreviations: WBH, whole body hypothermia; chol, cholesterol; sat, saturated; unsat, unsaturated, DPPC, dipalmitoylphosphatidylcholine; PC, palmitoylphosphatidylcholine; α, anti; hSP-B, purified human surfactant protein B; hSP-C, human surfactant protein C; sPLA$_2$, secretory phospholipase A2.

As a second step, the content of hydrophobic surfactant proteins, SP-B and SP-C, with respect to total surfactant PC was also analysed in the same four neonates. Interestingly, as shown in **Figure 40A-C**, SP-C and SP-B tend to decrease together with cholesterol after 72

hours of cooling (orange arrowheads). As described in normothermic newborn rabbits, both SP-B and SP-C as well as SP-A are turned over at a faster rate than saturated PC (Baritussio *et al.*, 1994). In humans, SP-B kinetics shows a peak after 20-30 hours and this may plausibly occur even for the other hydrophobic protein (Simonato *et al.*, 2011). Since both SP-C and SP-B are important for surfactant to adsorb properly (Creuwels *et al.*, 1993; Possmayer *et al.*, 2001; Wang *et al.*, 2005a), their decrease under WBH may start after 48 hours and explain the reduction in initial adsorption observed at this time point for NLD babies. Moreover, **Figure 40D** shows that SP-A levels tested in eight neonates were found significantly increased after 72 hours, probably with a rebalancing effect on surfactant adsorption (**Figure 35**, first row). In this regard, future specific studies should be addressed in a larger population of neonates to better define the exact kinetics of those surfactant proteins.

Interestingly, at the same PC amount, together with the rise in SP-A under WBH, the activity of $sPLA_2$ also tends to decrease ($p=0.06$). This confirms the presence of a WBH-mediated anti-inflammatory response, taking place upon 72 hours of cooling and involving additional factors than IL-6 and IL-8 (De Luca *et al.*, 2014).

Discussion

In this chapter, the *in vivo* effect of WBH on lung surfactant activity and composition was investigated in neonates with and without lung injury. In detail, the following relevant changes emerged: (1) the oxygenation index of neonates with severe meconium aspiration improves after 72 hours of the WBH; (2) the content in cholesterol with respect to total PC tends to decrease upon cooling, reaching a significant reduction after 72 hours in both NLD and MAS neonates; (3) cooling decreases the adsorption of surfactant material after 48 hours in NLD neonates, whereas meconial cholesterol has an opposite effect rising surfactant adsorption when present in the sample; (4) surfactant dynamic properties significantly improve after 72 hours of WBH in neonates with and without lung injury. This effect only occurs when samples are tested at 33 °C and is also evident after rewarming of neonates; (5) proteins SP-C and SP-B tend to decrease together with cholesterol levels in NLD babies after 72 hours of WBH; (6) at the same time, SP-A levels significantly increase, modulating the total activity of $sPLA_2$.

Scanty evidences are available about the effect of therapeutic hypothermia on the biophysical activity of human surfactant. The only previous data were obtained by SAT, suggesting a significant improvement in surfactant surface saturation after 48 hours of WBH, followed by a worse tendency after 72 hours (De Luca *et al.*, 2014). However, as extensively explained in chapter I, the SAT technique analyses the mere kinetics of surfactant accumulation at the air-liquid interface by a simplified plate fluorescent assay (Ravasio *et al.*, 2008). The method can only test the capability of material to form a surface-associated layer, but it cannot provide any detailed information about surface tension reduction capabilities and how surfactant complexes stabilise the interface during breathing-like compression-expansion dynamics. On the contrary, CBS can be considered as the “gold standard” technique to simulate the respiratory cycles under dynamic conditions. Interestingly, using this method, opposite results emerged comparing to the previous SAT evidences. The adsorption of surfactant was indeed slower after 48 hours of WBH irrespective of the experimental temperature, and then improved after 72 hours (**Figure 35**, first row). This result could be explained by the different timing used for the assays. The saturation of the interface as revealed by SAT started to be significant after 15 minutes from the beginning of the experiment

and it is assessed at very diluted surfactant concentration (De Luca *et al.*, 2014). Conversely, the initial adsorption rate is tested for 5 minutes in the CBS at much higher concentration. It is clear that the most appropriate *in vivo*-like model, provided that enough amount of material is available, is a method able to reproduce the lung dynamics such as CBS. Using this technique, an overall reduction in the adsorption rate at 33 °C irrespective of WBH time points was observed. This result confirms previous data assayed on PS at 25 °C (Suri *et al.*, 2012) and suggests the counterbalance effect of low temperature on surfactant fluidity, influencing membrane bending (Steinkühler *et al*, 2019), thus reducing the dynamics of the system and the adsorption activity mediated by SP-C and SP-B.

Cholesterol tends instead to fluidify the system and increase membrane curvature. This may explain why the meconial sterol improves the adsorption rate before and after 24 hours of WBH, when cholesterol was found at higher levels in MAS and MSAF samples (**Figure 35**, second and third rows). Interestingly, the initial adsorption in surfactant from these babies came back to values similar to those of NLD neonates after 48 hours and this took place at the same time of a reduction in the content of cholesterol. The lowest values in the sterol were detectable after 72 hours and post WBH along with a simultaneous reduction in SP-C and SP-B content and an increase in SP-A levels (**Figure 39A**, **Figure 40A-C**).

The interdependency between cholesterol and SP-C is expected since several evidences have shown their association. The protein increases the sterol mobilisation upon lipid membrane fragmentation (Parra *et al.*, 2011; Roldan *et al.*, 2016), probably promoting a stabilising effect on cholesterol-containing surfactant films (Gómez-Gil *et al.*, 2009a; Gómez-Gil *et al.*, 2009b). According to the squeeze-out model, upon shrinking of the air-liquid interface, less active lipid species are removed, to end in a highly packed film rich in saturated lipids at the interface that may sustain minimum surface tension under expiration (Egberts *et al.*, 1989; Pastrana-Rios *et al.*, 1994; Xu *et al.*, 2020). It has been proposed that part of the lost material is removed as small aggregates. On this basis, since SP-C is important to enhance both adsorption and the rapid movement of lipids at the interface (Creuwels *et al.*, 1993; Possmayer *et al.*, 2001; Wang *et al.*, 2005a), a synergistic role of the protein and cholesterol may be proposed allowing for a proper conversion of large surfactant complexes into small aggregates that could be taken up by macrophages (Roldan *et al.*, 2016).

It was also demonstrated that a temperature of 30 °C or lower reduce the adsorption of lamellar bodies particle by a decrease in the fluidity of the surfactant phases (Hobi *et al*, 2014). Thus, focusing on the obtained data, and as a consequence of the decrease in adsorption at 33 °C, a quick physiological response could lead to the raise in surfactant fluidity that occur in NLD babies under WBH. This response could include a release of cholesterol at 24 hours. This variation is subtle and not significant, still maintaining the sterol at physiological levels to promote its critical role in membrane organisation and spreading properties without impairing the capability of material to drastically reduce surface tension. With this purpose, cholesterol might be rapidly mobilised from pre-existing surfactant stores, allowing for very rapid changes in material organisation and adaptation to the environmental condition. Its rapid efflux, changing surfactant sterol/PC ratio, could perhaps be promoted by NPC1 and NPC2 in lamellar bodies of AT-II cells (Roszell *et al.*, 2012). This may explain its apparent increase in surfactant membranes of NLD babies after one day (**Figure 35**, first row) and confirm the hypothermia-mediated quick rise in the sterol previously observed in animal models (Langman *et al.*, 1996).

At the same time, this increase may be connected to other mechanisms in which cholesterol may also mediate gene expression. A decrease in the amount of the sterol in the

lipid rafts of macrophage plasma membranes seems to inhibit the proinflammatory signalling promoted by TLRs (Fessler & Parks, 2011). In this regard, the cholesterol efflux may be mediated by ABCG1 towards extracellular acceptors like HDL or moved directly to surfactant complexes (Choi *et al*, 2018). This mechanism could trigger an anti-inflammatory response and may be the cause of an increase in cholesterol/PC ratios. Moreover, mobilisation of the sterol in AT-II cells may be also a signal to modulate surfactant protein expression in the following 72 hours. As a result, increased SP-A levels may promote the movement of surfactant aggregates towards the air-liquid interface (Lopez-Rodriguez *et al.*, 2016b) and reduce the degradation of surfactant lipids by $sPLA_2$ (Arbibe *et al.*, 1998; Chabot *et al.*, 2003). Thus, a better adsorption, despite the decline in both cholesterol and hydrophobic surfactant proteins, was observed after 72 hours of WBH along with a reduction in the activity of the enzyme (**Figure 35**, first row and **Figure 40D**). Moreover, SP-A seems to *in vitro* inhibit the inflammation response in the absence of an infection. SP-A may also bind the signal-regulatory protein alfa on macrophages by its globular head group (Gold *et al*, 2004), potentially blocking its association to cluster of differentiation 47 (Gardai *et al*, 2003). This may explain the decrease in cytokines previously observed in NLD neonates after 72 hours of WBH (De Luca *et al.*, 2014). The ELISA kit used in the present study is not able to discern among SP-A1 and SP-A2 isoforms. However, because of the improvement in surfactant adsorption and the cytokine reduction after 72 hours of cooling, an overall increase in the two SP-A isoforms is the most likely event occurring upon WBH.

The secretion of lamellar bodies diminishes in the presence of SP-A (Mason & Voelker, 1998). This may create an unbalance between the recycling of small aggregates (rich in SP-C and cholesterol) and a proper replenishment of those components. However, SP-A in the presence of 1% SP-B seems to also inhibit the *in vitro* conversion of large to small aggregates (Veldhuizen *et al*, 1994), suggesting an alternative mechanism for the decrease in SP-C and cholesterol. Due to the interdependence of these two components, an alternative hypothesis could imply the WBH-mediated reduction in SP-C expression and cholesterol mobilisation. This may decrease the uptake of surfactant aggregates by macrophages (Poelma *et al.*, 2004) and maintain a proper pool of material at the interface, in spite of the reduction in lamellar bodies secretion. Indeed, as reported in humans with and without ARDS (Simonato *et al.*, 2011), the kinetics of SP-B has a peak at around 30 hours. A similar mechanism may involve SP-C, which could already decline at 48 hours, justifying the adsorption reduction at this time point, especially for material tested at 33 °C (**Figure 35**, first row).

Promotors of surfactant protein SP-A, B and C are activated by TTF-1 in the lungs (Das *et al*, 2011). Interestingly, a recent evidence suggests that this protein is also involved in ABCA1 repression and reduction of cholesterol efflux by regulating miR-33a (Lai *et al*, 2018). This increases the intracellular levels of the steroid, reducing its movement towards HDL and probably promotes its accumulation in lung surfactant. Starting from these evidences, it could be argued that the rapid mobilisation of cholesterol at 24 hours as well as its excess due to meconium may somehow exerts a negative feedback on TTF-1, reducing its action on ABCA1, increasing the cholesterol efflux towards HDL. This may explain the overtime decrease in both surfactant cholesterol and surfactant hydrophobic proteins under WBH.

On the other hand, the selective action on SP-C and SP-B expression may occur through different mechanisms: (1) a differential TTF phosphorylation status, (2) the simultaneous increase in other transcription factors that specifically influence SP-A, but not the expression of SP-B and SP-C. Future detailed studies focusing on both surfactant expression and kinetics under WBH in a larger population, may contribute to clarify this question.

Interestingly, when surfactant is tested at hypothermia temperature there is always a tendency to improve the dynamic properties of the system compared with 37 °C, despite the significant reduction in initial adsorption. This suggests a possible re-organisation of surfactant structure at 33 °C. The temperature reduction might cause a selective exclusion of lipids that pack at less content under compression (such as unsaturated phospholipids) from the alveolar interface, to end in a DPPC-enriched film with a solid-ordered type of phase during expiration. This process may be evident upon testing surfactant *in vitro* under breathing-like compression-expansion cycles, and would not require the *in vivo* metabolic production of DPPC (Nespeca *et al.*, 2016) (**Figure 39B** and **40B**). Consistently, the compositional changes that seem to take place after 72 hours of WBH (higher SP-A levels, lower SP-B and SP-C levels and a lower cholesterol content) convert this result from a tendency to a significant difference. In this regard, SP-C and cholesterol may have the same dynamic effect on surfactant membranes as the high temperature: they may increase the fluidity of the system, promoting fragmentation (Roldan *et al.*, 2016) and improving adsorption, but reducing surfactant rigidity and packing under compression (**Figure 41**). This means that once two of these three components decrease, e.g. SP-C and the sterol, lipid packing at the interface only depends on temperature variation, revealing the difference between 33 and 37 °C (**Figure 39B**). In this scenario, SP-A may promote the adsorption and spreading of material, suppling a surplus of surfactant at the interface for this mechanism to take place, despite the reduction in SP-B and SP-C.

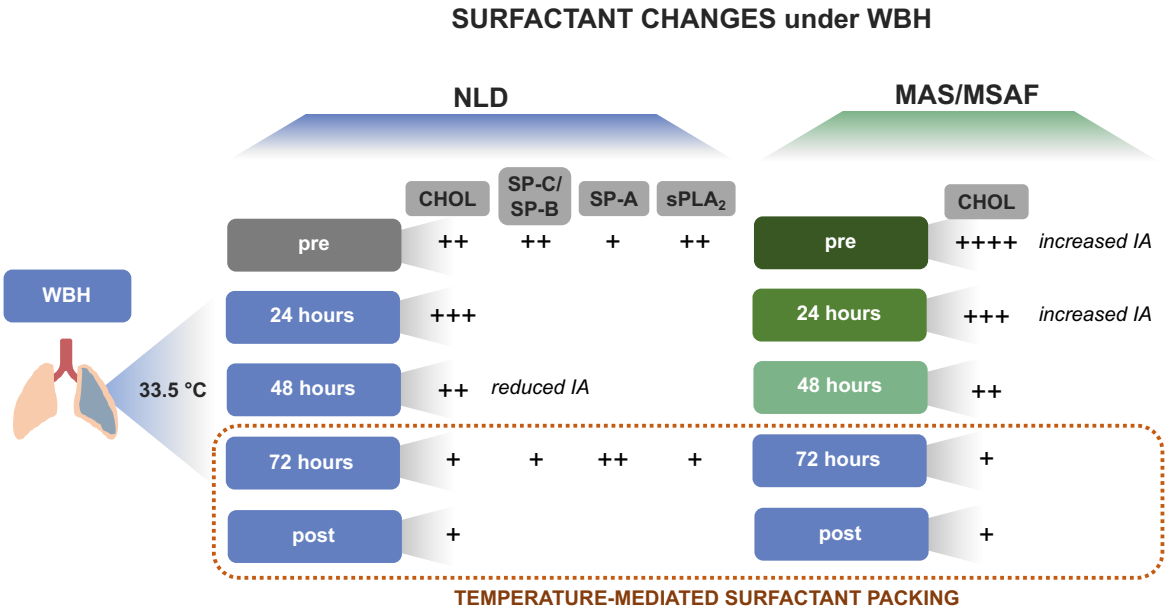

Figure 41. Schematic representation of surfactant changes under WBH in neonates with and without lung injury. The level of increase or reduction in surfactant components and $sPLA_2$ are illustrated more or less by plus symbols. The resulting effect on surfactant activity is also specified. Abbreviations: WBH, whole body hypothermia, NLD, no lung disease; MAS, meconium aspiration syndrome; MSAF, meconium stained amniotic fluid; CHOL, cholesterol; $sPLA_2$, secretory phospholipase A2; IA, initial adsorption.

These results occur in both NLD and MAS neonates. In the latter group surface tension under dynamic cycling also reached the lowest value after 48-72 hours of hypothermia, while surfactant compressibility was at its highest and oxygenation index improved. Consistently, these data were not confirmed when running the experiment at 37 °C or in BAL samples

obtained before WBH instigation. This confirms the positive effects of WBH reported in neonates with MAS (De Luca *et al.*, 2016) and in some cases of ARDS (Hayek *et al.*, 2017; Karnatovskaia *et al.*, 2014; Slack *et al.*, 2017; White *et al.*, 2017).

Moreover, a very high level of cholesterol was detected in samples of MAS neonates (52 and 87% with respect to total PC choline). The amount was two/three times higher than that obtained in NLD babies as observed in chapter II. Moreover, surfactant activity in MAS neonates was impaired during pre-hypothermia and improved only when a cholesterol reduction occured during cooling (from 48 hours onward). Thus, a dual-role for cholesterol emerges in physiological and pathological contexts. A slight variation of the steroid may occur during physiological responses to environmental conditions, modulating surfactant performance. Conversely, its excess together with the increase in other compounds, such as PuPC, causes a exacerbated surfactant fluidity in MAS, impairing the capability of the material to achieve minimal surface tension regardless of its concentration (see chapter II).

An improvement in oxygenation was observed in MAS patients when minimum surface tension was achieved. Beside these findings, other physiopathological mechanisms cannot be excluded such as: 1) WBH-induced reduction in metabolic demand and CO_2 production with consequent need for a less aggressive ventilation (Aslami *et al*, 2010; Pietrini *et al.*, 2012), 2) the effect of surfactant lavage and replacement in MAS babies and 3) the reduction in lung inflammation and protein extravasation as a consequence of WBH (Altınsoy *et al*, 2014; Aslami *et al*, 2012; Ball *et al.*, 2010; De Luca *et al.*, 2014; Hong *et al.*, 2005).

In spite of the promising results, several limitations should be considered: (1) there is no control group of babies with repeated BAL under normothermia. This group cannot be recruited because it is unethical to keep intubated healthy neonates for 72 hours only to perform nBALs; conversely, neonates may stay intubated so long only if they have lung diseases or perinatal asphyxia needing WBH, and thus they cannot represent healthy controls. Measurements before WBH must be considered as a sort of control, although with a sub-optimal performance due to the following critical points: the material is only precipitated and not purified as it happens in animal studies, a very low concentration was obtained from nBALs, and relatively limiting condition was used to allow for the detection of subtle differences in the biophysical parameters at different temperatures. (2) The sample size was small. This is due to the rarity of these patients, especially those affected by MAS. (3) nBALs were performed instead of fibroscopic BALs. However, this technique is well standardised and is known to describe the alveolar milieu better than simple tracheal aspirates (Dargaville *et al*, 1999). A total lung lavage would have also retrieved a surfactant of better quality, as done in animal studies (Suri *et al*, 2013; Suri *et al.*, 2012), but this technique is not applicable to human patients for ethical reasons. The nBAL might affect results, as it may harvest surfactant also from the upper airways and not only from the alveolar milieu. (4) Moreover, NLD babies cannot be considered as a perfect control group of healthy neonates, since they are anyway affected by perinatal asphyxia. Ideally, normal surfactant should be studied in spontaneously breathing neonates, as there is the theoretical risk that mechanical ventilation, even if provided according to the best current clinical practice, might affect surfactant quality/function. However, performing a BAL on non-intubated babies is unethical and unfeasible, making NLD the best control available for this type of study.

To conclude this chapter, the interfacial dynamic properties of lung surfactant of neonates under WBH significantly improve when material is tested at 33 °C, especially after 72 hours of hypothermia. This occurs together with several compositional changes, mainly a

reduction in cholesterol, an apparent decrease in surfactant hydrophobic proteins and an increase in SP-A content. This refinement of surfactant material together with the low temperature may influence both the rigidity and stability of surfactant complexes as well as the packing of surfactant under compression, promoting an effective reduction in surface tension at 33 °C compared with 37 °C.

Part of these data and text has been included in a paper in press:
Autilio C, Echaide M et al., Sci Rep. 2020

Chapter V

“Therapeutic hypothermia boosts surfactant biophysical properties: when surfactant composition counts”

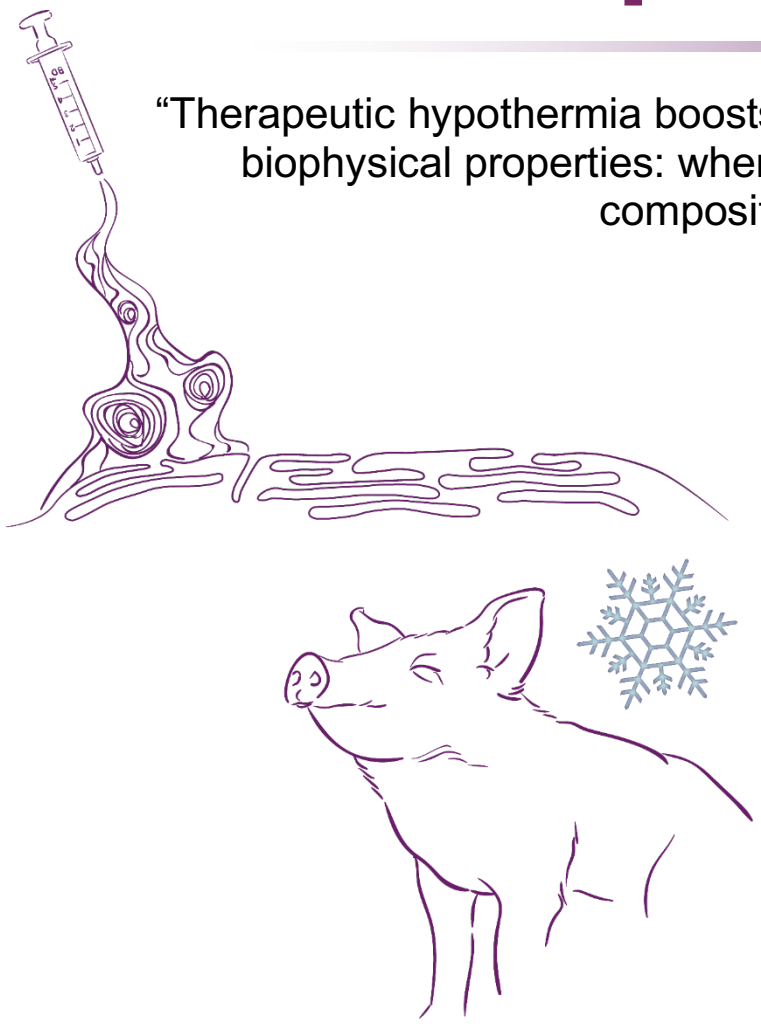

Introduction

In the previous chapter, the positive effect of WBH on lung surfactant activity was demonstrated in neonates with and without lung injury. Interestingly, a tendency to improve the interfacial dynamic properties of surfactant always takes place, testing samples at 33 °C compared with 37 °C. This trend becomes significant after 72 hours of hypothermia along with a surfactant refinement characterised by the increase in SP-A and the simultaneous reduction in both cholesterol and surfactant hydrophobic proteins. These results open new avenues to the use of therapeutic hypothermia for severe MAS, but may also shine a light on its potential to treat other direct lung injuries. Consistently, early studies have suggested some possible benefits in cooled patients suffering of ARDS (Hayek *et al.*, 2017; Karnatovskaia *et al.*, 2014; Slack *et al.*, 2017; White *et al.*, 2017). This syndrome accounts for 10% of all cases in intensive care units worldwide. Mortality remains at 30–40% and no effective treatments are available to date (Matthay *et al.*, 2019). Primary ARDS occurs after a direct insult to the lung, whereas secondary ARDS is triggered by an extra-pulmonary pro-inflammatory event (Calfee *et al.*, 2015; Matthay *et al.*, 2019; Sinha & Calfee, 2019). Theoretically, therapeutic hypothermia may be useful to treat primary but might be harmful in secondary ARDS (Itenov *et al*, 2018; Rumbus *et al*, 2017). Conversely, during primary ARDS the injury is at first confined to the lung, resulting in a lower compliance and more severe surfactant dysfunction than in the secondary form of the syndrome (Calfee *et al.*, 2015; Matthay *et al.*, 2019; Sinha & Calfee, 2019).

As extensively discussed in the introduction, during ARDS, surfactant function is impaired in several ways (Autilio & Pérez-Gil, 2019; Günther *et al.*, 2001). Protein-rich oedema fluid, high levels of cholesterol and $sPLA_2$ are the main actors inhibiting surfactant activity directly and enhancing the production of ROS. Lung surfactant is dramatically needed to reduce surface tension under the expiration-mediated shrinking of the alveolar air-liquid interface. On this basis, the precise proportions of DPPC, unsaturated phospholipids and SP-B and SP-C are essential for its function in a healthy lung (Autilio & Pérez-Gil, 2019).

However, oedema proteins, such as albumin, increase in ARDS patients (Sprung *et al*, 1981) and may compete with surfactant complexes to reach the air-liquid interface. The resulting interfacial steric barrier affects surfactant adsorption and the reduction in surface tension under compression as demonstrated *in vitro* (Taeusch *et al.*, 2005). Beyond the physiological range, the drastic rise in cholesterol compared to the portion of saturated lipid leads to fluidification of surfactant membranes (Autilio & Pérez-Gil, 2019). This impairs the ability of clinical and native surfactants to reduce surface tension upon breathing-like cycles (Keating *et al*, 2007; López-Rodríguez *et al.*, 2012). In this line, methyl-β-cyclodextrin, a molecule that binds and extracts cholesterol from membranes, can overcome the cholesterol-mediated inhibition when surfactant from a mouse model of ARDS is treated *ex vivo* (Al-Saiedy *et al*, 2018; Gunasekara *et al*, 2010). PLA_2 targets and hydrolyses the condensed domains of phosphatidylcholine monolayers with a crumbling effect at the air-liquid interface (Grainger *et al*, 1989). Consistently, high levels of the secretory form of the enzyme was detected in ARDS patients along with changes in surfactant phospholipid composition and surface tension properties (Seeds *et al.*, 2012). As a result, surfactant amount and performance are reduced and the work of breathing increases upon ARDS (Günther *et al.*, 2001).

Since a tendency to improve surfactant activity is always evident at 33 °C and enhanced by the compositional changes occurring in surfactant after 72 hours of WBH, a certain biophysical mechanism may soon take place, probably involving changes in surfactant

structure and packing/condensation under cooling. Besides, the surface activity of rabbit lung extracts tends to improve decreasing temperature from 40 to 15° C (Lempert & Macklem, 1971).

It is well known that the organisation and physical properties of lipid membranes, like those in lung surfactant, can be influenced by shifting temperatures towards their melting points (de la Serna *et al.*, 2004). Cooling to values below 30 °C decreases the adsorption of lung surfactant in the presence of plasma compounds (Enhorning *et al*, 2000). However, the reduction from 37 °C to 33 °C may have a different consequence, especially upon the interface compression, as it is still above surfactant melting temperature (≈32 °C) (de la Serna *et al.*, 2004).

With this in mind, to investigate the biophysical mechanisms supporting the effects of therapeutic hypothermia on surfactant activity, in this fifth chapter both the interfacial structure and the composition of lung surfactant films subjected to compression were studied at 33 °C compared with 37 °C. Surfactant function and resistance to inhibition by plasma was also studied under cooling, as well as its restoration as a consequence of further surfactant supplementation. The molecular mechanisms governing the enhanced performance at 33 °C were dissected and a feasible biophysical model was proposed including a crucial role of surfactant disaturated phospholipids. Finally, based on the obtained data, an *in vivo* experiment was performed, using a model of lung injury in newborn piglets. This served as a proof of concept to demonstrate the effectiveness of WBH with and without surfactant replacement therapy.

Part of data were obtained during the PhD candidate external stay at National Research Centre for the Working Environment (NFA) in Copenhagen under the supervision of Dr. Jorid Birkelund Sørli. At the same time, the experiments with newborn piglets were performed in collaboration with Dr. María Carmen Rey Santano at Hospital Universitario Cruces in Bilbao.

Key techniques and piglet model

Sample collection and handling

PS and purified SP-B and C were obtained from porcine BAL as previously reported and detailed in the Materials and Methods chapter (Taeusch *et al.*, 2005). Porcine plasma was obtained by centrifuging (500 g for 10 minutes at 4 °C) and pooling blood from 6 pigs with different sexes coming from the same slaughterhouse. Similarly, PS was purified from the BAL pool obtained from the 6 pig lungs.

PS and synthetic phospholipid concentrations were determined by phosphorus mineralisation. Plasma total protein concentration was measured with the Lowry method. Poractant alfa was obtained from Chiesi Farmaceutici S.p.A., lyophilised and stored at -80 °C until use. The same buffer solution containing 5 mM Tris and 150 mM NaCl at pH 7.4 was used for every experiment.

Biophysical activity and lateral structure of surfactant films

The biophysical activity of both PS and reconstituted lipid-protein surfactant suspensions was tested at limiting concentrations (1.5, 2, 5 and 8 mg/mL) under slow (2 cycles/min) and quick breathing-like (20 cycles/min) compression-expansion cycling in Constrained Drop Surfactometer (CDS) (Yu *et al*, 2004) and CBS (Schürch *et al.*, 2010). Surfactant capability to reduce surface tension was not inhibited during quick cycles in the CDS after bulk replacement with serum (Saad *et al*, 2009). Thus, both plasma inhibition and therapy restoration experiments were performed under slow cycles. A Langmuir-Blodgett surface balance was used to study PS lateral structure before and after subjecting the material (around 30 μg at 5 mg/mL) at the interface to 10 compression-expansion cycles (65 cm^2/min).

All methods were applied keeping the target temperature (33 °C or 37 °C) constant along the experiments. Details about protocols and techniques are described in the Materials and Methods chapter.

Composition of interfacial films and thermotropic properties

The temperature-dependent changes in lipid composition of PS films under compression at the air-liquid interface were analysed in a Langmuir-Blodgett balance. Briefly, PS (around 50 μg at 5 mg/mL), pre-heated to 33 °C or 37 °C, was deposited drop by drop at the air-liquid interface of the trough filled with buffer at the same temperature. After 10 minutes of equilibration (≈25 mN/m surface pressure), surfactant films were compressed, reducing interfacial area at a velocity of 25 cm^2/min and simultaneously transferred onto a glass slide. Immediately after drying, the glass slide was rinsed with chloroform/methanol (2:1 v/v) to collect lipids from the film. Five experiments per condition were pooled in a single sample for lipidomic analysis by LC-HRMS. Each lipid class was expressed as molar % of the total phospholipids. This characterisation was carried out at the RUBAM at the Department of Biomedicinal Chemistry (IQAC-CSIC) in Barcelona in Barcelona under the supervision of Dr. Josefina Casas.

DSC was performed on both PS and lipid/protein suspensions, testing materials at 3 mg/mL as described in Materials and Methods chapter.

Newborn piglets with lung injury due to surfactant deficiency

The experimental protocol used for the animal model followed the European and Spanish regulations for protection of experimental animals (UE2010/63 and RD53/2013) and was approved by the Ethical Committee for Animal Welfare of Hospital Universitario Cruces in Bilbao. The study was performed in newborn piglets between days 2-4 of life with lung injury due to surfactant deficiency induced by repeated BALs (Lachmann *et al*, 1980).

Five piglets of 2 to 4 days old were sedated with intramuscular injection of ketamine (15 mg/kg), diazepam (2 mg/kg) and atropine (0.05 mg/kg) and were anesthetised with sevofluorane (2-3 %). The starting positive pressure ventilator was set as follows: fraction of inspired oxygen (FiO_2)= 0.25-0.28, respiratory frequency (fR)= 20 breaths/min, PEEP= 3 cmH_2O and positive inspiratory pressure (PIP)= 9-11 cmH_2O. All procedures were performed aseptically. Lung injury due to surfactant deficiency was achieved by repetitive saline lavage (30 mL/Kg; 37 ºC with FIO_2= 1) via an endotracheal tube. Lavage procedures were repeated

at 5 minutes interval until PaO_2 values < 100 mmHg. After 15 minutes of reaching a PaO_2 value < 100 mmHg, two extra BALs were performed with the objective of developing a more severe lung injury model. After the period of stabilisation of 30 minutes, the piglets were assigned to 4 different conditions as follows:

(1) controlled mechanical ventilation (CMV) group (n= 1): a newborn piglet with lung injury was maintained in CMV during 3 days (72 hours), without exogenous surfactant treatment. The piglet was moved from right to left position during experimental study every 8-12 hours.

(2) CMV-WBH group (n= 2): newborn piglets with lung injury were maintained in CMV and WBH (33.5 ºC) during 3 days (72 hours), without surfactant replacement treatment. Piglets were moved from right to left position during experimental study every 8-12 hours.

(3) CMV-CHF5633 group (n= 1): a newborn piglet with lung injury received a 200 mg/Kg of clinical surfactant CHF 5633. With the animal in supine position, the surfactant bolus was administered in about one minute without disconnecting the ventilator. After 30 minutes from surfactant administration, the newborn piglet was keeping in CMV during 3 days (72 hours). After the establishment of CMV ventilation, the animal was changed to the left and right side every 6 hours.

(4) CMV-CHF5633-WBH group (n= 1): a newborn piglet with lung injury received a 200 mg/Kg of clinical surfactant CHF 5633. After 30 minutes from surfactant administration, the newborn piglet was kept in CMV and hypothermia during 3 days. After the establishment of CMV ventilation, the animal was changed to the left and right side every 8-12 hours.

Anaesthesia and analgesia were maintained using sevofluorane (0.5 - 1%) with a continuous intravenous infusion of midazolam (1.75 mg/Kg/h; 5 mg/mL) plus fentanyl (7.5 μg/kg/h; 50 μg/ml) during all the experimental period. During CMV, the respiratory parameters, peak inspiratory pressure, respiratory rate and FiO_2 were tuned attempting to keep $PaCO_2$ values between 35-45 mmHg and PaO_2 between 90-110 mmHg with a tidal volume between 7-10 mL, with a maximum PIP of 25 cmH_2O to avoid pneumothorax. After the stabilisation period (CMV-WBH group) or after 30 minutes of CHF 5633 administration (CMV-CHF5633-WBH), hypothermia was provided using whole body, core temperature servo-controlled, water-filled mattresses set at 33.5 ºC. After 72 hours of hypothermia, rewarming was performed at a rate of 0.5% per hour until the body temperature reached 37 ºC (approximately 6 hours). The ventilator efficiency index (VEI) was calculated as follows: [3,800/(PIP/PEEP) x respiratory frequency x $PaCO_2$]. VEI scores decrease as pulmonary function impairs; it is used as an index of CO_2 elimination efficiency. The OI was calculated as follows: mean airway pressure (Paw) x FIO_2/PaO_2.

Statistics

Data were expressed as mean (standard deviation). Results comparisons were conducted using One-Way ANOVA followed by post-hoc Tukey's test or Two-Way ANOVA followed by post-hoc paired and unpaired t-test when appropriate. Details are described in figure captions. Correlation analysis was performed using Spearman (ρ) coefficient. Analyses were carried out with Sigma Plot (v. 11, Systat Software, San Jose, USA) and IBM SPSS Statistics 25 (v.25, IBM Corp., Armonk, NY, USA). $p < 0.05$ was considered to be significant.

Moderate hypothermia enhances surfactant activity in a concentration-dependent manner

The activity of PS was tested at different concentrations (1.5, 2.5 and 5 mg/mL) under slow (2 cycles/min) dynamic cycles by CDS. As shown in **Figure 42**, PS initial adsorption did not change among conditions, whereas dynamic activity significantly depended on sample concentration.

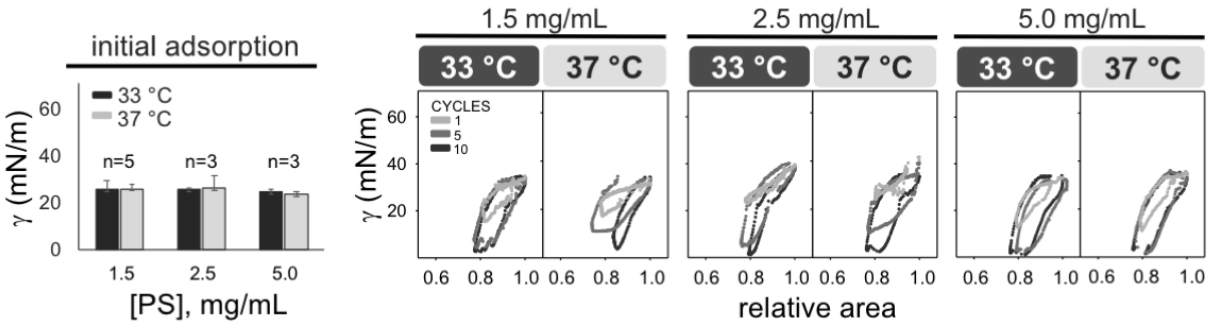

Figure 42. PS initial adsorption and dynamic γ-Δarea isotherms depending on temperature and concentration under slow compression-expansion cycling. On the left, surface tension values (γ, mN/m) reached by PS 10 seconds after the buffer deposition on top of the pedestal (initial adsorption). On the right, one typical replicate of isotherms representative of the ten slow compression-expansion cycles (2 cycles/min, shrinking the interface area by 20 %, 0.2 cm^2/min). Black and light grey bars represent experiments performed at 37 and 33 °C, respectively. Means and standard deviation of at least three replicates are shown. Compression-expansion cycles are depicted in grey scale. Abbreviations: PS, purified porcine surfactant; γ, surface tension.

At limiting concentration (1.5 mg/mL), PS significantly reduced surface tension after 5 slow cycles at 33 °C, whereas it needed 10 cycles at 37 °C (**Figure 42** and **Figure 43**). This trend was also evident at a PS concentration of 2.5 mg/mL. Using the latter condition, there was a significant difference in the minimum surface tension (γ_{min}) comparing cycle 5 and 10 for material tested at 37 °C, but it was not the case for PS assayed at 33 °C. However, this trend was not observed at higher PS concentration (5 mg/mL).

Overall, there were not significant differences among maximum surface tensions, apart from an increase in the maximum surface tension (γ_{max}) after 10 cycles at 37 °C for material tested at 5 mg/mL.

CDS experiments were performed under slow compression-expansion cycles (2 cycles/min), giving limiting information about breathing-like conditions. Thus, to recreate a physiological-like context, PS was also tested in CBS, using a very low concentration and subjected material to 20 cycles/min.

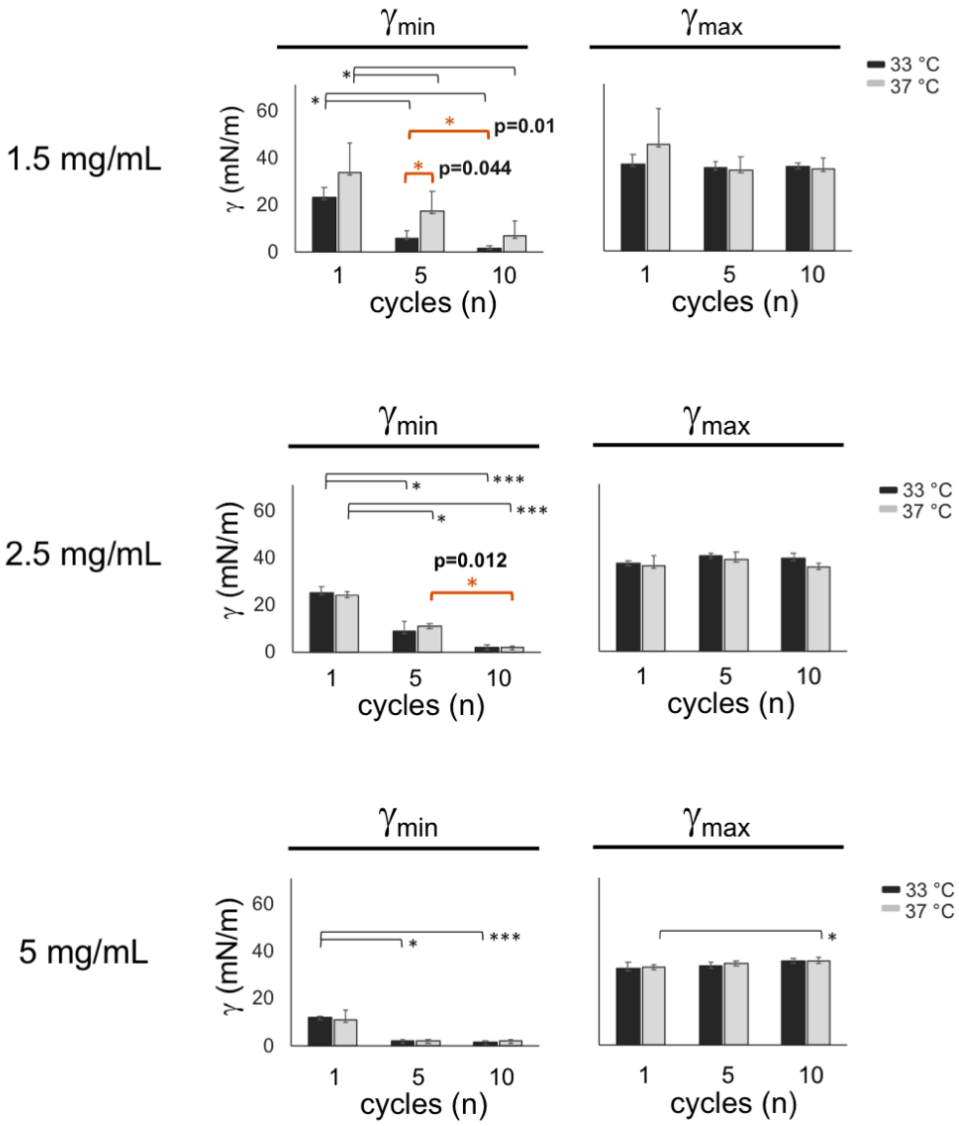

Figure 43. Effect of temperature and concentration on dynamic parameters of PS films subjected to compression-expansion cycling. Minimum (γ_{min}) and maximum (γ_{max}) surface tensions reached during cycles 1, 5 and 10 are compared in the bar plots, testing surfactant at 1.5, 2.5 or 5 mg/mL. Black and light grey bars represent experiments performed at 33 and 37 °C, respectively. Means and standard deviation of at least three replicates are shown. Horizontal lines represent statistical comparisons. Two-way ANOVA test followed by post-hoc test: * $p< 0.05$, *** $p< 0.005$. The exact p values of the most relevant post-hoc tests are indicated (the comparison bars and symbols highlighted in orange colour). Abbreviations: γ, surface tension; n, number.

As shown in **Figure 44**, PS was progressively diluted until reaching a concentration of 1.5 mg/mL, to perform experiments using a very limiting condition in which the differences among temperatures could be detected. Indeed, PS still maintained optimal surface-active properties until concentrations of around 4 mg/mL when tested at 37 °C (**Figure 44**, fourth column). PS diluted to 1.5 mg/mL showed a worsening in both initial adsorption and post expansion adsorption rates. Moreover, surface tensions fell down to values less than 2 mN/m only during dynamic cycling. This behaviour resembles the biophysical activity of lung surfactant collected from nBALs of NLD neonates, as shown in chapter II. Thus, the

concentration of 1.5 mg/mL was chosen for assaying the interfacial properties of PS in the CBS, comparing 33 and 37 °C.

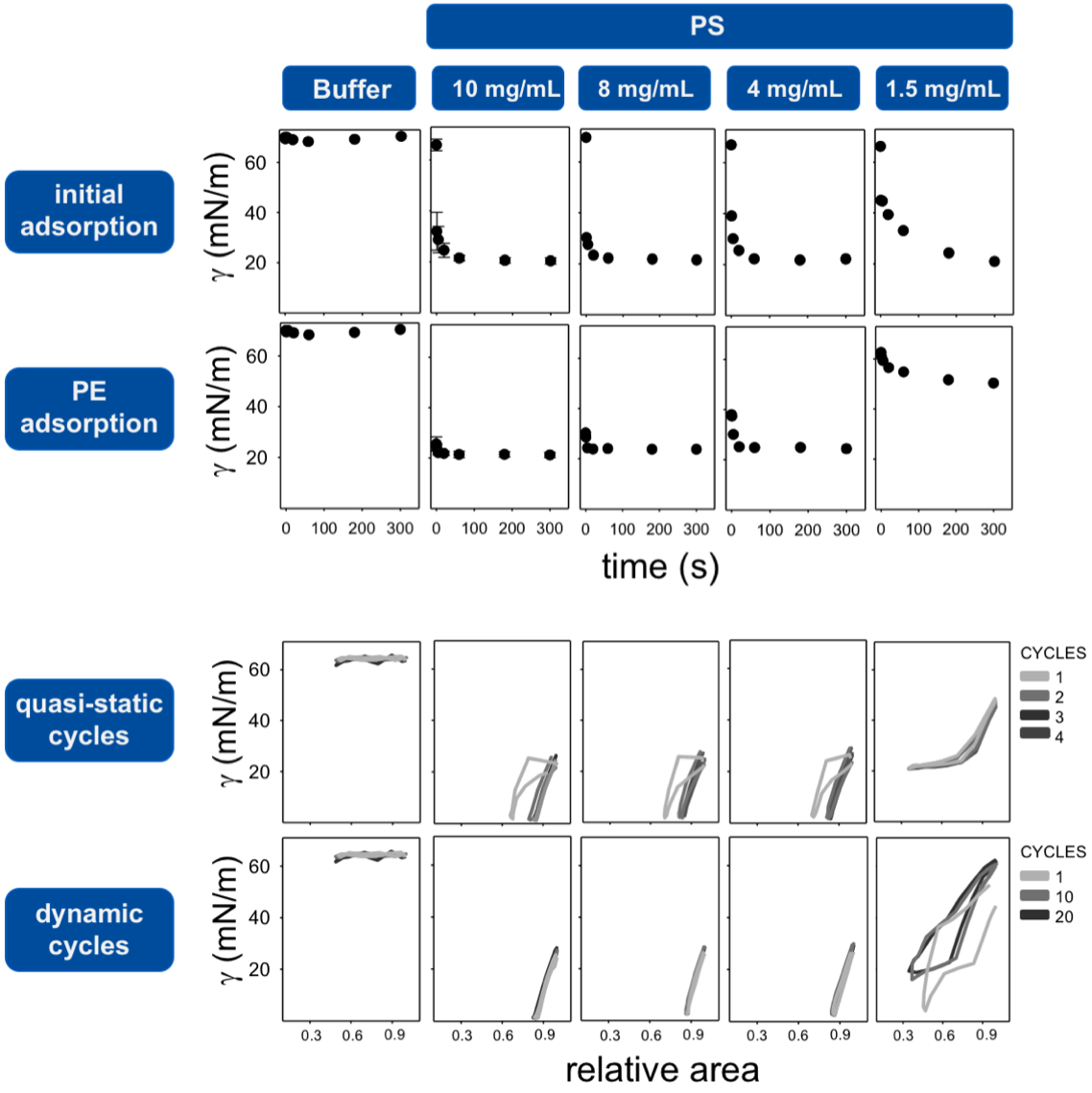

Figure 44. CBS analysis performed using different concentrations of PS at 37 °C. Mean and SD of three replicates are shown for initial adsorption and post-expansion adsorption. A representative isotherm is shown for the 4 quasi-static and the first, 10th and 20th dynamic cycles. Buffer alone is used as negative control and shown in black. Abbreviations: PS, purified porcine surfactant; γ, surface tension; PE, post expansion.

As shown in **Figure 45 A**, no differences were detected in both initial and post-expansion adsorption of PS. At the same time, and unlike CDS experiments, PS films subjected to slow quasi-static cycles (0.5 cycle/min) was not able to reduce surface tension regardless of the experimental temperature in the CBS.

This different result may be due to the different amount of PS used to saturate the interface for the two techniques. Indeed, although using the same PS concentration (1.5 mg/mL), 300 nL at 1.5 mg/mL (0.45 μg) were used for CBS tests, whereas 5 μl at 1.5 mg/mL

(7.5 μg) were employed in the CDS experiments. Thus, a higher amount of PS phospholipids was released in CDS, probably allowing for a better dynamic performance under slow compression-expansion cycles. Moreover, the speed employed to compress and expand the interface is also lower in the CBS compared to the CDS (0.5 cycle/min vs 2 cycles/min) and this may further explain the different result.

Although not temperature-dependent changes were detected under slow cycles, a different trend was observed when testing material upon quick cycles (20 cycles/min) at the CBS (**Figure 45B**).

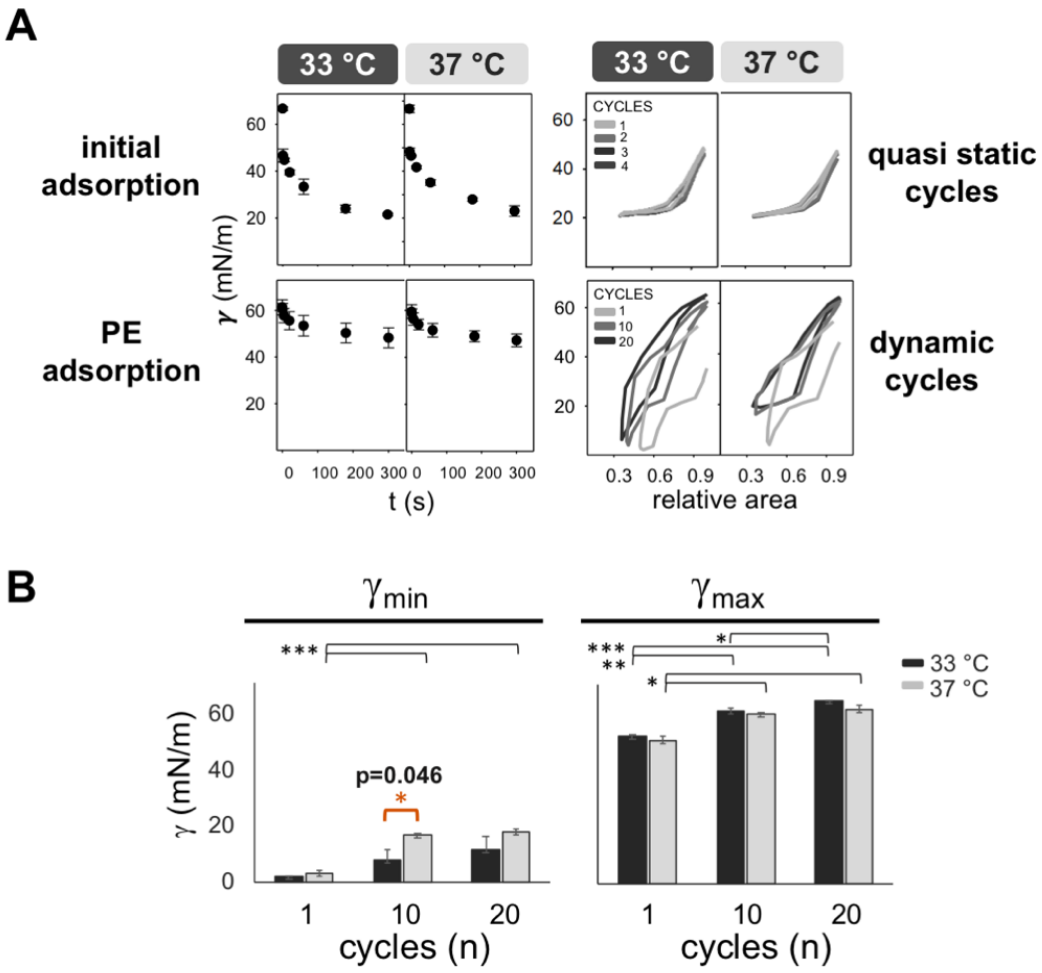

Figure 45. Effect of temperature on PS activity under slow and quick compression-expansion cycling. (A) On the left, γ values were followed during 5 minutes (300 s) of PS adsorption after injecting material onto the bubble or 5 minutes of re-adsorption after expanding the bubble volume (initial adsorption and post-expansion adsorption, respectively). On the right, one representative replicate (n= 3) of γ-Δarea isotherms corresponding to 4 slow cycles (quasi-static cycles) and 10 quick compression-expansion cycles (20 cycles/min). **(B)** Minimum and maximum surface tensions reached during cycles 1, 5 and 20. Black and light-grey bars represent experiments performed at 33 °C and 37 °C, respectively. Means and standard deviation of at least three replicates are shown. Horizontal lines represent statistical comparisons**.** Two-way ANOVA test followed by post-hoc test: * p< 0.05, **p < 0.01, *** p< 0.005. The exact p values of the most relevant post-hoc tests are indicated (the comparison bars and symbols highlighted in orange colour). Abbreviations: γ, surface tension; PE, post expansion; n, number.

At limiting concentration, the minimum surface tension was significantly lower after 10 quick cycles at 33 °C compared with 37 °C. Consistently, the minimum surface tension was

significantly higher along cycles at 37 °C. At the same time, the maximum surface tension significantly rose upon the interfacial dynamics irrespective of the experimental temperature. This is probably related to the highly diluted lung surfactant used for the experiments and the resulting progressive loss of material from the air-liquid interface under subsequent compression phases.

Moderate hypothermia increases the size of condensed domains in surfactant films, promoting the exclusion of unsaturated phospholipids upon breathing

To further understand the temperature-mediated improvement of PS interfacial properties when assayed at 33 °C, the activity and structure of PS were tested in a Langmuir-Blodgett trough (**Figure 46**) before and after 10 compression-expansion cycles (0.3 cycles/min). Starting from the same initial surface pressures, PS activity was slightly better at 33° C compared with 37 °C under interfacial dynamics. Maximum surface pressures were significantly higher (minimum surface tensions significantly lower) at 33 °C compared with 37 °C. This occurred during compression of the interface before and after the first cycle of the experiments (**Figure 46A** and **Figure 46C**).

Upon cycling, the plateau of the expansion moiety of the isotherms was visible at higher surface pressures at 33 °C than 37 °C (**Figure 46A**). This suggests that the compressed phase was more stable at 33 °C while the material tended to relax quicker at physiological temperature. Moreover, under compression of the air-liquid interface, a higher amount of surfactant seems to be excluded at 37 °C than at 33 °C and not replaced during the subsequent expansion. This results in a tendency to increase minimum surface pressures at 33 °C taking the last cycles into account ($p= 0.09$) (**Figure 46A** and **Figure 46C**).

Upon compression, and before further cycling, the condensed black domains observed at the surface films were rounder and less polymorphic than after compression-expansion cycling, as observed under epifluorescence microscopy (**Figure 46B**). This result was detected regardless of the temperature, suggesting an intrinsically fluid character of the ordered phase before cycling, reducing the contact perimeter with the coexisting surrounding disordered phases to a minimum. On the contrary, a de-mixing of lipids, together with larger areas of condensed phases, were observed after cycling, especially at 33 °C. These phases were apparently organised as smaller domains forming clusters.

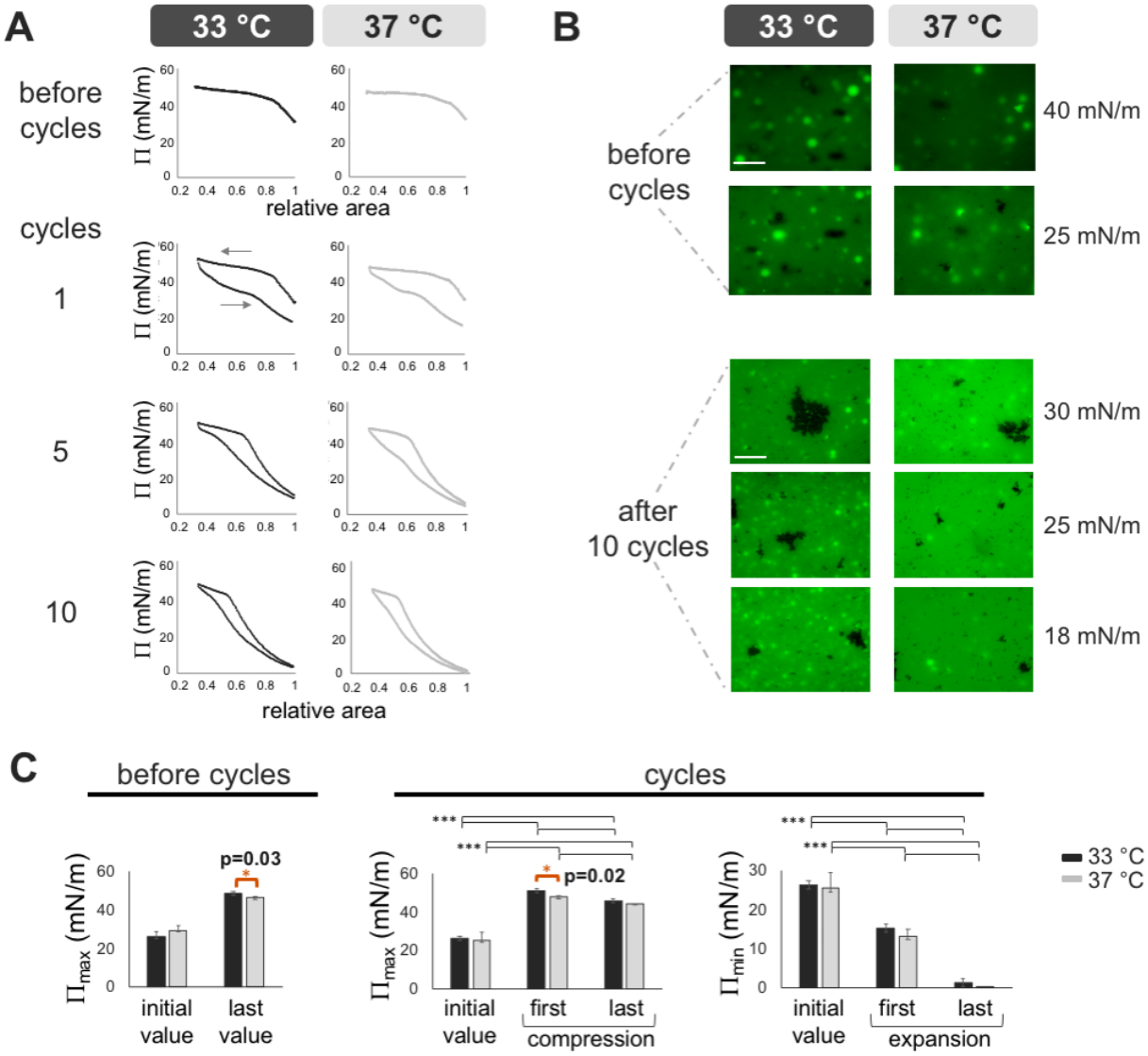

Figure 46. Temperature-dependent changes in PS activity and structure as assessed in a Langmuir-Blodgett trough. (A) One representative replicate (n= 5) of Π-Δarea isotherms before and during 10 slow compression-expansion cycles of the interface (0.3 cycles/min, ≈65 cm^2/min, reducing the interface area by ≈65 %) at 33° C or 37° C. Around 50 μg (at 5 mg/mL) of PS was spread at the interface before starting the experiment. Cycles 1, 5, and 10 are shown. **(B)** Epifluorescence analysis (n= 2) of PS lateral structure upon slow interfacial compressions (25 cm^2/min), before and after 10 quicker compression-expansion cycles (65 cm^2/min). PS was previously doped with the fluorescent probe BODIPY-PC (1% mol/mol). The lateral structure of PS is shown at several surface pressures before reaching the equilibrium plateau. White scale bars, 100 μm. For each image, histogram stretching has been performed to enhance contrast without deleting pixel data. **(C)** On the left, the initial and the maximum surface pressures obtained before and after the first compression (25 cm^2/min). On the right, the initial surface pressure obtained before starting the experiment together with the maximum and minimum surface pressures during the 1st and 10th compression-expansion cycles (65 cm^2/min). Mean and SD of 5 replicates are shown. Black and light-grey colours represent experiments performed at 33° C and 37° C, respectively. Black horizontal lines represent statistical comparisons. Paired t-test or Two-way ANOVA test followed by post-hoc test: * p< 0.05, *** p< 0.005. The exact p values of the most relevant post-hoc tests are indicated (the comparison bars and symbols highlighted in orange colour). Abbreviations: Π, surface pressure; Π_{max}, maximum surface pressure; Π_{min}, minimum surface pressure.

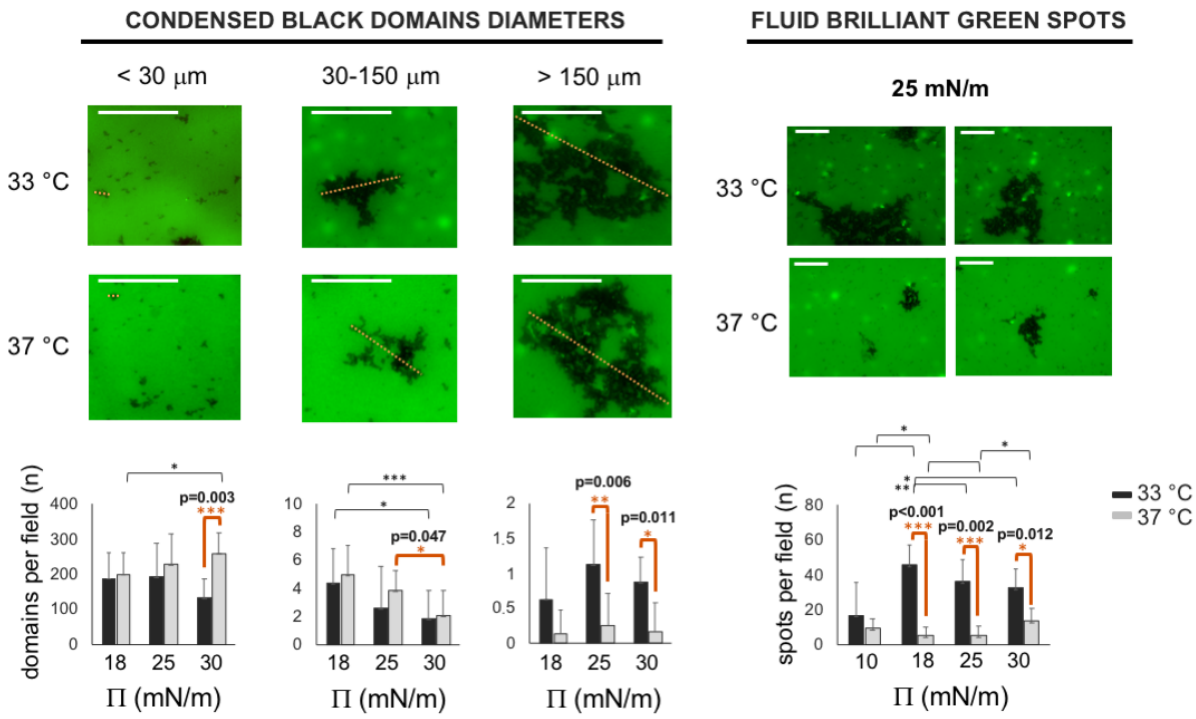

Figure 47. Temperature-dependent changes in surfactant lateral structure under compression in a Langmuir-Blodgett through. Representative images and statistical analysis of condensed and expanded regions observed at 33 °C and 37 °C, transferring the interface upon compression after 10 compression-expansion cycles. On the left, temperature-dependent changes in the count of black condensed domains with different diameters (< 30 μm, 30-150 μm, > 150 μm) at several surface pressures (18, 25, 30 mN/m). Due to the heterogenous and irregular shapes, the longer diameter for each condensed domain was considered for the analysis. An orange dotted line was shown as an example. On the right, temperature-dependent changes in the count of bright green spots per field at several surface pressures (10, 18, 25 and 30 mN/m). White scale bars, 100 μm. Black and light-grey colours represent experiments performed at 33° C and 37 °C, respectively. Mean and SD of 8 images per condition are shown. For each image, histogram stretching has been performed to enhance contrast without deleting pixel data. Black horizontal lines represent statistical comparisons. Two-way ANOVA test followed by post-hoc test: * p< 0.05, ** p< 0.01, *** p< 0.005. The exact p values of the most relevant post-hoc tests are indicated (the comparison bars and symbols highlighted in orange colour). Abbreviations: Π: surface pressure.

Moreover, brilliant fluorescent spots were present associated with the interface at both temperatures and remained visible after cycles, especially at 33 °C. As explained in chapter III, these probe-rich spots are likely areas of three-dimensional exclusion that appear bright due to the light scattering. Their apparent size was reduced after cycling associated with a lighter green liquid-expanded phase. Interestingly, due to the lower lipid miscibility at 33 °C than at 37 °C, phase-coexistence was more evident under hypothermia temperature. This leads to larger green spots, presumably excluded from the interface, along with larger and darker condensed domains at 33 °C than 37 °C (**Figure 47**). Indeed, at high surface pressures (> 25 mN/m), the size of black condensed domains increases at 33 °C compared with 37 °C along with the number of bright green spots (> 18 mN/m).

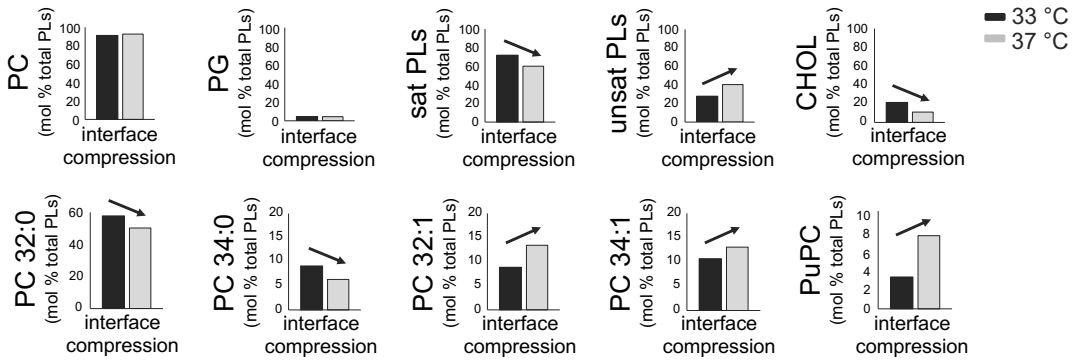

Figure 48. Temperature-dependent changes in the composition of surfactant interfacial films. Lipidomic analysis of PS proximally associated to the surface during compression of the interface (25 cm^2/min) at 33° C or 37° C. The interface recollected from 5 replicates were pooled per condition and analysed by lipidomic analysis. Each lipid species detected was normalised with respect of the total amount of phospholipids and reported as percentage. Black and light-grey colours represent experiments performed at 33° C and 37° C, respectively. Black arrows highlight the variation in PS lipid species at 33 °C compared with 37 °C. Abbreviations: PC: phosphatidylcholine; PLs: phospholipids; PG: phosphatidylglycerol; sat: saturated; unsat: unsaturated; CHOL: cholesterol; PuPC: polyunsaturated phosphatidylcholine.

Lipids (% total PLs)	33 °C	37 °C	PC-O (% total PLs)	33 °C	37 °C
PC	91.40	92.70	PC O-30:0	0.47	0.27
PC-O	1.84	1.27	PC O-32:0	1.18	0.76
LPC	1.79	0.97	PC O-34:0	0.10	0.05
PE	0.63	1.09	PC O-32:1/P-32:0	0.02	0.06
PG	4.34	3.96	PC O-34:1/P-34:0	**0.07**	**0.13**
CHOL	21.19	11.11	PC O-34:2/P-34:1	**0.00**	**0.01**
PC (% total PLs)	**33 °C**	**37 °C**	**PE (% total PLs)**	**33 °C**	**37 °C**
PC 32:0, DPPC	57.95	50.35	PE (34:0)	0.02	0.02
PC 34:0	9.18	6.35	PE (32:1)	0.00	0.04
PC 36:0	0.17	0.11	PE (34:1)	0.02	0.02
PC 38:0	0.02	0.02	PE (34:2)	0.09	0.17
PC 40:0	0.03	0.09	PE (36:1)	0.24	0.27
PC (32:1)	8.92	13.51	PE (36:2)	0.15	0.26
PC (32:2)	0.00	0.00	PE (36:3)	0.12	0.28
PC (34:1), POPC	10.70	13.00	PE (36:4)	0.00	0.02
PC (34:2)	2.28	4.96	**PG (% total PG)**	**33 °C**	**37 °C**
PC (36:1)	1.15	1.72	PG (32:0)	1.42	1.09
PC (36:2)	0.88	2.06	PG (34:0)	0.05	0.06
PC (36:3)	0.06	0.41	PG (32:1)	0.35	0.43
PC (36:4)	0.01	0.05	PG (34:1), POPG	1.73	1.30
PC (38:1)	0.01	0.02	PG (34:2)	0.31	0.49
PC (38:2)	0.02	0.04	PG (36:1)	0.23	0.32
PC (38:3)	0.00	0.00	PG (36:2)	0.25	0.27
PC (38:4)	0.00	0.00	**% total PLs**	**33 °C**	**37 °C**
PC (40:1)	0.02	0.02	saturated PLs	72.18	59.99
PuPC (≥ 2 double bonds)	3.24	7.52	unsaturated PLs	27.82	40.01

Table 10. Temperature-dependent changes in surfactant lipid species at the surface film, under compression of the interface. Lipidomic analysis of PS lipid species associated to the surface during compression of the interface (25 cm^2/min) at 33 °C or 37 °C. 5 replicates were pooled per condition. Each lipid species was normalised with respect of total phospholipids and reported as percentage. Abbreviations as in **Table 6** (chapter II).

The composition of PS lipids that were proximally associated to the surface under compression was analysed by LC-HRMS. **Table 10** shows raw data for all lipid species identified by lipidomic analysis, while the main lipid variations are depicted in **Figure 48**. The percentage of saturated lipids (especially DPPC) and cholesterol increased at 33 °C compared with 37 °C, whereas the amount of unsaturated lipids, especially those with more than 2 double bonds (polyunsaturated phosphatidylcholine (PuPC)), decreased.

Moderate hypothermia increases the size of condensed domains in surfactant films, promoting the exclusion of unsaturated phospholipids upon breathing-like cycling

Starting from the lipidomic results, the interfacial properties of simplified models of surfactant lipids and proteins were analysed in the CBS. The aim was to understand the contribution of saturated and unsaturated lipids along with hydrophobic surfactant proteins to the temperature-mediated improvement of surfactant activity. To do so, several mixtures of surfactant lipid (DPPC, POPG, POPC and DOPC at different proportions) with decreasing capability to pack under compression were combined with SP-B alone (1% total protein-to-lipid by weight) or with the fraction obtained from LH-20 column of size-molecular exclusion chromatography (MEC), containing both SP-B and SP-C (2% total protein-to-lipid by weight).

The combination of DPPC, POPC and POPG roughly simulates the composition of a typical lung surfactant in terms of saturated/unsaturated and zwitterionic/anionic phospholipid species. The presence of DOPC brings the contribution of phospholipids with a large area per molecule, such as it is the case with polyunsaturated species.

The surface properties of each mixture were assayed under quick cycles (20 cycles/min) in the CBS (**Figure 49**). No differences among 33 and 37 °C were noticed for PS at 8 mg/mL since its activity was optimal at this concentration (**Figure 44**). Thus, only results at physiological temperature (37 °C) for PS are shown and considered as control for ideal biophysical performance (γ_{min}< 2mN/m).

The presence of both SP-B and SP-C increased the adsorption and dynamic activity of all tested materials regardless of the experimental temperature. Upon dynamic cycling, there was a significant reduction in minimal surface tensions at 33 °C compared with 37 °C when a high percentage of DPPC (65%) with respect to POPG (35%) was present (**Figure 49**, second row). This difference was more evident in the absence of SP-C, suggesting the importance of both hydrophobic proteins to exclude POPG from the interface under compression. Moreover, although both SP-B and SP-C were present (**Figure 49,** second row), a trend to significance was observed at 33 °C for the reduction in area that is required to reach minimal surface tension: [13.6 (2.3)% at 33 °C vs 23.8 (2.2)% at 37 °C, p= 0.05].

Together with the DPPC content, the steric hindrance of excluded phospholipids under compression also enhanced surfactant activity at 33 °C. The difference among temperatures was significant in the presence of DOPC (**Figure 49**, fourth row). Conversely, the lipid-protein mixture containing POPC did not show any temperature-mediated changes in surface-active properties. Phospholipids of this mixture probably did not mix well, leading to a marked variability among replicates in CBS and the co-existence of 2 peaks in DSC (**Figure 50**).

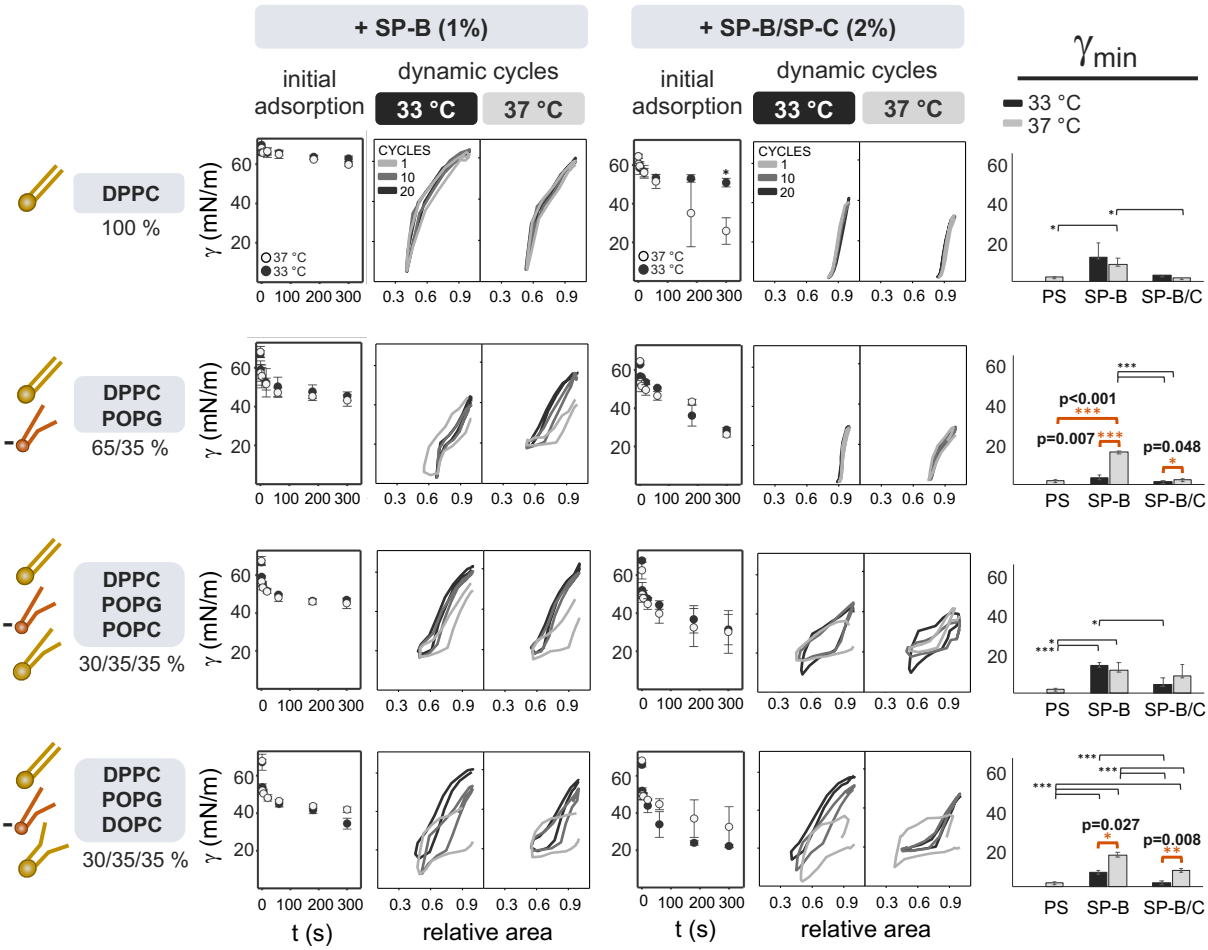

Figure 49. Contribution of lipid species and hydrophobic surfactant proteins in the temperature-mediated improvement of surfactant activity. Several surfactant lipid mixtures (DPPC, POPG, POPC and DOPC at different proportions) with decreasing capability to pack under compression were combined with purified porcine surfactant protein SP-B alone (1% w/w) or both SP-B and SP-C (2% total protein-to-lipid by weight). CBS experiments, using a concentration of 8 mg/mL of each lipid-protein mixture, were performed at 33° C or 37° C. On the left, the mass percent of the lipids used in each experiment is shown. Drawings of the lipids are also shown to illustrate the different space occupied at the interface according to their unsaturation grade. Graphs of initial adsorption show means and SD of three replicates per condition. One representative replicate (n= 3) of γ-Δarea isotherms under 10 quick compression-expansion cycles (20 cycles/min) is also shown. Graphs on the right compare minimum surface tensions (γ_{min}) reached upon 20 dynamic cycles (n= 3), also with purified PS (8 mg/mL). Isotherms of compression-expansion cycles are depicted in grey scale. Means and SD of three replicates are shown. Horizontal lines represent statistical comparisons. Black and light-grey colours represent experiments performed at 33° C and 37° C, respectively. Two-way ANOVA test followed by post-hoc test: * p< 0.05, ** p< 0.01, *** p< 0.005. The exact p values of the most relevant post-hoc tests are indicated (the comparison bars and symbols highlighted in orange colour). Abbreviations: γ, surface tension; γ_{min}, minimum surface tension; DPPC, dipalmitoylphosphatidylcholine; POPG, palmitoyloleoylphosphatidylglycerol; POPC, palmitoyloleoylphosphatidylcholine; DOPC, dioleoylphosphatidylcholine; PS, purified porcine surfactant.

When the minimum surface tension for each mixture under breathing-like interfacial dynamic were compared to PS (**Figure 49**, plots on the right), PS activity was similar to the activity of the mixture containing DPPC/POPG (65/35 %, w/w) with SP-B alone or with SP-C. This result was more evident for material tested at 33 °C.

A

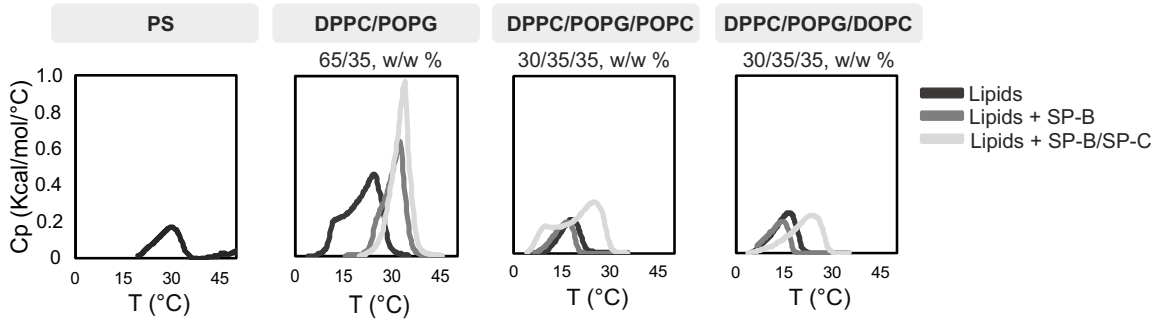

B

Samples	Tm (°C), mean (SD)
PS	29.7 (0.4)
DPPC/POPG	12.4 (0.3) - 24.5 (0.1)
DPPC/POPG + SP-B	**32.4 (0.1)**
DPPC/POPG + SP-B/C	**33.9 (0.1)**
DPPC/POPG/POPC	17.8 (0.1)
DPPC/POPG/POPC + SP-B	16.7 (0.2)
DPPC/POPG/POPC + SP-B/C	10.2 (0.6) - 24.9 (0.2)
DPPC/POPG/DOPC	15.6 (1.0)
DPPC/POPG/DOPC + SP-B	14.8 (0.3)
DPPC/POPG/DOPC + SP-B/C	23.5 (0.3)

Figure 50. Differential scanning calorimetry of PS and lipid-protein mixtures used in the CBS experiments. (A) One representative thermogram (n= 3) for PS, lipid mixtures alone, lipid mixtures with SP-B (1% w/w) or SP-B/SPC (2% w/w). **(B)** Summary table of the different melting temperatures. The melting temperatures of PS, [DPPC/POPG + SP-B] and [DPPC/POPG + SP-B/SP-C] mixtures are similar and close to the temperature used during moderate hypothermia (33 °C). Abbreviations: Cp: Specific heat capacity; T_m: melting temperature; DPPC: dipalmitoylphosphatidylcholine; POPG: palmitoyloleoylphosphatidylglycerol; POPC: palmitoyloleoylphosphatidylcholine; DOPC: dioleoylphosphatidylcholine; PS: porcine surfactant.

In the DSC experiments, the presence of both hydrophobic proteins (light-grey plot) increases the melting temperature in each condition, shifting the thermogram to right in the graphs (**Figure 50A**). This is likely due to the establishment of electrostatic interactions between the cationic proteins and the anionic PG, as previously reports (Shiffer *et al*, 1993).

The presence of SP-B alone increases the melting temperature for the lipid-protein mixture containing DPPC and POPG. Moreover, the melting temperatures of the mixtures containing DPPC/POPG (65/35 %, w/w) with SP-B alone or with SP-C were very close to that of therapeutic hypothermia: 32.4 (0.1) and 33.9 (0.1) °C. Interestingly, these samples showed the most evident temperature-mediated improvement in their surface-active properties (**Figure 49**, second row).

Moderate hypothermia decreases surfactant inhibition by plasma and enhances the restoration capability of therapeutic surfactants

To understand whether the boost in surfactant properties under therapeutic hypothermia was also present in an inhibitory environment and to study the effect of temperature on the restoration of surfactant activity, plasma was employed to recreate *in vitro* pulmonary inflammation-caused oedema and acute injury contexts. Moreover, the contribution of surfactant dilution and the restoration properties with further surfactant supplementation were also studied, comparing hypothermia and physiological temperatures.

The inhibition of PS activity by plasma was tested by CDS upon slow cycling (2 cycles/min) at different surfactant concentrations (1.5, 2.5 and 5 mg/mL), both at 33 and 37 °C (**Figure 51**). Within each condition, no differences between temperatures in initial adsorption and γ_{max} were noticed. Conversely, the dynamic activity (γ_{min}) of PS at 1.5 mg/mL was clearly impaired in the presence of plasma (**Figure 51**, middle panel). Interestingly, at this concentration, PS capability to produce very low surface tension was reduced with and without plasma at 37 °C, but it was still functional in the absence of plasma at 33 °C. On the other hand, when PS was tested at 2.5 mg/mL it worked properly in the presence of plasma at 33 °C, but it was inactivated at 37 °C. With this in mind, restoration experiments (**Table 11**) were then performed, maintaining the same amount of plasma, but using different concentrations of PS depending on the experimental temperature: 1.5 mg/mL at 33 °C and 2.5 mg/mL at 37 °C.

The restoration capability of two different materials were studied under these conditions: 1) Poractant alfa, a widely used therapeutic surfactant, and 2) the mixture DPPC/POPG (65/35, w/w) + SP-B/SP-C (2% total protein-to-lipid by weight), the lipid-protein mixture that had shown the best surface-activity (comparable to PS). Several amounts of these materials were used to mimic a therapy, by adding small volumes at increasing concentrations on top of plasma-inhibited surfactant until reaching restoration of low surface tension values (**Table 11**). These amounts were calculated as the mass percentage of dispensed phospholipids with respect to the amount of phospholipids in the inhibited surfactant (e.g. 5 μL of PS at 1.5 mg/mL were used at 33 °C, thus 80% of therapy means that 6 μg of therapy was required to restore surface tension reduction). Since the concentration of surfactant material highly influences its surface-active properties (Gunasekara *et al.*, 2008), the same therapy concentration for both temperatures was used. This required dispensing larger volumes of surfactant therapy at 37 °C compared with 33 °C, still maintaining values up to 4% of the constrained drop volume.

As a result, the same percentage (with respect to total phospholipids in the inhibited PS) and concentration of therapy were used regardless of the experimental temperature. Moreover, due to the different starting PS concentration (1.5 and 2.5 mg/mL for 33 and 37 °C, respectively), the percentage of therapy necessary to rescue PS activity was considered for data interpretation. The effects of adding buffer alone to the inhibited PS were also analysed as a reference (**Figure 52**).

Regardless of the therapy used, the amount of surfactant necessary to restore PS activity was always lower at 33 °C compared with 37 °C, being more evident for the protein-lipid mixture. The latter showed better restoration (required 80-100% therapy), compared to Poractant alfa (only restoring upon addition of 200% therapy) with a temperature-mediated improvement in the restoration capability (**Figure 52**). This was probably due to the better

exclusion of POPG from the interface under compression at 33 °C, leaving enough DPPC to reduce surface tension.

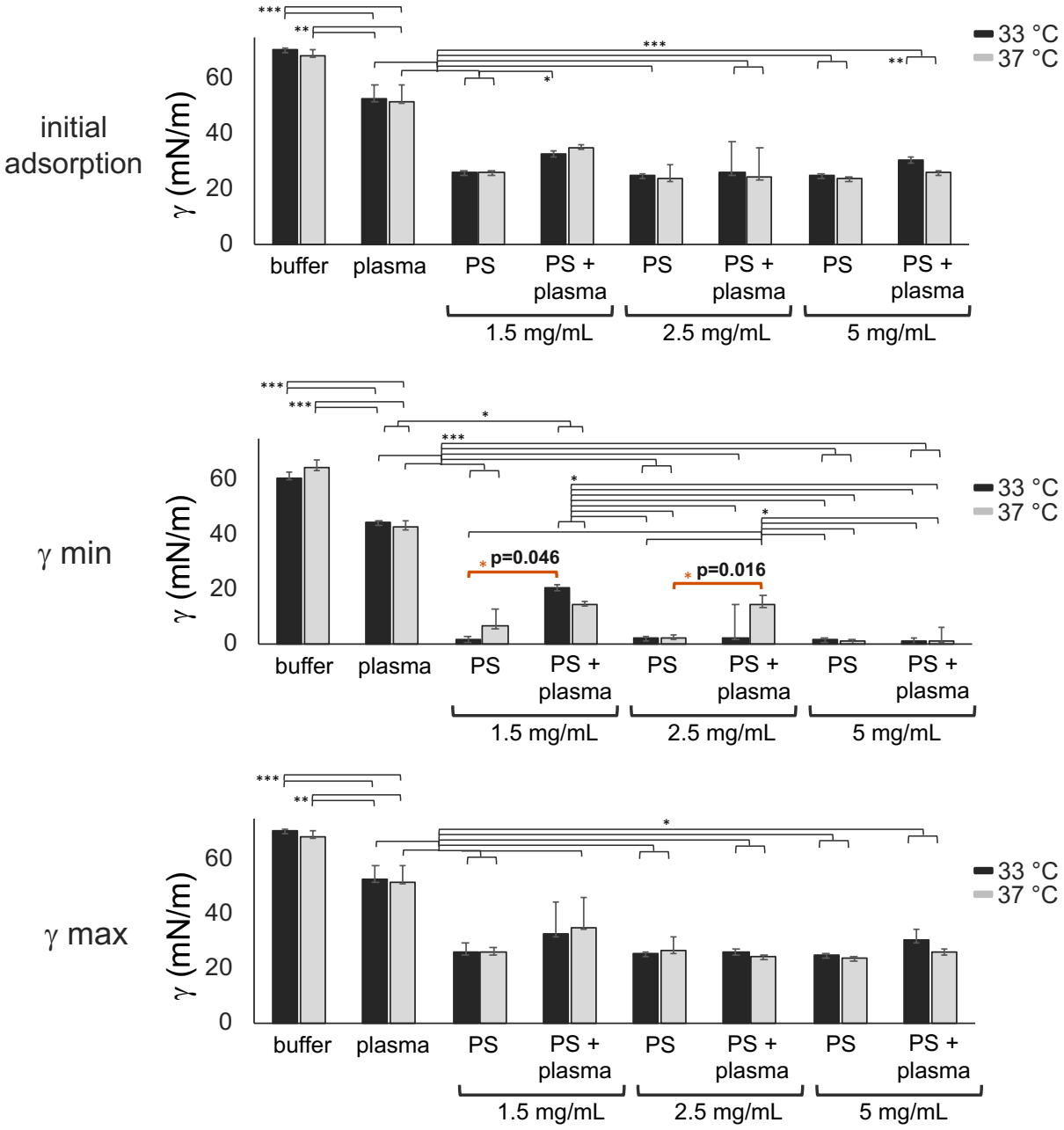

Figure 51. Inhibition of PS by plasma at different temperatures. CDS experiments of different concentrations of PS (1.5 (n= 4), 2.5 (n= 3) and 5 (n= 3) mg/mL) with and without plasma (68 mg/mL of total plasma proteins), corresponding to 1.6, 2.6 and 5.2% PLs/plasma total proteins. Surface tension after 10 second of material adsorption along with minimum and maximum surface tensions upon 10 slow compression-expansion cycles (2 cycles/min, reducing the interface area by 20 %, 0.2 cm^2/min) are depicted compared to plasma (n= 3) and buffer alone (n= 3). Black and light-grey bars represent experiments performed at 33° C and 37° C, respectively. Means and standard deviation of at least three replicates are shown. Horizontal lines represent statistical comparisons. Two-way ANOVA test followed by post-hoc test: * p< 0.05, ** p< 0.01 and ≥ 0.005, *** p< 0.005. The exact p values of the most relevant post-hoc tests are indicated (the comparison bars and symbols highlighted in orange colour). Abbreviations: PS, purified porcine surfactant; γ, surface tension; min, minimum; max, maximum.

DPPC/POPG (65/35, w/w %) + SP-B/C (2% of total w)							
33 °C				37 °C			
Therapy (%)	Volume (nL)	[ ], mg/mL	PS restoration	Therapy (%)	Volume (nL)	[ ], mg/mL	PS restoration
50	200	20	✘	50	-	-	✘
80	150	40	✔	80	250	40	✘
-	-			100	300	40	✔
PORα							
33 °C				37 °C			
Therapy (%)	Volume (nL)	[ ], mg/mL	PS restoration	Therapy (%)	Volume (nL)	[ ], mg/mL	PS restoration
50	200	20	✘	50	-	-	✘
80	150	40	✘	80	-	-	✘
100	150	50	✘	100	250	50	✘
200	150	100	✔	200	250	100	✔

Table 11. Different concentrations and volumes used for the *in vitro* restoration experiments in the CDS. The different percentages of therapy required [(μg phospholipids therapy/μg phospholipids in inhibited PS) x 100] are summarised together with the concentrations of materials and volumes dispensed on the top of the drop. The percentages of therapy able to restore PS activity are highlighted in green. Abbreviations: DPPC, dipalmitoylphosphatidylcholine; POPG, palmitoyloleoylphosphatidylglycerol; PORα: Poractant alfa; [ ]: concentration.

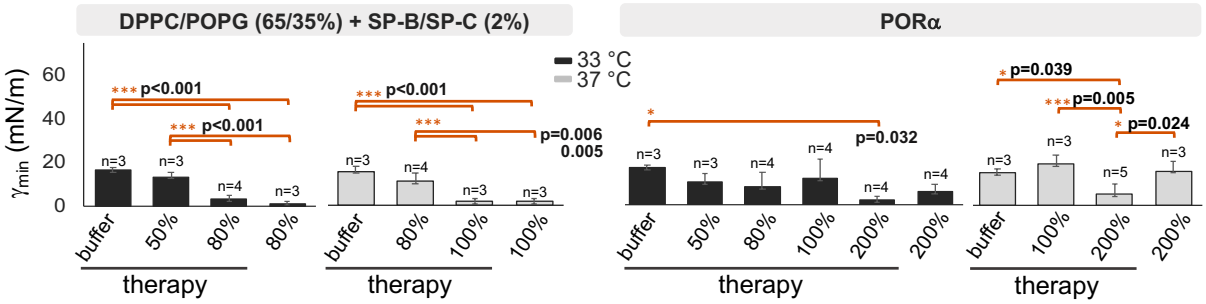

Figure 52. Restoration of inhibited PS at different temperatures. Restoration of PS activity was carried out after plasma inhibition, with 1.5 mg/mL or 2.5 mg/mL of PS at 33° C and 37° C. Once PS was inhibited, several amounts of further surfactant were supplemented to mimic therapy, using Poractant alfa or the lipid-protein mixture [DPPC/POPG (65/35%, w/w) + SP-B/SP-C (2% total protein-to-lipid by weight)]. These supplemented amounts were calculated as the percentage of μg of phospholipids of therapy with respect to the μg of inhibited PS. As further controls, only buffer was dispensed as a mock therapy for inhibited PS and the restoration therapy was analysed in the presence of plasma alone. Black and light-grey bars represent experiments performed at 33° C and 37° C, respectively. Means and standard deviation of at least three replicates are shown. Horizontal lines represent statistical comparisons. Two-way ANOVA test followed by post-hoc test: * p< 0.05, ** p< 0.01, *** p< 0.005. The exact p values of the most relevant post-hoc tests are indicated (the comparison bars and symbols highlighted in orange colour). Abbreviations: PS, purified porcine surfactant; γ, surface tension; min, minimum; DPPC, dipalmitoylphosphatidylcholine; POPG, palmitoyloleoylphosphatidylglycerol; PORα: Poractant alfa.

To further investigate this hypothesis, three lipid-protein mixtures with decreasing DPPC/POPG ratios were tested with plasma in the CDS at 33 and 37 °C and compared to Poractant alfa (**Figure 53**). Materials were released directly at the air liquid interface of a plasma drop which was previously subjected to 6 expansion-compression cycles. Subsequently, initial spreading and variation in surface tension under four slow dynamic cycles were detected.

Interestingly, the lipid-protein mixtures with DPPC ≥ 50% and POPG ≤ 50%, seem to be more resistant to plasma inhibition than Poractant alfa regardless of the experimental temperature. On the contrary, when increasing the amount of POPG to 65%, the activity was inhibited at 37 °C but still functional at 33 °C (**Figure 53)**.

A tendency to obtain a higher hysteresis at 37 °C compared with 33 °C was always present, but was more evident in the case of Poractant alfa. This may somehow be related to the presence of a more complex mixture, also containing PuPC, in the case of the animal-derived surfactant, produced from an organic extract of minced porcine lungs.

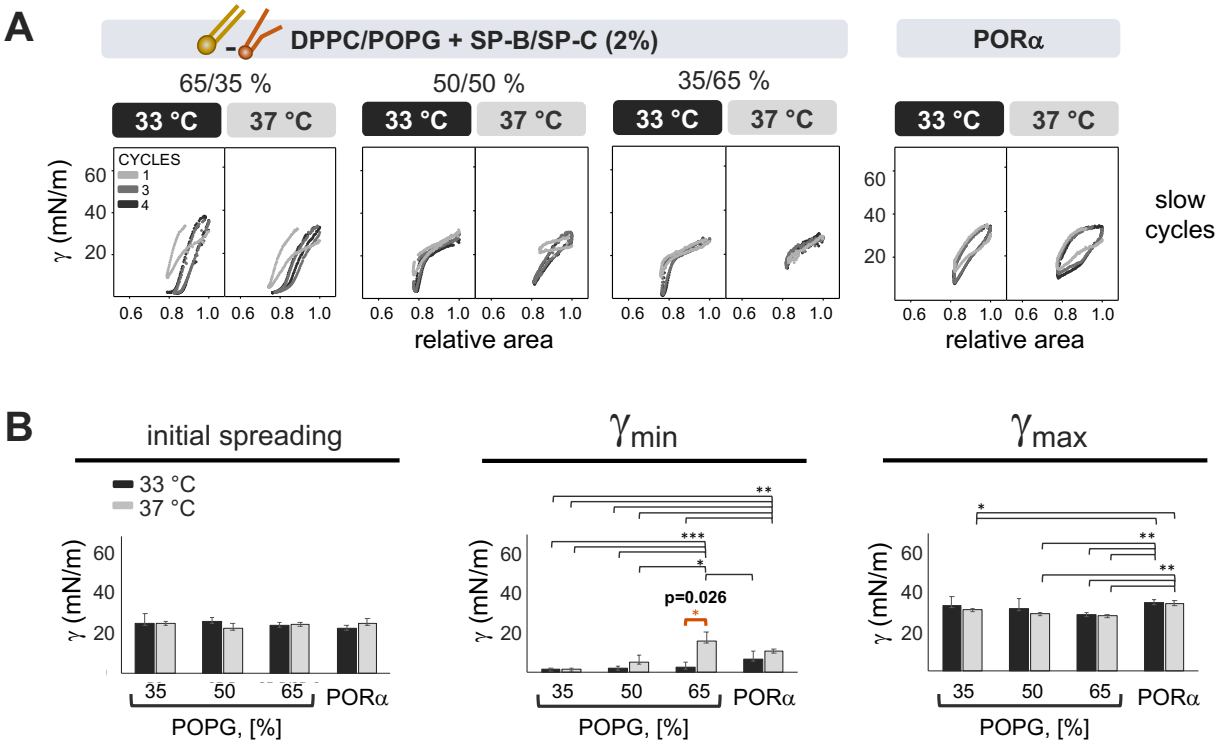

Figure 53. Temperature-mediated resistance to plasma inhibition, depending on DPPC/POPG ratio. About 200 nL at 40 mg/mL of Poractant alfa (n= 5, 33 °C; n= 3, 37 °C) or the lipid-protein mixtures [DPPC/POPG + SP-B/SP-C (2% total protein-to-lipid by weight)] with increasing percentages of POPG (n= 3 for each mixture and temperature), were dispensed at the interface of a plasma drop and subjected to 4 slow cycles in CDS (2 cycles/min, reducing the interface area by 20%, 0.2 cm^2/min). **(A)** One representative replicate of γ-Δarea isotherms at the 2 temperatures is shown for each tested material. **(B)** On the left, γ values reached after 10 seconds of material spreading at the plasma interface (initial spreading). In the middle and on the right, γ_{min} and γ_{max} reached during cycling. Compression-expansion cycles are depicted in grey scale. Black and light-grey bars represent experiments performed at 33 °C and 37 °C, respectively. Means and SD of at least three replicates are shown. Horizontal lines represent statistical comparisons. Two-way ANOVA test followed by post-hoc test: * p< 0.05, ** p< 0.01, *** p< 0.005. The exact p values of the most relevant post-hoc tests are indicated (the comparison bars and symbols highlighted in orange colour). Abbreviations: DPPC, dipalmitoylphosphatidylcholine; POPG, palmitoyloleoylphosphatidylglycerol; PORα, Poractant alfa; γ, surface tension; min, minimum; max, maximum.

Moderate hypothermia and CHF 5633 therapy: the proof of concept

As previously described, the lipid-protein mixture containing the same proportion of DPPC and POPG (50/50%, w/w) showed a good performance at both 37 and 33 °C in the presence of plasma with an enhanced activity at hypothermia temperature (**Figure 53**). Interestingly, this model mixture is quite similar to the synthetic clinical surfactant CHF 5633 in both lipid and protein composition, although CHF 5633 does not contain the whole native hydrophobic surfactant proteins. Thus, the next step was to move from these *in vitro* evidences to an *in vivo* model of lung injury in newborn piglets, investigating how the combination of WBH treatment and a surfactant replacement therapy with CHF 5633 may restore surfactant function and breathing under lung injury. To do so, a very preliminary study was performed, enrolling only 5 piglets to explore the feasibility of such clinically relevant model. However, the results may serve as a first proof of concept for future detailed investigation on larger sample size. The study design was summarised in **Figure 54**.

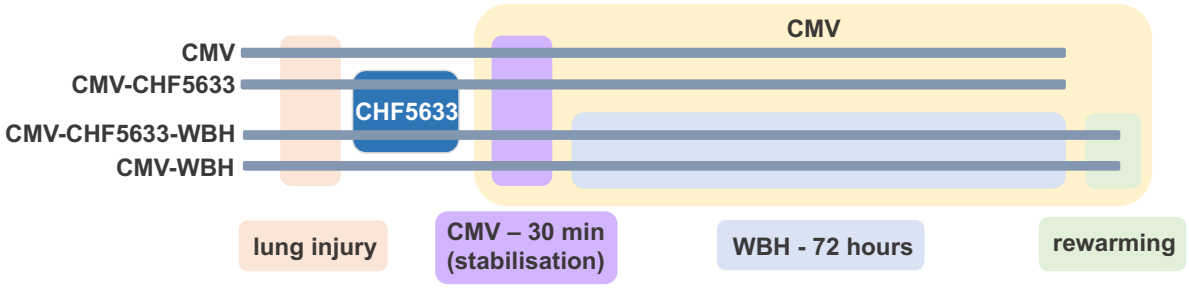

Figure 54. Study design of newborn piglets in a lung injury model. Four different groups were used for the study: (1) one piglet with lung injury subjected to controlled mechanical ventilation (CMV) for 72 hours after 30 minutes of stabilisation (CMV), (2) two piglets with lung injury subjected to CMV and WBH for 72 hours after 30 minutes of stabilisation under CMV (CMV-WBH), (3) two piglets with lung injury receiving CHF 5633 before 30 minutes of stabilisation and 72 hours of CMV (CMV-CHF5633), (4) one piglet with lung injury receiving CHF 5633 before 30 minutes of stabilisation and 72 hours of CMV under WBH (CMV-CHF5633-WBH). Lung injury was induced by subsequent BALs and depletion of surfactant before starting CMV. The three piglets under WBH were also subjected to rewarming (approximately 6 hours). Abbreviations: CMV, controlled mechanical ventilation; WBH, whole body hypothermia.

Animals used for each group were similar in size (≈2 Kg) and age (≈4 days). Lung injury was induced by multiple BALs (CMV group: 8; CMV-WBH group: 8±1; CMV-CHF5633 group: 8; CMV-CHF5633-WBH group: 8). All animals showed similar gas exchange and ventilatory parameters at baseline. Repeated BALs produced a drastic decrease of PaO_2/FiO_2 and VEI with an increase of OI and $PaCO_2$ level (**Figure 55**) in all piglets. Moreover, after BALs, all groups showed a decrease of tidal volume and dynamic compliance (Cdyn), although maintaining similar mean airway pressure (Paw=11 cmH_2O at BAL and 30 cmH_2O at stabilisation point). The impairment of those parameters suggested that repetitive BALs in newborn piglets produced a stable moderate respiratory distress.

As shown in **Figure 55A**, when comparing the CMV piglet with CMV-WBH piglets, there were an increase in PaO_2/FiO_2 and VEI and a decrease in OI under hypothermia treatment. At the same time, the replacement therapy with CHF 5633 rapidly improved PaO_2/FiO_2, VEI and OI values regardless of the WBH treatment. The enhancement in the respiratory parameters

were maintained during all WBH period (72 hours). Moreover, the CMV-CHF5633-WBH piglet showed better VEI than the other studied groups, apparently since a lower respiratory rate was needed to maintain normal $PaCO_2$ values (**Figure 55B**). However, VEI slightly decreased during rewarming, probably due to the simultaneous increase in respiratory rate (**Figure 55A**, second row).

When CHF 5633 was administered, FIO_2, namely the fraction of inspired oxygen needed to maintain normoxia values, was rapidly reduced in both groups regardless of hypothermia treatment (**Figure 55C**, first row).

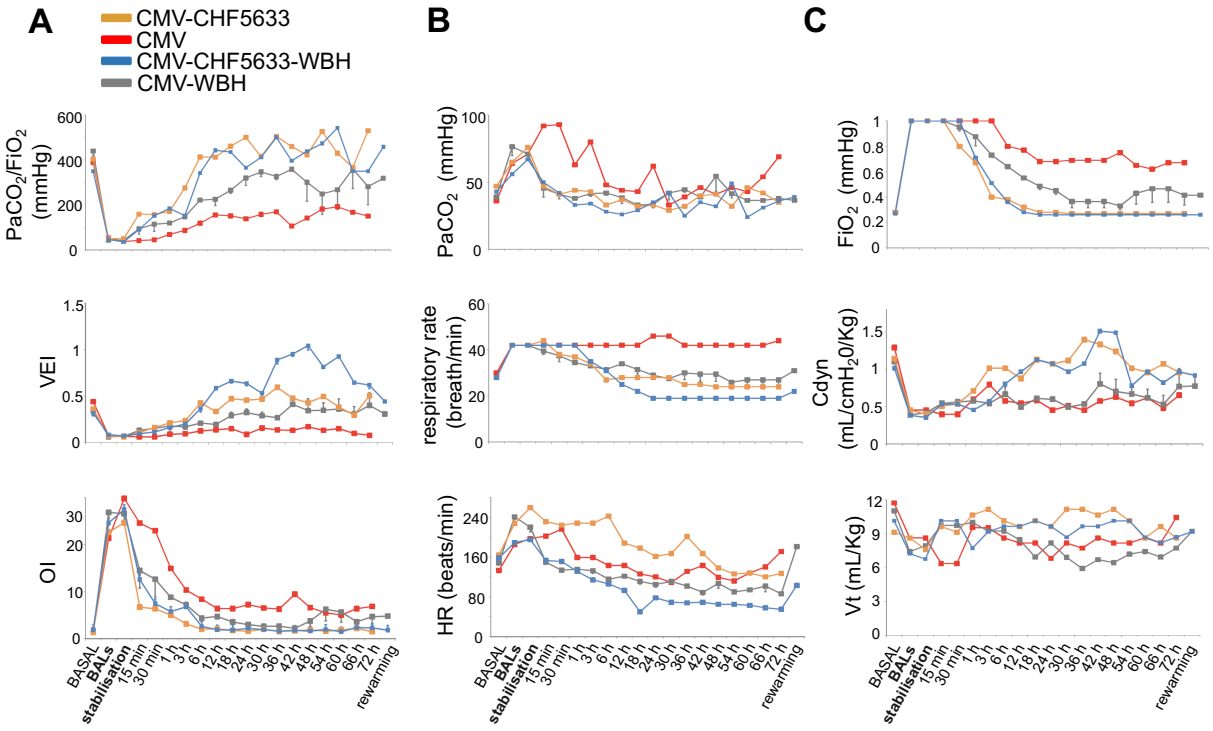

Figure 55. Respiratory parameters and heart rate of the studied groups. Each value was measured at basal time point, after repeated BALs (lung injury), after 30 minutes of stabilisation, after 15 minutes, 30 minutes, 1 hour, 3 and 6 hours from stabilisation and every 6 hours during the following three days. As for WBH groups, values were also measured 6 hours after rewarming. Abbreviations: PaCO2, partial pressure of carbon dioxide; FiO_2, fraction of inspired oxygen; VEI, ventilator efficiency index; OI, oxygenation index; HR, heart rate; Cdyn, dynamic compliance; Vt, tidal volume; BALs, bronchoalveolar lavages; CMV, controlled mechanical ventilation; WBH, whole body hypothermia.

Besides, a slight delay in the FIO_2 reduction (of around 30 minutes) was observed in the CMV-CHF5633-WBH piglet compared to the CMV-CHF5633 piglet. This trend could be also appreciated in the PaO_2/FIO_2 values. Both tidal volume and dynamic compliance were lower in CMV- and CMV-WBH groups compared with piglets treated with CHF 5633 (**Figure 55C**, second and third rows). Moreover, there were not significant differences between groups in mean arterial blood pressure values along the three days and, as expected, both WBH groups showed a decrease in heart rate during hypothermia treatment, which was recovered after rewarming (**Figure 55B**, third row).

Thus, although very preliminary, this study seems to confirm the protective role of WBH during lung injury due to surfactant deficiency. At the same time, the administration of CHF

5633 seems to promote a rapid improvement of PaO_2/FiO_2, VEI and OI as well as dynamic compliance and tidal volume, regardless of WBH treatment. Interestingly, the CMV-CHF5633-WBH piglet shows better VEI than the other studied groups, validating the effectiveness of coupling WBH and surfactant therapy *in vivo* upon lung injury characterised by diluted surfactant material in the airways.

Discussion

In this chapter, the *in vitro* effect of therapeutic-like hypothermia on lung surfactant activity and composition was investigated in the presence and absence of plasma inhibition. In detail, therapeutic hypothermia induces several *in vitro* effects on surfactant properties, compared with its performance at physiological temperature: (1) the capability of PS to drastically reduce surface tension under breathing-like conditions is enhanced in a concentration-dependent manner; (2) surfactant structure and composition at the air-liquid interface re-organise differently under compression (expiration): larger DPPC-enriched condensed domains and lower percentages of less active lipids are detected at 33 °C; (3) PS resistance to plasma inhibition is boosted under cooling; (4) *in vitro* restoration therapies are more effective at 33 than at 37 °C; (5) the higher the DPPC proportion, the better the restoration performance under therapeutic hypothermia. Moreover, the proof of concept of coupling WBH treatment and a therapy with the synthetic surfactant CHF 5633 was demonstrated by using a piglet model of lung injury due to surfactant deficiency. Although neonatal, this model may also resemble lung conditions under which surfactant is injured and diluted, such as ARDS.

Up to now, no causal therapies are available for ARDS. Although surfactant inhibition is not necessarily the primary pathogenic factor during ARDS (Matthay *et al.*, 2019), the protein-rich oedema fluid leaking into the alveoli and the local inflammation make its inactivation a secondary and critical feature of the syndrome (Günther *et al.*, 2001; Gunther *et al.*, 1996; Schmidt *et al.*, 2007; Schmidt *et al.*, 2001). This occurs through different biological mechanisms. For instance, several plasma proteins (albumin, fibrinogen) inhibit the proper adsorption of surfactant, creating a steric barrier at the interface, fluidifying surfactant membranes (CRP) or degrading surfactant lipids (lipases, $sPLA_2$) and proteins (proteases) (Autilio & Pérez-Gil, 2019; Echaide *et al.*, 2017; Günther *et al.*, 2001). The results described here suggest that the initial adsorption of diluted PS in the presence of plasma was similar at 33 °C and 37 °C. However, plasma compounds seem to be better excluded at 33 °C upon interfacial dynamics. Consistently, the γ_{min} was very low regardless of the plasma presence, testing surfactant at 2.5 mg/mL and 33 °C. On the contrary, there was a significant increase in γ_{min} when PS was assayed with plasma at 37 °C (**Figure 51**).

Interestingly, some plasma proteins, such as fibrinogen, can be found into the liquid-expanded phase during lateral compression (Williams *et al.*, 2019). Due to the lipid de-mixing, larger condensed (DPPC-enriched) domains were observed at 33 °C and a liquid-expanded phase with larger excluded three-dimensional structures also appeared at this temperature (**Figure 46** and **Figure 47**). A temperature-dependent segregation of condensed domains during interfacial compression was already described for DPPC and bovine surfactant (Discher *et al*, 1996). Thus, a similar mechanism may probably occur with plasma compounds. As it happens with unsaturated phospholipids (Egberts *et al.*, 1989), plasma proteins might be better (at lower pressures) squeezed out from the interface at 33 °C, thus increasing the resistance to plasma inactivation under therapeutic hypothermia. Moreover, in both adult and meconial

ARDS, as also demonstrated in the previous chapters, high cholesterol and PuPC levels are present, either associated to a lung response or due to plasma extravasation and meconium injury (Autilio *et al*, 2018; Autilio *et al*, 2020; Markart *et al.*, 2007). This may impede surfactant to properly reduce surface tension during expiration. For instance, increasing the amount of cholesterol with respect to DPPC leads to changes in the proper packing of DPPC domains, affecting the capability to rise surface pressure (reduce surface tension) upon lateral compression (Miyoshi & Kato, 2015).

Interestingly, the surface elasticity of spread DPPC monolayers at high surface pressures seems to lower under increasing temperatures (Bykov *et al*, 2019). This reduces the interfacial activity of the material, probably due to the quicker relaxation of DPPC films that lose their capability to sustain high surface pressure. In the present experiments, an increased percentage of cholesterol and saturated lipids was detected at the air-liquid interface at 33 °C. The sterol presence seems to influence the dynamic surface elasticity of DPPC monolayers under compression (Vrânceanu *et al*, 2008). However, we still observed a temperature-mediated effect on the lateral organisation of DPPC/unsaturated PC domains of PS at the air-liquid interface (**Figure 46** and **Figure 47**). This is probably associated with the simultaneous increase in both cholesterol and saturated lipids detected at hypothermia temperature (**Figure 56**). In this regard, we demonstrated formation of larger condensed interfacial domains at 33 °C than at 37 °C during lateral compression (**Figure 47**). Cholesterol may insert preferentially into these ordered structures (Andreev *et al*, 2020). Thus, a larger DPPC proportion at the interface at 33 °C might cause a higher amount of cholesterol to partition from the surrounding disordered phases.

These results may suggest a protective role of therapeutic hypothermia reducing the cholesterol-mediated inhibition. This might occur by promoting DPPC de-mixing and thus increasing the amount of DPPC at the interface during compression at 33 °C compared with 37 °C. This indirectly contributes to higher sterol captures into ordered domains at hypothermia temperature. This model may also explain why the differences in dynamic properties of lung surfactant are more evident after 72 hours of WBH in neonates. At this time point, although maintaining the same amount of DPPC, there was a decrease in both cholesterol and the content of surfactant hydrophobic proteins. The reduction in cholesterol may result in a reduction in the sterol present in the ordered DPPC domains. This increases the amount of condensed DPPC domains without cholesterol as well as the presence of disordered domains no longer ordered by the sterol. Thus, a reduced amount of cholesterol may contribute to enhance the interfacial properties under compression of DPPC-enriched films and simultaneously decrease those of film containing higher unsaturated phospholipid levels. Since at 37 °C there is an increase in unsaturated phospholipids and a simultaneous decrease in saturated phospholipids at the air-liquid interface under compression, this may explain the drastic difference among temperatures observed after 72 hours of WBH in films subjected to fast breathing-like compression-expansion cycles of the interface (**Figure 39**). This evidence was also confirmed by the *in vitro* experiments performed using the protein-mixtures containing DPPC, POPG and DOPC that showed drastic temperature-mediated differences without cholesterol, especially in the absence of SP-C (**Figure 49**). In this regard, as discussed in chapter IV, SP-C could probably mediate similar effects than increasing temperature, such as membrane bending, on the dynamics of the system. This leads to (1) an improvement in the adsorption of material at the air-liquid interface, reducing the dilution of surfactant and (2) an effect that counterbalances the system stabilisation promoted by low temperatures. Thus, the

presence of SP-C could reduce the hypothermia-mediated effects in both *ex vivo* and *in vitro* experiments.

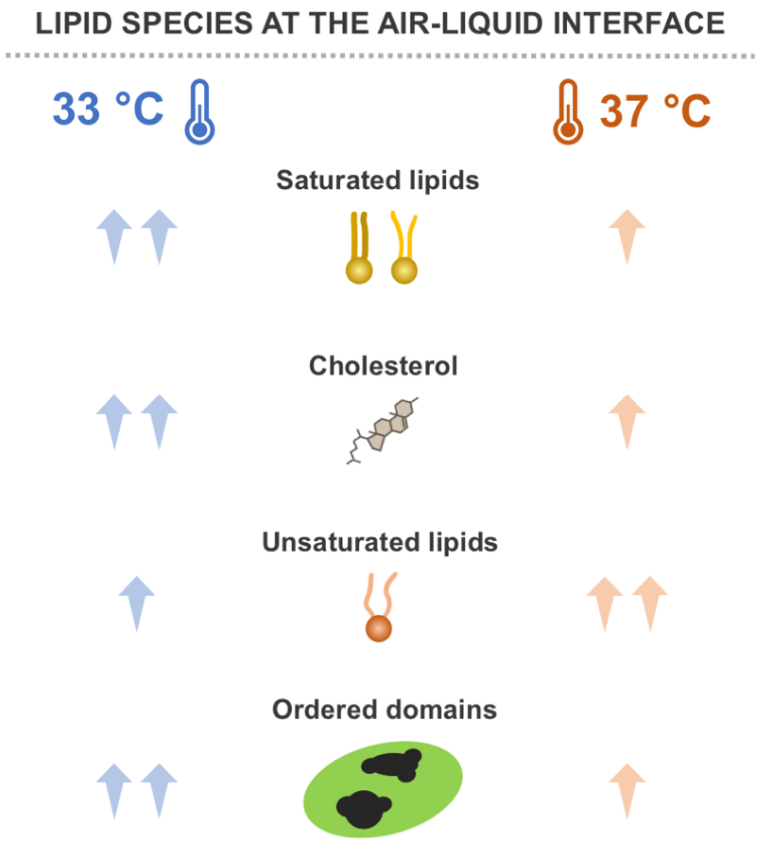

Figure 56. Schematic representation of possible candidates involved in the temperature-mediated improvement of surfactant performance at the air-liquid interface. Therapeutic hypothermia (33 °C) seems to promote the presence of higher levels of cholesterol and saturated lipids (mainly DPPC) along with reduced amount of unsaturated lipid species at the interfacial surfactant film, compared with 37 °C. This promotes the formation of ordered condensed domains with larger size at hypothermia temperature compared with 37 °C.

During ARDS, higher levels of $sPLA_2$ lead to a significant reduction in both surfactant DPPC (Günther *et al.*, 2001; Gunther *et al.*, 1996; Schmidt *et al.*, 2007; Schmidt *et al.*, 2001) and PG amounts (Seeds *et al.*, 2012). At the same time, surfactant proteins decrease (Günther *et al.*, 2001) and ROS increase, oxidizing the lipid-protein membranes (Autilio & Pérez-Gil, 2019). As a result, the availability of surface-active material is drastically reduced and surfactant complexes become inactivated. Interestingly, as suggested by the current results, therapeutic hypothermia could be beneficial under these impaired surfactant conditions: (1) at lower concentration, as in a ARDS context, surfactant performance is better at 33 °C than 37 °C (**Figure 42-44**), (2) surfactant exhibits higher resistance to plasma inhibition under therapeutic hypothermia (**Figure 51**); (3) due to the lower miscibility of lipids at 33 °C, unsaturated lipids (e.g. PuPC and DOPC) and plasma components are removed more efficiently from the interface. This occurs with a lower loss of DPPC during the interfacial compression (at expiration) (**Figure 49** and **Figure 53**). This last mechanism (outlined in

Figure 57) fits with the first two effects perfectly. A better performance of surfactant at 33 °C with and without plasma is closely linked to the concentration of tested material. Lower concentrations mean lower DPPC amounts at the air-liquid interface, that are even more reduced under compression at 37 °C.

Finally, an increase in both the endogenous and therapeutic surfactant performance under cooling was demonstrated (**Figure 52**). Regardless of the material applied (Poractant alfa or lipid-protein mixtures containing different proportions of DPPC and POPG), lower doses were more resistant to plasma inhibition and able to restore PS activity at 33 °C compared with 37 °C. Moreover, the resistance to plasma inactivation was higher at high DPPC ratios regardless of the temperature (**Figure 53**). Altogether, these results are promising for primary ARDS patients. In those patients, the maximum beneficial effect of exogenous surfactant should be warranted with the minimum dose.

The present data show a better plasma resistance for the lipid-protein mixture containing ≥ 50% DPPC when compared to Poractant alfa at both 33 °C and 37 °C (**Figure 53**). Similar results were obtained when studying the resistance of the synthetic clinical surfactant CHF 5633 to serum inactivation at physiological temperature. CHF 5633 composition is similar to the lipid-protein mixtures employed in the present study: 50/50 DPPC/POPG (w/w%) and 1.8% by mass of SP-B/SP-C analogues. Thus, it could be argued that the mechanism involved in plasma resistance of the studied synthetic lipid-protein mixture upon dynamic cycles may probably be analogous to that of CHF 5633 in the presence of serum, and particularly enhanced at 33 °C. In this line, the lipid-protein mixture with increased POPG/DPPC ratio showed a reduced activity at 37 °C, but was still functional at 33 °C. Plasma and serum proteins are excluded from the interface together with POPG during compression, presumably in a process lead by surfactant proteins/peptides. The same mechanism might occur under therapeutic hypothermia, with less DPPC lost from the interface during compression (**Figure 56**). The lower lipid miscibility at 33 °C may contribute to reduce DPPC mixing into the liquid-expanded phase and its interfacial exclusion under compression. This would explain the good performance of the material at low DPPC ratio (35%) (**Figure 53**).

Interestingly, promising preliminary results were obtained combining WBH and CHF 5633 in a model of lung injury related to surfactant deficiency. In spite of the small number of piglets, a positive effect of WBH on respiratory parameters were confirmed as well as the synergistic action of administrating the synthetic surfactant preparation together with therapeutic hypothermia. In this line, the ventilator efficiency index (VEI) which scores the pulmonary function, improves in the cooled piglet treated with CHF 5633 and this boosting occurs around 12 hours from WBH, reaching a peak at around 36-66 hours of cooling, suggesting an anticipation in the effect of WBH alone.

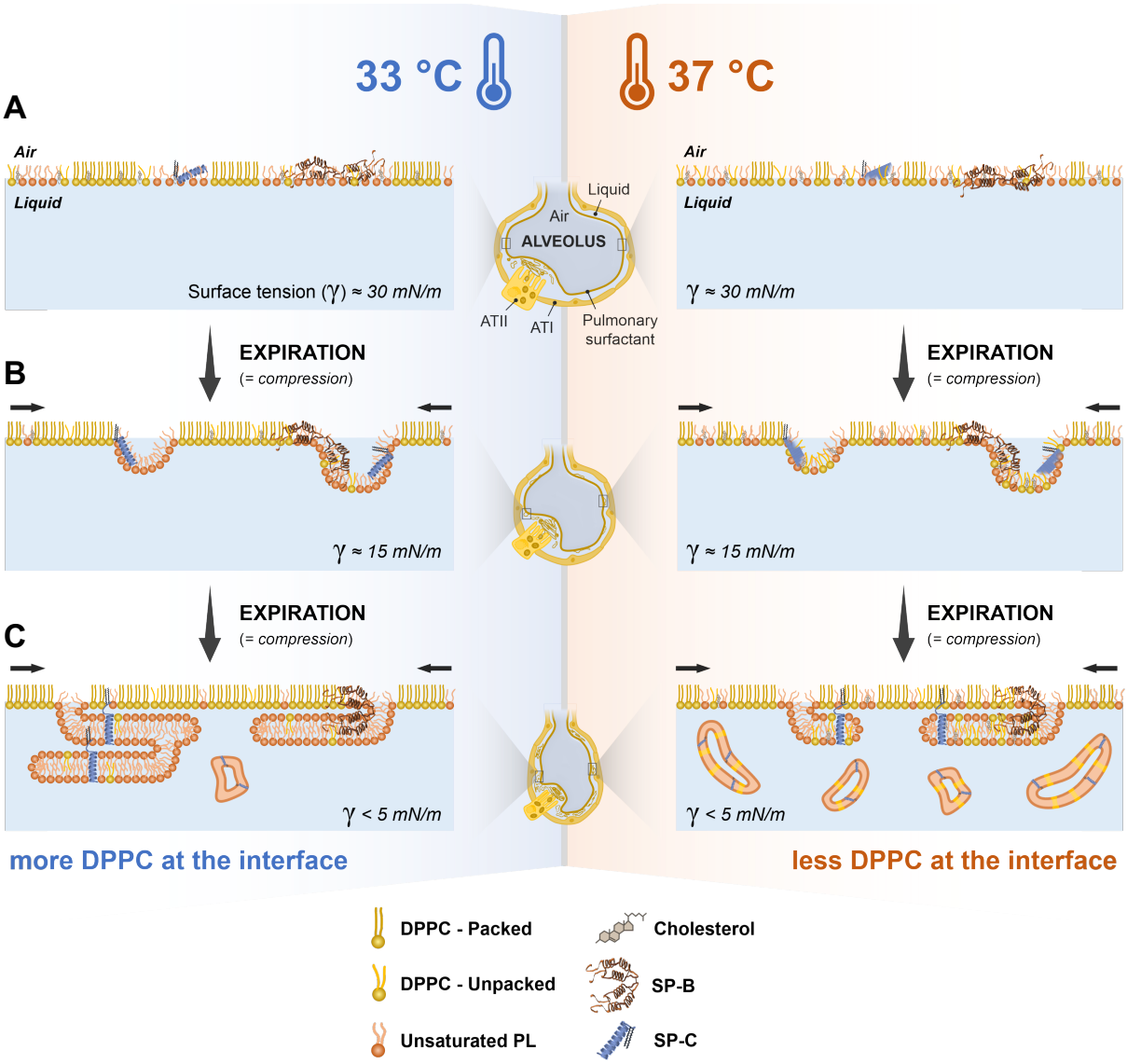

Figure 57. Temperature-mediated compression-driven reorganisation of surfactant at the air-liquid interface. (A) When surfactant adsorbs at the air-liquid interface, the lateral segregation between packed ordered domains (DPPC enriched) and expanded disordered lipids is less evident at 37 °C due to temperature-facilitated mixing. Larger condensed domains are visible at 33 °C. **(B)** During compression (at expiration), SP-B and SP-C promote surfactant reorganisation at the air-liquid interface, facilitating maximal reduction in surface tension. Areas rich in lipids with lower stability at high pressures, and therefore poorer surface-active properties (unsaturated lipids) are laterally and three-dimensional excluded from the air-liquid interface. Due to lipid de-mixing, the condensed ordered/liquid-expanded disordered phase segregation is more evident at 33 °C. This leads to compression-driven preferential exclusion of unsaturated lipids. Conversely, a fraction of DPPC is also lost from the interface at 37 °C because of the temperature-dependent partial mixing. **(C)** At the highest compression rates of the alveolar interface (at the end of expiration), lipids excluded from the interface are organised in three-dimensional structures that remain associated to the interfacial film. These structures might be more stable and firmly associated to the surface at 33 °C than 37 °C. Indeed, part of those membranes, containing higher DPPC proportions, may detach from the surface at 37 °C. This probably fuels both catabolism and recycling of surfactant lipids under physiological conditions when new surfactant components continuously adsorb and replenish the material lost at the interface. Conversely, the adsorption of surfactant would be compromised by several plasma compounds when they pass from systemic circulation to the alveolar space. This affects the amount of DPPC available to reduce surface tension at 37 °C and suggests a protective role at 33 °C. Abbreviations: DPPC, dipalmitoylphosphatidylcholine; γ, surface tension; AT-I, alveolar type I cell; AT-II, alveolar type II cell.

These results serve as a proof of concept for future detailed studies, which should increase the number of animals tested as well as performing biochemical and biophysical analysis on nBAL content. Moreover, in spite of the promising *in vitro* data, several limitations should be enumerated: (1) PS undergoes a temperature-mediated collapse under compression in the Langmuir-Blodgett balance (Rugonyi *et al.*, 2008). This prevents analysing surfactant interfacial structure and composition at surface pressures higher than 40 mN/m (surface tensions lower than 30 mN/m) like those presumably existing at the alveolar spaces, as measured in excised rat lungs under transpulmonary pressure (γ< 10 mN/m) (Schürch *et al*, 1978). In addition, a lipidomic analysis after several compression-expansion cycles could better define the compositional changes at the interface in a dynamic system. However, these experiments would have an intrinsic limitation since they last around 30 minutes and the lipids at the interface are prone to oxidation during this period. At the same time, physiologically, new material is continuously secreted from the AT-II cells, replacing the spent surfactant at the interface and this mechanism is difficult to recreate in a Langmuir Blodgett trough. Also, experiments using lipid-protein mixtures containing only SP-C could not be carried out in the CBS, because the presence of SP-B is indeed essential for the adsorption and re-adsorption of a significant proportion of lipids at the bubble interface (Schürch *et al.*, 2010). As previously described, surfactant is resistant to plasma inactivation under quick cycles in the CDS (Saad *et al.*, 2009). For that reason, the use of slow cycles was necessary to facilitate the competition of plasma proteins for the air-liquid interface. Finally, it cannot be excluded that the lower interfacial activity at 37 °C, especially for the mixture containing high percentages of POPG or DOPC, was influenced by a higher lipid oxidation at increased temperatures (Ghnimi *et al*, 2017).

Altogether, in this chapter the influence of therapeutic hypothermia on surfactant structure and composition at the air-liquid interface was demonstrated, dissecting the molecular mechanism under the temperature-mediated boosting of lung surfactant activity. This is mainly due to an increase in the interfacial proportion of DPPC upon compression and leads to improved lung and therapeutic surfactant activity both under physiological and inhibitory conditions. These evidences are added to the multiple physiological effects of WBH on the lung: a temperature-mediated decrease in cytokines (De Luca *et al.*, 2014), a temperature-mediated surfactant refinement and a depuration from meconial cholesterol in the case of MAS. All these evidences contribute to explain the better respiratory mechanics in several cases of cooled patients with ARDS (Hayek *et al.*, 2017; Karnatovskaia *et al.*, 2014; Slack *et al.*, 2017; White *et al.*, 2017) and upon MAS.

Part of this text has been published in the following paper:

Piñeiro-Hermida S, Autilio C, et al., J Cell Biol. 2020, 219(10):e202002120

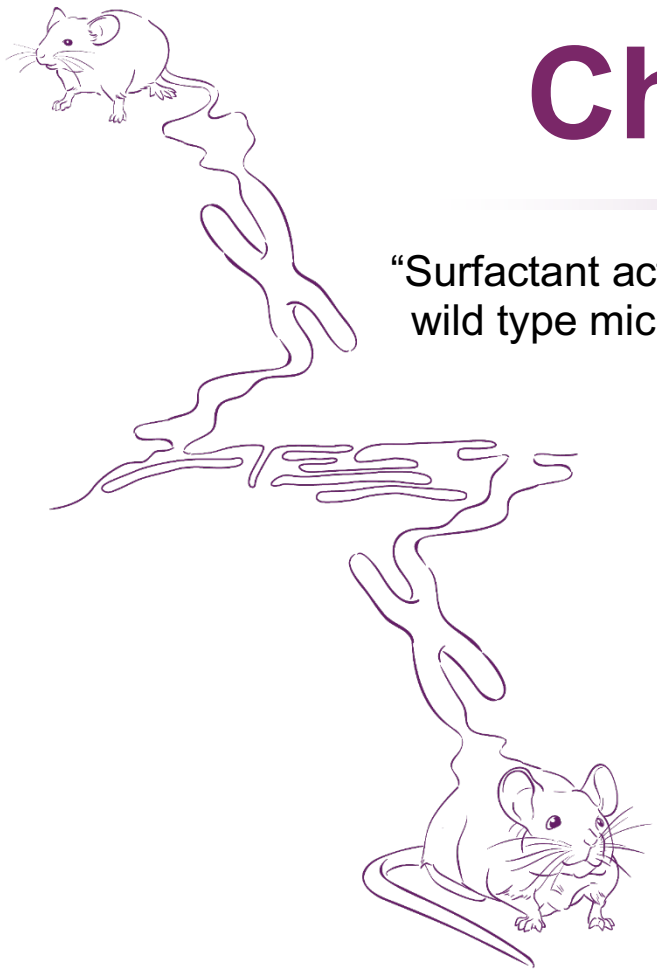

Chapter VI

"Surfactant activity is compromised in old wild type mice and in young *Tert*$^{-/-}$ mice"

Introduction

In the previous chapters, an important role played by lung surfactant in the early or late response to environmental changes emerged, under both physiological and pathological conditions. This lipid-protein complex may be considered a pulmonary sensor whose slight changes may proportionate variegated effects. For instance, several compositional alterations take place in lung surfactant soon after a pro-inflammatory injury due to meconium aspiration. A rise in both PuPC and cholesterol, together with degradation of surfactant lipids and proteins and protein oxidation and deoligomerisation early impair the activity of the system in neonates with severe MAS. At the same time, early variations in cholesterol amount and its delayed reduction, together with a decrease in hydrophobic proteins, occur as a response to WBH in neonates, improving the interfacial properties of lung surfactant at 33 °C. With this in mind, it could be argued that this lipid-protein complex may be altered in physiological contexts in which less pulmonary reserves and increased basal levels of inflammation are involved, such as aging (Fulop *et al*, 2017; Lowery *et al*, 2013) or age-related diseases. In this scenario, IPF can be considered one of the diseases mainly associated to elderly (Collard, 2010), affecting around 3 million people worldwide with a median survival time from diagnosis between 2 and 4 years (Richeldi *et al*, 2017). Interestingly, between 8% and 15% of familial cases of IPF are related to mutations in telomerase or in telomere-protective proteins (Alder *et al*, 2008).

Telomeres are structures at the end of eukaryotic chromosomes, involved in chromosome stability (Blackburn, 2001). This protective machinery consists in mammals of DNA containing TTAGGG repeats associated to a six-protein complex, called “shelterin” (de Lange, 2005). During cell divisions, an incomplete replication of DNA ends may occur and this may lead to telomere shortening, but it is compensated by the *de novo* addition of telomeric repeats onto chromosome ends. This mechanism is mediated by the action of telomerase, a reverse transcriptase consisting of a catalytic subunit, namely TERT, and an RNA component (Terc) that acts as a template for telomere elongation (Greider & Blackburn, 1985).

Short telomeres may be considered one of the primary signs of aging together with genomic instability, cellular senescence, apoptosis and loss of regenerative capacity (Selman & Pardo, 2014). Moreover, IPF patients show shorter telomeres than healthy individuals even in the absence of mutations in telomerase or in telomere-protective proteins (Alder *et al.*, 2008). Besides, single nucleotide polymorphisms within the *Tert* gene increase the risk of lung fibrosis (Fingerlin *et al*, 2013), and mutations in telomere maintenance genes are associated with the clinical manifestations of IPF (Piñeiro-Hermida *et al*, 2020). Previous studies in mice demonstrate that (1) telomere dysfunction in AT-II cells leads to a progressive and lethal pulmonary fibrosis (Povedano *et al*, 2015), (2) short telomeres in lung cells of telomerase-deficient animals treated with subtoxic bleomycin doses may cause IPF, and (3) a therapy that activates telomerase in the lungs may revert this phenotype (Povedano *et al*, 2018).

Interestingly, patients with IPF may develop an acute exacerbation that shares some similarities with ARDS, leading to hypoxemic respiratory failure (Marchioni *et al*, 2018). In that case, the diffuse alveolar damage may occur in both diseases together with cellular infiltrates, mainly neutrophils, and increased pro-inflammatory cytokines (Collard *et al*, 2016; Matthay *et al.*, 2019; Schupp *et al*, 2015). With this in mind, it could be possible that alterations in the lung surfactant system of IPF patients may contribute to a worsening under this acute exacerbation and/or get worse upon this condition. In fact, several reports suggest variations in pulmonary surfactant components during IPF. PI and sphingomyelin increase in BAL fluids, while PG

levels are reduced (Gunther *et al*, 1999; Low, 1989; Robinson *et al*, 1988; Suryadevara *et al*, 2020) and this correlates with the disease severity. Moreover, low ratio between SP-A and phospholipids are observed in IPF patients (McCormack *et al*, 1995). Different results were reported in wild type mice after bleomycin-induced fibrosis in which SP-B levels decreased, while SP-A and SP-C content did not change. However, a very marked fibrotic phenotype was observed in *SFTPC*$^{-/-}$ mice (Lawson *et al*, 2005).

The overexpression of TGF-β1 in mice causes an early reduction in SP-B and SP-C levels with concomitant high surface tension values, alveolar derecruitment and mechanical stress before a fibrotic tissue remodelling appears (Lopez-Rodriguez *et al*, 2016a). Interestingly, SP-C knockout showed an age-dependent murine phenotype similar to that of IPF (Ruwisch et al., 2020). These evidences confirmed the association between several cases of IPF and mutations in the *SFTPC* gene (Lawson & Loyd, 2006).

Starting from these considerations, it could be argued that short and dysfunctional telomeres may be involved in lung fibrosis development and act as a cofactor in lung surfactant alteration upon aging. Thus, in this chapter, the interfacial properties as well as the changes in hydrophobic surfactant proteins of lung surfactant were investigated in wild type and *Tert*$^{-/-}$ mice upon aging and after a telomerase gene therapy. This was possible thanks to a collaboration with the research group of Prof. Maria Antonia Blasco Marhuenda at Spanish National Cancer Research Center (CNIO) that provide all mice and gene therapy.

Animal model and key techniques

Mice and gene therapy

Tert heterozygous mice (*Tert*$^{+/-}$) were generated with >98% C57/BL6 background and intercrossed to generate *Tert*$^{+/+}$ and *Tert*$^{-/-}$ first generation (*G1*). *G1 Tert*$^{-/-}$ were then successive breading until generating *G3 Tert*$^{-/-}$ mice. Male *G3 Tert*$^{-/-}$ and *Tert*$^{+/+}$ of 4-7 weeks, 23-34 weeks and 71-72 weeks were used for the experiments. All animals were bred and maintained under specific pathogen–free conditions in laminar flow caging at CNIO animal facility in accordance with the recommendations of the Federation of European Laboratory Animal Science Associations. All animal procedures were approved by the CNIO Institutional Animal Care and Use Committee and the Ethics Committee for Research and Animal Welfare.

The production of virus particles and their use in treatments are well stablished and standardise in CNIO laboratories. Briefly, HEK 293 cells were cultured in corning roller bottles in DMEM supplemented with 10% FBS to 80% confluence and cotransfected with a plasmid carrying the expression cassette flanked by the AAV2 viral inverted terminal repeats, a helper plasmid carrying the AAV rep2 and cap9 genes, and a plasmid carrying the adenovirus helper functions. The expression cassettes were under the control of the cytomegalovirus promoter and contained a SV40 polyadenylation signal for eGFP and the 39-untranslated region of the *Tert* gene as polyadenylation signal for *Tert*. AAV9 particles were purified using two caesium chloride gradients, dialysed against PBS, filtered, and stored at −80°C until use. Then, 27-30 weeks old *Tert*$^{+/+}$ and *G3 Tert*$^{-/-}$ mice were administered with 2*E^{12} vector genome of AAV9-Tert and AAV9-empty virus particles in a volume of 100 µl 0.001% Pluronic F-68 in PBS 1X by a single intravenous tail injection. Animals were then sacrificed 21 weeks after the administration of the AAV9-Tert and AAV9-empty virus particles.

BAL collection and sample handling

Animals were euthanised by intraperitoneal injection of 10 µl/g of a ketamine/xylazine anaesthetic combination in saline (100:10 mg/kg, respectively) before performing BAL lavages. After BAL collection, cellular components were precipitated at 500 g for 10 minutes and supernatants were stored at -80 °C until use. Before each analysis, samples were slowly thawed and ultracentrifuged at 100,000 g for 1 hour at 4 °C. The amount of PC in the resulting pellets were measured by a colorimetric and enzymatic method. Further details are described in Materials and Methods chapter.

Lung surfactant activity and composition

Mice lung surfactant was diluted to a concentration of 10 mg/mL with a buffer containing 5 mM Tris and 150 mM NaCl at pH 7.4. Around 300 nL was then used for CBS analysis, studying the interfacial properties during initial adsorption, post expansion adsorption, quick dynamic cycles (30 cycles/min) and stability. SP-B and SP-C content were analysed by PAGE and Western blotting followed by band densitometry, loading 3 µg of PC from isolated mice surfactant into each line of the gel. Further details of these techniques are available in Materials and Methods chapter.

Statistics

A one-way ANOVA test or a Kruskal-Wallis test were used, following a Shapiro–Wilk normality test. The post hoc Dunn-Sidak multiple test was then performed for multiple comparisons. According to the sample distribution, either a Mann-Whitney or unpaired t test was used to compare *Tert*$^{+/+}$ and *G3 Tert*$^{-/-}$ mice of the same age or 71-72 weeks-old mice with and without telomerase therapy. Results are shown as mean values ± standard error of the mean (SE). For all analyses, a p value < 0.05 was considered statistically significant.

Impaired pulmonary surfactant activity in aged wild-type lungs is anticipated in telomerase-deficient mice

As shown in **Figure 57**, the adsorption of pulmonary surfactant at the air-liquid interfaces tested by CBS was significantly better in the youngest *Tert*$^{+/+}$ mice (4-7 weeks old) compared with *G3 Tert*$^{-/-}$ mice of different age. However, the difference in adsorption properties disappeared with increasing age of *Tert*$^{+/+}$ mice, from 23 weeks on. At the same time, the difference in post expansion properties was only present when the youngest mice (4-7 weeks old) were compared, showing a decrease in the interfacial spreading of *Tert*$^{-/-}$ mice. Interestingly, lung surfactant of the oldest *Tert*$^{+/+}$ mice (71-72 weeks) was characterised by a further impairment in interfacial properties during dynamic cycles when compared with younger *Tert*$^{+/+}$ mice (4-7 or 23-34 weeks old). As shown in **Figure 58**, once subjected to compression-expansion dynamic under breathing-like conditions, physiological aging affected the capability of surfactant to achieve γ values less than 9 mN/m under the conditions tested (upper row). Indeed, significant differences in γ_{min} among 71-72-and 23-34-weeks old mice were observed as well as a significant increase in the relative area of compression required to reach γ_{min} (lower row, right) upon aging.

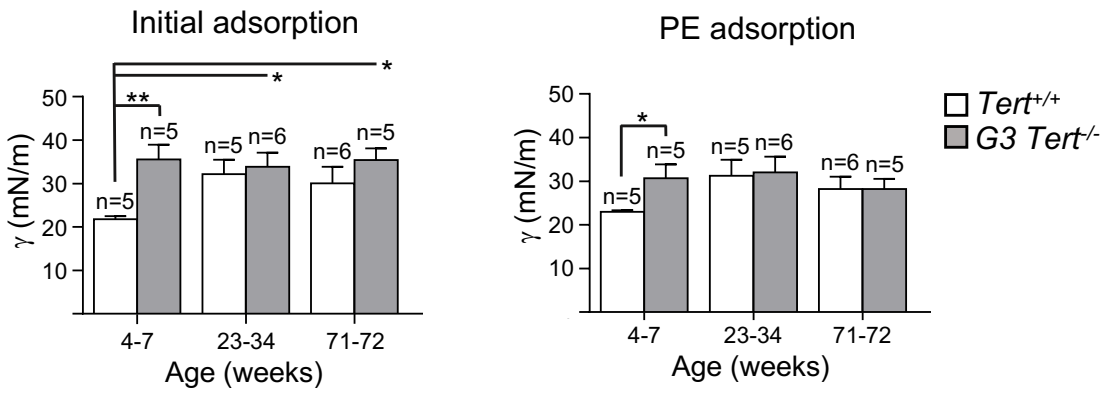

Figure 57. Initial and post-expansion (PE) adsorption of surfactant from mice with and without *Tert*, as tested in CBS. On the left, surface tension values obtained 1 second after applying surfactant material onto the air bubble (initial adsorption) or 1 second after bubble expansion (PE adsorption). White bars represent *Tert*$^{+/+}$ mice. Grey bars represent *G3 Tert*$^{-/-}$ mice. Data are expressed as mean ± SE (n= 5-6 animals per group). One-way ANOVA with post hoc Dunn–Sidak multiple comparison test. Between different conditions within the same age: following a Shapiro–Wilk normality test, two-sample unpaired t test, or Mann–Whitney test when appropriate: * p< 0.05, ** p< 0.01. Abbreviations: γ, surface tension; PE, post-expansion.

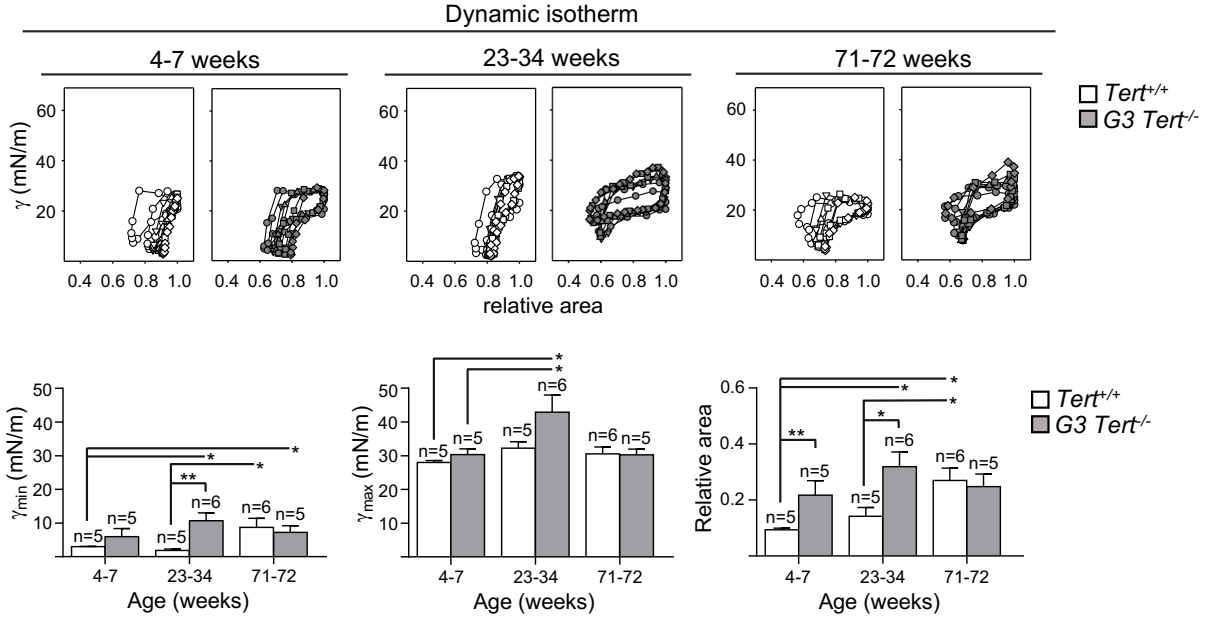

Figure 58. Interfacial properties under breathing-like compression-expansion cycles of surfactant from mice with and without *Tert*, as tested in CBS. In the first row representative γ-relative area isotherms are shown for each group tested. On the bottom, minimum and maximum γ along with the relative area of compression required to obtain the minimum γ during the 20th cycle**.** White bars represent *Tert*$^{+/+}$ mice. Grey bars represent *G3 Tert*$^{-/-}$ mice. Data are expressed as mean ± SE (n= 5-6 animals per group). One-way ANOVA with post hoc Dunn–Sidak multiple comparison test. Between different conditions within the same age: following a Shapiro–Wilk normality test, two-sample unpaired t test, or Mann–Whitney test when appropriate: * p< 0.05, ** p< 0.01. Abbreviations: γ, surface tension; min, minumun; max, maximum.

This reduced surfactant activity was anticipated in *G3 Tert*$^{-/-}$ mice that already showed an early worsening in the relative area of compression at 4-7 weeks of age (second row, on

the right). Similarly, at 23 weeks of age, *G3 Tert*$^{-/-}$ mice presented a significantly higher γ_{min} when compared with *Tert*$^{+/+}$ mice of the same age (lower row, left).

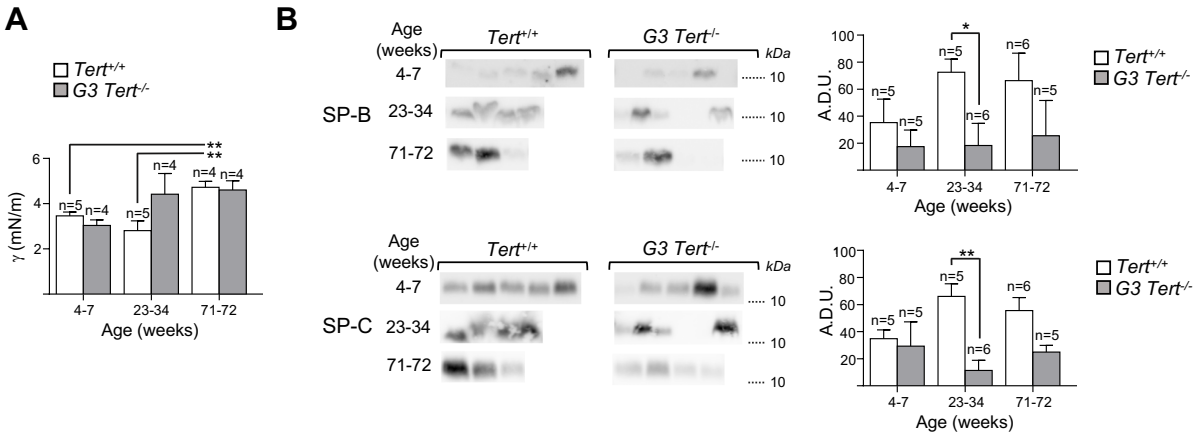

Figure 59. Interfacial film stability and Western blot analysis of hydrophobic surfactant proteins in surfactant isolated from *Tert*$^{+/+}$ and *G3 Tert*$^{-/-}$ mice with increasing weeks of age. (A) Surface tension maintained after discharging five shocking mechanical perturbation on films compressed at the CBS to test their stability. **(B)** SP-B and SP-C bands obtained by performing Western blot analysis under reducing conditions, upon loading equivalent amounts of PC for each sample. Densitometry analysis was performed using as reference the most intense band among the samples tested within each run. White bars represent *Tert*$^{+/+}$ mice. Grey bars represent *G3 Tert*$^{-/-}$ mice. One-way ANOVA with post hoc Dunn–Sidak multiple comparison test. Between different conditions within the same age: following a Shapiro–Wilk normality test, two-sample unpaired t test, or Mann–Whitney test when appropriate: * p< 0.05, ** p< 0.01. Abbreviations: γ, surface tension; A.D.U., arbitrary densitometry units.

As shown in **Figure 59**, a low stability of compressed interfacial films against shockly mechanical perturbation was also observed in surfactant from the oldest *Tert*$^{+/+}$ mice (71-72 weeks). The content in surfactant proteins SP-B and SP-C also tended to decrease in *G3 Tert*$^{-/-}$ mice with increasing age (**Figure 59**). As described for healthy mice (Mahavadi *et al*, 2010), the levels of SP-B and SP-C at the extracellular lavage exhibit a substantial variability in the control group. Moreover, the extreme hydrophobicity of SP-B and SP-C and their strong association with lipids typically make the Western Blot bands appear blurred, especially in the case of SP-C. In spite of this limitation, the two proteins in the lung fluid at 23-34 weeks of age appeared with a significantly lower content in the lavage, becoming only a trend when 71-72-weeks old *Tert*$^{+/+}$ and *G3 Tert*$^{-/-}$ mice were compared. This confirms a worsening in surfactant biophysical properties during physiological aging regardless of *Tert* presence, since surfactant proteins are required to stabilise the respiratory surface and facilitate breathing mechanics.

Telomerase gene therapy prevents age-related worsening in surfactant activity in wild type and telomerase-deficient mice

As a second step, to address whether telomerase gene therapy may improve the age-related pulmonary surfactant inactivation in both *Tert*$^{+/+}$ and *G3 Tert*$^{-/-}$ mice, the activity of surfactant from *G3 Tert*$^{-/-}$ and *Tert*$^{+/+}$ mice of 71-72 weeks old was compared with that of the same mice treated with AAV9-empty or AAV9-Tert gene expressing vectors.

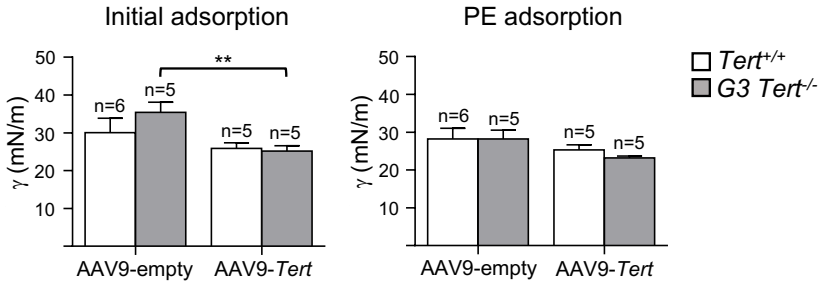

Figure 60. Initial and post-expansion (PE) adsorption of surfactant from 71-72 weeks mice with and without *Tert*, and receiving or not gene therapy, as tested in CBS. On the left, surface tension values obtained 1 second after applying surfactant material onto the air bubble (initial adsorption) or 1 second after the bubble expansion (PE adsorption). White bars represent *Tert*$^{+/+}$ mice. Grey bars represent *G3 Tert*$^{-/-}$ mice. Data are expressed as mean ± SE (n= 5-6 animals per group). One-way ANOVA with post hoc Dunn–Sidak multiple comparison test. Between different conditions within the same age: following a Shapiro–Wilk normality test, two-sample unpaired t test, or Mann–Whitney test when appropriate: ** p< 0.01. Abbreviations: γ, surface tension; PE, post-expansion.

Telomerase activity seemed to be beneficial, overall improving the interfacial properties of lung surfactant in old animals. In fact, *G3 Tert*$^{-/-}$ mice treated with AAV9-Tert showed an enhanced surfactant adsorption, but no significant changes in post-expansion interfacial respreading (**Figure 60**). Moreover, when the activity of material was tested under dynamic breathing-like compression-expansion cycles, there was a significant reduction in the relative area of compression required to achieve minimum surface tension after telomerase gene therapy, when compared with the behaviour of surfactant from AAV9-empty group, regardless of the presence of *Tert* (**Figure 61**). This may suggest a physiological impairment in telomerase activity upon aging that can be at least partially reverted by telomerase gene therapy.

The stability of interfacial films compressed after dynamic cycles and subjected to five mechanical perturbations tends to reduce, but this variation was not significant. Interestingly, telomerase gene therapy did not change SP-B and SP-C content in *G3 Tert*$^{-/-}$ mice, but reduced significantly the amount of SP-B in *Tert*$^{+/+}$ mice (**Figure 62**), with a tendency to decrease SP-C content. This may be due to a therapy-mediated rebalance of surfactant homeostasis that is more evident when endogenous *Tert* is also present.

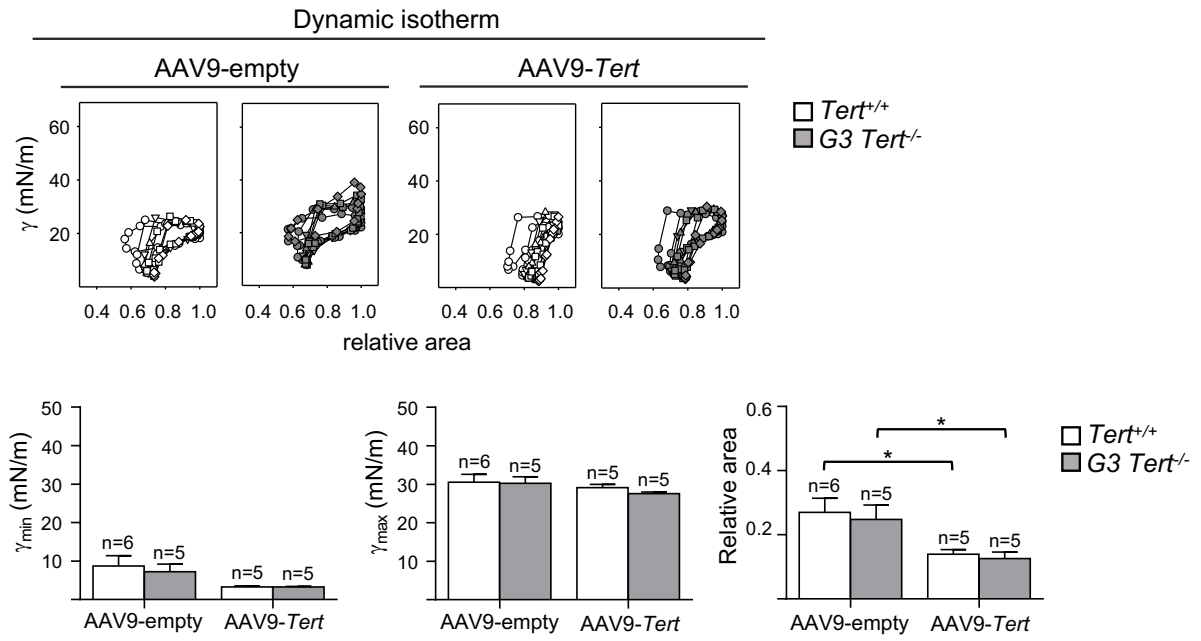

Figure 61. Interfacial properties under breathing-like compression-expansion cycles of surfactant from 71-72 weeks mice with and without *Tert,* and receiving or not gene therapy, as tested in CBS. In the first row, representative γ-relative area isotherms are shown for each group tested. On the bottom, minimum and maximum γ along with the relative area of compression producing the minimal tension during the 20th cycle**.** Grey bars represent *G3 Tert*$^{-/-}$ mice. White bars represent *Tert*$^{+/+}$ mice. Data are expressed as mean ± SE (n= 5-6 animals per group). One-way ANOVA with post hoc Dunn–Sidak multiple comparison test. Between different conditions within the same age: following a Shapiro–Wilk normality test, two-sample unpaired t test, or Mann–Whitney test when appropriate: * p< 0.05. Abbreviations: γ, surface tension; min, minumun; max, maximum.

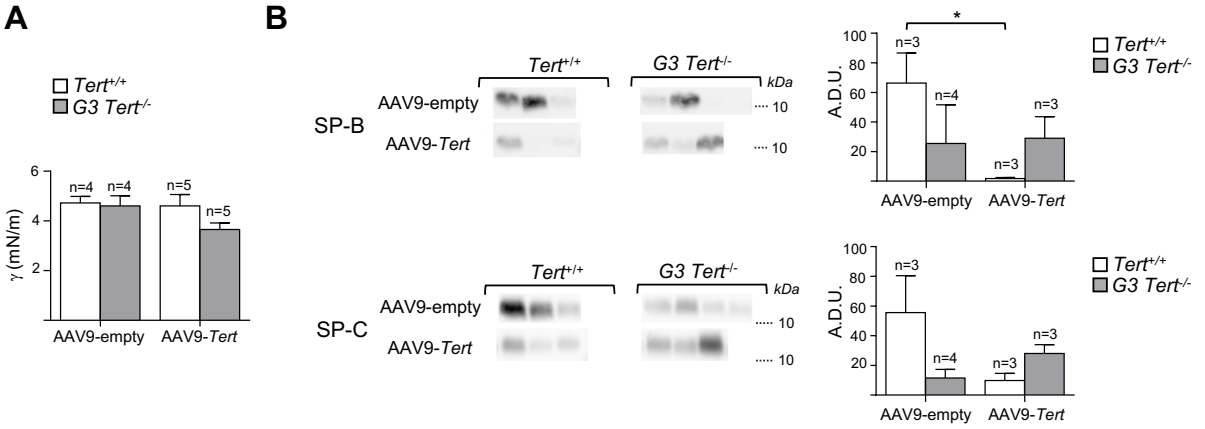

Figure 62. Interfacial film stability and Western blot analysis of hydrophobic surfactant proteins in surfactant isolated from 71-72 weeks mice with and without *Tert*, and receiving or not gene therapy. (A) Surface tension obtained after discharging five shocking mechanical perturbations on films compressed at the CBS. **(B)** SP-B and SP-C bands obtained by performing Western blot analysis under reducing conditions, upon loading equivalent amounts of PC for sample. Densitometry analysis was performed using as reference the most intense band among the samples tested within each run. White bars represent *Tert*$^{+/+}$ mice. Grey bars represent *G3 Tert*$^{-/-}$ mice. One-way ANOVA with post hoc Dunn–Sidak multiple comparison test. Between different conditions within the same age: following a Shapiro–Wilk normality test, two-sample unpaired t test, or Mann–Whitney test when appropriate: * p< 0.05, ** p< 0.01. Abbreviations: γ, surface tension; A.D.U., arbitrary densitometry units.

Discussion

In this chapter, the effect of aging and the presence of an active telomerase system (TERT) on lung surfactant function and composition was investigated in mice with different age. Moreover, the capability of a gene therapy with *Tert* to revert the surfactant alterations was also demonstrated in the group of oldest mice (71-72 weeks). In detail, the following results emerged: (1) the activity of lung surfactant is impaired in the oldest mice regardless of the *Tert* presence; (2) this alteration is anticipated by 48 weeks in $Tert^{-/-}$ mice; (3) no apparent differences in SP-B and SP-C content have been observed when comparing mice with different ages within the same group ($Tert^{-/-}$ or $Ter^{+/+}$ mice); (4) there is a significant decrease in both SP-B and SP-C content in 23-34-weeks-old $Tert^{-/-}$ mice compared with $Tert^{+/+}$ animals of the same age. This reduction remains present in the oldest mice, although as a tendency; (5) the therapy with telomerase improves the interfacial properties of lung surfactant in 71-72-weeks-old mice regardless of the *Tert* presence. The latter seems to be determined by changes in hydrophobic surfactant proteins upon telomerase therapy. Indeed, SP-B and SP-C do not vary in $Tert^{-/-}$ mice, but decrease in $Ter^{+/+}$ mice.

IPF is a chronic and progressive disease associated to elderly. Patients with this condition show apparently shorter telomeres than healthy individuals (Alder *et al.*, 2008). Moreover, studies in a mouse model of fibrosis induced by bleomycin or TGF-1β, suggested a decrease in both SP-B and SP-C content as a consequence of the fibrotic process (Lawson *et al.*, 2005; Lopez-Rodriguez *et al.*, 2016a). In spite of the few studies in the field and the controversial results, physiological aging seems also to be associated with lung surfactant alterations affecting lipids and proteins (Orgeig *et al*, 2014). In Beagle dogs, the proportion of surfactant PC seems to decrease upon aging, whereas the content in phosphatidyl serine and sphingomyelin increases. This results in a modest improvement of surfactant adsorption in old dogs (Clercx *et al*, 1989). Similarly, a reduction in saturated PC content was described in rats upon aging (Ueda *et al*, 2000). Studies performed in horses did not report age-related compositional changes in surfactant, but only an overall decrease of phospholipids (Christmann *et al*, 2009). On the contrary, in a recent study, no variations in phospholipid amount as well as in large and small aggregates subfractions were described in old mice compared to young animals (Veldhuizen *et al*, 2019). As for humans, autopsy from subjects died because of non-pulmonary reasons did not show differences in the percentage of saturated PC (Rebello *et al*, 1996), which remained constant along adult life (around 35%) (Yasuoka *et al*, 1977).

Interestingly, in a recent study the interfacial properties of lung surfactant were analysed in old and young mice both under healthy physiological conditions and upon acute lung injury (Yazicioglu *et al*, 2020). Testing the same amount of PC at limiting concentrations, the capability of pulmonary surfactant to reduce surface tension during breathing-like dynamics was severely compromised in old mice, compared with young animals. Moreover, acute lung injury induced by LPS impaired the activity of the system regardless of age, although a decline in pulmonary function and a higher mortality rate was noticed in old, compared with young mice. This may be explained by the simultaneous alteration in AT-II cells and their adaptive response in old animals, which showed age-related damages in surfactant metabolism, rise in inflammation signalling (Yazicioglu *et al.*, 2020) and previously described degenerative alterations in both lamellar bodies and tubular myelin structures (Walski *et al*, 2009). These results are in accordance with the data described here.

The activity of lung surfactant impairs upon aging regardless of the presence of *Tert*, but this alteration is anticipated in time when the telomerase is absent. At the same time, no changes in hydrophobic surfactant proteins were observed in the oldest mice. This is in line with previous evidences that describe no variation in the amount of SP-A upon aging in rats (Ueda *et al.*, 2000). Conversely, a physiologically decrease of this collectin without changes in SP-D was reported in humans (Betsuyaku *et al*, 2004). Moreover, an increase in the fraction of the SP-A1 gene variant was observed in BAL fluids of old healthy subjects (Tagaram *et al*, 2007). This protein is less active in host defence activities than SP-A2, but seems to contribute to the interfacial adsorption of surfactant material (Lopez-Rodriguez *et al.*, 2016b). Thus, the potential contribution of changes in the amount of hydrophilic surfactant proteins SP-A and SP-D to contribute on counteracting the effects of aging with and without a proper TERT activity should be explored in future studies.

The absence of *Tert* predisposes lungs to a fibrotic process, early reducing the levels of SP-B and SP-C and anticipating the impairment of lung surfactant activity. This explains why telomerase-deficient animals treated with bleomycin are much more prone to develop a fibrotic process compared with wild type mice, a phenotype that may be at least partially reverted by telomerase therapy (Povedano *et al.*, 2018).

Interestingly, aging reduces the number of alveolar macrophages and impairs their phagocytosis action in C57BL/6 mice (Wong *et al*, 2017). Those cells have a crucial role in maintaining the correct surfactant homeostasis, preventing the accumulation of already used surfactant with a limited biophysical performance at the alveolar spaces (Autilio & Pérez-Gil, 2019). An impairment of surfactant activity has been already proposed as an early marker of fibrosis in a model of bleomycin-induced fibrosis in mice (Lopez-Rodriguez *et al.*, 2016a). It is therefore conceivable that the age-related intrinsic deficiency in operative surfactant, both as a consequence of deactivated material that is not properly cleared by aged macrophages because of the lack of enough amounts of newly synthetised surfactant by a reduced population of type II cells (Yazicioglu *et al.*, 2020), leads to progressively impaired pulmonary mechanics, contributing ultimately to reduction in lung tissue elasticity and its abnormal remodelling.

Overall, these results suggest a correlation between impaired interfacial properties of lung surfactant upon aging and the presence of TERT activity. Moreover, they pave the way to potential future therapies for age-related disorders characterised by less pulmonary reserves and surfactant alterations like IPF, especially in patients whose pulmonary fibrosis is associated with short telomeres.

General discussion & future perspectives

The lack and/or inactivation of the lung surfactant system are considered as the primary event or co-factor in the development of several lung diseases such as RDS or direct ARDS, which contribute to premature mortality, disability and health costs of pulmonary disorders. Lung surfactant is a lipid-protein complex that lines the fluid covering the alveolar epithelium, reducing surface tension and minimizing the work of breathing during the whole life. Since it is essential for respiration, dissecting the role of the system in both health and disease may help to seek new diagnostic and therapeutic strategies, rising the health benefits and the efficacy of clinical interventions. With this in mind, in the present Thesis biophysical techniques, such as CBS and SAT, combined with molecular and biochemical methods (e.g. lipidomic and western blot analysis) were used to assess the activity and compositional changes of lung surfactant, obtained from AFs, nBALs and whole BALs, in the context of several pulmonary diseases (i.e. neonatal ARDS due to meconium aspiration, RDS or age-dependent fibrotic processes resembling IPF due to telomerase disfunction). Moreover, this Thesis also addresses the use of novel synthetic surfactant preparations (i.e. CHF 5633) and therapeutic hypothermia as a potential therapy to improve surfactant activity upon inflammation-related and surfactant deficiency-associated lung injury (i.e. in asphyxiated neonates with and without ARDS due to meconium aspiration and in a piglet model of surfactant depletion under WBH). Additionally, a biophysical *in vitro* model based on PS and lipid-protein mixtures has been developed to explain the improvements observed in the interfacial performance of lung surfactant during therapeutic hypothermia. Finally, an *in vitro* characterisation by using several biophysical techniques (i.e. CBS, Langmuir-Blodgett balance, SAT and DSC) was also performed to highlight the major resistance to serum inactivation of the synthetic clinical surfactant CHF 5633 compared to the animal-derived preparation Poractant alfa. Overall, the data obtained in this Thesis highlights the importance of translational biophysics in order to understand the key role of pulmonary surfactant to sense changes in the alveolar milieu upon physiological and pathological conditions.

The inactivation of surfactant lipid-protein complexes can be considered an early biomarker, a co-factor or a secondary component in the development and evolution of several respiratory diseases. Additionally, the improvement in pulmonary surfactant activity is also a robust indicator of how effective a treatment is (e.g. therapeutic hypothermia) to reduce lung injury. These results suggest the importance of studying lung surfactant biophysical and compositional properties towards a personalised medicine of respiratory diseases. In the last few years, the advent of precision medicine has revolutionised the paradigm of clinical care from the traditional evidence-based approach, centred on data collected from large population studies, towards an individual-based prediction of a treatment response or risk of disease (Hodson, 2016). Personalised medicine has been mainly focused on cancer treatments, growing slowly in the contexts of other pathologies. Recently, several approaches were proposed for different respiratory diseases, from asthma to ARDS and IPF (Chung, 2017; Silva *et al*, 2020; Thannickal & Antony, 2018), to seek the proper therapy to the right person at the right time, based on the patient phenotype. These algorithms are mainly related to genetic risks such as gene polymorphisms involved in the response to inflammation and disease progression, or circulating biochemical parameters amenable to monitorise the lung inflammation status (Ball *et al*, 2020; Horhat *et al*, 2017; Portelli & Sayers, 2012; Spadaro *et al*, 2019; Thannickal & Antony, 2018). However, as extensively discussed along this Thesis, changes in the lung surfactant system may also play a role in several lung diseases. In this regard, depending on the extent of surfactant alteration and the patient susceptibility, the severity of pulmonary distress may vary. Addressing this point could contribute to optimise

individualised therapies. Nonetheless, the approach suggested so far for precision medicine of lung diseases does not contemplate considering the lipid and protein composition along with the activity of pulmonary surfactant. At the same time, CPAP and surfactant replacement therapy in RDS neonates typically follow a collective strategy that should be more personalised to maximise the efficacy of the treatments (Sweet *et al.*, 2019).

As a pulmonary sensor, slight changes or drastic inactivation of pulmonary surfactant may provide variegated effects, being a cofactor in the development of respiratory distress. In this context, the results obtained in the present Thesis demonstrate several compositional and structural alterations in the lung surfactant system of neonates after a pro-inflammatory injury - due in this case to meconium aspiration. These changes - an increase in PuPC and cholesterol, the degradation of surfactant lipids by $sPLA_2$ activity and the modification of a proper SP-B profile – all contribute to impair the interfacial properties of lung surfactant, resulting in a reduced lung aeration. At the same time, using a mouse model of IPF due to telomerase dysfunction, pulmonary surfactant impairment was also observed during this chronic lung disease, which seems to be influenced by aging. Interestingly, the obtained results also suggest how the restoration of lung surfactant activity may be a good indicator for the efficacy of therapeutic treatments like WBH. In fact, the overtime reduction in cholesterol together with the restoration of equilibrated levels of hydrophobic surfactant proteins and $sPLA_2$ activity and the concomitant increase in SP-A levels occur as a response in neonates after 72 hours of cooling. This process improves the interfacial properties of neonatal lung surfactant in physiological and meconium-related lung injury by a mechanism that seems to partially depend on the organisation of the sterol and DPPC at the air-liquid interface together with a more evident exclusion of unsaturated phospholipids under breathing-like interfacial compression. These results may introduce the possibility to study novel replacement therapies in same cases of severe ARDS, including the administration of DPPC-enriched synthetic lipid-protein mixtures, such as CHF 5633, which seems also to be more resistant to serum/plasma inhibition. Moreover, the therapeutic effect of clinical surfactants may be enhanced under WBH, paving the way to future strategies combining therapeutic hypothermia and surfactant replacement therapy.

The data obtained in the present Thesis also illustrate how the interfacial adsorption and accumulation properties of lung surfactant, using surface-active materials from AFs or nBALs, can be considered a reliable indicator to identify RDS neonates who will not in principle fail CPAP as well as the lung injury progression that can end in a reduced lung aeration upon severe ARDS due to meconium aspiration. In this line, SAT has been already successfully applied in respiratory research by testing BAL fluids from animal and neonates (Danhaive *et al.*, 2015; De Luca *et al.*, 2014; Ravasio *et al.*, 2008). Moreover, the data emerged in the Thesis also suggest the superiority of SAT, compared to other biophysical methods, to detect slight differences in the surface-active properties of animal-derived and synthetic materials in the presence of serum. This technique, developed by Ravasio *et al.*, can be considered a simple, reliable and quick method based on only two steps: the quantification of surfactant present in a sample followed by its fluorescently labelling and the measurement of its overtime accumulation at the air-liquid interface. The adjustment of the classic protocol as suggested in the present Thesis, allows for a further improvement of the technique, obtaining simple-to-interpret results in less than 3 hours. Moreover, data are not biased by any intrinsic sample dilution since a fixed amount of PC is used for testing. This is very important and make the difference with other available methods to assess the quality rather than the quantity of surfactant, such as the stable microbubble test (Bhatia *et al.*, 2013; Pattle *et al.*, 1979).

With a view to integrate surfactant activity and its compositional and structural changes in the personalisation of respiratory medicine, the need to bridge knowledge and expertise gaps between biophysical investigations and clinical practice, is essential. In this line, translational biophysics may heal the rift between lung clinics and basic science. This was possible in the present Thesis, successful to demonstrate how variations in composition and activity of lung surfactant are a threat shared by several respiratory diseases. The surfactant lipid-protein complex is altered, sooner or later, causing or contributing to lung injury and reduced aeration. From this angle, modified SAT has proven to reliably detect unfunctional pulmonary surfactant, when assaying materials from several sources: porcine whole BALs, neonatal nBALs and AFs. Thus, this quick and simple technique may be a good candidate to be included in future algorithms towards a precise respiratory medicine in different contexts. As demonstrated in the present Thesis, together with LUS, SAT performed in AFs may contribute for screening CPAP-treated RDS neonates needing for surfactant replacement therapy. Additionally, the activity of lung surfactant as proved by SAT may be analysed in nBALs or BALs of ARDS patients to be combined with circulating markers to differentiate subjects with high or low- lung inflammation status (Ball *et al.*, 2020). This may help to correctly identify the ARDS phenotype, improving the outcome by decreasing the bias due to the intrinsic multi-factorial complexity of the disease. Moreover, the SAT may be performed at the same time of -omics approaches. By means of these techniques the activity of lung surfactant may be co-analysed together with the genetic dissection of crucial genes involved in immune-response, vascular permeability (Hernández-Beeftink *et al*, 2019) and surfactant metabolism (ABCA3, SFTPB, SFTPD, SPTPA1/2, SFTPC) as well as to mass spectrometry-based approaches able to provide information on surfactant lipid and protein composition. This could be useful in personalised strategies to monitorise the disease progression and address the best specific treatments for ARDS. Indeed, this algorithm has the potential to develop novel genetic and lipidomic panels as potentially useful tools for clinicians, to better understand which ARDS patient would need a surfactant replacement therapy, its timing and doses of administration as well as the importance of coupling therapeutic surfactants with complementary anti-inflammatory drugs. With this in mind, future studies should also investigate the composition and structure of surfactant system as a function of age and sex in order to better address a personalised therapy for ARDS in both neonates and adults. At the same time, the status of lung surfactant, from its surface-active properties to its lipid-protein composition, together with genetic factors, may be also useful to define the disease progression in IPF patients.

Thinking about today, a simple bench to bedside method, such as SAT, can also cut ice in the early detection of impaired or absent surfactant in lung pathologies, for which a quick intervention can make the difference. COVID-19 is spreading rapidly worldwide this year and an effective therapy is still not available for all patients to date. According to WHO data, more than 35 million people are globally infected by severe acute respiratory syndrome coronavirus 2 and this wave is still cresting (Alwan *et al*, 2020). The virus enters and replicates into AT-II cells and this may probably affect the synthesis and secretion of surfactant material. With this in mind, the administration of exogenous surfactant preparations as a possible therapy in the most severe cases was contemplated in several studies (Pramod *et al*, 2020; Schousboe *et al*, 2020; Weiskirchen, 2020). Thus, the use of SAT in the early phase of COVID-19 by testing virus-inactivated surfactant materials from nBALs or BALs of intubated patients can also be a good strategy, helping to identify which patient should be selected for a replacement therapy.

To summarise, the data obtained in this Thesis shed light on the role of pulmonary surfactant as a reliable indicator of the lung environment under several pathological and physiological conditions (**Figure 63**).

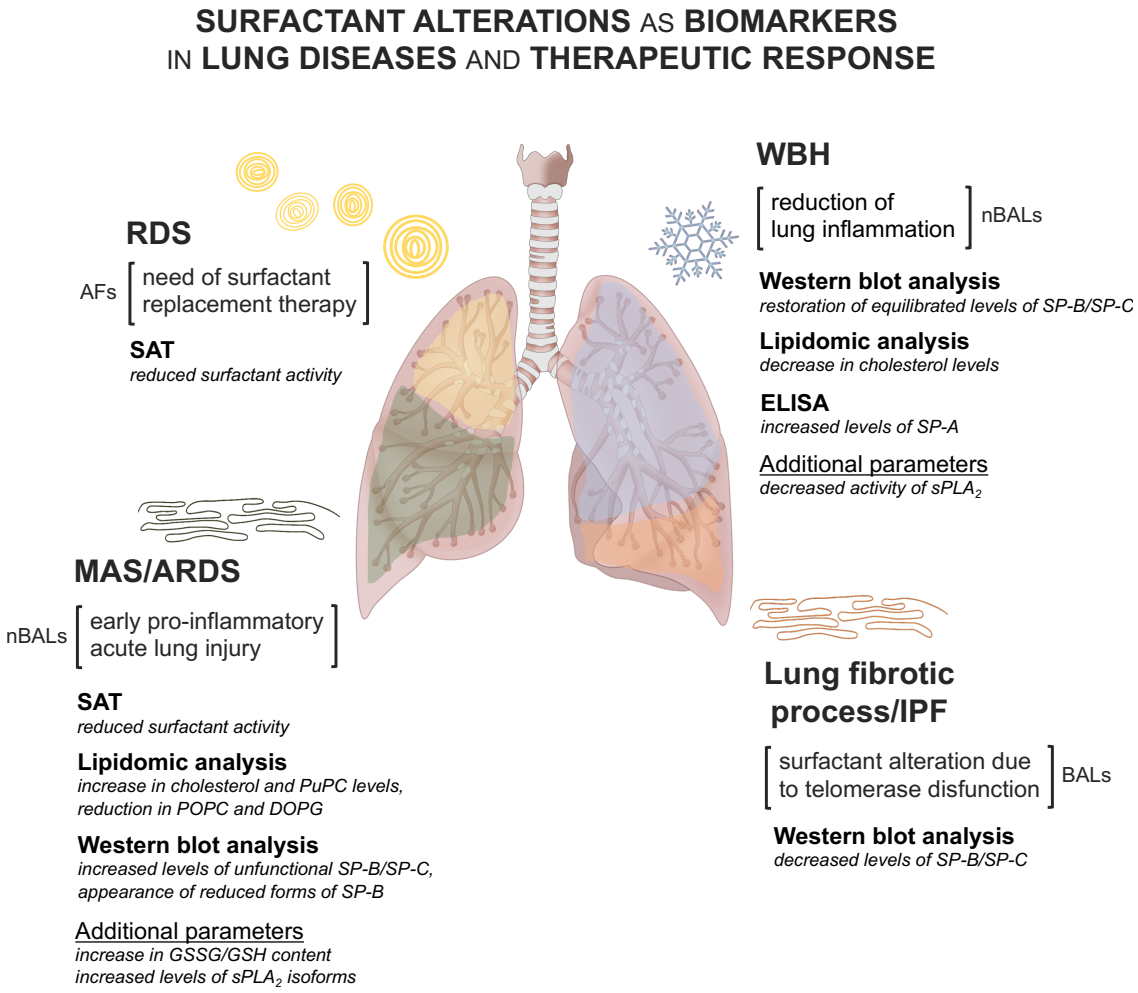

Figure 63. Pulmonary surfactant as a reliable indicator of the lung environment under several pathological and physiological conditions. Abbreviations: RDS, neonatal respiratory distress syndrome; AFs, amniotic fluids; SAT, surfactant adsorption test; MAS, meconium aspiration syndrome; ARDS, acute respiratory distress syndrome; nBALs, non-bronchoscopic bronchoalveolar lavages; PuPC, polyunsaturated PC; POPC, palmitoyloleoylphosphatidylcholine; DOPG, dioleoylphosphatidylglycerol; GSSG, oxidised glutathione; GSH, reduced glutathione; $sPLA_2$, secretory phospholipase A2; IPF, idiopathic pulmonary fibrosis; BALs, bronchoscopic bronchoalveolar lavages.

The possibility to test human and animal samples of different sources by basic biophysical techniques make doable to study lung surfactant modifications in physiological processes and disease, replacing simplified *in vitro* models that could not represent the full *in vivo* complexity. This highlights the importance of translational research thought the constant feedback between lung physicians and basic science researchers, motivating the ongoing investigations in biophysics and contributing to seek novel diagnostic methods, towards promoting the conversion from bench to bedside.

Conclusions

Lung surfactant is essential for breathing by maintaining reduced surface tension values at the air-liquid interface of alveoli, preventing their collapse. Since it plays a vital role in the respiratory system, this lipid-protein complex is also a reliable indicator of slightly and drastic variations of the alveolar milieu that may influence lung aeration under pathological and physiological conditions. Given the background, in this Thesis, using human and animal samples of different sources as well as *in vitro* biophysical models, it has been demonstrated that:

1. lamellar bodies from AFs of neonates who fail CPAP and need surfactant replacement therapy do not adsorb and accumulate properly at the air-liquid interface. This behaviour is reliably assessed by SAT and can be used to identify CPAP-treated neonates who do not need a replacement therapy with a clinical surfactant.

2. Neonatal pulmonary surfactant undergoes different compositional changes in the early 3 hours of ARDS due to meconium aspiration (increase in hydrophobic proteins, cholesterol and PuPC levels, $sPLA_2$-mediated reduction in PC species and a deoligomerisation of SP-B) that affect both its structure and activity, resulting in a diminished lung aeration.

3. The activity of lung surfactant is improved and the oxygen demand is reduced after 72 hours of WBH treatment in intubated and asphyxiated neonates with and without ARDS due to meconium aspiration. At the same time, the levels of cholesterol, hydrophobic surfactant proteins and $sPLA_2$ activity decrease, whereas the content in SP-A increases in nBALs after 72 hours of cooling.

4. The boosting in pulmonary surfactant activity under WBH is due to a temperature-mediated reorganisation of cholesterol and DPPC at the air-liquid interface together with a more evident exclusion of unsaturated phospholipid species under breathing-like interfacial compression, as demonstrated *in vitro*. This is mainly related to the ratio between DPPC and unsaturated phospholipids and occurs for exogenous and therapeutic surfactants in both physiological and oedema-like inhibition contexts.

5. The synthetic clinical surfactant CHF 5633 is more resistant to serum inactivation, as tested *in vitro*, than the animal-derived preparation Poractant alfa. Administering CHF 5633 under WBH improves the ventilator efficiency index in a piglet models of lung injury due to surfactant deficiency.

6. The activity of lung surfactant is impaired upon aging and this alteration occurs 6 months earlier in the absence of TERT, an essential component in the active telomerase system, as demonstrated *in vivo* using a mouse model. Moreover, the therapy with telomerase restores interfacial properties of lung surfactant in old mice regardless of the *Tert* presence.

Part of this text has been published in the following reviews:

Echaide M, Autilio C, et al., Sci. Rep., 2020, in press

Autilio C & Perez-Gil J., Arch Dis Child Fetal Neonatal Ed. 2019, 104(4):F443-F451

Materials & Methods

Material collection and purification

Neonatal BAL

The lavages collection was performed by the NICU team from the Division of Pediatrics and Neonatal Critical Care directed by Prof. Daniele De Luca at "A.Béclère" Medical Center of Paris. The study protocol was approved by the local ethical committee of the South Paris University Hospitals (n. PP13-046) and parental consent was obtained upon NICU admission.

The neonate was left supine with the head turned to the left so that the right lung would be predominantly sampled. One mL/Kg of 0.9% NaCl at 37 °C was instilled through an end hole catheter inserted into the endotracheal tube through a Y-piece, while continuing ventilation and until a resistance was felt. After three ventilator cycles, the suction was gently applied and the fluid was aspirated into a sterile polypropylene trap. The same approach was repeated with the head turned to the right in order to sample the left lung and recover two aliquots. The latter were pooled with an average of 50% of recovered instilled volume, namely 1-3 mL for each patient. Visible blood-stained lavages were discarded, excluding the patient from the study.

Mice BAL

All animals were bred and maintained under specific pathogen–free conditions in laminar flow caging at CNIO animal facility in accordance with the recommendations of the Federation of European Laboratory Animal Science Associations. All animal procedures were approved by the CNIO Institutional Animal Care and Use Committee and the Ethics Committee for Research and Animal Welfare.

The mouse belly was wet with 70% ethanol, the top layer of fur was pinched from the middle of the belly, using forceps and scissors, and the skin was flayed up to the chin, leaving thin muscle layer intact and visible. The muscle layer was cut below diaphragm which was punctured on both sides. The tissue covering trachea on throat was then removed by gently pulling it to the sides with forceps. Using curved forceps, a piece of suture thread was pulled under the trachea without damaging it. By using 1 mL syringe with non-puncturing curved tip, 1 mL of buffer (5 mM Tris and 150 mM NaCl at pH 7.4, 25 °C) was pulled up into the syringe. The trachea was then cut by using the tip of a syringe and a tip catheter was put down into the trachea. The suture thread was then wrapped around the trachea containing the tip catheter, forming a tight knot. The tip catheter was connected to the syringe containing 1 mL of buffer and the majority of the saline solution was released into the lungs, pushing down the plunger to the 1 mark of the syringe. The plunger was then pulled back to 4, pushed down to 2 and back up to 6 mark. Finally, the plunger was pushed down to 4 before retaining as much liquid as possible and ejecting the recovered BAL in a tube on ice. This procedure was performed 3 times per mouse.

Purification of surfactant from human and porcine sources

Porcine BALs were obtained by washing excised porcine lungs with buffer (5 mM Tris and 150 mM NaCl at pH 7.4) (**Figure 64A**). Subsequently, BALs were centrifuged (1000 g for 10' at 4 °C) to remove cells and debris and the obtained supernatant was ultra-centrifuged at 100,000 g for 1h (70 Ti fixed-angle rotor; Beckman Coulter, Brea, CA) at 4 °C to obtain full

surfactant complexes. The same protocol was used to precipitate surfactant from the BAL of the patient with alveolar proteinosis, which was obtained by therapeutic lavages. As for AFs, the pooled cell-free samples were passed through a gaze before centrifugation to remove traces of mucus. In all cases, the resulting pellets were resuspended in a sodium bromide solution (16% NaBr and 0.9% NaCl) with a Potter-Elvehjem homogenizer. These homogenised pellets were loaded onto a sodium bromide gradient centrifugation to remove potential blood contaminants, as previously described (Taeusch *et al.*, 2005). In detail, two saline solutions were carefully added to 1 volume of resuspended pellets (16% NaBr/ 0.9% NaCl), following this order: 1.5 volume of (13% NaBr/ 0.9% NaCl) and 0.6 volume of 0.9% NaCl. The suspensions were then ultra-centrifuged at 120,000 g for 2h at 4 °C (SW40 Ti swinging-bucket rotor; Beckman Coulter). After centrifugation, purified materials were obtained as a disc between the 13% NaBr/ 0.9% NaCl solution and the 0.9% NaCl cushion layers. This surfactant disc was then collected, resuspended in 0.9% NaCl and stored in aliquots at -80 °C.

Purification of porcine and human surfactant proteins

Porcine and human hydrophobic surfactant proteins SP-B and SP-C were purified by two sequential MEC steps, as described earlier (Perez-Gil *et al*, 1993), using the organic extract of PS or that obtained from the purified surfactant of the patient with alveolar proteinosis (**Figure 64A**). The organic extraction was performed by using the Bligh and Dyer method that is a variation of the Folch method and allows for a simultaneous extraction and partitioning of lipids (and part of the hydrophobic proteins associated to them) in one of the two liquid phases that are generated by the procedure (Bligh & Dyer, 1959). At the same time, the hydrophilic proteins are precipitated and isolated between the two liquid phases. In detail, milliQ water, pure methanol and chloroform were added to purified materials in the following volume proportions: 1:1:2:1 (Purified surfactant:Water:Methanol:Chloroform). After mixing thoroughly for 30'', the obtained solution was incubated at 40 °C for 30' to allow for the water-soluble protein flocculation. Subsequently, one more volume of chloroform and water were added to the sample, before mixing thoroughly for 30''. The obtained biphasic solution was centrifuged for 5' at 600 g at 4 °C. The organic fraction, namely organic extract (OE), formed at the bottom of the tube was collected. Other 2 volumes of chloroform were added to the remained aqueous fraction, repeating the centrifugation step. This last process was performed twice to yield full hydrophobic material recovery. OE was stored at -20 °C.

After OE concentration under vacuum in a rotary evaporator, OE hydrophobic constituents were fractioned by MEC using a gel filtration resin (Sephadex LH-20), with chloroform:methanol (2:1, v/v) as the eluent in a 1000mm-SR25 column (GE Healthcare, Little Chalfont, UK). The LH-20 resin allows for the separation by gravity of three OE fractions according to the capability to cross the pores, which depends on their size and structure. Thus the bigger molecules elute before than the smaller ones with the following elution order: (1) hydrophobic surfactant proteins SP-B/SPC that present a molecular weight ranging from 4200 Da for SP-C to 16000 Da for SP-B dimers, with a molecular weight larger than the cut-off threshold of LH-20, in an appropriate proportion of 40% for SP-B and 60% for SP-C (Schürch *et al.*, 2010); (2) phospholipids that are characterised by a molecular weight of around 700 Da and may generate inverse micelle aggregates; (3) neutral lipids that present a molecular weight of around 400 Da. The absorbance at 240 and 280 nm was monitored to detect both lipids and proteins in the eluted fractions. Subsequently, a fraction of delipidised SP-B/SP-C was used to separate the 2 surfactant proteins by a gel filtration resin with larger pore diameter

(Sephadex LH-60) eluted in chloroform:methanol (1:1, v/v) acidified with 0.05% HCl (0.1N, to reduce hydrophobic interactions between the proteins and the resin). The larger pores are responsible for the delay of the smallest protein (SP-C), which is the only able to cross the pores. Thus, LH-60 resin also allows for the separation by gravity of the two hydrophobic proteins according to their size, the bigger (SP-B, ranging from 8000 to 16000 Da) eluting before than the smaller (SP-C of around 4000 Da).

The protein concentration of SP-B/C, SP-B and SP-C fractions was quantified by amino acid analysis in a High-Performance Liquid Ion-Exchange Chromatographer. In detail, a volume of protein fractions (200 μL for porcine OE, 500 μL for human OE) was dried under a nitrogen flow and subjected to acidic hydrolysis (HCl 6N, 0.1% phenol w/v, containing a known amount of *nor*-leucine as internal standard) for 24h at 100 °C under vacuum. The high temperature optimises the hydrolysis, whereas the vacuum is necessary to reduce the oxidation of sensible amino acids.

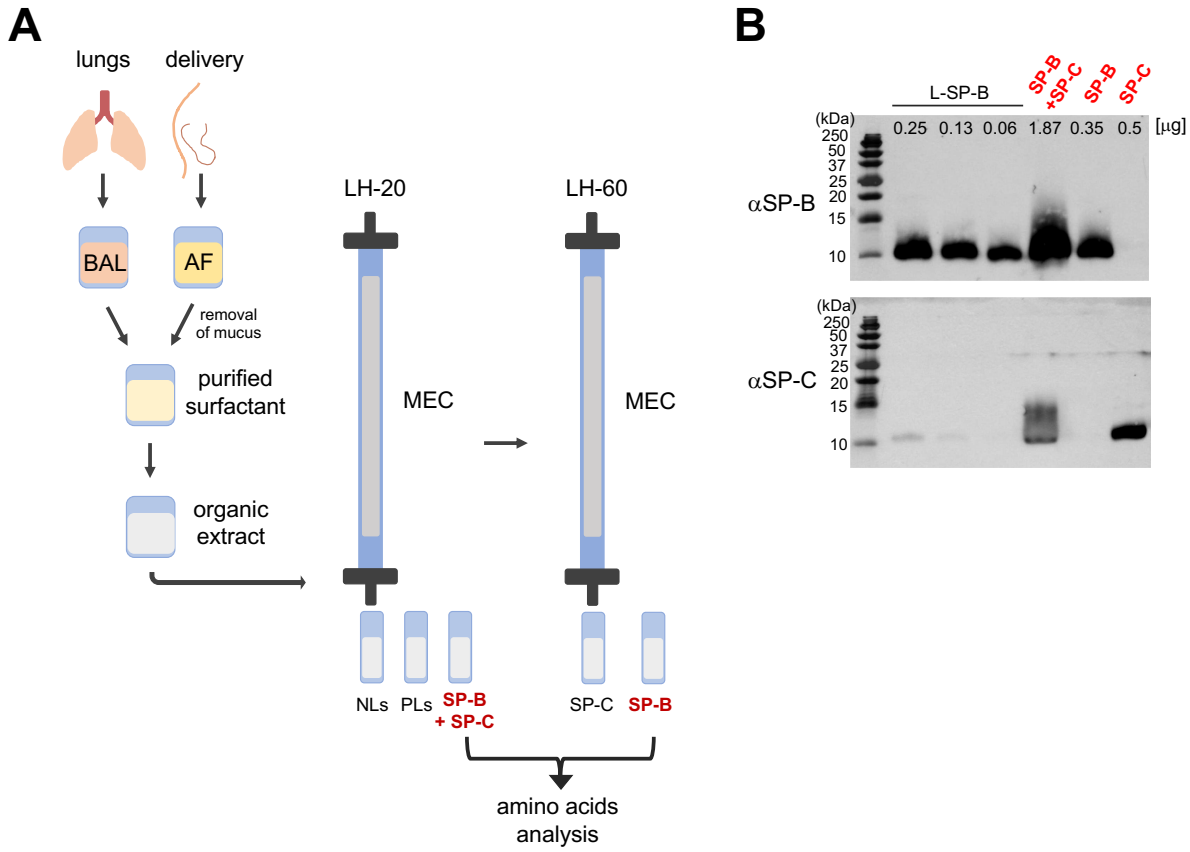

Figure 64. Schematic protocol for surfactant purification and isolation of SP-B/SP-C, SP-B and SP-C protein fractions. (A) Surfactant material derived from lavages of excised porcine lungs, therapeutic lavages of a proteinosis patient or a pool of cell-free AFs after removal of mucus. The scheme of the procedure applied to isolate the hydrophobic proteins, using sephadex LH-20 (SP-B/C), followed by LH60 columns (SP-B, SP-C) is shown. **(B)** Western blot analysis, using anti-SP-B and anti-SP-C antibodies to test the presence of the two proteins and their cross-contaminations into the eluted fractions. 10 μL of sample was loaded into each lane of the polyacrylamide gel. This volume corresponded to around 2 μg of SP-B/C, 0.35 μg of SP-B and 0.5 μg of SP-C. Moreover, several amounts of SP-B previously purified from porcine lung tissues were also loaded as internal controls (L-SP-B). Abbreviations: BAL, bronchoalveolar lavage; MEC, molecular exclusion chromatography; SP-B, surfactant protein B; SP-C, surfactant protein C; PLs, phospholipids; NLs, neutral lipids; L-SP-B, SP-B purified from porcine lung tissues; α, anti.

After hydrolysis, HCl was evaporated under a nitrogen flow and dried tubes were subjected to two milliQ washing and evaporation steps that help to remove all traces of HCl (SpeedVac Concentrator System, Thermo Fisher Scientific; Waltham, MS). Hydrolysed samples were then resuspended in citrate buffer for injection into the analyser (Biochrom 30+ amino acid analyser, Harvard Bioscience, Holliston, MA, USA) and separated by a 35 mL/hr protein hydrolysate/oxidised High-Performance column. Knowing the amino acid sequence of each protein (human or porcine), the amino acids present in both SP-B and SP-C were used to quantify the concentration of whole SP-B/C fraction (LH-20), whereas the amino acids present in SP-B or SP-C were used to quantify the purified SP-B or SP-C fractions (LH-60), respectively. Each concentration was corrected considering the recovery of the internal standard (*nor*-leucine). In detail, the less sensible amino acids are chosen for the quantification analysis. Indeed, during acid hydrolysis, methionine is very sensible to oxidation, tryptophan and cysteine are destroyed, while both threonine and serine are partially lost. Moreover, glycine and serine are common contaminants, thus should be excluded from the analysis (Bartolomeo & Maisano, 2006). The amino acids shared by the two proteins were used for quantifying the LH-20 fraction. Porcine SP-B/C concentration resulted in around 200 μg/mL, whereas porcine SP-B and SP-C concentrations were in the range of 36 μg/mL and 50 μg/mL, respectively. **Figure 64B** shows the PAGE performed to exclude a cross-contamination between purified porcine SP-B and SP-C fractions. Around 10 μL of each purified surfactant fraction was used to load a PAGE (16% polyacrylamide) followed by a Western blot analysis as described below. Less amount of the proteins was obtained from the purified human surfactant: 4 μg/mL for hSP-C and 9 μg/mL for hSP-B. The PAGE of these fractions, loading 50 μL each, is shown in **Figure 18** of chapter II.

Samples/materials handling

The materials used in the present Thesis are included in **Table 12**. Samples of patients, PS, purified AF, glutathione, Poractant alfa, CHF 5633, protein-lipid mixtures and surfactant from mice were resuspended or diluted in the same buffer to reach the experimental concentrations: 5 mM Tris and 150 mM NaCl at pH 7.4.

Phospholipids DPPC, POPC, POPG and DOPC, bought as dry powders, were weighed and resuspended in chloroform:methanol (2:1, v/v) before quantifying their concentration by phosphorus mineralisation as described below. Different volumes of lipids and surfactant proteins were mixed as organic solutions according to the required proportions. These mixtures were dried under a nitrogen flow, resuspended in buffer to reach a final concentration of 8 mg/mL and incubated 1h at 45 °C by intermittent shaking (every 10', 1400 rpm) to reconstitute multilamellar suspensions. The samples were then chilled to 37 or 33 °C before testing their activity. Glutathione was weighed immediately before the experiment, resuspended in buffer and added in the correct proportions to the dried SP-B and lipids for incubation.

Material	Producer/Country
Sodium bromide (NaBr)	Merck KGaA, St. Louis, Missouri, USA
Sodium chloride (NaCl)	Merck KGaA, St. Louis, Missouri, USA
Sephadex LH-20	Ge Healthcare, Little Chalfont, UK
Sephadex LH-60	Ge Healthcare, Little Chalfont, UK
Hydrochloric acid (HCl)	Scharlau Science Group, Barcelona, Spain
Hydroxybenzene (Phenol)	Merck KGaA, St. Louis, Missouri, USA
L-(+)-Norleucine	Merck KGaA, St. Louis, Missouri, USA
tris(hydroxymethyl)aminomethane (Tris)	Merck KGaA, St. Louis, Missouri, USA
Chloroform	Avantor, Inc, Pennsylvania,USA
Methanol	Avantor, Inc, Pennsylvania,USA
1,2-dipalmitoyl-sn-glycero-3-phosphocholine (DPPC)	Avanti Polar Lipids, Inc., Alabaster, USA
1-palmitoyl-2-oleoyl-sn-glycero-3-phosphocholine (POPC)	Avanti Polar Lipids, Inc., Alabaster, USA
1-Palmitoyl-2-oleoyl-sn-glycero-3-phosphoglycerol (POPG)	Avanti Polar Lipids, Inc., Alabaster, USA
1,2-dioleoyl-sn-glycero-3-phosphocholine (DOPC)	Avanti Polar Lipids, Inc., Alabaster, USA
γ-glutamyl-cysteinylglycine (gluthatione)	Merck KGaA, St. Louis, Missouri, USA
Poractant alfa	Chiesi farmaceutici S.p.a, Parma, Italy
CHF 5633	Chiesi farmaceutici S.p.a, Parma, Italy
Bis-BODIPY® FL C11-PC; 1,2-Bis-(4,4-Difluoro-5,7-Dimethyl-4-Bora-3a,4a-Diaza-s-Indacene-3-Undecanoyl)-sn-Glycero-3-Phosphocholine) (BODIPY-PC)	Thermo Fisher Scientific, Massachusetts, USA
1-palmitoyl-2-{6-[(7-nitro-2-1,3-benzoxadiazol-4-yl)amino]hexanoyl}-sn-glycero-3-phosphocholine (NBD-PC)	Avanti Polar Lipids, Inc., Alabaster, USA
Dimethyl sulfoxide (DMSO)	Merck KGaA, St. Louis, Missouri, USA
Ammonium heptamolybdate tetrahydrate	Merck KGaA, St. Louis, Missouri, USA
L-Threoascorbic acid (L-Ascorbic acid)	Merck KGaA, St. Louis, Missouri, USA
Sodium Dodecyl Sulfate	Merck KGaA, St. Louis, Missouri, USA
Glycerol	Merck KGaA, St. Louis, Missouri, USA
3′,3″,5′,5″-Tetrabromophenolsulfonphthalein (Bromophenol Blue)	Merck KGaA, St. Louis, Missouri, USA
β-mercapto-ethanol	Merck KGaA, St. Louis, Missouri, USA
Acrylamide/Bis Acrylamide	Bio-Rad, Hercules, CA, USA
polyvinylidene fluoride membrane	Bio-Rad, Hercules, CA, USA
Di-Sodium hydrogen phosphate (Na_2HPO_4)	Merck KGaA, St. Louis, Missouri, USA
Monobasic potassium phosphate (KH_2PO_4)	Merck KGaA, St. Louis, Missouri, USA
Tween 20	Bio-Rad, Hercules, CA, USA
Skim milk	Merck KGaA, St. Louis, Missouri, USA
Millipore Immobilon® Western Chemiluminescent HRP Substrate (ECL)	Merck KGaA, St. Louis, Missouri, USA
Ethanol	PanReac AppliChem, Chicago IL, USA
Acetic acid	Carl Roth, Karlsruhe, Germany
Glutaraldehyde	Merck KGaA, St. Louis, Missouri, USA
Sodium thiosulfate ($Na_2S_2O_3.xH_2O$)	Merck KGaA, St. Louis, Missouri, USA
Sodium acetate (CH_3COONa)	Merck KGaA, St. Louis, Missouri, USA
Silver nitrate	PanReac AppliChem, Chicago IL, USA
Formaldehyde	PanReac AppliChem, Chicago IL, USA
Sodium carbonate (Na_2CO_3)	Merck KGaA, St. Louis, Missouri, USA
Ethylenediaminetetraacetic acid calcium disodium salt (EDTA)	PanReac AppliChem, Chicago IL, USA
Folin	Bio-Rad, Hercules, CA, USA
Sodium hydroxide (NaOH)	Merck KGaA, St. Louis, Missouri, USA
L(+)-Tartaric acid potassium Sodium salt (sodium potassium tartrate)	Merck KGaA, St. Louis, Missouri, USA
Copper(II) sulfate pentahydrate	Merck KGaA, St. Louis, Missouri, USA
Aqueous 5-sulfo-salicylic acid dihydrate	Merck KGaA, St. Louis, Missouri, USA
2-vinylpyridine	Merck KGaA, St. Louis, Missouri, USA
Agarose	Merck KGaA, St. Louis, Missouri, USA
Sucrose	Merck KGaA, St. Louis, Missouri, USA

Table 12. All materials used in the present Thesis. The generic name and the producer specifications are shown.

Poractant alfa was used as commercialised or lyophilised and resuspended in buffer at the time of the experiments, using different volumes to achieve the required final

concentrations. CHF 5633 was used as obtained from Chiesi Famraceutici S.p.A.. To perform the epifluorescence and SAT experiments, surfactant was doped with BODIPY-PC or NBD-PC, previously resuspended in dimethyl sulfoxide to reach a concentration of 1 μg/μL. Plasma and serum aliquots were thawed slowly and used immediately after thawing.

Surfactant composition

Phospholipid quantification

Phospholipid content was quantified by Rouser assay (Rouser *et al.*, 1966). Samples were dried out in glass tubes previously delipidised with chloroform:methanol (2:1, v/v). A standard curve was also included, drying out known amounts of phosphate. Then, lipid hydrolysis and phosphorus mineralisation were performed by incubating the dried material at 260 °C into a sand bath with perchloric acid (70%), capping the tubes with glass ampoules. The acid solution was then diluted, adding the following compounds and thoroughly vortex after each addition, in this order: (1) 3.5 mL of milliQ water, (2) 0.5 mL of 2.5% molybdate, (3) 0.5 mL of 10% ascorbic acid. Subsequently, tubes were incubated at 100°C in boiling water, to promote a colorimetric reaction in which ascorbic acid reduced the phosphomolibdic complexes that were generated. This results in a blueish/green/yellow colours according to the initial phosphate content. Samples were then measured in a spectrophotometer within 15 minutes to obtain absorbance at 820 nm. PS used for the experiments of the present Thesis resulted in a concentration of 78 mg/mL of phospholipids.

Phosphatidylcholine and cholesterol kits

PC amount was quantified by (1) directly dispensing 10 μL of nBAL/AF from patients, (2) by diluting 1:20 isolated human surfactant from nBALs, or (3) by diluting 1:20 isolated mice surfactant, using the buffer solution (see above). Cholesterol content was measured by diluting 1:5 the isolated surfactants with the buffer solution. According to the PC kit (Spinreact, Girona, Spain), phospholipids were previously hydrolysed by PLA D and the generated choline was oxidised by a choline oxidase to betaine, producing hydrogen peroxide. Similarly, in the cholesterol kit (Spinreact, Girona, Spain), cholesterol esters were hydrolysed by cholesterol esterase and the generated free cholesterol reacts with a cholesterol oxidase, also producing hydrogen peroxide. The latter, in the presence of peroxidase, couples oxidatively 4-Aminophenazone (4-AP) and dichlorophenol, forming a quinonimine dye. This generates a pink colour whose intensity is proportional to the choline or cholesterol content, with an absorption wavelength of 505 nm. Phospholipids (300 mg/dL) and cholesterol (200 mg/dL) were used as internal aqueous standards, respectively.

Lipidomic analysis

Lipidomic analysis was carried out at the RUBAM at the Department of Biomedicinal Chemistry (IQAC-CSIC) in Barcelona under the supervision of Dr. Josefina Casas. This characterisation was performed by liquid-chromatography (LC) high resolution mass spectrometry (HRMS) analysis. By means of this technique, firstly, the molecules are separated chromatographically based on lipid species or classes. Subsequently, they are

ionised by the ion source and the detection of particular ions is performed by a mass analyser, resulting in different peaks. Several volumes of nBALs from patients, corresponding to 50 μg of total PC, were evaporated in a SpeedVac Concentrator System (Thermo Fisher Scientific; Waltham, MS). These samples as well as meconium (around 50 g) and surfactant large aggregates isolated from nBALs of patients (50 μg of total PC), were subjected to an organic extraction according to the Bligh and Dyer method. The OE was then dried under nitrogen flux and stored under argon atmosphere at -20 °C, to avoid oxidation. Interfacial films of PS after compression in a Langmuir Blodgett trough were collected in chloroform:methanol (2:1, v/v). The entire volume (15 μg PC) was dried under nitrogen flux and stored under argon atmosphere at -20 °C, to avoid oxidation.

Internal standards were added to all samples: 16:0 D31_18:1 phosphocholine, 16:0 D31_18:1 phosphoethanolamine, 16:0 D31-18:1 phosphoserine, 16:0 D31_18:1 phosphatidylglycerol, 17:0 lyso-phosphocholine, 17:1 lyso- phosphoethanolamine, 17:1 lyso-phosphoserine, 17:1 lyso- phosphatidylglycerol, 17:0 cholesteryl, 0.2 nmol each, (Avanti Polar Lipids, Inc., Alabaster, USA). Subsequently, LC-HRMS analysis was performed using an Acquity ultra-high-performance liquid chromatography (UHPLC) system (Waters, USA) connected to a Time of Flight (LCT Premier XE) Detector. Briefly, lipid extracts were injected onto an Acquity UHPLC BEH C_8 column (1.7 µm particle size, 100 mm x 2.1 mm, Waters, Ireland) at a flow rate of 0.3 mL/min and a column temperature of 30 ºC. The mobile phases were: (1) methanol with 2 mM ammonium formate and 0.2% formic acid, (2) water with 2 mM ammonium formate and 0.2% formic acid. A linear gradient was programmed as follows: 0.0 min: 20% B; 3 min: 10% B; 6 min: 10% B; 15 min: 1% B; 18 min: 1% B; 20 min: 20% B; 22 min: 20% B.

Full scan spectra from 50 to 1800 Da were acquired, and individual spectra were summed to produce data points each of 0.2 s. Results are express as equivalent picomoles, which are obtained as follows:

$$eq\ pmol_A = Area_A \times pmol_{IS} / Area_{IS} \times Q_{sample}$$

Q_{Sample} is the amount of sample in mg, $pmol_{IS}$ are the picomoles used as internal standard, $Area_A$ y $Area_{IS}$ are the analyte and internal standard areas, respectively. To further normalise data, the levels of lipid classes are expressed as the percentage of the total lipids analysed, whereas the levels of lipid molecular species are expressed as the percentage of the total lipids in the respective class.

PAGE and Western Blot analysis

Electrophoresis Laemmli buffer (2% sodium dodecyl sulfate, 62.5 mM Tris, pH 6.8, 10% glycerol, and 0.03% bromophenol blue) containing or not 4% β-mercaptoethanol was added to samples before incubating the tubes 15 minutes at 90°C. Subsequently, samples were loaded into the gel, using different amounts per condition: 2 μg of phospholipids from lipid-protein mixtures, 4 μg PC of isolated large aggregates from nBALs, 11 μg of lyophilised nBALs, 3 μg PC of isolated surfactant from mice. Purified porcine surfactant SP-B (200 ng) or human surfactant SP-B and SP-C (50 ng) were used as internal reference.

Polyacrylamide gel (16%) was run for around 1 h, and proteins were transferred onto polyvinylidene fluoride membranes with a humid chamber (1 h; 4°C; 300 mA) and blocked in PBS-T (100 mM Na_2HPO_4/KH_2PO_4-1% Tween) with 5% skim milk at room temperature for 2 h. Membranes were then incubated overnight with the primary human/mouse polyclonal antibodies in PBS-T 5% milk at 4°C, washed thoroughly in PBS-T, and incubated with the secondary antibody for 1h at room temperature. Membranes were then developed (1 minute of exposition or 2 minutes of overexposition) using a commercial ECL system for horseradish peroxidase (HRP) substrate and chemiluminescence was read in ImageQuant LAS 500 (GE Healthcare Life Sciences, Logan, USA). Bands densitometry was performed by using ImageJ for Mac OS X. Stripping of membranes was carried out by their incubation with guanidine thiocyanate (4 M in distilled water) for several seconds at room temperature until they became transparent. Membranes were then left in PBS 1% for 30 minutes before starting the incubation with the primary antibody. All primary and HRP-conjugated secondary antibodies are included in **Table 13**.

Western blot antibody	Type	Experimental dilution	Producer/Country
anti-SP-C	primary, polyclonal rabbit, WRAB-76696	1:5000 (human/porcine samples) 1:10000 (mice samples)	Seven Hills , Cincinnati, OH, USA
anti-SP-B	primary, polyclonal rabbit, WRAB-48604	1:5000 (all samples)	Seven Hills , Cincinnati, OH, USA
anti-SP-A	primary, polyclonal rabbit	1:10000 (all samples)	kindly supplied by Joanna Floros's Laboratory (Pennsylvania State University, USA)
anti-pro-SP-B	primary, polyclonal rabbit, WRAB-55522	1:2500 (all samples)	Seven Hills , Cincinnati, OH, USA
HRP-conjugated-antibody	secondary, polyclonal swain anti-rabbit Ig (P0217)	1:5000 (all samples)	Dako, Agilent technologies, Santa Clara, CA, USA

Table 13. Antibodies used for Western Blot analysis in the present Thesis. The type, the experimental dilution and the producer specifications are shown.

SP-A

SP-A content was measured directly in nBALs by using a specific ELISA kit, which detects the total amount of SP-A (both SP-A1 and SP-A2 isoforms) (BioVendor - Laboratorní medicína a.s., Karásek, Czech Republic). nBAL samples were diluted 1:100 to perform the assay and results were normilised for the PC amount of each sample, detected by the phosphatidylcholine colorimetric kit.

Silver staining

Gels were treated as follows: 30 minutes in fixing solution (40% ethanol, 10% acetic acid) and 30 minutes in sensitizing solution (30% ethanol, 0.5% glutaraldehyde, 12.6 mM sodium thiosulphate, 0.8 M sodium acetate). Subsequently, gels were washed three times in miliQ water for 5 minutes to eliminate the solution excess and incubated with silver solution (0.6 mM silver nitrate, 0.04% formaldehyde) for 20 minutes. Then, after a quick wash with miliQ water, the developing solution (0.2 M sodium carbonate, 0.02% formaldehyde) was used to develop bands and the reaction was stopped by adding 50 mM EDTA (pH 8.0).

Biochemical parameters

The levels of total proteins in nBALs of patients were measured in a microplate using the Pierce™ Bicinchoninic acid (BCA) Protein Assay Kit (Thermo Fisher Scientific, Waltham, USA) with an intra-assay coefficient of variation < 7 %. Different amounts of bovine serum albumin (6.25-0.125 μg) were used as internal standard. The method is characterised by two reactions that are performed in one step at high temperature. Peptide bonds in an alkaline solution (pH 11.25) reduce Cu^{2+} from copper(II) sulfate pentahydrate to a cuprous cation (Cu^{1+}). This reduction is proportional to the amount of the protein in the solution. Then, chelation of two molecules of BCA with one Cu^{1+} results in a purple-coloured complex that strongly absorbs light at a wavelength of 562 nm. The incubation at high temperature (37-60°C) for 30 minutes is essential since it increases the assay sensitivity and reduces the variances due to unequal amino acid composition in the sample. Indeed, the BCA-Cu^{1+} complex at lower temperature is mainly influenced by the presence of cysteine, cystine, tryptophan and tyrosine residues of the protein. Conversely, when increasing temperature, the peptide bond also seems to take part to the formation of the BCA-Cu^{1+} complex.

Total proteins in porcine plasma and serum were tested by the Lowry method, as previously described (Lowry *et al*, 1951), using different amounts of bovine serum albumin (5-50 μg) as internal standard. In an alkaline solution and at room temperature, Cu^{2+} forms a complex with peptide bonds of proteins, in which it is reduced to Cu^{1+}. The latter and the radical groups of cysteine, tyrosine and tryptophan react with Folin's phenol reagent (a mixture of phosphomolybdate and phosphotungstate) to generate an unstable complex. This leads to the oxidation of aromatic/thiol residues and the reduction of Folin's phenol reagent to heteropolymolybdenum Blue, which adsorbs light at around 700 nm. This is proportional to the amount of proteins present in the sample, containing cysteine, tyrosine and tryptophan. Briefly, samples and standard amounts were diluted in milliQ water with 3% sodium dodecyl sulfate (to solubilise relatively insoluble lipoproteins) to a final volume of 200 μL. Then, three reagents (A= 2% Na_2CO_3 and 0.1 M NaOH, B= 2% sodium potassium tartrate and C= Copper(II) sulfate pentahydrate) were prepared separately and mixed (A:B:C, 100:1:1, v/v/v) just before adding 1mL of the mixture to samples and standard tubes. After thoroughly vortexing, the tubes were left at room temperature for 15 minutes. Then, 100 μL of Folin's phenol reagent were added to the tubes that were thoroughly vortexed again. After 30 minutes, the absorbance was measured at 700 nm. Total proteins from porcine serum and plasma used in the present Thesis resulted in around 70 mg/mL.

The content of different $sPLA_2$ subtypes (IB, V and X) in nBALs were analysed by specific ELISA kits (intra- and inter-assay coefficient of variation < 15%): Cayman Chemical (Michigan, USA), Cusabio Technology LLC (Houston, USA) and Cloud-Clone Corp (Texas, USA), respectively. The assays were performed without diluting nBALs and the obtained values were normalised by the PC amount contained in each sample.

The activity of $sPLA_2$ was analysed by a colorimetric enzymatic assay (Enzo Life Sciences, Inc., New York, USA) with an intra- and inter-assay coefficient of variation below 5 and 10%, respectively. In detail, this is a nonradioactive method on microplate, which uses 1,2-dithio analogue of diheptanoylphosphatidylcholine as substrate for $sPLA_2$. Upon hydrolysis of the thiol ester bond at *sn-2* position, free thiols are generated and react with 5,5'-dithio-*bis*-2-nitrobenzoic acid, producing a sulfhydryl compound, which is proportional to the total enzyme activity against PC species, and detected at a wavelength of 405 nm with a correction at 590

nm. Different dilutions of porcine $sPLA_2$ IB in the presence of mM levels of calcium are used as internal standards, corresponding to an activity from 40 to 5 units/mL. An additional dilution for the standard curve (2.5 units/mL) was also included, still remaining beyond the detection limit of the assay (2.34 units/mL). This allows detecting the activity of the enzyme in samples with low levels of $sPLA_2$ as expected in nBALs of healthy neonates, although maintaining a good Pearson correlation coefficient (r=0.995).

The content of total, reduced and oxidised glutathione were measured by a colorimetric assay (Glutathione Colorimetric Detection Kit, Invitrogen, Carlsbar, Ca, USA). Firstly, proteins in nBALs samples were precipitated by complexation with the strong acid 5-sulfo-salicylic acid dehydrate (SSA) (5% weight in a phosphate buffer) to remove any thiol-bearing proteins and to reduce the oxidation of free GSH. Briefly, one volume of cold 5% SSA was added to the sample and mix thoroughly, before incubating the mixture for 10 minutes at 4°C. Samples were then centrifuged at 22,000 g for 10 minutes at 4 °C. Only the supernatant was carefully recollected and diluted with a phosphate buffer at pH 6.5 to 1% SSA before performing the assay. To detect GSSG amount, both standard dilutions (25-0.78 µM of oxidised glutathione) and diluted samples were incubated with 2-vinylpyridine to derivatise GSH through the bond that is generated between the CH_2 group on 2-vinylpyridine and the thiol group of GSH. Briefly, 27 µL of 2-vinylpyridine were added to 98 µL of ethanol in a fume hood and the solution was immediately used to incubate samples and standards (2-vinylpyridine/standards-samples, 1:50, v/v) for 1 hour at room temperature. This allows blocking free GSH or other thiols present in samples. Afterwards, standard dilutions and samples, subjected or not to the blocking with 2-vinylpyridine, were incubated with glutathione reductase. This enzyme, in the presence of NADPH, reduces total GSSG to two molecules of GSH, but has no effect on GSH-vinylpyridine conjugate. Thus, GSH produced from GSSG reduction as well as the starting GSH amount were measured, adding a colorimetric substrate (5-5'- dithiobis [2-nitrobenzoic acid]) to generate a yellow colour chromophore (5-thionitrobenzoic acid (TNB)) and GS-TNB. The latter is then further reduced to GSH and TNB by glutathione reductase, increasing the sensitivity of the assay. The optical density was read at 405 nm. The total amount of glutathione species is yielded by the values of any sample not treated with 2-vinylpyridine. The free GSH (corresponding to the masked GSH) is obtained by the difference between the values of total glutathione and the values detected when treating glutathione with 2-vinylpyridine, which only correspond to total GSSG since GSH is masked.

Surfactant interfacial properties

Wilhelmy balance

The Wilhelmy balance is a simple model typically used to study the adsorption and spreading properties of surface-active materials. It was first applied by the pioneer work of Clements (Clements, 1957) in the middle of 20th century, when the existence of lung surfactant as a surface-active material in the lungs was proven.

To test surfactant adsorption, a controlled amount of material is injected at the bottom of a small hydrophobic trough (typically made of Teflon) that is filled with an aqueous solution and rest on a water-thermostatic module to adjust the subphase temperature. To evaluate the spreading properties, surfactant is distributed directly at the air-liquid interface. The subsequent reduction in surface tension is usually detected by a Wilhelmy plate, typically a

small piece of filter paper or a platinum plate, the bottom edge of which is immersed into the aqueous subphase and in contact with the air-liquid interface. Thus, when surfactant accumulates at the aqueous surface, a force transducer detects the increase in lateral molecular pressure, which is related to the reduction in surface tension. In detail, the sensor connected to the plate is able to detect the downward force applied by the liquid meniscus wetting the plate. This is proportionally reduced in presence of increasing amounts of surfactant phospholipids at the interface, which displace the molecules of water from the interface, reducing the surface tension and thus decreasing both the liquid meniscus and the downward force on the plate. With this in mind, the surface tension can be calculated as follows (Cruz & Pérez-Gil, 2007):

Force on the plate (F)= (Weight of the plate) + [2 x (thickness + width of the plate) x surface tension of the liquid x cos(Θ)] – (Buoyant Force)

The weight of the plate can be adjusted to zero by specific calibration, whereas the Buoyant Force (depending on the density of liquid, the volume of the plate that is immersed into the liquid and the gravitation acceleration) can be excluded, assuming that the force is around zero due to the depth of immersion. In this way, the surface tension force is the only parameter necessary to calculate the force on the plate (F). Thus, the latter is equal to:

F= 2 x (thickness + width of the plate) x surface tension of the liquid x cos(contact angle)

Since the contact angle (Θ, that is the angle generated between a solid surface and the liquid-vapor interface) is zero if the plate is perfectly wet and cos(0)=1, knowing the thickness and the width of the plate, the force on the plate (surface pressure) will be only proportional to the surface tension values as follows:

$$\Pi = \gamma_0 - \gamma_1$$

Where γ_0 is the surface tension of the aqueous solution before applying surfactant material and γ_1 is the surface tension reached by lung surfactant at the interface.

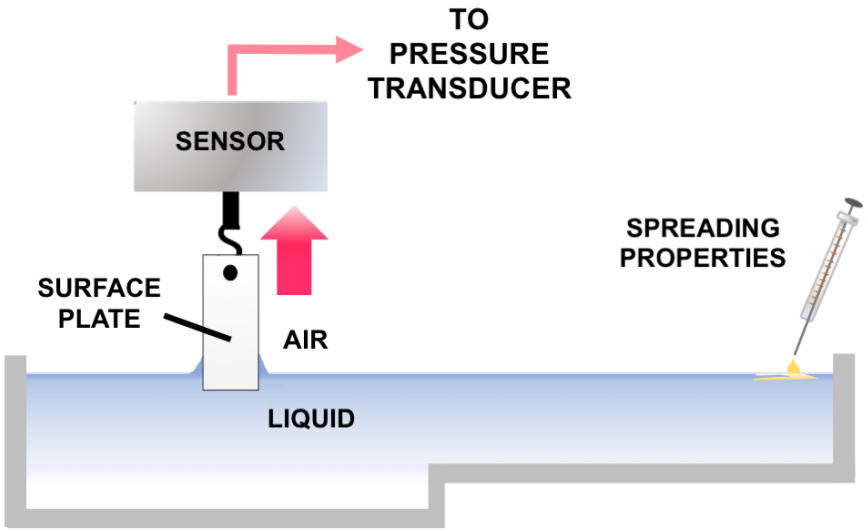

Figure 65. Schematic representation of the Wilhelmy balance used for the experiments. A small arm was added to the trough. Samples were tested, distributing material in one drop at the end of the smaller arm.

As shown in **Figure 65**, the spreading capability of lung surfactant was assayed by using a Wilhelmy balance whose design was modified by adding a small arm to the trough (total area arm = 6.45 cm^2, total area trough = 21.45 cm^2) to increase the distance between the injection point and the pressure sensor. The design was specially created in the mechanical service of Complutense University of Madrid (Spain). The maximum temperature variation was around ±1°C. The Wilhelmy plate was a piece of filter paper with a thickness of 0.5 mm and a width of 10 mm (Whatman, GE Healthcare Life Sciences, Logan, USA). The pressure sensor was purchased from NIMA Technology, Inc., Coventry, UK. PS, Poractant alfa and CHF 5633 were tested at 25 °C by spreading, directly at the air-liquid interface, 10 µL of the different materials containing 50, 100 or 150 µg of phospholipids. The sample was distributed only in one drop at the end of the smaller arm of the trough on the opposite side to the pressure sensor. Each experiment was performed in triplicate and the changes in surface pressure were recorded for 40 minutes.

Captive Bubble and Constrained Drop Surfactometers

Adsorption, spreading and dynamic properties of surfactant materials were tested under breathing-like conditions by CBS and CDS. CBS is a non-commercial device, specially created by a collaboration between Prof. Perez-Gil research group (Complutense University of Madrid, Spain) and research group of Prof. Samuel Schürch (University of Calgary, Alberta, Canada). Most parts of the device are specially created in the mechanical and glass services of Complutense University of Madrid (Spain). CDS was purchased from Prof. Yi Zuo laboratory (University of Hawaii, Honolulu, Hawaii).

The two devices recreate an alveolus *in vitro* as an air-liquid interface subjected to continuous breathing-like compression-expansion cycles at controlled temperatures. CBS is characterised by an air bubble, resting on an agarose roof (10% weight), and enclosed in a glass chamber filled with buffer containing sucrose (10% weight) (**Figure 66)**.

CDS consists of a buffer drop, constrained on the top of a pedestal with a sharp knife edge. The drop is enclosed in an air chamber and connected to a syringe filled with the same buffer (**Figure 67)**. Both the bubble and the drop are continuously recorded during experiments by a video camera: Pulnix TM 7 CN (Sunnyvale, CA, USA). Temperature is kept constant by a heater in the CBS and both a heater and a Peltier module in the CDS. Changes in temperature are checked overtime using temperature probes to maintain a maximum temperature variation of around ±1 °C.

Samples can be injected below or onto the bubble/drop surfaces to study adsorption and spreading surfactant properties, respectively. In CBS experiments, a microliter Hamilton syringe is connected to a transparent capillary (polyethylene tube, BD Clay Adams, New Jersey, USA) and used to enter the chamber and inject material close to the bubble. As for CDS, material is dispensed as a drop directly on top of the pedestal or released dropwise at the interface of the buffer drop that is previously generated. Once the material is adsorbed or spread, compression-expansion cycles are performed as following, depending on the device. In CBS, a piston is moved up and down above the chamber. This reduces the volume of the chamber, introduces hydrostatic pressure and changes the distribution of water molecules with respect to air, according to the surface tension values. In the CDS, the drop volume is modified by using the syringe. Thus, since the air-liquid interface of the drop is enclosed by the sharp knife edge, this variation in volume can decrease or increase the surface exposed to air of the drop.

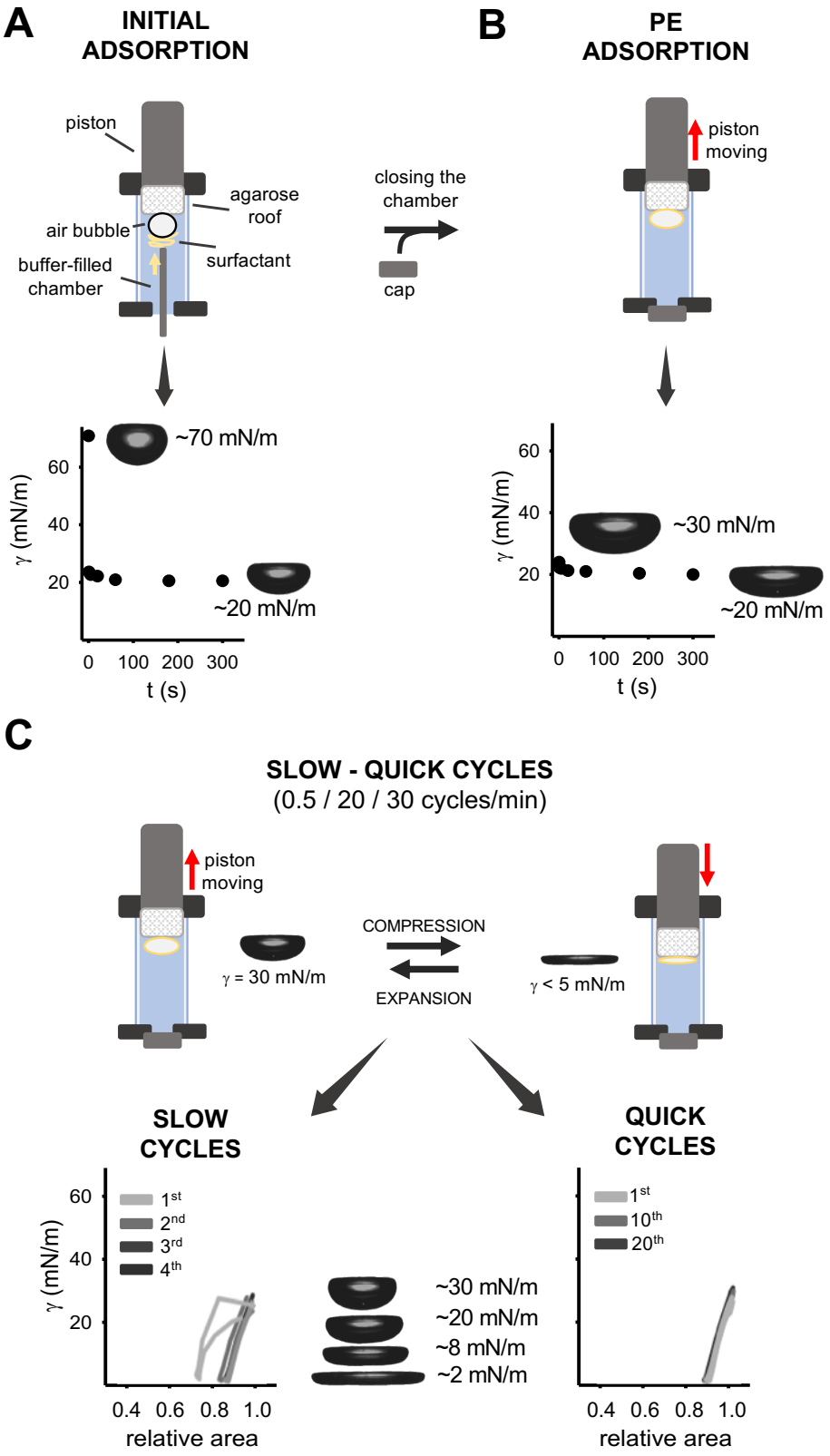

Figure 66. Schematic representation of a CBS experiment and the analysis of data, after recording the variation in surface tension under static and dynamic conditions. (A) Material is dispensed close to the bubble and the initial adsorption is recorded along 5 minutes. **(B)** The chamber is then closed and the bubble is expanded, recording the PE adsorption for another 5 minutes. **(C)** Subsequently, four slow quasi-static cycles (0.5 cycle/min) or 20/30 dynamic quick cycles per minute are started, continuously recording the variation in γ per surface area variations. Abbreviations: γ, surface tension; PE, post-expansion.

The presence of a surfactant material that is well organised at the air-liquid interface and able to reduce surface tension leads to changes in the shape of either the bubble or the drop. In fact, surfactant coats the liquid surface, decreasing the contact between liquid molecules and air. This leads to variations in the surface geometry, resulting in a disc-like shape of the bubble or the drop under low γ values (< 5 mN/m). In both devices, these changes in shape can be monitored overtime and transformed into γ variations by Axisymmetric drop shape analysis (ADSA) software (Yu *et al.*, 2004) in CDS and an analogous software designed by Schoel (Schoel *et al*, 1994) in CBS. The determination of γ values in the CSD uses the contact angle and shape of the drop. Briefly, ADSA creates a profile with a certain surface tension (set to 40 mN/m) and check if this profile matches the profile of the picture of the drop obtained from the experiment. If it is not the case, the program creates drop profiles smaller (with lower surface tensions) until reaching the match. ADSA then considers the next picture having similar surface tension, starting the analysis from the matched γ. As for CBS, the surface area and the volume of the bubble as well as γ values are calculated from the height and diameter of the bubble, using functions with several approximations, obtained from experimental data of 118 bubbles.

CBS experiments (**Figure 66**) were performed by injecting 300 nL of surfactant material onto the bubble and waiting 5 minutes for surfactant adsorption. The chamber was then sealed and the bubble was expanded by moving up the piston, increasing its volume by ≈25% and waiting other 5 minutes to test surfactant spreading. Subsequently, one or four slow compression-expansion cycles were performed. In detail, the bubble was compressed and expanded once during 2 minutes or four times during 8 minutes, changing its volume by ≈25%. The bubble was then subjected to 20 or 30 quick cycles, maintaining the same variation of the bubble volume (20-30 cycles/min). Finally, when possible, the stability of the multi-lamellar structure created by the interfacial surfactant upon dynamic cycling was tested by introducing shocking mechanical perturbations into the bubble chamber. This was done by hitting several times the chamber with a pendulum hammer, as previously described and illustrated (Schürch *et al.*, 2010). The position of the hammer with respect to the CBS chamber needs to be the same along hitting, generating an angle of 90 degrees. All the experiments were performed in triplicate and the results were analysed as γ/t and γ/hits graphs and γ/area isotherms.

Like CBS, CDS experiments can be performed under breathing-like conditions (20 cycles/min). However, in the present Thesis, a different protocol was ideated to allow for PS inhibition by plasma, avoiding as much as possible the contribution of drop evaporation. In particular, the speed to change the bubble volume was reduced to perform 2 cycles/min (**Figure 67**) and the timing of each experiment was set to 6 minutes. Indeed, due to the spontaneous process of evaporation, the drop volume decreases of around 25% in 6 minutes regardless of the experimental temperature (37 or 33 °C), reaching already 50% in 8 minutes. This process was slower at 25 °C. Thus, to make replicates reproducible, the maximum timing for an experiment was set to 6 minutes, as following. PS (5 μl at 1.5, 2.5 or 5 mg/mL) was dispensed on top of the pedestal and kept down until reaching the buffer inside the pedestal. A buffer drop was then immediately added on top (7 μl), waiting 10 seconds (initial adsorption) before performing 10 slow compression-expansion cycles (2 cycles/min, shrinking the interface area by 20 %). For lipid-protein mixtures, materials (40 mg/mL) were dispensed directly on top of the plasma drop (previously subjected to 6 slow compression-expansion cycles), and subjected to further 4 slow cycles. All the experiments were performed in triplicate and the results were analysed as γ/t and γ/area isotherms.

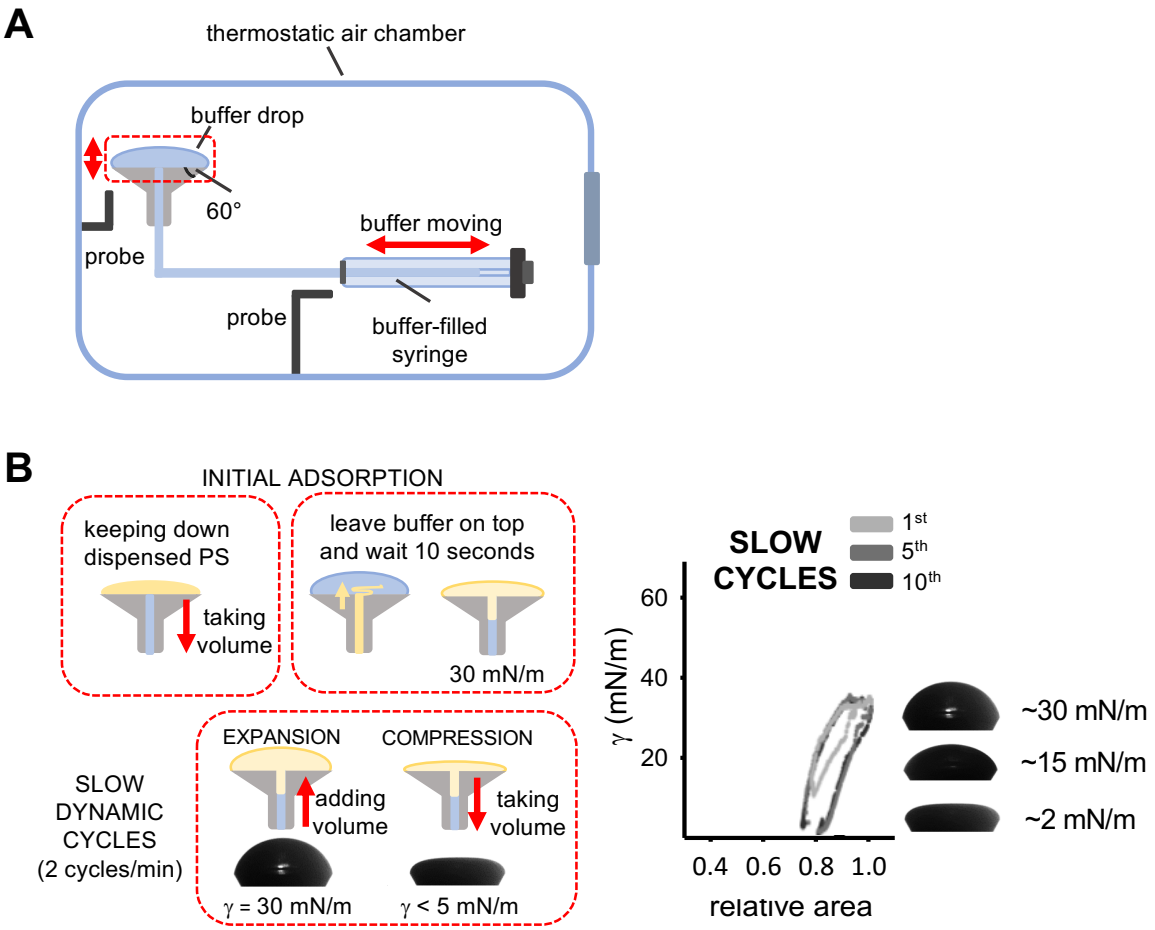

Figure 67. Schematic representation of a CDS experiment and the analysis of data, after recording the variation in surface tension under slow dynamic conditions. (A) Schematic illustration of a CDS device. **(B)** Different steps of the experiment to test the activity of material under a limiting condition: dispensed PS and immediately keeping it down; leave a drop of buffer on top of the pedestal; waiting 10 seconds for the adsorption; starting the slow dynamic cycles. Abbreviations: γ, surface tension; PS, purified porcine surfactant.

Serum inhibition and surfactant resistance to this inhibition were tested in CBS as previously published (**Figure 68A**) (López-Rodríguez *et al.*, 2012). In detail, an excess of total serum proteins, namely 3 µL of whole porcine serum (at 68 mg/mL of total proteins, around 200 µg) was first injected at the air-liquid interface of the bubble. After 5 minutes, surfactant was introduced and distributed over the bubble surface without touching the bubble, to initiate the experiment as described above from the Initial Adsorption, but in the presence of serum.

In **Figure 68B** the restoration experiment is illustrated for the CDS. The device was maintained at the target temperatures (33 or 37 °C) by using a thermostatic chamber and temperature was continuously recorded by 2 internal probes: the first one close to the syringe containing the buffer and the second one close to the drop.

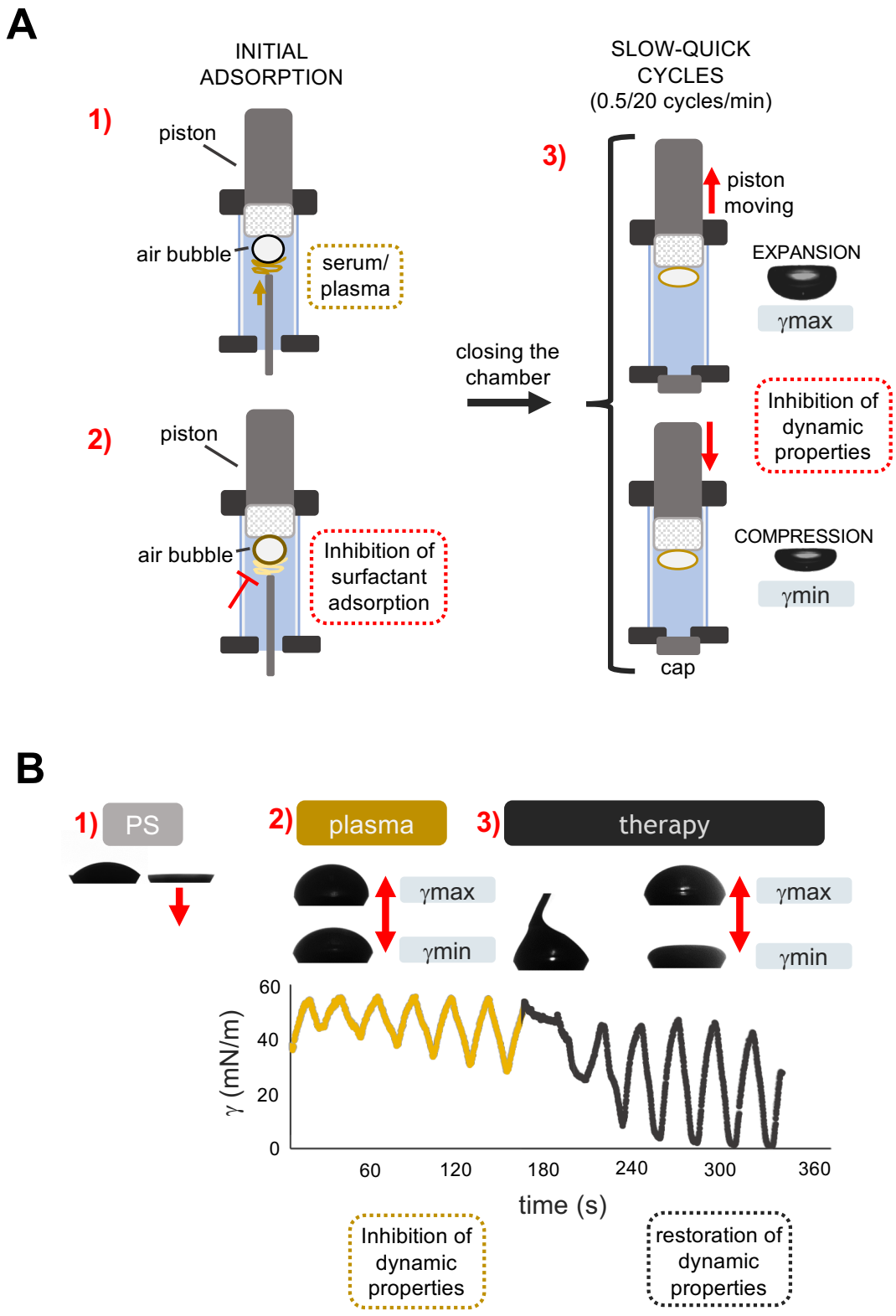

Figure 68. Schematic representation of an experiment to test PS inhibition by plasma/serum (CBS, CDS) and restoration of its capability to reduce surface tension by further supplementation of surfactant (CDS). (A) CBS: an excess of serum/plasma is first dispensed at the interface of the bubble, waiting 5 minutes before leaving PS close to the bubble and starting the experiment. **(B)** CDS: an excess of plasma instead of buffer was dispensed on top of the pedestal before starting the experiment. After 6 dynamic cycles, small volumes of the surfactant therapy are released at the drop interface. Abbreviations: γ, surface tension; PS, purified porcine surfactant.

The restoration experiment was carried out in around 6 minutes with the following steps:

1. 5 μL of PS at different concentrations was left on top of the pedestal and taken down slowly into the pedestal, which was filled with buffer.
2. Subsequently, an excess of total proteins of plasma (7 μL at 67.9 mg/mL, namely around 480 μg) or buffer for the control, were dispensed on top of the pedestal. Plasma was dispensed immediately after thawing. After 10 seconds, materials at the interface were subjected to slow expansion-compression cycles (2 cycles/min, shrinking the interface area by 20 %, 0.2 cm^2/min). As for the restoration experiments, the syringe movement was stopped at the end of the seventh expansion.
3. At this point, "therapeutic treatment" was applied at the air-liquid interface of the drop, touching once the drop. A syringe of 1 μL was used, dispensing small volumes (150-600 nL). After 15 seconds, the same slow cycles were started again (from compression) for another 5 cycles.

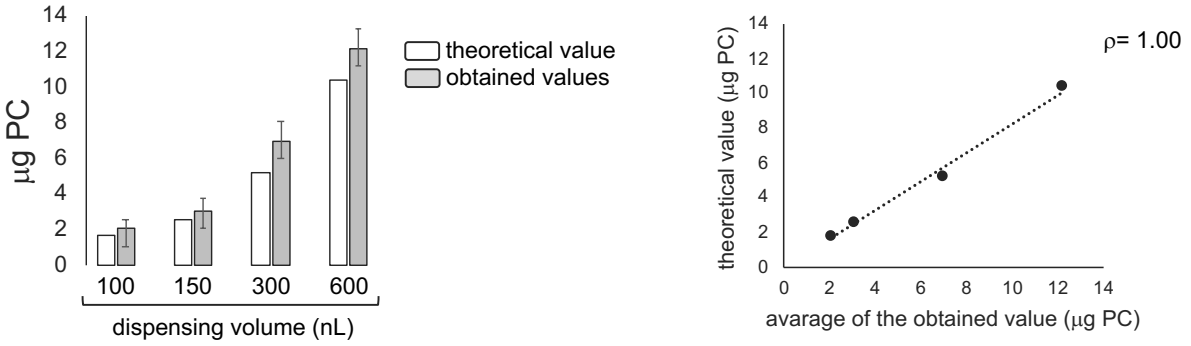

Figure 69. Dispensing linearity of a 1μL syringe, leaving material at the interface of a buffer drop (10 μL) at room temperature. A protein-lipid mixture containing DPPC/POPG (65/35, w/w%) and SP-B/C (2% of total w) at ≈25 mg/mL was used for the experiments. On the left, comparison of theoretical values of PC amount and obtained values determined by an enzymatic assay. Results for different volumes (100, 150, 300 and 600 nL) of material were analysed. On the right, correlation between theoretical and obtained values, using a Spearman (rho) coefficients. Results show a good linearity and a strong correlation (ρ=1), suggesting very small errors in dispensing the therapy. White and light-grey bars represent theoretical and obtained values, respectively. Means and SD of three replicates are shown. Abbreviations: PC, phosphatidylcholine.

The linearity of the 1 μL syringe used to leave therapy at the air-liquid interface was also studied and shown in **Figure 69A**. To do so, several volumes of the protein-lipid mixture used for the restoration experiments (at ≈ 25 mg/mL of PC), were dispensed in triplicate at the air-liquid interface of a buffer drop (10 μL). The resulting PC amounts were tested by an enzymatic method (Spinreact, Girona, Spain) and compared to the theoretical values. As shown in the figure, there was a strong correlation (ρ=1) between theoretical and obtained values, suggesting very small errors in dispensing material.

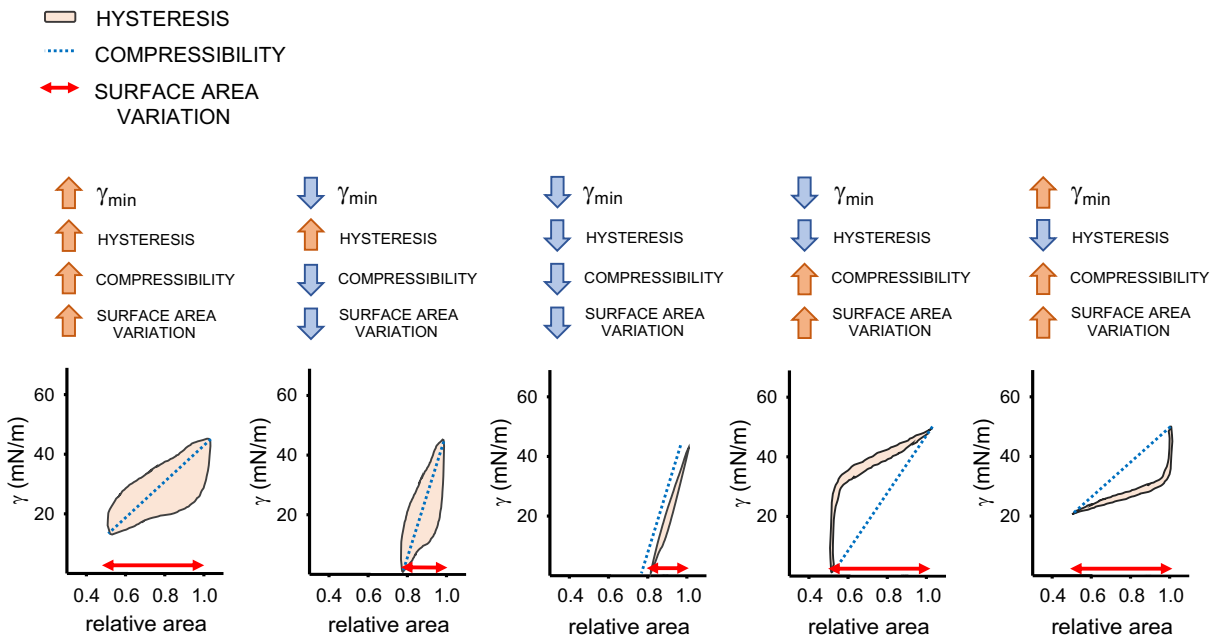

Figure 70. Schematic illustration of hysteresis, compressibility and surface area variation as defined from γ/area isotherms of surfactant subjected to compression-expansion cycles. Five different examples are shown, suggesting several possible behaviours for surfactant material to organise under dynamic cycling regardless of the achieved minimum surface tension. The enclosed area (salmon colour) between the compression and expansion segments defines the hysteresis, the red dash with double arrow corresponds to the change in relative area (surface area variation required to reach minimal tension), whereas the light blue dotted line defines compressibility (as the slope of the line passing through the minimum and maximum points of compression). Salmon and light-blue arrows on top of the graphs indicate increase and reduction in the values of any of the parameters. Abbreviations: γ, surface tension

Apart from γ values, other informative parameters can be obtained from the analysis of γ/area isotherms of CBS and CDS experiments that may illustrate further details on the organisation and properties of surfactant films at the air-liquid interface under cycles: compressibility, hysteresis and surface area variation under compression (**Figure 70**). Compressibility measures the changes in relative volume of a substance under stress. Lipids able to highly pack at the interface, as it is the case for DPPC, are less deformable than unsaturated lipids that occupy higher surface area. As a consequence, low compressibility indicates a tight packing of surfactant components in monolayers, favouring a quick surface tension reduction upon compression. Hysteresis defines the difference in the rate of surface tension variation between the compression and the expansion of the interface area. Thus, this parameter measures indirectly the work associated to surfactant for reorganising itself at the air-liquid interface upon cycling. The surface area variation under compression suggests how much the surface area of the bubble needs to be reduced to allow a proper reorganisation of material at the interface in order to reduce surface tension to the minimum. Compressibility ($\Delta\Pi/\Delta A$) is calculated as the slope value of the line passing through the minimum and maximum points of compression (minimum and maximum areas of the bubble) in the dynamic cycling curves (the steeper the slope, the lower the surfactant compressibility). Hysteresis (J/m^2) is calculated as the enclosed area between the compression and expansion segments of the isotherms in the dynamic cycling curves (the higher the hysteresis, the higher the work needed for surfactant to reorganise). This is done by approximating the curves to a third-

degree polynomial function. The surface area variation under compression, namely the relative area of compression (Δarea), is calculated by subtracting the minimum area of compression from the maximum one.

Langmuir-Blodgett trough

The use of Langmuir-Blodgett balances allows for the study of both structure and dynamic properties of surfactant material. It enables the compression and expansion of the adsorbed/spread surfactant film by moving the horizontal barrier that delimits one side (or two sides, if two symmetrical barriers are set) of the trough. At the same time, the interface can be transferred onto a solid support (i.e., glass or mica) and the microstructures and nanostructures formed by surfactant at the interface can be evaluated at different surface pressures, for example, by epifluorescence (which can also be applied in situ at the trough) or atomic force microscopy. Problems with leakage are reduced considerably by using a balance, which is specifically designed, with a special continuous Teflon ribbon barrier that encloses the whole area, which can be reduced or enlarged, and has no junctions (Cruz & Pérez-Gil, 2007). **Figure 71** shows an illustrative example of a Langmuir-Blodgett experiment of a doped DPPC monolayer subjected to lateral compression with the corresponding [Π/Area occupied by the Phospholipid (Å^2)] isotherm and the concurrent transference to a glass support for observation under epifluorescence microscopy. DPPC at the interface shows a specific Π/Area isotherm that corresponds to different phase organisations under interfacial compression and increased Π (**Figure 71B**). On this basis, depending on the lipid mobility and packing, under increasing lateral pressure, DPPC monolayer passes through a gas-like 2D phase (G), a co-existence of G and Le, a co-existence of Le and Lc and only Lc and then a solid-like phase until the monolayer collapses upon the high compression of the interface. Since the fluorescent analogue of PC occupies a higher area per molecule due to the presence of the bulky fluorophore group on its acyl chain, DPPC clusters exclude the probe at increased surface pressure. This is visible by epifluorescence microscopy as black starry-shape domains against a green background (which represents the mixture of unpacked DPPC and probe) (**Figure 71A)**.

A Langmuir-Blodgett balance with a special continuous Teflon ribbon barrier (total area= 184 cm^2, NIMA Technology, Inc., Coventry, UK) was used to study surfactant interfacial activity and lateral structure before and after subjecting material at the interface to 10 compression-expansion cycles (65 cm^2/min). This device is characterised by a Teflon trough filled with buffer on top of a water-thermostatic module to heat the liquid. Buffer subphase was maintained wormer than the interface to reach the target temperature right at the air-liquid interface. The latter was continuously recorded by a temperature probe resting at the interface and away from any possible contact with the walls of the trough. The maximum temperature variation was around ±1°C. The Wilhelmy plate was a piece of filter paper with a thickness of 0.5 mm and a width of 10 mm (Whatman, GE Healthcare Life Sciences, Logan, USA). The pressure sensor was purchased from NIMA Technology, Inc., Coventry, UK. Compression-expansion cycles were performed by moving the Teflon ribbon barrier, shrinking the interface area by ≈65 %.

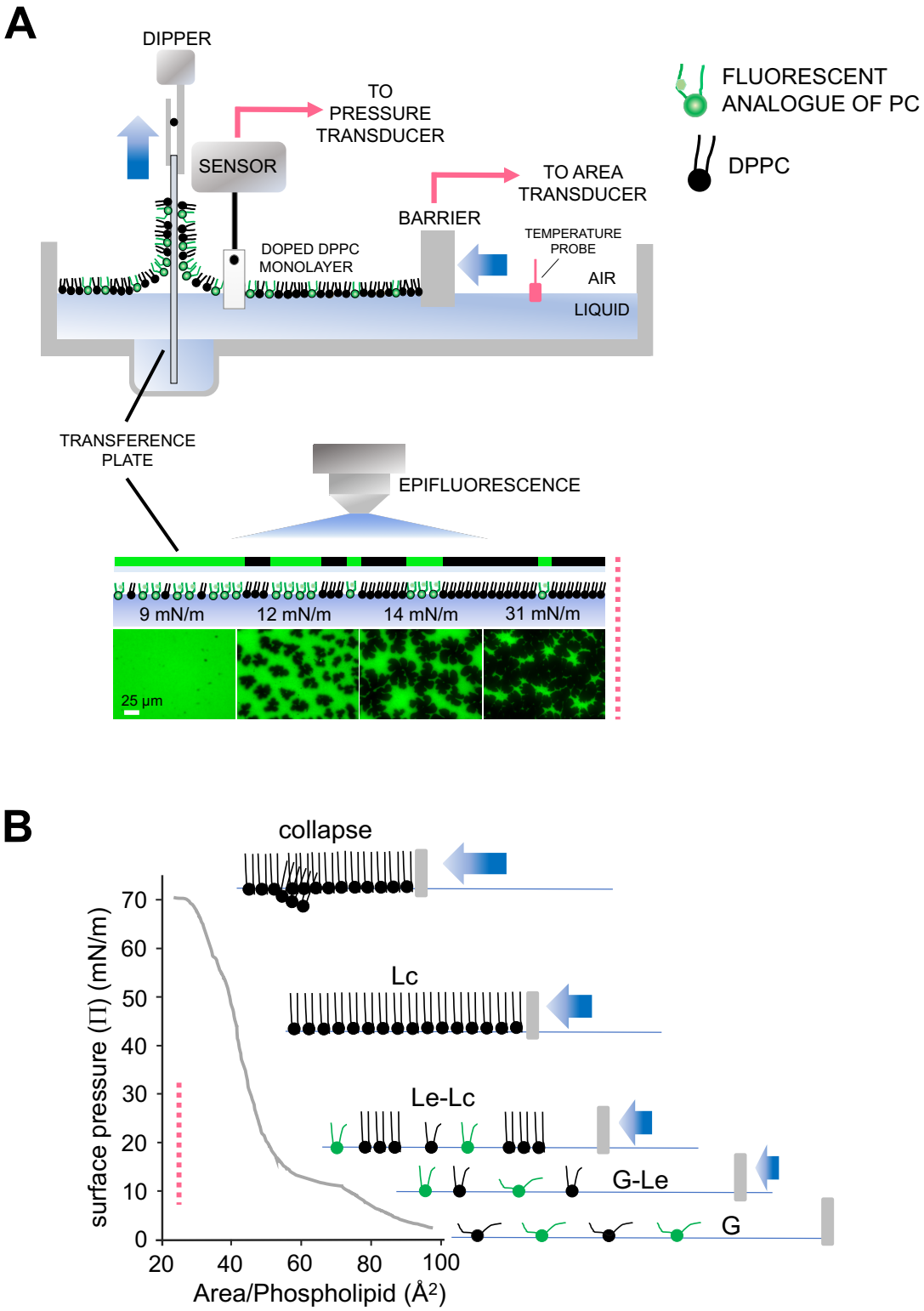

Figure 71. An illustrative diagram of the Langmuir-Blodgett trough subjected to lateral compression and the concurrent transference of a DPPC-reach interfacial film. (A) A schematic representation of the device and the images obtained by epifluorescence microscopy of DPPC doped with a fluorescent analogue of PC. **(B)** The classic Π/area isotherm of a pure DPPC film under increasing lateral pressure together with the corresponding segregation of condensed DPPC domains at the interface. The possible organisation of the fluorescent probe is also included. *Figure adapted from (González et al, 2015)*. Abbreviations: PC, phosphatidylcholine; Π, surface pressure, G, gaseous phase; Le, liquid-expanded phase; Lc, liquid-condensed phase.

This continuous Teflon ribbon barrier encloses the interface and avoids the leakage of the film during compression (Cruz & Pérez-Gil, 2007). Surfactant material was deposited dropwise at the air-liquid interface and the reduction in surface tension was recorded overtime as the increase in surface pressure against a paper plate sensor. The interfacial compression was started 10 minutes after surfactant deposition, to allow for equilibration of the material at the interface, before starting compression. As regards lipidomic analysis, around 50 μg of PS at 5 mg/mL was dispensed at the interface, before transferring material (25 cm^2/min). Lipids at the interface were rinsed with chloroform:methanol (2:1, v/v) and dried by a nitrogen flow. Five replicates per condition were pooled and analysed by LC-HRMS.

Structure of surfactant membranes and films

Epifluorescence Microscopy

The sample at the air-liquid interface of the Langmuir-Blodgett balance after 10 minutes of equilibration or after 10 compression-expansion cycles, was transferred onto a glass slide, moving up the lift with the glass coverslip (that had been previously immersed into the subphase) (5 mm/min) under the simultaneous compression of the interface (25 cm^2/min). The resulting supported film, captured at different surface pressures (COVASP (continuously varying surface pressures) films, (Wang *et al.*, 2007)), was observed under a epifluorescence microscope: Leica microsystems with Hamamatsu digital camera (experiments performed in chapter III) or Olympus BX-60 with an Olympus DP71 camera (experiments performed in chapter V).

To study the interfacial structure of PS, Poractant alfa and CHF 5633, the experiments in the Langmuir-Blodgett balance were performed in darkness, maintaining constant the temperature at 25 °C. Briefly, 2.5 μg/μL of PS or Poractant alfa or 50 μg/μL of CHF 5633 were labelled with NBD-PC for 1 hour at 37 °C to obtain a final molar ratio of 1% (dye/surfactant). In the case of PS and Poractant alfa, 15 μL of dye/surfactant suspension were spread at the air-liquid interface. As for CHF 5633, 3 μL of dye/surfactant suspension were applied with the barrier totally closed before opening it at a constant speed of 5 cm^2/min.

To study the interfacial structure of PS at 37 °C or 33 °C, around 30 μg of PS at 5 mg/mL previously doped with BODIPY-PC (1% mol/mol) was dispensed at the interface and transferred onto the glass slide before and after 10 cycles (65 cm^2/min), performing experiments in darkness. Lateral segregated domain structures in PS films were observed by epifluorescence microscopy.

Two replicates per condition were carried out and 4 images for each tested surface pressure were acquired per replicate. For each image, histogram stretching has been performed to enhance contrast without deleting pixel data by Adobe Photoshop CS4.

Cryo-electron Microscopy

Cryo-TEM allows for the study of samples at high-resolution under cryogenic temperatures without any staining agent. In this way, both ultrastructure and morphology of surfactant lipid membranes are preserved by the process of cryogenisation. The nanostructure

of surfactant large aggregates at around 8-10 mg/mL PC was analyzed by cryo-EM (from seven neonates with NLD and six with MAS).

Around 1 μl of sample was applied to the holey carbon copper grids (R2/2; Quantifoil, Großlöbichau, DE) and vitrified using a Cryoplunge (Gatan, Pleasanton, CA). The grids were observed in a JEM-1230 transmission electron microscope (JEOL; Tokyo, JP) operated at 100 kV and imaged at a final magnification of 5.68 Å/px, using an F416 CMOS camera from TVIPS (Gauting, DE). Four images per sample were taken. All surfactant vesicles present in each image from all of the samples of each group were evaluated by measuring their vertical and horizontal diameters and then averaged. The number of layers per vesicle was also counted.

Differential Scanning Calorimetry

The existence of different phases and membrane organisations and their interconversion as a function of temperature, as well as the determination of T_m values governing the phase transitions and the associated energy (enthalpy) can all be characterised by differential scanning calorimetry (DSC). DSC thermograms from surfactant membranes can be obtained in a microcalorimeter, which measures the differential heat (Cp) required to raise the temperature of the sample (surfactant) to the same value reached by a reference (buffer) along a ramp of increasing (or decreasing) temperature (**Figure 72A**) (Chiu & Prenner, 2011).

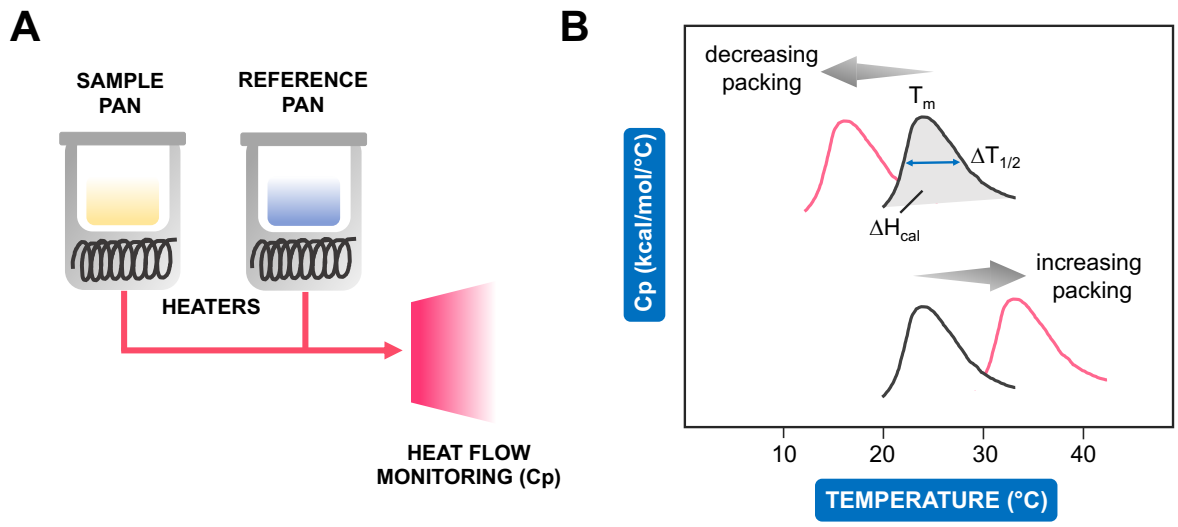

Figure 72. Heat transfer inside a differential scanning calorimetry (DSC). (A) A schematic representation of a DSC. **(B)** An illustrative example of the different parameters obtained from a DSC thermogram. The peak of temperature at which the Cp occurs is the T_m, the area under the peak (grey colour) is the energy needed to complete the phase transition and the grey blue line with double arrows indicate the cooperativity, namely the width of the transition at half peak height. The movement of the peak towards higher temperature suggests an increase in the packing of the material and a relative stabilisation of the ordered state. Abbreviations: Cp, differential heat capacity.

As schematised in **Figure 72B**, a typical membrane or lung surfactant sample undergoes an endothermic molecular reorganisation, with an increase in Cp, illustrating the T_m (peak temperature at which maximum Cp occurs), the energy needed to complete the phase transition (ΔH_{cal}) (area under peak, grey colour) and the cooperativity ($\Delta T_{1/2}$, light blue arrow) (the width of the transition at half peak height). The latter defines the capability of “cooperative

domains" to undergo a concerted phase transition. This phenomenon reduces the temperature range to reach a transition, thus decreasing the width of the peak.

If the T_m of a sample rises, the order of the system and the surfactant capability to stably pack under compression also increase. This may be due to (1) an increase in the amount of most packable lipid species (i.e., DPPC), (2) the presence of external molecules that influence packing, reducing the hydration status of surfactant membranes, (3) changes in the three-dimensional structure of the system versus more dehydrated supramolecular organisation. Conversely, a movement of T_m towards a lower temperature defines the opposite because of an increase in the disorder and destablisation of the system.

DSC experiments were performed as follows. Each lipid/protein mixture resuspended in buffer was assayed at 3 mg/mL. PS, CHF 5633 and Poractant alfa were diluted to reach the same concentration before testing. The sample and the reference material (buffer) were degassed prior to being inserted into the two microcalorimeter pans of a VP-DSC microcalorimeter (No. MC-2, MicroCal, Amherst, MA, USA). Samples were consecutively heated to 60 °C and cooled to 2 °C (30 °C/h) for 10 cycles of temperature scanning. The same heat was applied to the sample and the reference cells. Data from the 10^{th} cycle were analyzed by the software Origin (Origin Labs, Northampton, MA, USA).

Bibliography

Agassandian M, Mallampalli RK (2013) Surfactant phospholipid metabolism. *Biochim Biophys Acta* 1831: 612-625

Al-Saiedy M, Gunasekara L, Green F, Pratt R, Chiu A, Yang A, Dennis J, Pieron C, Bjornson C, Winston B *et al* (2018) Surfactant Dysfunction in ARDS and Bronchiolitis is Repaired with Cyclodextrins. *Mil Med* 183: 207-215

Alder JK, Chen JJ, Lancaster L, Danoff S, Su SC, Cogan JD, Vulto I, Xie M, Qi X, Tuder RM *et al* (2008) Short telomeres are a risk factor for idiopathic pulmonary fibrosis. *Proc Natl Acad Sci U S A* 105: 13051-13056

Altınsoy C, Tuzun F, Duman N, Sever AH, Dilek M, Ozbal S, Ergur BU, Yesilirmak DC, Yılmaz O, Kumral A *et al* (2014) Effect of induced hypothermia on lipopolysaccharide-induced lung injury in neonatal rats. *J Matern Fetal Neonatal Med* 27: 421-429

Alwan NA, Burgess RA, Ashworth S, Beale R, Bhadelia N, Bogaert D, Dowd J, Eckerle I, Goldman LR, Greenhalgh T *et al* (2020) Scientific consensus on the COVID-19 pandemic: we need to act now. *Lancet* 396: e71-72

Amrein M, von Nahmen A, Sieber M (1997) A scanning force- and fluorescence light microscopy study of the structure and function of a model pulmonary surfactant. *Eur Biophys J* 26: 349-357

Andreev K, Martynowycz MW, Kuzmenko I, Bu W, Hall SB, Gidalevitz D (2020) Structural Changes in Films of Pulmonary Surfactant Induced by Surfactant Vesicles. *Langmuir*: doi: 10.1021/acs.langmuir.1020c01813

Arbibe L, Koumanov K, Vial D, Rougeot C, Faure G, Havet N, Longacre S, Vargaftig BB, Béréziat G, Voelker DR *et al* (1998) Generation of lyso-phospholipids from surfactant in acute lung injury is mediated by type-II phospholipase A2 and inhibited by a direct surfactant protein A-phospholipase A2 protein interaction. *J Clin Invest* 102: 1152-1160

Ardell S, Pfister RH, Soll R (2015) Animal derived surfactant extract versus protein free synthetic surfactant for the prevention and treatment of respiratory distress syndrome. *Cochrane Database Syst Rev* 8: Cd000144

Arrich J, Holzer M, Havel C, Müllner M, Herkner H (2016) Hypothermia for neuroprotection in adults after cardiopulmonary resuscitation. *Cochrane Database Syst Rev* 2: Cd004128

Arroyo R, Echaide M, Moreno-Herrero F, Perez-Gil J, Kingma PS (2020) Functional characterization of the different oligomeric forms of human surfactant protein SP-D. *Biochim Biophys Acta Proteins Proteom* 1868: 140436

Arroyo R, Martín-González A, Echaide M, Jain A, Brondyk WH, Rosenbaum J, Moreno-Herrero F, Pérez-Gil J (2018) Supramolecular Assembly of Human Pulmonary Surfactant Protein SP-D. *J Mol Biol* 430: 1495-1509

Ashino Y, Ying X, Dobbs LG, Bhattacharya J (2000) [Ca(2+)](i) oscillations regulate type II cell exocytosis in the pulmonary alveolus. *Am J Physiol Lung Cell Mol Physiol* 279: L5-13

Aslami H, Binnekade J, Horn J, Huissoon S, Juffermans N (2010) The effect of induced hypothermia on respiratory parameters in mechanically ventilated patients. *Resuscitation* 81: 1723-1725

Aslami H, Kuipers MT, Beurskens CJ, Roelofs JJ, Schultz MJ, Juffermans NP (2012) Mild hypothermia reduces ventilator-induced lung injury, irrespective of reducing respiratory rate. *Transl Res* 159: 110-117

Autilio C, Echaide M, De Luca D, Pérez-Gil J (2018) Controlled hypothermia may improve surfactant function in asphyxiated neonates with or without meconium aspiration syndrome. *PLoS One* 13: e0192295

Autilio C, Echaide M, Shankar-Aguilera S, Bragado R, Amidani D, Salomone F, Pérez-Gil J, De Luca D (2020) Surfactant Injury in the Early Phase of Severe Meconium Aspiration Syndrome. *Am J Respir Cell Mol Biol* 63: 327-337

Autilio C, Pérez-Gil J (2019) Understanding the principle biophysics concepts of pulmonary surfactant in health and disease. *Arch Dis Child Fetal Neonatal Ed* 104: F443-f451

Azzopardi DV, Strohm B, Edwards AD, Dyet L, Halliday HL, Juszczak E, Kapellou O, Levene M, Marlow N, Porter E *et al* (2009) Moderate hypothermia to treat perinatal asphyxial encephalopathy. *N Engl J Med* 361: 1349-1358

Bae CW, Takahashi A, Chida S, Sasaki M (1998) Morphology and function of pulmonary surfactant inhibited by meconium. *Pediatr Res* 44: 187-191

Bagatolli LA, Ipsen JH, Simonsen AC, Mouritsen OG (2010) An outlook on organization of lipids in membranes: searching for a realistic connection with the organization of biological membranes. *Prog Lipid Res* 49: 378-389

Bahadue FL, Soll R (2012) Early versus delayed selective surfactant treatment for neonatal respiratory distress syndrome. *Cochrane Database Syst Rev* 11: Cd001456

Ball L, Silva PL, Rocco PRM, Pelosi P (2020) A critical approach to personalised medicine in ARDS. *Lancet Respir Med* 8: 218-219

Ball MK, Hillman NH, Kallapur SG, Polglase GR, Jobe AH, Pillow JJ (2010) Body temperature effects on lung injury in ventilated preterm lambs. *Resuscitation* 81: 749-754

Ban N, Matsumura Y, Sakai H, Takanezawa Y, Sasaki M, Arai H, Inagaki N (2007) ABCA3 as a lipid transporter in pulmonary surfactant biogenesis. *J Biol Chem* 282: 9628-9634

Bañares-Hidalgo A, Pérez-Gil J, Estrada P (2014) Acidic pH triggers conformational changes at the NH2-terminal propeptide of the precursor of pulmonary surfactant protein B to form a coiled coil structure. *Biochim Biophys Acta* 1838: 1738-1751

Baritussio A, Alberti A, Quaglino D, Pettenazzo A, Dalzoppo D, Sartori L, Pasquali-Ronchetti I (1994) SP-A, SP-B, and SP-C in surfactant subtypes around birth: reexamination of alveolar life cycle of surfactant. *Am J Physiol* 266: L436-447

Bartolomeo MP, Maisano F (2006) Validation of a reversed-phase HPLC method for quantitative amino acid analysis. *J Biomol Tech* 17: 131-137

Basu S, Kumar A, Bhatia BD, Satya K, Singh TB (2007) Role of steroids on the clinical course and outcome of meconium aspiration syndrome-a randomized controlled trial. *J Trop Pediatr* 53: 331-337

Bates SR (2010) P63 (CKAP4) as an SP-A receptor: implications for surfactant turnover. *Cell Physiol Biochem* 25: 41-54

Bates SR, Dodia C, Tao JQ, Fisher AB (2008) Surfactant protein-A plays an important role in lung surfactant clearance: evidence using the surfactant protein-A gene-targeted mouse. *Am J Physiol Lung Cell Mol Physiol* 294: L325-333

Baumgart F, Ospina OL, Mingarro I, Rodríguez-Crespo I, Pérez-Gil J (2010) Palmitoylation of pulmonary surfactant protein SP-C is critical for its functional cooperation with SP-B to sustain compression/expansion dynamics in cholesterol-containing surfactant films. *Biophys J* 99: 3234-3243

Benoit J, Merrill S, Rundell C, Meeker CI (1986) Amniostat-FLM: an initial clinical trial with both vaginal pool and amniocentesis samples. *Am J Obstet Gynecol* 154: 65-68

Bernhard W, Schmiedl A, Koster G, Orgeig S, Acevedo C, Poets CF, Postle AD (2007) Developmental changes in rat surfactant lipidomics in the context of species variability. *Pediatr Pulmonol* 42: 794-804

Besnard AE, Wirjosoekarto SA, Broeze KA, Opmeer BC, Mol BW (2013) Lecithin/sphingomyelin ratio and lamellar body count for fetal lung maturity: a meta-analysis. *Eur J Obstet Gynecol Reprod Biol* 169: 177-183

Betsuyaku T, Kuroki Y, Nagai K, Nasuhara Y, Nishimura M (2004) Effects of ageing and smoking on SP-A and SP-D levels in bronchoalveolar lavage fluid. *Eur Respir J* 24: 964-970

Bezzine S, Koduri RS, Valentin E, Murakami M, Kudo I, Ghomashchi F, Sadilek M, Lambeau G, Gelb MH (2000) Exogenously added human group X secreted phospholipase A(2) but not the group IB, IIA, and V enzymes efficiently release arachidonic acid from adherent mammalian cells. *J Biol Chem* 275: 3179-3191

Bhatia R, Morley CJ, Argus B, Tingay DG, Donath S, Davis PG (2013) The stable microbubble test for determining continuous positive airway pressure (CPAP) success in very preterm infants receiving nasal CPAP from birth. *Neonatology* 104: 188-193

Blackburn EH (2001) Switching and signaling at the telomere. *Cell* 106: 661-673

Blanco O, Cruz A, Ospina OL, López-Rodriguez E, Vázquez L, Pérez-Gil J (2012) Interfacial behavior and structural properties of a clinical lung surfactant from porcine source. *Biochim Biophys Acta* 1818: 2756-2766

Blanco O, Pérez-Gil J (2007) Biochemical and pharmacological differences between preparations of exogenous natural surfactant used to treat Respiratory Distress Syndrome: role of the different components in an efficient pulmonary surfactant. *Eur J Pharmacol* 568: 1-15

Bligh EG, Dyer WJ (1959) A rapid method of total lipid extraction and purification. *Can J Biochem Physiol* 37: 911-917

Bohlin K, Merchak A, Spence K, Patterson BW, Hamvas A (2003) Endogenous surfactant metabolism in newborn infants with and without respiratory failure. *Pediatr Res* 54: 185-191

Bossuyt PM, Reitsma JB, Bruns DE, Gatsonis CA, Glasziou PP, Irwig LM, Moher D, Rennie D, de Vet HC, Lijmer JG (2003) The STARD statement for reporting studies of diagnostic accuracy: explanation and elaboration. *Ann Intern Med* 138: W1-12

Botas C, Poulain F, Akiyama J, Brown C, Allen L, Goerke J, Clements J, Carlson E, Gillespie AM, Epstein C *et al* (1998) Altered surfactant homeostasis and alveolar type II cell morphology in mice lacking surfactant protein D. *Proc Natl Acad Sci U S A* 95: 11869-11874

Brasch F, Johnen G, Winn-Brasch A, Guttentag SH, Schmiedl A, Kapp N, Suzuki Y, Müller KM, Richter J, Hawgood S *et al* (2004) Surfactant protein B in type II pneumocytes and intra-alveolar surfactant forms of human lungs. *Am J Respir Cell Mol Biol* 30: 449-458

Brat R, Yousef N, Klifa R, Reynaud S, Shankar Aguilera S, De Luca D (2015) Lung Ultrasonography Score to Evaluate Oxygenation and Surfactant Need in Neonates Treated With Continuous Positive Airway Pressure. *JAMA Pediatrics* 169: e151797-e151797

Bridges JP, Ikegami M, Brilli LL, Chen X, Mason RJ, Shannon JM (2010) LPCAT1 regulates surfactant phospholipid synthesis and is required for transitioning to air breathing in mice. *J Clin Invest* 120: 1736-1748

Bui KC, Walther FJ, David-Cu R, Garg M, Warburton D (1992) Phospholipid and surfactant protein A concentrations in tracheal aspirates from infants requiring extracorporeal membrane oxygenation. *J Pediatr* 121: 271-274

Bunnell E, Pacht ER (1993) Oxidized glutathione is increased in the alveolar fluid of patients with the adult respiratory distress syndrome. *Am Rev Respir Dis* 148: 1174-1178

Bunt JE, Zimmermann LJ, Wattimena JL, van Beek RH, Sauer PJ, Carnielli VP (1998) Endogenous surfactant turnover in preterm infants measured with stable isotopes. *Am J Respir Crit Care Med* 157: 810-814

Butler PL, Mallampalli RK (2010) Cross-talk between remodeling and de novo pathways maintains phospholipid balance through ubiquitination. *J Biol Chem* 285: 6246-6258

Bykov AG, Guzman E, Rubio RG, Krycki MM, Milyaeva OY, Noskov BA (2019) Influence of temperature on dynamic surface properties of spread DPPC monolayers in a broad range of surface pressures. *Chem Phys Lipids* 225: 104812

Cabré EJ, Malmström J, Sutherland D, Pérez-Gil J, Otzen DE (2009) Surfactant protein SP-B strongly modifies surface collapse of phospholipid vesicles: insights from a quartz crystal microbalance with dissipation. *Biophys J* 97: 768-776

Cairo MJ (2019) Pilbeam's Mechanical Ventilation: Physiological and Clinical Applications, 7th Edition. *Mosby*

Calfee CS, Janz DR, Bernard GR, May AK, Kangelaris KN, Matthay MA, Ware LB (2015) Distinct molecular phenotypes of direct vs indirect ARDS in single-center and multicenter studies. *Chest* 147: 1539-1548

Calkovska A, Mokra D, Drgova A, Zila I, Javorka K (2008) Bronchoalveolar lavage with pulmonary surfactant/dextran mixture improves meconium clearance and lung functions in experimental meconium aspiration syndrome. *Eur J Pediatr* 167: 851-857

Cañadas O, Olmeda B, Alonso A, Pérez-Gil J (2020) Lipid-Protein and Protein-Protein Interactions in the Pulmonary Surfactant System and Their Role in Lung Homeostasis. *Int J Mol Sci* 21

Carnielli VP, Cogo PE (2018) Surfactant Metabolism in Neonatal Lung Diseases. In: *Neonatology: A Practical Approach to Neonatal Diseases*, Buonocore G., Bracci R., Weindling M. (eds.) pp. 809-822. Springer International Publishing: Cham

Cavicchioli P, Zimmermann LJ, Cogo PE, Badon T, Giordano G, Torresin M, Zacchello F, Carnielli VP (2001) Endogenous surfactant turnover in preterm infants with respiratory distress syndrome studied with stable isotope lipids. *Am J Respir Crit Care Med* 163: 55-60

Cerrada A, Haller T, Cruz A, Pérez-Gil J (2015) Pneumocytes Assemble Lung Surfactant as Highly Packed/Dehydrated States with Optimal Surface Activity. *Biophys J* 109: 2295-2306

Chabot S, Koumanov K, Lambeau G, Gelb MH, Balloy V, Chignard M, Whitsett JA, Touqui L (2003) Inhibitory effects of surfactant protein A on surfactant phospholipid hydrolysis by secreted phospholipases A2. *J Immunol* 171: 995-1000

Chaby R, Garcia-Verdugo I, Espinassous Q, Augusto LA (2005) Interactions between LPS and lung surfactant proteins. *J Endotoxin Res* 11: 181-185

Chander A, Johnson RG, Reicherter J, Fisher AB (1986) Lung lamellar bodies maintain an acidic internal pH. *J Biol Chem* 261: 6126-6131

Chavarha M, Loney RW, Rananavare SB, Hall SB (2013) An anionic phospholipid enables the hydrophobic surfactant proteins to alter spontaneous curvature. *Biophys J* 104: 594-603

Chernomordik LV, Kozlov MM (2003) Protein-lipid interplay in fusion and fission of biological membranes. *Annu Rev Biochem* 72: 175-207

Chintagari NR, Mishra A, Su L, Wang Y, Ayalew S, Hartson SD, Liu L (2010) Vacuolar ATPase regulates surfactant secretion in rat alveolar type II cells by modulating lamellar body calcium. *PLoS One* 5: e9228

Chiu MH, Prenner EJ (2011) Differential scanning calorimetry: An invaluable tool for a detailed thermodynamic characterization of macromolecules and their interactions. *J Pharm Bioallied Sci* 3: 39-59

Choi HJ, Hahn S, Lee J, Park B-J, Lee SM, Kim H-S, Bae C-W (2012) Surfactant lavage therapy for meconium aspiration syndrome: a systematic review and meta-analysis. *Neonatology* 101: 183-191

Choi SH, Wallace AM, Schneider DA, Burg E, Kim J, Alekseeva E, Ubags ND, Cool CD, Fang L, Suratt BT *et al* (2018) AIBP augments cholesterol efflux from alveolar macrophages to surfactant and reduces acute lung inflammation. *JCI Insight* 3: e120519

Christmann U, Hite RD, Witonsky SG, Elvinger F, Werre SR, Thatcher CD, Tan RH, Buechner-Maxwell VA (2009) Influence of age on surfactant isolated from healthy horses maintained on pasture. *J Vet Intern Med* 23: 612-618

Chung KF (2017) Personalised medicine in asthma: time for action: Number 1 in the Series "Personalised medicine in respiratory diseases" Edited by Renaud Louis and Nicolas Roche. *Eur Respir Rev* 26: 170064

Clark JC, Wert SE, Bachurski CJ, Stahlman MT, Stripp BR, Weaver TE, Whitsett JA (1995) Targeted disruption of the surfactant protein B gene disrupts surfactant homeostasis, causing respiratory failure in newborn mice. *Proc Natl Acad Sci U S A* 92: 7794-7798

Cleary GM, Antunes MJ, Ciesielka DA, Higgins ST, Spitzer AR, Chander A (1997) Exudative lung injury is associated with decreased levels of surfactant proteins in a rat model of meconium aspiration. *Pediatrics* 100: 998-1003

Clements JA (1957) Surface tension of lung extracts. *Proc Soc Exp Biol Med* 95: 170-172

Clercx C, Venker-van Haagen A, Den Breejen J, Haagsman H, van den Brom W, de Vries H, van Golde L (1989) Effects of age and breed on the phospholipid composition of canine surfactant. *Lung* 167: 351

Cochrane CG, Revak SD, Merritt TA, Schraufstätter IU, Hoch RC, Henderson C, Andersson S, Takamori H, Oades ZG (1998) Bronchoalveolar lavage with KL4-surfactant in models of meconium aspiration syndrome. *Pediatr Res* 44: 705-715

Cogo PE, Zimmermann LJ, Rosso F, Tormena F, Gamba P, Verlato G, Baritussio A, Carnielli VP (2002) Surfactant synthesis and kinetics in infants with congenital diaphragmatic hernia. *Am J Respir Crit Care Med* 166: 154-158

Collard HR (2010) The age of idiopathic pulmonary fibrosis. *Am J Respir Crit Care Med* 181: 771-772

Collard HR, Ryerson CJ, Corte TJ, Jenkins G, Kondoh Y, Lederer DJ, Lee JS, Maher TM, Wells AU, Antoniou KM *et al* (2016) Acute Exacerbation of Idiopathic Pulmonary Fibrosis. An International Working Group Report. *Am J Respir Crit Care Med* 194: 265-275

Confalonieri M, Salton F, Fabiano F (2017) Acute respiratory distress syndrome. *Eur Respir Rev* 26

Copland I, Post M (2004) Lung development and fetal lung growth. *Paediatr Respir Rev* 5 Suppl A: S259-264

Creuwels LA, Demel RA, van Golde LM, Benson BJ, Haagsman HP (1993) Effect of acylation on structure and function of surfactant protein C at the air-liquid interface. *J Biol Chem* 268: 26752-26758

Crouch EC (1998) Structure, biologic properties, and expression of surfactant protein D (SP-D). *Biochim Biophys Acta* 1408: 278-289

Cruces P, Erranz B, Donoso A, Carvajal C, Salomón T, Torres MF, Díaz F (2013) Mild hypothermia increases pulmonary anti-inflammatory response during protective mechanical ventilation in a piglet model of acute lung injury. *Pediatric Anesthesia* 23: 1069-1077

Cruz A, Pérez-Gil J (2007) Langmuir films to determine lateral surface pressure on lipid segregation. *Methods Mol Biol* 400: 439-457

Cruz A, Vázquez L, Vélez M, Pérez-Gil J (2004) Effect of pulmonary surfactant protein SP-B on the micro- and nanostructure of phospholipid films. *Biophys J* 86: 308-320

Cruz A, Worthman LA, Serrano AG, Casals C, Keough KM, Pérez-Gil J (2000) Microstructure and dynamic surface properties of surfactant protein SP-B/dipalmitoylphosphatidylcholine interfacial films spread from lipid-protein bilayers. *Eur Biophys J* 29: 204-213

Curstedt T, Halliday HL, Speer CP (2015) A unique story in neonatal research: the development of a porcine surfactant. *Neonatology* 107: 321-329

Curstedt T, Johansson J (2010) Different effects of surfactant proteins B and C - implications for development of synthetic surfactants. *Neonatology* 97: 367-372

D'Aronco S, Simonato M, Vedovelli L, Baritussio A, Verlato G, Nobile S, Giorgetti C, Nespeca M, Carnielli VP, Cogo PE (2015) Surfactant protein B and A concentrations are increased in neonatal pneumonia. *Pediatr Res* 78: 401-406

Danhaive O, Chapin C, Horneman H, Cogo PE, Ballard PL (2015) Surface film formation in vitro by infant and therapeutic surfactants: role of surfactant protein B. *Pediatr Res* 77: 340-346

Dargaville PA, Copnell B, Mills JF, Haron I, Lee JK, Tingay DG, Rohana J, Mildenhall LF, Jeng MJ, Narayanan A *et al* (2011) Randomized controlled trial of lung lavage with dilute surfactant for meconium aspiration syndrome. *J Pediatr* 158: 383-389.e382

Dargaville PA, Mills JF (2005) Surfactant therapy for meconium aspiration syndrome: current status. *Drugs* 65: 2569-2591

Dargaville PA, South M, McDougall PN (1999) Comparison of two methods of diagnostic lung lavage in ventilated infants with lung disease. *Am J Respir Crit Care Med* 160: 771-777

Das A, Acharya S, Gottipati KR, McKnight JB, Chandru H, Alcorn JL, Boggaram V (2011) Thyroid transcription factor-1 (TTF-1) gene: identification of ZBP-89, Sp1, and TTF-1 sites in the promoter and regulation by TNF-α in lung epithelial cells. *Am J Physiol Lung Cell Mol Physiol* 301: L427-440

de Blic J, Midulla F, Barbato A, Clement A, Dab I, Eber E, Green C, Grigg J, Kotecha S, Kurland G *et al* (2000) Bronchoalveolar lavage in children. ERS Task Force on bronchoalveolar lavage in children. European Respiratory Society. *Eur Respir J* 15: 217-231

de la Serna JB, Perez-Gil J, Simonsen AC, Bagatolli LA (2004) Cholesterol rules direct observation of the coexistence of two fluid phases in native pulmonary surfactant membranes at physiological temperatures. *J Biol Chem* 279: 40715-40722

de la Serna JB, Vargas R, Picardi V, Cruz A, Arranz R, Valpuesta JM, Mateu L, Pérez-Gil J (2013) Segregated ordered lipid phases and protein-promoted membrane cohesivity are required for pulmonary surfactant films to stabilize and protect the respiratory surface. *Faraday Discuss* 161: 535-548; discussion 563-589

de Lange T (2005) Shelterin: the protein complex that shapes and safeguards human telomeres. *Genes Dev* 19: 2100-2110

De Luca D (2019) Personalising care of acute respiratory distress syndrome according to patients' age. *Lancet Respir Med* 7: 100-101

De Luca D, Lopez-Rodriguez E, Minucci A, Vendittelli F, Gentile L, Stival E, Conti G, Piastra M, Antonelli M, Echaide M *et al* (2013) Clinical and biological role of secretory phospholipase A2 in acute respiratory distress syndrome infants. *Crit Care* 17: R163

De Luca D, Minucci A, Trias J, Tripodi D, Conti G, Zuppi C, Capoluongo E (2012) Varespladib inhibits secretory phospholipase A2 in bronchoalveolar lavage of different types of neonatal lung injury. *J Clin Pharmacol* 52: 729-737

De Luca D, Minucci A, Tripodi D, Piastra M, Pietrini D, Zuppi C, Conti G, Carnielli VP, Capoluongo E (2011) Role of distinct phospholipases A2 and their modulators in meconium aspiration syndrome in human neonates. *Intensive Care Med* 37: 1158-1165

De Luca D, Shankar-Aguilera S, Autilio C, Raschetti R, Vedovelli L, Fitting C, Payré C, Jeammet L, Perez-Gil J, Cogo PE *et al* (2020) Surfactant-secreted phospholipase A(2) interplay and respiratory outcome in preterm neonates. *Am J Physiol Lung Cell Mol Physiol* 319: L95-l104

De Luca D, Tingay DG, van Kaam A, Brunow de Carvalho W, Valverde E, Christoph Roehr C, Mosca F, Matassa PG, Danhaive O, Carnielli VP *et al* (2016) Hypothermia and Meconium Aspiration Syndrome: International Multicenter Retrospective Cohort Study. *Am J Respir Crit Care Med* 194: 381-384

De Luca D, van Kaam AH, Tingay DG, Courtney SE, Danhaive O, Carnielli VP, Zimmermann LJ, Kneyber MCJ, Tissieres P, Brierley J *et al* (2017) The Montreux definition of neonatal ARDS: biological and clinical background behind the description of a new entity. *Lancet Respir Med* 5: 657-666

De Luca D, Vázquez-Sánchez S, Minucci A, Echaide M, Piastra M, Conti G, Capoluongo ED, Pérez-Gil J (2014) Effect of whole body hypothermia on inflammation and surfactant function in asphyxiated neonates. *Eur Respir J* 44: 1708-1710

Dennis EA, Cao J, Hsu YH, Magrioti V, Kokotos G (2011) Phospholipase A2 enzymes: physical structure, biological function, disease implication, chemical inhibition, and therapeutic intervention. *Chem Rev* 111: 6130-6185

Desai O, Winkler J, Minasyan M, Herzog EL (2018) The role of immune and inflammatory cells in idiopathic pulmonary fibrosis. *Front Med (Lausanne)* 5: 43

Diemel RV, Snel MM, Waring AJ, Walther FJ, van Golde LM, Putz G, Haagsman HP, Batenburg JJ (2002) Multilayer formation upon compression of surfactant monolayers depends on protein concentration as well as lipid composition. An atomic force microscopy study. *J Biol Chem* 277: 21179-21188

Discher BM, Maloney KM, Schief WR, Jr., Grainger DW, Vogel V, Hall SB (1996) Lateral phase separation in interfacial films of pulmonary surfactant. *Biophys J* 71: 2583-2590

Dluhy RA, Shanmukh S, Leapard JB, Krüger P, Baatz JE (2003) Deacylated pulmonary surfactant protein SP-C transforms from alpha-helical to amyloid fibril structure via a pH-dependent mechanism: an infrared structural investigation. *Biophys J* 85: 2417-2429

Doyle IR, Jones ME, Barr HA, Orgeig S, Crockett AJ, McDonald CF, Nicholas TE (1994) Composition of human pulmonary surfactant varies with exercise and level of fitness. *Am J Respir Crit Care Med* 149: 1619-1627

Drost EM, Skwarski KM, Sauleda J, Soler N, Roca J, Agusti A, MacNee W (2005) Oxidative stress and airway inflammation in severe exacerbations of COPD. *Thorax* 60: 293-300

Eastoe J, Dalton JS (2000) Dynamic surface tension and adsorption mechanisms of surfactants at the air–water interface. *Adv Colloid Interface Sci* 85: 103-144

Echaide M, Autilio C, Arroyo R, Perez-Gil J (2017) Restoring pulmonary surfactant membranes and films at the respiratory surface. *Biochim Biophys Acta Biomembr* 1859: 1725-1739

Echaide M, Autilio C, López-Rodríguez E, Cruz A, Pérez-Gil J (2020) In Vitro Functional and Structural Characterization of A Synthetic Clinical Pulmonary Surfactant with Enhanced Resistance to Inhibition. *Sci Rep* 10: 1-10

Egberts J, Sloot H, Mazure A (1989) Minimal surface tension, squeeze-out and transition temperatures of binary mixtures of dipalmitoylphosphatidylcholine and unsaturated phospholipids. *Biochim Biophys Acta* 1002: 109-113

Enhorning G, Hohlfeld J, Krug N, Lema G, Welliver RC (2000) Surfactant function affected by airway inflammation and cooling: possible impact on exercise-induced asthma. *Eur Respir J* 15: 532-538

Fakhoury G, Daikoku NH, Benser J, Dubin NH (1994) Lamellar body concentrations and the prediction of fetal pulmonary maturity. *Am J Obstet Gynecol* 170: 72-76

Fan E, Brodie D, Slutsky AS (2018) Acute respiratory distress syndrome: advances in diagnosis and treatment. *Jama* 319: 698-710

Ferkol T, Schraufnagel D (2014) The global burden of respiratory disease. *Ann Am Thorac Soc* 11: 404-406

Fessler MB, Parks JS (2011) Intracellular lipid flux and membrane microdomains as organizing principles in inflammatory cell signaling. *J Immunol* 187: 1529-1535

Fessler MB, Summer RS (2016) Surfactant Lipids at the Host-Environment Interface. Metabolic Sensors, Suppressors, and Effectors of Inflammatory Lung Disease. *Am J Respir Cell Mol Biol* 54: 624-635

Fetus Co, Newborn (2014) Respiratory support in preterm infants at birth. *Pediatrics* 133: 171-174

Filgueiras OM, Possmayer F (1990) Purification and characterization of a phospholipase A2 associated with rabbit lung microsomes: some evidence for its mitochondrial origin. *Biochim Biophys Acta* 1046: 258-266

Finer NN, Merritt TA, Bernstein G, Job L, Mazela J, Segal R (2010) An open label, pilot study of Aerosurf® combined with nCPAP to prevent RDS in preterm neonates. *J Aerosol Med Pulm Drug Deliv* 23: 303-309

Fingerlin TE, Murphy E, Zhang W, Peljto AL, Brown KK, Steele MP, Loyd JE, Cosgrove GP, Lynch D, Groshong S *et al* (2013) Genome-wide association study identifies multiple susceptibility loci for pulmonary fibrosis. *Nat Genet* 45: 613-620

Fisher AB, Dodia C (2001) Lysosomal-type PLA2 and turnover of alveolar DPPC. *Am J Physiol Lung Cell Mol Physiol* 280: L748-754

Fisher AB, Dodia C, Ruckert P, Tao JQ, Bates SR (2010) Pathway to lamellar bodies for surfactant protein A. *Am J Physiol Lung Cell Mol Physiol* 299: L51-58

Fitzgerald ML, Xavier R, Haley KJ, Welti R, Goss JL, Brown CE, Zhuang DZ, Bell SA, Lu N, McKee M *et al* (2007) ABCA3 inactivation in mice causes respiratory failure, loss of pulmonary surfactant, and depletion of lung phosphatidylglycerol. *J Lipid Res* 48: 621-632

Foligno S, De Luca D (2020) Porcine versus bovine surfactant therapy for RDS in preterm neonates: pragmatic meta-analysis and review of physiopathological plausibility of the effects on extra-pulmonary outcomes. *Respir Res* 21: 8

Frick M, Bertocchi C, Jennings P, Haller T, Mair N, Singer W, Pfaller W, Ritsch-Marte M, Dietl P (2004) Ca2+ entry is essential for cell strain-induced lamellar body fusion in isolated rat type II pneumocytes. *Am J Physiol Lung Cell Mol Physiol* 286: L210-220

Fulop T, Larbi A, Dupuis G, Le Page A, Frost EH, Cohen AA, Witkowski JM, Franceschi C (2017) Immunosenescence and Inflamm-Aging As Two Sides of the Same Coin: Friends or Foes? *Front Immunol* 8: 1960

Gage A (2018) Music and the Road: Essays on the Interplay of Music and the Popular Culture of the American Road. *CAML Review / REVUE DE L'ACBM* 46

García-Álvarez B, Alonso A, Pérez-Gil J (2019) Structure and Function of Pulmonary Surfactant Proteins. *eLS John Wiley & Sons*

Garcia-Verdugo I, Garcia de Paco E, Espinassous Q, Gonzalez-Horta A, Synguelakis M, Kanellopoulos J, Rivas L, Chaby R, Perez-Gil J (2009) Synthetic peptides representing the N-terminal segment of surfactant protein C modulate LPS-stimulated TNF-alpha production by macrophages. *Innate Immun* 15: 53-62

García-Verdugo I, Wang G, Floros J, Casals C (2002) Structural analysis and lipid-binding properties of recombinant human surfactant protein a derived from one or both genes. *Biochemistry* 41: 14041-14053

Gardai SJ, Xiao YQ, Dickinson M, Nick JA, Voelker DR, Greene KE, Henson PM (2003) By binding SIRPalpha or calreticulin/CD91, lung collectins act as dual function surveillance molecules to suppress or enhance inflammation. *Cell* 115: 13-23

Ghio AJ, Stonehuerner JG, Richards JH, Crissman KM, Roggli VL, Piantadosi CA, Carraway MS (2008) Iron homeostasis and oxidative stress in idiopathic pulmonary alveolar proteinosis: a case-control study. *Respir Res* 9: 10

Ghnimi S, Budilarto E, Kamal-Eldin A (2017) The new paradigm for lipid oxidation and insights to microencapsulation of Omega-3 fatty acids. *Compr Rev Food Sci Food Saf* 16: 1206-1218

Glaser K, Fehrholz M, Henrich B, Claus H, Papsdorf M, Speer CP (2017) Anti-inflammatory effects of the new generation synthetic surfactant CHF5633 on Ureaplasma-induced cytokine responses in human monocytes. *Expert Rev Anti Infect Ther* 15: 181-189

Glaser K, Fehrholz M, Papsdorf M, Curstedt T, Kunzmann S, Speer CP (2016) The new generation synthetic reconstituted surfactant CHF5633 suppresses LPS-induced cytokine responses in human neonatal monocytes. *Cytokine* 86: 119-123

Gold JA, Hoshino Y, Tanaka N, Rom WN, Raju B, Condos R, Weiden MD (2004) Surfactant protein A modulates the inflammatory response in macrophages during tuberculosis. *Infect Immun* 72: 645-650

Gómez-Gil L, Pérez-Gil J, Goormaghtigh E (2009a) Cholesterol modulates the exposure and orientation of pulmonary surfactant protein SP-C in model surfactant membranes. *Biochim Biophys Acta* 1788: 1907-1915

Gómez-Gil L, Schürch D, Goormaghtigh E, Pérez-Gil J (2009b) Pulmonary surfactant protein SP-C counteracts the deleterious effects of cholesterol on the activity of surfactant films under physiologically relevant compression-expansion dynamics. *Biophys J* 97: 2736-2745

González CM, Pizarro-Guerra G, Droguett F, Sarabia M (2015) Artificial biomembrane based on DPPC--Investigation into phase transition and thermal behavior through ellipsometric techniques. *Biochim Biophys Acta* 1848: 2295-2307

Gouyon JB, Ribakovsky C, Ferdynus C, Quantin C, Sagot P, Gouyon B, Network BP (2008) Severe respiratory disorders in term neonates. *Paediatr Perinat Epidemiol* 22: 22-30

Grainger D, Reichert A, Ringsdorf H, Salesse C (1989) An enzyme caught in action: direct imaging of hydrolytic function and domain formation of phospholipase A2 in phosphatidylcholine monolayers. *FEBS Lett* 252: 73-82

Green RM, Graham M, O'Donovan MR, Chipman JK, Hodges NJ (2006) Subcellular compartmentalization of glutathione: correlations with parameters of oxidative stress related to genotoxicity. *Mutagenesis* 21: 383-390

Greider CW, Blackburn EH (1985) Identification of a specific telomere terminal transferase activity in Tetrahymena extracts. *Cell* 43: 405-413

Griese M, Kirmeier HG, Liebisch G, Rauch D, Stückler F, Schmitz G, Zarbock R (2015) Surfactant lipidomics in healthy children and childhood interstitial lung disease. *PloS one* 10: e0117985

Gunasekara L, Schoel WM, Schürch S, Amrein MW (2008) A comparative study of mechanisms of surfactant inhibition. *Biochim Biophys Acta* 1778: 433-444

Gunasekara L, Schürch S, Schoel WM, Nag K, Leonenko Z, Haufs M, Amrein M (2005) Pulmonary surfactant function is abolished by an elevated proportion of cholesterol. *Biochim Biophys Acta* 1737: 27-35

Gunasekara LC, Pratt RM, Schoel WM, Gosche S, Prenner EJ, Amrein MW (2010) Methyl-beta-cyclodextrin restores the structure and function of pulmonary surfactant films impaired by cholesterol. *Biochim Biophys Acta* 1798: 986-994

Günther A, Ruppert C, Schmidt R, Markart P, Grimminger F, Walmrath D, Seeger W (2001) Surfactant alteration and replacement in acute respiratory distress syndrome. *Respir Res* 2: 353

Günther A, Schmidt R, Feustel A, Meier U, Pucker C, Ermert M, Seeger W (1999) Surfactant subtype conversion is related to loss of surfactant apoprotein B and surface activity in large surfactant aggregates. Experimental and clinical studies. *Am J Respir Crit Care Med* 159: 244-251

Günther A, Schmidt R, Harodt J, Schmehl T, Walmrath D, Ruppert C, Grimminger F, Seeger W (2002) Bronchoscopic administration of bovine natural surfactant in ARDS and septic shock: impact on biophysical and biochemical surfactant properties. *Eur Respir J* 19: 797-804

Gunther A, Schmidt R, Nix F, Yabut-Perez M, Guth C, Rosseau S, Siebert C, Grimminger F, Morr H, Velcovsky H (1999) Surfactant abnormalities in idiopathic pulmonary fibrosis, hypersensitivity pneumonitis and sarcoidosis. *Eur Respir J* 14: 565-573

Gunther A, Siebert C, Schmidt R, Ziegler S, Grimminger F, Yabut M, Temmesfeld B, Walmrath D, Morr H, Seeger W (1996) Surfactant alterations in severe pneumonia, acute respiratory distress syndrome, and cardiogenic lung edema. *Am J Respir Crit Care Med* 153: 176-184

Guo X, Luo S, Amidani D, Rivetti C, Pieraccini G, Pioselli B, Catinella S, Murgia X, Salomone F, Xu Y (2020) In vitro characterization and in vivo comparison of the pulmonary outcomes of Poractant alfa and Calsurf in ventilated preterm rabbits. *PloS one* 15: e0230229

Hahn S, Choi HJ, Soll R, Dargaville PA (2013) Lung lavage for meconium aspiration syndrome in newborn infants. *Cochrane Database Syst Rev*: Cd003486

Hall NJ, Eaton S, Peters MJ, Hiorns MP, Alexander N, Azzopardi DV, Pierro A (2010) Mild controlled hypothermia in preterm neonates with advanced necrotizing enterocolitis. *Pediatrics* 125: e300-e308

Haller T, Dietl P, Stockner H, Frick M, Mair N, Tinhofer I, Ritsch A, Enhorning G, Putz G (2004) Tracing surfactant transformation from cellular release to insertion into an air-liquid interface. *Am J Physiol Lung Cell Mol Physiol* 286: L1009-1015

Halliday HL (2017) The fascinating story of surfactant. *J Paediatr Child Health* 53: 327-332

Hawgood S, Poulain FR (2001) The pulmonary collectins and surfactant metabolism. *Annu Rev Physiol* 63: 495-519

Hayek AJ, White HD, Ghamande S, Spradley C, Arroliga AC (2017) Is therapeutic hypothermia for acute respiratory distress syndrome the future? *J Intensive Care Med* 32: 460-464

Henn R, Fiori RM, Fiori HH, Pereira MR, Colvero MO, Ramos Garcia PC, Padoim P, Stivanin JB (2016) Surfactant with and without bronchoalveolar lavage in an experimental model of meconium aspiration syndrome. *J Perinat Med* 44: 685-689

Hentschel R, Bohlin K, van Kaam A, Fuchs H, Danhaive O (2020) Surfactant replacement therapy: From biological basis to current clinical practice. *Pediatr Res* 88: 176-183

Hernández-Beeftink T, Guillen-Guio B, Villar J, Flores C (2019) Genomics and the Acute Respiratory Distress Syndrome: Current and Future Directions. *Int J Mol Sci* 20: 4004

Herting E, Rauprich P, Stichtenoth G, Walter G, Johansson J, Robertson B (2001) Resistance of different surfactant preparations to inactivation by meconium. *Pediatr Res* 50: 44-49

Hiansen JQ, Keating E, Aspros A, Yao LJ, Bosma KJ, Yamashita CM, Lewis JF, Veldhuizen RA (2015) Cholesterol-mediated surfactant dysfunction is mitigated by surfactant protein A. *Biochim Biophys Acta* 1848: 813-820

Hidalgo A, Salomone F, Fresno N, Orellana G, Cruz A, Perez-Gil J (2017) Efficient interfacially driven vehiculization of corticosteroids by pulmonary surfactant. *Langmuir* 33: 7929-7939

Hilgendorff A, Doerner M, Rawer D, Leick J, Trotter A, Ebsen M, Ruppert C, Günther A, Gortner L, Reiss I (2006) Effects of a recombinant surfactant protein-C-based surfactant on lung function and the pulmonary surfactant system in a model of meconium aspiration syndrome. *Crit Care Med* 34: 203-210

Hilgendorff A, Rawer D, Doerner M, Tutdibi E, Ebsen M, Schmidt R, Guenther A, Gortner L, Reiss I (2003) Synthetic and natural surfactant differentially modulate inflammation after meconium aspiration. *Intensive Care Med* 29: 2247-2254

Hite RD, Grier BL, Waite BM, Veldhuizen RA, Possmayer F, Yao LJ, Seeds MC (2012) Surfactant protein B inhibits secretory phospholipase A2 hydrolysis of surfactant phospholipids. *Am J Physiol Lung Cell Mol Physiol* 302: L257-265

Hite RD, Seeds MC, Jacinto RB, Grier BL, Waite BM, Bass DA (2005) Lysophospholipid and fatty acid inhibition of pulmonary surfactant: non-enzymatic models of phospholipase A2 surfactant hydrolysis. *Biochim Biophys Acta* 1720: 14-21

Hobi N, Giolai M, Olmeda B, Miklavc P, Felder E, Walther P, Dietl P, Frick M, Pérez-Gil J, Haller T (2016) A small key unlocks a heavy door: The essential function of the small hydrophobic proteins SP-B and SP-C to trigger adsorption of pulmonary surfactant lamellar bodies. *Biochim Biophys Acta* 1863: 2124-2134

Hobi N, Siber G, Bouzas V, Ravasio A, Pérez-Gil J, Haller T (2014) Physiological variables affecting surface film formation by native lamellar body-like pulmonary surfactant particles. *Biochim Biophys Acta* 1838: 1842-1850

Hodson R (2016) Precision medicine. *Nature* 537: S49-S49

Holm B, Notter R, Finkelstein J (1985) Surface property changes from interactions of albumin with natural lung surfactant and extracted lung lipids. *Chem Phys Lipids* 38: 287-298

Holm BA, Enhorning G, Notter RH (1988) A biophysical mechanism by which plasma proteins inhibit lung surfactant activity. *Chem Phys Lipids* 49: 49-55

Holm BA, Wang Z, Notter RH (1999) Multiple mechanisms of lung surfactant inhibition. *Pediatr Res* 46: 85-93

Hong S-B, Koh Y, Lee I-C, Kim MJ, Kim WS, Kim D-S, Kim WD, Lim C-M (2005) Induced hypothermia as a new approach to lung rest for the acutely injured lung. *Crit Care Med* 33: 2049-2055

Horhat FG, Gundogdu F, David LV, Boia ES, Pirtea L, Horhat R, Cucui-Cozma A, Ciuca I, Diaconu M, Nitu R *et al* (2017) Early Evaluation and Monitoring of Critical Patients with Acute Respiratory Distress Syndrome (ARDS) Using Specific Genetic Polymorphisms. *Biochem Genet* 55: 204-211

Ikegami M (2006) Surfactant catabolism. *Respirology* 11 Suppl: S24-27

Ikegami M, Grant S, Korfhagen T, Scheule RK, Whitsett JA (2009) Surfactant protein-D regulates the postnatal maturation of pulmonary surfactant lipid pool sizes. *J Appl Physiol (1985)* 106: 1545-1552

Ikegami M, Hull WM, Yoshida M, Wert SE, Whitsett JA (2001) SP-D and GM-CSF regulate surfactant homeostasis via distinct mechanisms. *Am J Physiol Lung Cell Mol Physiol* 281: L697-703

Ikegami M, Na CL, Korfhagen TR, Whitsett JA (2005) Surfactant protein D influences surfactant ultrastructure and uptake by alveolar type II cells. *Am J Physiol Lung Cell Mol Physiol* 288: L552-561

Ingenito EP, Mora R, Mark L (2000) Pivotal role of anionic phospholipids in determining dynamic behavior of lung surfactant. *Am J Respir Crit Care Med* 161: 831-838

Itenov TS, Johansen ME, Bestle M, Thormar K, Hein L, Gyldensted L, Lindhardt A, Christensen H, Estrup S, Pedersen HP *et al* (2018) Induced hypothermia in patients with septic shock and respiratory failure (CASS): a randomised, controlled, open-label trial. *Lancet Respir Med* 6: 183-192

Jacobs SE, Berg M, Hunt R, Tarnow-Mordi WO, Inder TE, Davis PG (2013) Cooling for newborns with hypoxic ischaemic encephalopathy. *Cochrane Database Syst Rev* 1: CD003311

Janssen DJ, Carnielli VP, Cogo P, Bohlin K, Hamvas A, Luijendijk IH, Bunt JEH, Tibboel D, Zimmermann LJ (2006) Surfactant phosphatidylcholine metabolism in neonates with meconium aspiration syndrome. *J Pediatr* 149: 634-639

Janssen DJ, Tibboel D, Carnielli VP, van Emmen E, Luijendijk IH, Wattimena JD, Zimmermann LJ (2003) Surfactant phosphatidylcholine pool size in human neonates with congenital diaphragmatic hernia requiring ECMO. *J Pediatr* 142: 247-252

Jeng MJ, Soong WJ, Lee YS, Tsao PC, Yang CF, Chiu SY, Tang RB (2010) Meconium exposure dependent cell death and apoptosis in human alveolar epithelial cells. *Pediatr Pulmonol* 45: 816-823

Johansson J (1998) Structure and properties of surfactant protein C. *Biochim Biophys Acta* 1408: 161-172

Johansson J, Curstedt T (2019) Synthetic surfactants with SP-B and SP-C analogues to enable worldwide treatment of neonatal respiratory distress syndrome and other lung diseases. *J Intern Med* 285: 165-186

Johansson J, Curstedt T, Jörnvall H (1991) Surfactant protein B: disulfide bridges, structural properties, and kringle similarities. *Biochemistry* 30: 6917-6921

Jouhet J (2013) Importance of the hexagonal lipid phase in biological membrane organization. *Front Plant Sci* 4: 494

Kairys V, Gilson MK, Luy B (2004) Structural model for an AxxxG-mediated dimer of surfactant-associated protein C. *Eur J Biochem* 271: 2086-2092

Karnatovskaia LV, Festic E, Freeman WD, Lee AS (2014) Effect of therapeutic hypothermia on gas exchange and respiratory mechanics: a retrospective cohort study. *Ther Hypothermia Temp Manag* 4: 88-95

Karray A, Ali MB, Raida J, Sofiane B (2020) Hydrolysis of three different head groups phospholipids by chicken group V phospholipase A2 using the monomolecular film technique. *Biosci Rep* 40: BSR20192053

Keating E, Rahman L, Francis J, Petersen A, Possmayer F, Veldhuizen R, Petersen NO (2007) Effect of cholesterol on the biophysical and physiological properties of a clinical pulmonary surfactant. *Biophys J* 93: 1391-1401

Kennedy MA, Barrera GC, Nakamura K, Baldán A, Tarr P, Fishbein MC, Frank J, Francone OL, Edwards PA (2005) ABCG1 has a critical role in mediating cholesterol efflux to HDL and preventing cellular lipid accumulation. *Cell Metab* 1: 121-131

Khemani RG, Smith LS, Zimmerman JJ, Erickson S (2015) Pediatric acute respiratory distress syndrome: definition, incidence, and epidemiology: proceedings from the Pediatric Acute Lung Injury Consensus Conference. *Pediatr Crit Care Med* 16: S23-40

Knudsen L, Ochs M (2018) The micromechanics of lung alveoli: structure and function of surfactant and tissue components. *Histochem Cell Biol* 150: 661-676

Kobayashi T, Ohta K, Tashiro K, Nishizuka K, Chen W-M, Ohmura S, Yamamoto K (1999) Dextran restores albumin-inhibited surface activity of pulmonary surfactant extract. *J Appl Physiol (1985)* 86: 1778-1784

Kopincova J, Calkovska A (2016) Meconium-induced inflammation and surfactant inactivation: specifics of molecular mechanisms. *Pediatr Res* 79: 514-521

Korfhagen TR, Sheftelyevich V, Burhans MS, Bruno MD, Ross GF, Wert SE, Stahlman MT, Jobe AH, Ikegami M, Whitsett JA *et al* (1998) Surfactant protein-D regulates surfactant phospholipid homeostasis in vivo. *J Biol Chem* 273: 28438-28443

Kothe TB, Royse E, Kemp MW, Schmidt A, Salomone F, Saito M, Usuda H, Watanabe S, Musk GC, Jobe AH (2018) Effects of budesonide and surfactant in preterm fetal sheep. *Am J Physiol Lung Cell Mol Physiol* 315: L193-L201

Krisans SK (1992) The role of peroxisomes in cholesterol metabolism. *Am J Respir Cell Mol Biol* 7: 358-364

Lachmann B, Robertson B, Vogel J (1980) In vivo lung lavage as an experimental model of the respiratory distress syndrome. *Acta Anaesthesiol Scand* 24: 231-236

Lai SC, Phelps CA, Short AM, Dutta SM, Mu D (2018) Thyroid transcription factor 1 enhances cellular statin sensitivity via perturbing cholesterol metabolism. *Oncogene* 37: 3290-3300

Lambeau G, Gelb MH (2008) Biochemistry and physiology of mammalian secreted phospholipases A2. *Annu Rev Biochem* 77: 495-520

Lang CJ, Postle AD, Orgeig S, Possmayer F, Bernhard W, Panda AK, Jurgens KD, Milsom WK, Nag K, Daniels CB (2005) Dipalmitoylphosphatidylcholine is not the major surfactant phospholipid species in all mammals. *Am J Physiol Regul Integr Comp Physiol* 289: R1426-R1439

Langman C, Orgeig S, Daniels CB (1996) Alterations in composition and function of surfactant associated with torpor in Sminthopsis crassicaudata. *Am J Physiol* 271: R437-445

Lawson WE, Loyd JE (2006) The genetic approach in pulmonary fibrosis: can it provide clues to this complex disease? *Proc Am Thorac Soc* 3: 345-349

Lawson WE, Polosukhin VV, Stathopoulos GT, Zoia O, Han W, Lane KB, Li B, Donnelly EF, Holburn GE, Lewis KG *et al* (2005) Increased and prolonged pulmonary fibrosis in surfactant protein C-deficient mice following intratracheal bleomycin. *Am J Pathol* 167: 1267-1277

Lempert J, Macklem PT (1971) Effect of temperature on rabbit lung surfactant and pressure-volume hysteresis. *J Appl Physiol* 31: 380-385

Liekkinen J, Enkavi G, Javanainen M, Olmeda B, Pérez-Gil J, Vattulainen I (2020) Pulmonary Surfactant Lipid Reorganization Induced by the Adsorption of the Oligomeric Surfactant Protein B Complex. *J Mol Biol* 432: 3251-3268

Lin S, Ikegami M, Moon C, Naren AP, Shannon JM (2015) Lysophosphatidylcholine Acyltransferase 1 (LPCAT1) Specifically Interacts with Phospholipid Transfer Protein StarD10 to Facilitate Surfactant Phospholipid Trafficking in Alveolar Type II Cells. *J Biol Chem* 290: 18559-18574

Lopez-Rodriguez E, Boden C, Echaide M, Perez-Gil J, Kolb M, Gauldie J, Maus UA, Ochs M, Knudsen L (2016a) Surfactant dysfunction during overexpression of TGF-β1 precedes profibrotic lung remodeling in vivo. *Am J Physiol Lung Cell Mol Physiol* 310: L1260-1271

Lopez-Rodriguez E, Echaide M, Cruz A, Taeusch HW, Perez-Gil J (2011) Meconium impairs pulmonary surfactant by a combined action of cholesterol and bile acids. *Biophys J* 100: 646-655

Lopez-Rodriguez E, Gay-Jordi G, Mucci A, Lachmann N, Serrano-Mollar A (2017) Lung surfactant metabolism: early in life, early in disease and target in cell therapy. *Cell Tissue Res* 367: 721-735

López-Rodríguez E, Ospina OL, Echaide M, Taeusch HW, Pérez-Gil J (2012) Exposure to polymers reverses inhibition of pulmonary surfactant by serum, meconium, or cholesterol in the captive bubble surfactometer. *Biophys J* 103: 1451-1459

Lopez-Rodriguez E, Pascual A, Arroyo R, Floros J, Perez-Gil J (2016b) Human Pulmonary Surfactant Protein SP-A1 Provides Maximal Efficiency of Lung Interfacial Films. *Biophys J* 111: 524-536

Lopez-Rodriguez E, Pérez-Gil J (2014) Structure-function relationships in pulmonary surfactant membranes: from biophysics to therapy. *Biochim Biophys Acta* 1838: 1568-1585

Lotze A, Whitsett JA, Kammerman LA, Ritter M, Taylor GA, Short BL (1990) Surfactant protein A concentrations in tracheal aspirate fluid from infants requiring extracorporeal membrane oxygenation. *J Pediatr* 116: 435-440

Low RB (1989) Bronchoalveolar lavage lipids in idiopathic pulmonary fibrosis. *Chest* 95: 3-5

Lowery EM, Brubaker AL, Kuhlmann E, Kovacs EJ (2013) The aging lung. *Clin Interv Aging* 8: 1489-1496

Lowry OH, Rosebrough NJ, Farr AL, Randall RJ (1951) Protein measurement with the Folin phenol reagent. *J Biol Chem* 193: 265-275

Lu KW, Goerke J, Clements JA, Taeusch HW (2005a) Hyaluronan decreases surfactant inactivation in vitro. *Pediatr Res* 57: 237-241

Lu KW, Goerke J, Clements JA, Taeusch HW (2005b) Hyaluronan reduces surfactant inhibition and improves rat lung function after meconium injury. *Pediatr Res* 58: 206-210

Lu KW, Robertson B, Taeusch HW (2005c) Dextran or polyethylene glycol added to Curosurf for treatment of meconium lung injury in rats. *Neonatology* 88: 46-53

Lu KW, Taeusch HW, Robertson B, Goerke J, Clements JA (2001a) Polyethylene glycol/surfactant mixtures improve lung function after HCl and endotoxin lung injuries. *Am J Respir Crit Care Med* 164: 1531-1536

Lu Z, Gu Y, Rooney SA (2001b) Transcriptional regulation of the lung fatty acid synthase gene by glucocorticoid, thyroid hormone and transforming growth factor-beta 1. *Biochim Biophys Acta* 1532: 213-222

Lugones Y, Blanco O, López-Rodríguez E, Echaide M, Cruz A, Pérez-Gil J (2018) Inhibition and counterinhibition of Surfacen, a clinical lung surfactant of natural origin. *PLoS One* 13: e0204050

Lyra JC, Mascaretti RS, Precioso AR, Haddad LB, Mauad T, Costa Vaz FA, Rebello CM (2009) Polyethylene glycol addition does not improve exogenous surfactant function in an experimental model of meconium aspiration syndrome. *Exp Lung Res* 35: 76-88

Mabrey S, Sturtevant JM (1976) Investigation of phase transitions of lipids and lipid mixtures by sensitivity differential scanning calorimetry. *Proc Natl Acad Sci U S A* 73: 3862-3866

Madsen J, Panchal MH, Mackay RA, Echaide M, Koster G, Aquino G, Pelizzi N, Perez-Gil J, Salomone F, Clark HW *et al* (2018) Metabolism of a synthetic compared with a natural therapeutic pulmonary surfactant in adult mice. *J Lipid Res* 59: 1880-1892

Mahavadi P, Korfei M, Henneke I, Liebisch G, Schmitz G, Gochuico BR, Markart P, Bellusci S, Seeger W, Ruppert C *et al* (2010) Epithelial stress and apoptosis underlie Hermansky-Pudlak syndrome-associated interstitial pneumonia. *Am J Respir Crit Care Med* 182: 207-219

Malcharek S, Hinz A, Hilterhaus L, Galla H-J (2005) Multilayer structures in lipid monolayer films containing surfactant protein C: effects of cholesterol and POPE. *Biophys J* 88: 2638-2649

Marchioni A, Tonelli R, Ball L, Fantini R, Castaniere I, Cerri S, Luppi F, Malerba M, Pelosi P, Clini E (2018) Acute exacerbation of idiopathic pulmonary fibrosis: lessons learned from acute respiratory distress syndrome? *Crit Care* 22: 80

Markart P, Ruppert C, Wygrecka M, Colaris T, Dahal B, Walmrath D, Harbach H, Wilhelm J, Seeger W, Schmidt R *et al* (2007) Patients with ARDS show improvement but not normalisation of alveolar surface activity with surfactant treatment: putative role of neutral lipids. *Thorax* 62: 588-594

Mart MF, Ware LB (2020) The long-lasting effects of the acute respiratory distress syndrome. *Expert Rev Respir Med* 14: 577-586

Martínez-Calle M, Alonso A, Pérez-Gil J, Olmeda B (2019) Native supramolecular protein complexes in pulmonary surfactant: Evidences for SP-A/SP-B interactions. *Nat Rev Dis Primers* 207: 103466

Martínez-Calle M, Olmeda B, Dietl P, Frick M, Pérez-Gil J (2018) Pulmonary surfactant protein SP-B promotes exocytosis of lamellar bodies in alveolar type II cells. *Faseb j* 32: 4600-4611

Martinez-Calle M, Prieto M, Olmeda B, Fedorov A, Loura LMS, Pérez-Gil J (2020) Pulmonary surfactant protein SP-B nanorings induce the multilamellar organization of surfactant complexes. *Biochim Biophys Acta Biomembr* 1862: 183216

Mason R, Broaddus VC, Martin T, King T, Schraufnagel D, Murray J, Nadel J (2010) Murray and Nadel's Textbook of Respiratory Medicine 5th Edition. *Saunders*

Mason RJ, Voelker DR (1998) Regulatory mechanisms of surfactant secretion. *Biochim Biophys Acta* 1408: 226-240

Matthay MA, Zemans RL, Zimmerman GA, Arabi YM, Beitler JR, Mercat A, Herridge M, Randolph AG, Calfee CS (2019) Acute respiratory distress syndrome. *Nature Reviews Disease Primers* 5: 1-22

McCormack F, King Jr T, Bucher BL, Nielsen L, Mason RJ, McCormac F (1995) Surfactant protein A predicts survival in idiopathic pulmonary fibrosis. *Am J Respir Crit Care Med* 152: 751-759

McDevitt TM, Gonzales LW, Savani RC, Ballard PL (2007) Role of endogenous TGF-beta in glucocorticoid-induced lung type II cell differentiation. *Am J Physiol Lung Cell Mol Physiol* 292: L249-257

McGinnis K, Brown J, Morrison J (2008) Changing patterns of fetal lung maturity testing. *J Perinatol* 28: 20-23

Meng SS, Chang W, Lu ZH, Xie JF, Qiu HB, Yang Y, Guo FM (2019) Effect of surfactant administration on outcomes of adult patients in acute respiratory distress syndrome: a meta-analysis of randomized controlled trials. *BMC Pulm Med* 19: 9

Merchak A, Janssen DJ, Bohlin K, Patterson BW, Zimmermann LJ, Carnielli VP, Hamvas A (2002) Endogenous pulmonary surfactant metabolism is not affected by mode of ventilation in premature infants with respiratory distress syndrome. *J Pediatr* 140: 693-698

Mikolka P, Kopincova J, Tomcikova Mikusiakova L, Kosutova P, Antosova M, Calkovska A, Mokra D (2016) Effects of surfactant/budesonide therapy on oxidative modifications in the lung in experimental meconium-induced lung injury. *J Physiol Pharmacol* 67: 57-65

Miles PR, Bowman L, Rao KM, Baatz JE, Huffman L (1999) Pulmonary surfactant inhibits LPS-induced nitric oxide production by alveolar macrophages. *Am J Physiol* 276: L186-196

Miyoshi T, Kato S (2015) Detailed Analysis of the Surface Area and Elasticity in the Saturated 1,2-Diacylphosphatidylcholine/Cholesterol Binary Monolayer System. *Langmuir* 31: 9086-9096

Moses D, Holm BA, Spitale P, Liu MY, Enhorning G (1991) Inhibition of pulmonary surfactant function by meconium. *Am J Obstet Gynecol* 164: 477-481

Moya FR, Gadzinowski J, Bancalari E, Salinas V, Kopelman B, Bancalari A, Kornacka MK, Merritt TA, Segal R, Schaber CJ *et al* (2005) A multicenter, randomized, masked, comparison trial of lucinactant, colfosceril palmitate, and beractant for the prevention of respiratory distress syndrome among very preterm infants. *Pediatrics* 115: 1018-1029

Mugford M (2006) Cost effectiveness of prevention and treatment of neonatal respiratory distress (RDS) with exogenous surfactant: What has changed in the last three decades? *Early Hum Dev* 82: 105-115

Murakami M, Kambe T, Shimbara S, Higashino K, Hanasaki K, Arita H, Horiguchi M, Arita M, Arai H, Inoue K *et al* (1999) Different functional aspects of the group II subfamily (Types IIA and V) and type X secretory phospholipase A(2)s in regulating arachidonic acid release and prostaglandin generation. Implications of cyclooxygenase-2 induction and phospholipid scramblase-mediated cellular membrane perturbation. *J Biol Chem* 274: 31435-31444

Murakami M, Koduri RS, Enomoto A, Shimbara S, Seki M, Yoshihara K, Singer A, Valentin E, Ghomashchi F, Lambeau G *et al* (2001) Distinct arachidonate-releasing functions of mammalian secreted phospholipase A2s in human embryonic kidney 293 and rat mastocytoma RBL-2H3 cells through heparan sulfate shuttling and external plasma membrane mechanisms. *J Biol Chem* 276: 10083-10096

Murakami M, Masuda S, Shimbara S, Bezzine S, Lazdunski M, Lambeau G, Gelb MH, Matsukura S, Kokubu F, Adachi M *et al* (2003) Cellular arachidonate-releasing function of novel classes of secretory phospholipase A2s (groups III and XII). *J Biol Chem* 278: 10657-10667

Murakami M, Shimbara S, Kambe T, Kuwata H, Winstead MV, Tischfield JA, Kudo I (1998) The functions of five distinct mammalian phospholipase A2S in regulating arachidonic acid release. Type IIa and type V secretory phospholipase A2S are functionally redundant and act in concert with cytosolic phospholipase A2. *J Biol Chem* 273: 14411-14423

Murakami M, Taketomi Y, Sato H, Yamamoto K (2011) Secreted phospholipase A2 revisited. *J Biochem* 150: 233-255

Muramatsu N, Kondo T (1992) Adsorption of bovine serum albumin on positively and negatively charged microcapsules. *J Colloid Interface Sci* 153: 23-29

Nag K, Taneva SG, Perez-Gil J, Cruz A, Keough K (1997) Combinations of fluorescently labeled pulmonary surfactant proteins SP-B and SP-C in phospholipid films. *Biophys J* 72: 2638-2650

Nakanishi H, Shindou H, Hishikawa D, Harayama T, Ogasawara R, Suwabe A, Taguchi R, Shimizu T (2006) Cloning and characterization of mouse lung-type acyl-CoA:lysophosphatidylcholine acyltransferase 1 (LPCAT1). Expression in alveolar type II cells and possible involvement in surfactant production. *J Biol Chem* 281: 20140-20147

Nakos G, Kitsiouli E, Hatzidaki E, Koulouras V, Touqui L, Lekka ME (2005) Phospholipases A2 and platelet-activating-factor acetylhydrolase in patients with acute respiratory distress syndrome. *Crit Care Med* 33: 772-779

Natarajan CK, Sankar MJ, Jain K, Agarwal R, Paul VK (2016) Surfactant therapy and antibiotics in neonates with meconium aspiration syndrome: a systematic review and meta-analysis. *J Perinatol* 36 Suppl 1: S49-54

Neerhof MG, Haney EI, Silver RK, Ashwood ER, Lee I-S, Piazze JJ (2001) Lamellar body counts compared with traditional phospholipid analysis as an assay for evaluating fetal lung maturity. *Obstet Gynecol* 97: 305-309

Neidleman SL (1987) Effects of temperature on lipid unsaturation. *Biotechnol Genet Eng Rev* 5: 245-268

Nespeca M, Giorgetti C, Nobile S, Ferrini I, Simonato M, Verlato G, Cogo P, Carnielli VP (2016) Does Whole-Body Hypothermia in Neonates with Hypoxic–Ischemic Encephalopathy Affect Surfactant Disaturated-Phosphatidylcholine Kinetics? *PloS one* 11: e0153328

Nishiyama O, Kume H, Kondo M, Ito Y, Ito M, Yamaki K (2004) Role of lysophosphatidylcholine in eosinophil infiltration and resistance in airways. *Clin Exp Pharmacol Physiol* 31: 179-184

Nkadi PO, Merritt TA, Pillers DA (2009) An overview of pulmonary surfactant in the neonate: genetics, metabolism, and the role of surfactant in health and disease. *Mol Genet Metab* 97: 95-101

Nogee LM, Garnier G, Dietz HC, Singer L, Murphy AM, deMello DE, Colten HR (1994) A mutation in the surfactant protein B gene responsible for fatal neonatal respiratory disease in multiple kindreds. *J Clin Invest* 93: 1860-1863

Ochs M, Hegermann J, Lopez-Rodriguez E, Timm S, Nouailles G, Matuszak J, Simmons S, Witzenrath M, Kuebler WM (2020) On Top of the Alveolar Epithelium: Surfactant and the Glycocalyx. *Int J Mol Sci* 21

Ochs M, Johnen G, Müller KM, Wahlers T, Hawgood S, Richter J, Brasch F (2002) Intracellular and intraalveolar localization of surfactant protein A (SP-A) in the parenchymal region of the human lung. *Am J Respir Cell Mol Biol* 26: 91-98

Ochs M, Schüttler M, Stichtenoth G, Herting E (2006) Morphological alterations of exogenous surfactant inhibited by meconium can be prevented by dextran. *Respir Res* 7: 86

Oh MH, Bae CW (2000) Inhibitory effect of meconium on pulmonary surfactant function tested in vitro using the stable microbubble test. *Eur J Pediatr* 159: 770-774

Olmeda B, García-Álvarez B, Gómez MJ, Martínez-Calle M, Cruz A, Pérez-Gil J (2015) A model for the structure and mechanism of action of pulmonary surfactant protein B. *Faseb j* 29: 4236-4247

Olmeda B, García-Álvarez B, Pérez-Gil J (2013) Structure-function correlations of pulmonary surfactant protein SP-B and the saposin-like family of proteins. *Eur Biophys J* 42: 209-222

Olmeda B, Martínez-Calle M, Pérez-Gil J (2017) Pulmonary surfactant metabolism in the alveolar airspace: Biogenesis, extracellular conversions, recycling. *Ann Anat* 209: 78-92

Olmeda B, Villén L, Cruz A, Orellana G, Perez-Gil J (2010) Pulmonary surfactant layers accelerate O(2) diffusion through the air-water interface. *Biochim Biophys Acta* 1798: 1281-1284

Oosterlaken-Dijksterhuis MA, van Eijk M, van Buel BL, van Golde LM, Haagsman HP (1991) Surfactant protein composition of lamellar bodies isolated from rat lung. *Biochem J* 274 (Pt 1): 115-119

Orgeig S, Daniels CB, Johnston SD, Sullivan LC (2003) The pattern of surfactant cholesterol during vertebrate evolution and development: does ontogeny recapitulate phylogeny? *Reprod Fertil Dev* 15: 55-73

Orgeig S, Hiemstra PS, Veldhuizen EJ, Casals C, Clark HW, Haczku A, Knudsen L, Possmayer F (2010) Recent advances in alveolar biology: evolution and function of alveolar proteins. *Respir Physiol Neurobiol* 173 Suppl: S43-54

Orgeig S, Morrison JL, Daniels CB (2014) Effect of Environment and Aging on the Pulmonary Surfactant System. In: *The Lung*, Elsevier (ed.) pp. 447-469.

Osanai K, Mason RJ, Voelker DR (1998) Trafficking of newly synthesized surfactant protein A in isolated rat alveolar type II cells. *Am J Respir Cell Mol Biol* 19: 929-935

Papazian L, Aubron C, Brochard L, Chiche JD, Combes A, Dreyfuss D, Forel JM, Guérin C, Jaber S, Mekontso-Dessap A *et al* (2019) Formal guidelines: management of acute respiratory distress syndrome. *Ann Intensive Care* 9: 69

Parra E, Alcaraz A, Cruz A, Aguilella VM, Pérez-Gil J (2013) Hydrophobic pulmonary surfactant proteins SP-B and SP-C induce pore formation in planar lipid membranes: evidence for proteolipid pores. *Biophys J* 104: 146-155

Parra E, Moleiro LH, López-Montero I, Cruz A, Monroy F, Pérez-Gil J (2011) A combined action of pulmonary surfactant proteins SP-B and SP-C modulates permeability and dynamics of phospholipid membranes. *Biochem J* 438: 555-564

Parra E, Pérez-Gil J (2015) Composition, structure and mechanical properties define performance of pulmonary surfactant membranes and films. *Chem Phys Lipids* 185: 153-175

Parry G, Tucker J, Tarnow-Mordi W (2003) CRIB II: an update of the clinical risk index for babies score. *Lancet* 361: 1789-1791

Pastrana-Rios B, Flach CR, Brauner JW, Mautone AJ, Mendelsohn R (1994) A Direct Test of the" Squeeze-Out" Hypothesis of Lung Surfactant Function. External Reflection FT-IR at the Air/Wave Interface. *Biochemistry* 33: 5121-5127

Pattle R, Kratzing C, Parkinson C, Graves L, Robertson R, Robards G, Currie J, Parsons J, Sutherland P (1979) Maturity of fetal lungs tested by production of stable microbubbles in amniotic fluid. *Br J Obstet Gynaecol* 86: 615-622

Pérez-Chacón G, Astudillo AM, Balgoma D, Balboa MA, Balsinde J (2009) Control of free arachidonic acid levels by phospholipases A2 and lysophospholipid acyltransferases. *Biochim Biophys Acta* 1791: 1103-1113

Pérez-Gil J (2008) Structure of pulmonary surfactant membranes and films: the role of proteins and lipid-protein interactions. *Biochim Biophys Acta* 1778: 1676-1695

Perez-Gil J, Cruz A, Casals C (1993) Solubility of hydrophobic surfactant proteins in organic solvent/water mixtures. Structural studies on SP-B and SP-C in aqueous organic solvents and lipids. *Biochim Biophys Acta* 1168: 261-270

Perez-Gil J, Weaver TE (2010) Pulmonary surfactant pathophysiology: current models and open questions. *Physiology (Bethesda)* 25: 132-141

Petrou S, Yiu HH, Kwon J (2019) Economic consequences of preterm birth: a systematic review of the recent literature (2009–2017). *Arch Dis Child* 104: 456-465

Pettenazzo A, Jobe A, Humme J, Seidner S, Ikegami M (1988) Clearance of surfactant phosphatidylcholine via the upper airways in rabbits. *J Appl Physiol (1985)* 65: 2151-2155

Phibbs RH, Tooley WH, Ballard RA, Sniderman SH, Clements JA, Schlueter MA, Wakeley A, Heilbron DC, Phibbs CS (1991) Initial clinical trial of EXOSURF, a protein-free synthetic surfactant, for the prophylaxis and early treatment of hyaline membrane disease. *Pediatrics* 88: 1-9

Piastra M, Yousef N, Brat R, Manzoni P, Mokhtari M, De Luca D (2014) Lung ultrasound findings in meconium aspiration syndrome. *Early Hum Dev* 90 Suppl 2: S41-43

Pietrini D, Piastra M, Luca E, Mancino A, Conti G, Cavaliere F, De Luca D (2012) Neuroprotection and hypothermia in infants and children. *Curr Drug Targets* 13: 925-935

Piñeiro-Hermida S, Autilio C, Martínez P, Bosch F, Pérez-Gil J, Blasco MA (2020) Telomerase treatment prevents lung profibrotic pathologies associated with physiological aging. *J Cell Biol* 219: e202002120

Poelma DL, Walther FJ, Waring AJ, Haitsma JJ, Zimmermann LJ, Lachmann B, van Iwaarden JF (2007) Effect of SP-B peptides on the uptake of liposomes by alveolar cells. *Neonatology* 91: 233-240

Poelma DL, Zimmermann LJ, van Cappellen WA, Haitsma JJ, Lachmann B, van Iwaarden JF (2004) Distinct effects of SP-B and SP-C on the uptake of surfactant-like liposomes by alveolar cells in vivo and in vitro. *Am J Physiol Lung Cell Mol Physiol* 287: L1056-1065

Pol A, Gross SP, Parton RG (2014) Review: biogenesis of the multifunctional lipid droplet: lipids, proteins, and sites. *J Cell Biol* 204: 635-646

Portelli M, Sayers I (2012) Genetic basis for personalized medicine in asthma. *Expert Rev Respir Med* 6: 223-236

Possmayer F, Nag K, Rodriguez K, Qanbar R, Schürch S (2001) Surface activity in vitro: role of surfactant proteins. *Comp Biochem Physiol A Mol Integr Physiol* 129: 209-220

Postle AD, Henderson NG, Koster G, Clark HW, Hunt AN (2011) Analysis of lung surfactant phosphatidylcholine metabolism in transgenic mice using stable isotopes. *Chem Phys Lipids* 164: 549-555

Povedano JM, Martinez P, Flores JM, Mulero F, Blasco MA (2015) Mice with Pulmonary Fibrosis Driven by Telomere Dysfunction. *Cell Rep* 12: 286-299

Povedano JM, Martinez P, Serrano R, Tejera Á, Gómez-López G, Bobadilla M, Flores JM, Bosch F, Blasco MA (2018) Therapeutic effects of telomerase in mice with pulmonary fibrosis induced by damage to the lungs and short telomeres. *Elife* 7: e31299

Pramod K, Kotta S, Jijith US, Aravind A, Abu Tahir M, Manju CS, Gangadharappa HV (2020) Surfactant-based prophylaxis and therapy against COVID-19: A possibility. *Med Hypotheses* 143: 110081

Raghavendran K, Willson D, Notter RH (2011) Surfactant therapy for acute lung injury and acute respiratory distress syndrome. *Crit Care Clin* 27: 525-559

Raimundo K, Chang E, Broder MS, Alexander K, Zazzali J, Swigris JJ (2016) Clinical and economic burden of idiopathic pulmonary fibrosis: a retrospective cohort study. *BMC Pulm Med* 16: 2

Ramanathan R, Bhatia JJ, Sekar K, Ernst F (2013) Mortality in preterm infants with respiratory distress syndrome treated with poractant alfa, calfactant or beractant: a retrospective study. *J Perinatol* 33: 119-125

Ramanathan R, Biniwale M, Sekar K, Hanna N, Golombek S, Bhatia J, Naylor M, Fabbri L, Varoli G, Santoro D *et al* (2020) Synthetic Surfactant CHF5633 Compared with Poractant Alfa in the Treatment of Neonatal Respiratory Distress Syndrome: A Multicenter, Double-Blind, Randomized, Controlled Clinical Trial. *J Pediatr* 225: 90-96.e91

Ramsingh R, Grygorczyk A, Solecki A, Cherkaoui LS, Berthiaume Y, Grygorczyk R (2011) Cell deformation at the air-liquid interface induces Ca2+-dependent ATP release from lung epithelial cells. *Am J Physiol Lung Cell Mol Physiol* 300: L587-595

Ranieri VM, Rubenfeld GD, Thompson BT, Ferguson ND, Caldwell E, Fan E, Camporota L, Slutsky AS (2012) Acute respiratory distress syndrome: the Berlin Definition. *Jama* 307: 2526-2533

Ravasio A, Cruz A, Pérez-Gil J, Haller T (2008) High-throughput evaluation of pulmonary surfactant adsorption and surface film formation. *J Lipid Res* 49: 2479-2488

Rebello CM, Jobe AH, Eisele JW, Ikegami M (1996) Alveolar and tissue surfactant pool sizes in humans. *Am J Respir Crit Care Med* 154: 625-628

Reitsma S, Slaaf DW, Vink H, van Zandvoort MA, oude Egbrink MG (2007) The endothelial glycocalyx: composition, functions, and visualization. *Pflugers Arch* 454: 345-359

Restrepo RD, Hirst KR, Wittnebel L, Wettstein R (2012) AARC Clinical Practice Guideline: Transcutaneous Monitoring of Carbon Dioxide and Oxygen: 2012. *Respiratory Care* 57: 1955-1962

Rezoagli E, Fumagalli R, Bellani G (2017) Definition and epidemiology of acute respiratory distress syndrome. *Ann Transl Med* 5: 282

Ricci F, Murgia X, Razzetti R, Pelizzi N, Salomone F (2017) In vitro and in vivo comparison between poractant alfa and the new generation synthetic surfactant CHF5633. *Pediatr Res* 81: 369-375

Richardson DK, Corcoran JD, Escobar GJ, Lee SK (2001) SNAP-II and SNAPPE-II: Simplified newborn illness severity and mortality risk scores. *J Pediatr* 138: 92-100

Richeldi L, Collard HR, Jones MG (2017) Idiopathic pulmonary fibrosis. *Lancet* 389: 1941-1952

Rider ED, Ikegami M, Jobe AH (1992) Localization of alveolar surfactant clearance in rabbit lung cells. *Am J Physiol* 263: L201-209

Ridsdale R, Post M (2004) Surfactant lipid synthesis and lamellar body formation in glycogen-laden type II cells. *Am J Physiol Lung Cell Mol Physiol* 287: L743-751

Riviello ED, Kiviri W, Twagirumugabe T, Mueller A, Banner-Goodspeed VM, Officer L, Novack V, Mutumwinka M, Talmor DS, Fowler RA (2016) Hospital Incidence and Outcomes of the Acute Respiratory Distress Syndrome Using the Kigali Modification of the Berlin Definition. *Am J Respir Crit Care Med* 193: 52-59

Robinson PC, Watters LC, King TE, Mason RJ (1988) Idopathic pulmonary fibrosis. *Am Rev Respir Dis* 137: 585-591

Rodríguez-Capote K, Manzanares D, Haines T, Possmayer F (2006) Reactive oxygen species inactivation of surfactant involves structural and functional alterations to surfactant proteins SP-B and SP-C. *Biophys J* 90: 2808-2821

Roldan N, Nyholm TKM, Slotte JP, Pérez-Gil J, García-Álvarez B (2016) Effect of Lung Surfactant Protein SP-C and SP-C-Promoted Membrane Fragmentation on Cholesterol Dynamics. *Biophys J* 111: 1703-1713

Ross M, Krol S, Janshoff A, Galla HJ (2002) Kinetics of phospholipid insertion into monolayers containing the lung surfactant proteins SP-B or SP-C. *Eur Biophys J* 31: 52-61

Roszell BR, Tao JQ, Yu KJ, Huang S, Bates SR (2012) Characterization of the Niemann-Pick C pathway in alveolar type II cells and lamellar bodies of the lung. *Am J Physiol Lung Cell Mol Physiol* 302: L919-932

Rouser G, Siakotos AN, Fleischer S (1966) Quantitative analysis of phospholipids by thin-layer chromatography and phosphorus analysis of spots. *Lipids* 1: 85-86

Roux JF, Nakamura J, Brown E, Sweet AY (1972) The lecithin-sphingomyelin ratio of amniotic fluid: an index of fetal lung maturity? *Pediatrics* 49: 464-466

Ruano ML, Miguel E, Perez-Gil J, Casals C (1996) Comparison of lipid aggregation and self-aggregation activities of pulmonary surfactant-associated protein A. *Biochem J* 313 (Pt 2): 683-689

Rubenfeld GD, Caldwell E, Peabody E, Weaver J, Martin DP, Neff M, Stern EJ, Hudson LD (2005) Incidence and outcomes of acute lung injury. *N Engl J Med* 353: 1685-1693

Rugonyi S, Biswas SC, Hall SB (2008) The biophysical function of pulmonary surfactant. *Respir Physiol Neurobiol* 163: 244-255

Rumbus Z, Matics R, Hegyi P, Zsiboras C, Szabo I, Illes A, Petervari E, Balasko M, Marta K, Miko A *et al* (2017) Fever Is Associated with Reduced, Hypothermia with Increased Mortality in Septic Patients: A Meta-Analysis of Clinical Trials. *PLoS One* 12: e0170152

Ruwisch J, Sehlmeyer K, Roldan N, Garcia-Alvarez B, Perez-Gil J, Weaver TE, Ochs M, Knudsen L, Lopez-Rodriguez E (2020) Air Space Distension Precedes Spontaneous Fibrotic Remodeling and Impaired Cholesterol Metabolism in the Absence of Surfactant Protein C. *Am J Respir Cell Mol Biol* 62: 466-478

Saad SM, Policova Z, Dang A, Acosta EJ, Hair ML, Neumann AW (2009) A double injection ADSA-CSD methodology for lung surfactant inhibition and reversal studies. *Colloids Surf B Biointerfaces* 73: 365-375

Saegusa J, Akakura N, Wu C-Y, Hoogland C, Ma Z, Lam KS, Liu F-T, Takada YK, Takada Y (2008) Pro-inflammatory secretory phospholipase A2 type IIA binds to integrins αvβ3 and α4β1 and induces proliferation of monocytic cells in an integrin-dependent manner. *J Biol Chem* 283: 26107-26115

Sáenz A, López-Sánchez A, Mojica-Lázaro J, Martínez-Caro L, Nin N, Bagatolli LA, Casals C (2010) Fluidizing effects of C-reactive protein on lung surfactant membranes: protective role of surfactant protein A. *FASEB J* 24: 3662-3673

Sakata A, Ida E, Tominaga M, Onoue K (1987) Arachidonic acid acts as an intracellular activator of NADPH-oxidase in Fc gamma receptor-mediated superoxide generation in macrophages. *J Immunol* 138: 4353-4359

Salvaterra E, Campo I (2020) Pulmonary alveolar proteinosis: from classification to therapy. *Breathe (Sheff)* 16: 200018

Salvesen B, Curstedt T, Mollnes TE, Saugstad OD (2014) Effects of natural versus synthetic surfactant with SP-B and SP-C analogs in a porcine model of meconium aspiration syndrome. *Neonatology* 105: 128-135

Sánchez Luna M, Bacher P, Unnebrink K, Martinez-Tristani M, Ramos Navarro C (2020) Beractant and poractant alfa in premature neonates with respiratory distress syndrome: a systematic review of real-world evidence studies and randomized controlled trials. *J Perinatol* 40: 1121-1134

Sánchez-Barbero F, Rivas G, Steinhilber W, Casals C (2007) Structural and functional differences among human surfactant proteins SP-A1, SP-A2 and co-expressed SP-A1/SP-A2: role of supratrimeric oligomerization. *Biochem J* 406: 479-489

Sankaram MB, Thompson TE (1991) Cholesterol-induced fluid-phase immiscibility in membranes. *Proc Natl Acad Sci U S A* 88: 8686-8690

Sano H, Kuroki Y, Honma T, Ogasawara Y, Sohma H, Voelker DR, Akino T (1998) Analysis of chimeric proteins identifies the regions in the carbohydrate recognition domains of rat lung collectins that are

essential for interactions with phospholipids, glycolipids, and alveolar type II cells. *J Biol Chem* 273: 4783-4789

Sarker M, Waring AJ, Walther FJ, Keough KM, Booth V (2007) Structure of mini-B, a functional fragment of surfactant protein B, in detergent micelles. *Biochemistry* 46: 11047-11056

Sato A, Ikegami M (2012) SP-B and SP-C containing new synthetic surfactant for treatment of extremely immature lamb lung. *PLoS One* 7: e39392

Schmidt R, Luboeinski T, Markart P, Ruppert C, Daum C, Grimminger F, Seeger W, Günther A (2004) Alveolar antioxidant status in patients with acute respiratory distress syndrome. *Eur Respir J* 24: 994-999

Schmidt R, Markart P, Ruppert C, Wygrecka M, Kuchenbuch T, Walmrath D, Seeger W, Guenther A (2007) Time-dependent changes in pulmonary surfactant function and composition in acute respiratory distress syndrome due to pneumonia or aspiration. *Respir Res* 8: 55

Schmidt R, Meier U, Yabut-Perez M, Walmrath D, Grimminger F, Seeger W, Gunther A (2001) Alteration of fatty acid profiles in different pulmonary surfactant phospholipids in acute respiratory distress syndrome and severe pneumonia. *Am J Respir Crit Care Med* 163: 95-100

Schmiedl A, Ochs M, Mühlfeld C, Johnen G, Brasch F (2005) Distribution of surfactant proteins in type II pneumocytes of newborn, 14-day old, and adult rats: an immunoelectron microscopic and stereological study. *Histochem Cell Biol* 124: 465-476

Schmölzer GM, Kumar M, Pichler G, Aziz K, O'Reilly M, Cheung PY (2013) Non-invasive versus invasive respiratory support in preterm infants at birth: systematic review and meta-analysis. *BMJ* 347: f5980

Schoel WM, Schurch S, Goerke J (1994) The captive bubble method for the evaluation of pulmonary surfactant: surface tension, area, and volume calculations. *Biochim Biophys Acta* 1200: 281-290

Schousboe P, Wiese L, Heiring C, Verder H, Poorisrisak P, Verder P, Nielsen HB (2020) Assessment of pulmonary surfactant in COVID-19 patients. *Crit Care* 24: 552

Schupp JC, Binder H, Jäger B, Cillis G, Zissel G, Müller-Quernheim J, Prasse A (2015) Macrophage activation in acute exacerbation of idiopathic pulmonary fibrosis. *PloS one* 10: e0116775

Schürch D, Ospina OL, Cruz A, Pérez-Gil J (2010) Combined and independent action of proteins SP-B and SP-C in the surface behavior and mechanical stability of pulmonary surfactant films. *Biophys J* 99: 3290-3299

Schürch S, Bachofen H, Possmayer F (2001) Surface activity in situ, in vivo, and in the captive bubble surfactometer. *Comp Biochem Physiol A Mol Integr Physiol* 129: 195-207

Schürch S, Goerke J, Clements JA (1978) Direct determination of volume- and time-dependence of alveolar surface tension in excised lungs. *Proc Natl Acad Sci U S A* 75: 3417-3421

Seeds MC, Grier BL, Suckling BN, Safta AM, Long DL, Waite BM, Morris PE, Hite RD (2012) Secretory phospholipase A2-mediated depletion of phosphatidylglycerol in early acute respiratory distress syndrome. *Am J Med Sci* 343: 446-451

Seehase M, Collins JJ, Kuypers E, Jellema RK, Ophelders DR, Ospina OL, Perez-Gil J, Bianco F, Garzia R, Razzetti R *et al* (2012) New surfactant with SP-B and C analogs gives survival benefit after inactivation in preterm lambs. *PLoS One* 7: e47631

Sehlmeyer K, Ruwisch J, Roldan N, Lopez-Rodriguez E (2020) Alveolar Dynamics and Beyond - The Importance of Surfactant Protein C and Cholesterol in Lung Homeostasis and Fibrosis. *Front Physiol* 11: 386

Selman M, Pardo A (2014) Revealing the pathogenic and aging-related mechanisms of the enigmatic idiopathic pulmonary fibrosis. an integral model. *Am J Respir Crit Care Med* 189: 1161-1172

Shiffer K, Hawgood S, Haagsman HP, Benson B, Clements JA, Goerke J (1993) Lung surfactant proteins, SP-B and SP-C, alter the thermodynamic properties of phospholipid membranes: a differential calorimetry study. *Biochemistry* 32: 590-597

Silva PL, Pelosi P, Rocco PRM (2020) Personalized pharmacological therapy for ARDS: a light at the end of the tunnel. *Expert Opin Investig Drugs* 29: 49-61

Silveyra P, Floros J (2012) Genetic variant associations of human SP-A and SP-D with acute and chronic lung injury. *Front Biosci (Landmark Ed)* 17: 407-429

Simonato M, Baritussio A, Ori C, Vedovelli L, Rossi S, Dalla Massara L, Rizzi S, Carnielli VP, Cogo PE (2011) Disaturated-phosphatidylcholine and surfactant protein-B turnover in human acute lung injury and in control patients. *Respir Res* 12: 36

Singh B, Clark R, Powers R, Spitzer A (2009) Meconium aspiration syndrome remains a significant problem in the NICU: outcomes and treatment patterns in term neonates admitted for intensive care during a ten-year period. *J Perinatol* 29: 497-503

Singh N, Halliday HL, Stevens TP, Suresh G, Soll R, Rojas-Reyes MX (2015) Comparison of animal-derived surfactants for the prevention and treatment of respiratory distress syndrome in preterm infants. *Cochrane Database Syst Rev*: CD010249

Sinha P, Calfee CS (2019) Phenotypes in acute respiratory distress syndrome: moving towards precision medicine. *Curr Opin Crit Care* 25: 12-20

Sinha SK, Lacaze-Masmonteil T, i Soler AV, Wiswell TE, Gadzinowski J, Hajdu J, Bernstein G, Sanchez-Luna M, Segal R, Schaber CJ (2005) A multicenter, randomized, controlled trial of lucinactant versus poractant alfa among very premature infants at high risk for respiratory distress syndrome. *Pediatrics* 115: 1030-1038

Sippola T, Aho H, Peuravuori H, Lukkarinen H, Gunn J, Kääpä P (2006) Pancreatic Phospholipase A 2 Contributes to Lung Injury in Experimental Meconium Aspiration. *Pediatr Res* 59: 641-645

Slack DF, Corwin DS, Shah NG, Shanholtz CB, Verceles AC, Netzer G, Jones KM, Brown CH, Terrin ML, Hasday JD (2017) Pilot feasibility study of therapeutic hypothermia for moderate to severe acute respiratory distress syndrome. *Crit Care Med* 45: 1152-1159

Soriano JB, Kendrick PJ, Paulson KR, Gupta V, Abrams EM, Adedoyin RA, Adhikari TB, Advani SM, Agrawal A, Ahmadian E (2020) Prevalence and attributable health burden of chronic respiratory diseases, 1990–2017: a systematic analysis for the Global Burden of Disease Study 2017. *Lancet Respir Med* 8: 585-596

Spadaro S, Park M, Turrini C, Tunstall T, Thwaites R, Mauri T, Ragazzi R, Ruggeri P, Hansel TT, Caramori G *et al* (2019) Biomarkers for Acute Respiratory Distress syndrome and prospects for personalised medicine. *J Inflamm (Lond)* 16: 1

Spragg RG, Lewis JF, Walmrath H-D, Johannigman J, Bellingan G, Laterre P-F, Witte MC, Richards GA, Rippin G, Rathgeb F (2004) Effect of recombinant surfactant protein C–based surfactant on the acute respiratory distress syndrome. *N Engl J Med* 351: 884-892

Sprung CL, Rackow EC, Fein IA, Jacob AI, Isikoff SK (1981) The spectrum of pulmonary edema: differentiation of cardiogenic, intermediate, and noncardiogenic forms of pulmonary edema. *Am Rev Respir Dis* 124: 718-722

Stadtman E, Levine R (2003) Free radical-mediated oxidation of free amino acids and amino acid residues in proteins. *Amino acids* 25: 207-218

Stahlman MT, Gray MP, Falconieri MW, Whitsett JA, Weaver TE (2000) Lamellar body formation in normal and surfactant protein B-deficient fetal mice. *Lab Invest* 80: 395-403

Steinkühler J, Sezgin E, Urbančič I, Eggeling C, Dimova R (2019) Mechanical properties of plasma membrane vesicles correlate with lipid order, viscosity and cell density. *Commun Biol* 2: 337

Stichtenoth G, Walter G, Lange R, Raith M, Bernhard W, Herting E (2014) Surface tension of airway aspirates withdrawn during neonatal resuscitation reflects lung maturity. *Pediatr Pulmonol* 49: 751-756

Subramaniam P, Ho JJ, Davis PG (2016) Prophylactic nasal continuous positive airway pressure for preventing morbidity and mortality in very preterm infants. *Cochrane Database Syst Rev*: CD001243

Sun B, Curstedt T, Robertson B (1993) Surfactant inhibition in experimental meconium aspiration. *Acta Paediatr* 82: 182-189

Suri LN, Cruz A, Veldhuizen RA, Staples JF, Possmayer F, Orgeig S, Perez-Gil J (2013) Adaptations to hibernation in lung surfactant composition of 13-lined ground squirrels influence surfactant lipid phase segregation properties. *Biochim Biophys Acta* 1828: 1707-1714

Suri LN, McCaig L, Picardi MV, Ospina OL, Veldhuizen RA, Staples JF, Possmayer F, Yao L-J, Perez-Gil J, Orgeig S (2012) Adaptation to low body temperature influences pulmonary surfactant composition thereby increasing fluidity while maintaining appropriately ordered membrane structure and surface activity. *Biochim Biophys Acta* 1818: 1581-1589

Suryadevara V, Ramchandran R, Kamp DW, Natarajan V (2020) Lipid Mediators Regulate Pulmonary Fibrosis: Potential Mechanisms and Signaling Pathways. *Int J Mol Sci* 21

Suwabe A, Mason RJ, Voelker DR (1991) Temporal segregation of surfactant secretion and lamellar body biogenesis in primary cultures of rat alveolar type II cells. *Am J Respir Cell Mol Biol* 5: 80-86

Sweet DG, Carnielli V, Greisen G, Hallman M, Ozek E, Plavka R, Saugstad OD, Simeoni U, Speer CP, Vento M *et al* (2013) European consensus guidelines on the management of neonatal respiratory distress syndrome in preterm infants--2013 update. *Neonatology* 103: 353-368

Sweet DG, Carnielli V, Greisen G, Hallman M, Ozek E, Te Pas A, Plavka R, Roehr CC, Saugstad OD, Simeoni U *et al* (2019) European Consensus Guidelines on the Management of Respiratory Distress Syndrome - 2019 Update. *Neonatology* 115: 432-450

Sweet DG, Turner MA, Stranak Z, Plavka R, Clarke P, Stenson BJ, Singer D, Goelz R, Fabbri L, Varoli G *et al* (2017) A first-in-human clinical study of a new SP-B and SP-C enriched synthetic surfactant (CHF5633) in preterm babies with respiratory distress syndrome. *Arch Dis Child Fetal Neonatal Ed* 102: F497-f503

Szallasi A, Gronowski AM, Eby CS (2003) Lamellar body count in amniotic fluid: a comparative study of four different hematology analyzers. *Clin Chem* 49: 994-997

Tabak S, Notter R (1977) Effect of plasma proteins on the dynamic Π—a characteristics of saturated phospholipid films. *J Colloid Interface Sci* 59: 293-300

Taeusch HW, Bernardino de la Serna J, Perez-Gil J, Alonso C, Zasadzinski JA (2005) Inactivation of pulmonary surfactant due to serum-inhibited adsorption and reversal by hydrophilic polymers: experimental. *Biophys J* 89: 1769-1779

Taeusch HW, Lu KW, Goerke J, Clements JA (1999) Nonionic polymers reverse inactivation of surfactant by meconium and other substances. *Am J Respir Crit Care Med* 159: 1391-1395

Tagaram HR, Wang G, Umstead TM, Mikerov AN, Thomas NJ, Graff GR, Hess JC, Thomassen MJ, Kavuru MS, Phelps DS *et al* (2007) Characterization of a human surfactant protein A1 (SP-A1) gene-specific antibody; SP-A1 content variation among individuals of varying age and pulmonary health. *Am J Physiol Lung Cell Mol Physiol* 292: L1052-1063

Takemura Y, Goodson P, Bao HF, Jain L, Helms MN (2010) Rac1-mediated NADPH oxidase release of O2− regulates epithelial sodium channel activity in the alveolar epithelium. *Am J Physiol Lung Cell Mol Physiology* 298: L509-L520

Taneva S, Keough KM (1994a) Pulmonary surfactant proteins SP-B and SP-C in spread monolayers at the air-water interface: I. Monolayers of pulmonary surfactant protein SP-B and phospholipids. *Biophys J* 66: 1137-1148

Taneva SG, Keough KM (1994b) Dynamic surface properties of pulmonary surfactant proteins SP-B and SP-C and their mixtures with dipalmitoylphosphatidylcholine. *Biochemistry* 33: 14660-14670

Thannickal VJ, Antony VB (2018) Is personalized medicine a realistic goal in idiopathic pulmonary fibrosis? *Expert Rev Respir Med* 12: 441-443

Thébaud B, Goss KN, Laughon M, Whitsett JA, Abman SH, Steinhorn RH, Aschner JL, Davis PG, McGrath-Morrow SA, Soll RF *et al* (2019) Bronchopulmonary dysplasia. *Nat Rev Dis Primers* 5: 78

Tian Y, Zhou R, Rehg JE, Jackowski S (2007) Role of phosphocholine cytidylyltransferase alpha in lung development. *Mol Cell Biol* 27: 975-982

Tokieda K, Ikegami M, Wert SE, Baatz JE, Zou Y, Whitsett JA (1999) Surfactant protein B corrects oxygen-induced pulmonary dysfunction in heterozygous surfactant protein B-deficient mice. *Pediatr Res* 46: 708-714

Touqui L, Arbibe L (1999) A role for phospholipase A2 in ARDS pathogenesis. *Mol Med Today* 5: 244-249

Tridente A, De Martino L, De Luca D (2019) Porcine vs bovine surfactant therapy for preterm neonates with RDS: systematic review with biological plausibility and pragmatic meta-analysis of respiratory outcomes. *Respir Res* 20: 28

Triggiani M, Granata F, Petraroli A, Loffredo S, Frattini A, Staiano RI, Monaco G, Marone G (2009) Inhibition of secretory phospholipase A2-induced cytokine production in human lung macrophages by budesonide. *Int Arch Allergy Immunol* 150: 144-155

Ueda T, Cheng G, Kuroki Y, Sano H, Sugiyama K, Motojima S, Fukuda T (2000) Effects of aging on surfactant forms in rats. *Eur Respir J* 15: 80-84

Ueda T, Ikegami M, Henry M, Jobe AH (1995) Clearance of surfactant protein B from rabbit lungs. *Am J Physiol* 268: L636-641

Um SJ, Lam S, Coxson H, Man SF, Sin DD (2013) Budesonide/formoterol enhances the expression of pro Surfactant Protein-B in lungs of COPD patients. *PLoS One* 8: e83881

van Meer G, Voelker DR, Feigenson GW (2008) Membrane lipids: where they are and how they behave. *Nat Rev Mol Cell Biol* 9: 112-124

Van Vliet BN, Montani J-P (2005) Circulation and Fluid Volume Control. In: *Integrative Physiology in the Proteomics and Post-Genomics Age*, Walz W., Humana press (ed.) pp. 43-66.

Veldhuizen R, Hearn S, Lewis J, Possmayer F (1994) Surface-area cycling of different surfactant preparations: SP-A and SP-B are essential for large-aggregate integrity. *Biochem J* 300: 519-524

Veldhuizen R, McCaig LA, Akino T, Lewis JF (1995) Pulmonary surfactant subfractions in patients with the acute respiratory distress syndrome. *Am J Respir Crit Care Med* 152: 1867-1871

Veldhuizen R, Nag K, Orgeig S, Possmayer F (1998) The role of lipids in pulmonary surfactant. *Biochim Biophys Acta* 1408: 90-108

Veldhuizen RA, McCaig LA, Pape C, Gill SE (2019) The effects of aging and exercise on lung mechanics, surfactant and alveolar macrophages. *Exp Lung Res* 45: 113-122

Verder H, Albertsen P, Ebbesen F, Greisen G, Robertson B, Bertelsen A, Agertoft L, Djernes B, Nathan E, Reinholdt J (1999) Nasal continuous positive airway pressure and early surfactant therapy for respiratory distress syndrome in newborns of less than 30 weeks' gestation. *Pediatrics* 103: e24-e24

Verlato G, Simonato M, Giambelluca S, Fantinato M, Correani A, Cavicchiolo ME, Priante E, Carnielli V, Cogo P (2018) Surfactant components and tracheal aspirate inflammatory markers in preterm infants with respiratory distress syndrome. *J Pediatr* 203: 442-446

Vieira AC, Fiori HH, Garcia PC, Piva JP, Munhoz TP, Fiori RM (2012) Lamellar body count and stable microbubble test on tracheal aspirates from infants for the diagnosis of respiratory distress syndrome. *Pediatr Crit Care Med* 13: 178-182

Voorhout WF, Veenendaal T, Kuroki Y, Ogasawara Y, van Golde LM, Geuze HJ (1992) Immunocytochemical localization of surfactant protein D (SP-D) in type II cells, Clara cells, and alveolar macrophages of rat lung. *J Histochem Cytochem* 40: 1589-1597

Vorbroker DK, Profitt SA, Nogee LM, Whitsett JA (1995) Aberrant processing of surfactant protein C in hereditary SP-B deficiency. *Am J Physiol* 268: L647-656

Vrânceanu M, Winkler K, Nirschl H, Leneweit G (2008) Surface rheology and phase transitions of monolayers of phospholipid/cholesterol mixtures. *Biophys J* 94: 3924-3934

Wagner PD (2015) The physiological basis of pulmonary gas exchange: implications for clinical interpretation of arterial blood gases. *Eur Respir J* 45: 227-243

Walani SR (2020) Global burden of preterm birth. *Int J Gynaecol Obstet* 150: 31-33

Walker SR, Williams MC, Benson B (1986) Immunocytochemical localization of the major surfactant apoproteins in type II cells, Clara cells, and alveolar macrophages of rat lung. *J Histochem Cytochem* 34: 1137-1148

Walski M, Pokorski M, Antosiewicz J, Rekawek A, Frontczak-Baniewicz M, Jernajczyk U, Di Giulio C (2009) Pulmonary surfactant: ultrastructural features and putative mechanisms of aging. *J Physiol Pharmacol* 60: 121-125

Walters RW, Jenq RR, Hall SB (2000) Distinct steps in the adsorption of pulmonary surfactant to an air-liquid interface. *Biophys J* 78: 257-266

Wang L, Cai P, Galla HJ, He H, Flach CR, Mendelsohn R (2005a) Monolayer-multilayer transitions in a lung surfactant model: IR reflection-absorption spectroscopy and atomic force microscopy. *Eur Biophys J* 34: 243-254

Wang L, Cruz A, Flach CR, Pérez-Gil J, Mendelsohn R (2007) Langmuir-Blodgett films formed by continuously varying surface pressure. Characterization by IR spectroscopy and epifluorescence microscopy. *Langmuir* 23: 4950-4958

Wang L, Magdaleno S, Tabas I, Jackowski S (2005b) Early embryonic lethality in mice with targeted deletion of the CTP:phosphocholine cytidylyltransferase alpha gene (Pcyt1a). *Mol Cell Biol* 25: 3357-3363

Wang N, Silver DL, Thiele C, Tall AR (2001) ATP-binding cassette transporter A1 (ABCA1) functions as a cholesterol efflux regulatory protein. *J Biol Chem* 276: 23742-23747

Wang Z, Gurel O, Baatz JE, Notter RH (1996a) Differential activity and lack of synergy of lung surfactant proteins SP-B and SP-C in interactions with phospholipids. *J Lipid Res* 37: 1749-1760

Wang Z, Hall SB, Notter RH (1996b) Roles of different hydrophobic constituents in the adsorption of pulmonary surfactant. *J Lipid Res* 37: 790-798

Warriner HE, Ding J, Waring AJ, Zasadzinski JA (2002) A concentration-dependent mechanism by which serum albumin inactivates replacement lung surfactants. *Biophys J* 82: 835-842

Watterberg KL, Aucott S, Benitz WE, Cummings JJ, Eichenwald EC, Goldsmith J, Poindexter BB, Puopolo K, Stewart DL, Wang KS (2015) The apgar score. *Pediatrics* 136: 819-822

Weaver TE (1998) Synthesis, processing and secretion of surfactant proteins B and C. *Biochim Biophys Acta* 1408: 173-179

Weaver TE, Conkright JJ (2001) Function of surfactant proteins B and C. *Annu Rev Physiol* 63: 555-578

Weiskirchen R (2020) Severity of Coronavirus Disease 2019 (COVID-19): Does Surfactant Matter? *Front Microbiol* 11: 1905

White HD, Ghamande S, Arroliga AC (2017) Therapeutic Hypothermia for Acute Respiratory Distress Syndrome. *Crit Care Med* 45: e1202-e1203

Wilder MA (2004) Surfactant protein B deficiency in infants with respiratory failure. *J Perinat Neonatal Nurs* 18: 61-67

Williams I, Zasadzinski JA, Squires TM (2019) Interfacial rheology and direct imaging reveal domain-templated network formation in phospholipid monolayers penetrated by fibrinogen. *Soft Matter* 15: 9076-9084

Wirtz HR, Dobbs LG (1990) Calcium mobilization and exocytosis after one mechanical stretch of lung epithelial cells. *Science* 250: 1266-1269

Wisnivesky J, de-Torres JP (2019) The global burden of pulmonary diseases: most prevalent problems and opportunities for improvement. *Ann Glob Health* 85: 1

Wissel H, Lehfeldt A, Klein P, Müller T, Stevens PA (2001) Endocytosed SP-A and surfactant lipids are sorted to different organelles in rat type II pneumocytes. *Am J Physiol Lung Cell Mol Physiol* 281: L345-360

Wiswell TE, Knight GR, Finer NN, Donn SM, Desai H, Walsh WF, Sekar KC, Bernstein G, Keszler M, Visser VE *et al* (2002) A multicenter, randomized, controlled trial comparing Surfaxin (Lucinactant) lavage with standard care for treatment of meconium aspiration syndrome. *Pediatrics* 109: 1081-1087

Wojciechowski WV (2005) Respiratory Care Sciences: An Integrated Approach 4th Edition. *Delmar Thomson Learning*

Wong CK, Smith CA, Sakamoto K, Kaminski N, Koff JL, Goldstein DR (2017) Aging Impairs Alveolar Macrophage Phagocytosis and Increases Influenza-Induced Mortality in Mice. *J Immunol* 199: 1060-1068

Wu N, Hanrahan J, Bornstein J, Chen S-Y, 2015. Healthcare costs utilization and costs of patients hospitalized with acute respiratory distress syndrome (ARDS) in US commercially-insured individuals and Medicare beneficiaries. Eur Respiratory Soc.

Wu YZ, Medjane S, Chabot S, Kubrusly FS, Raw I, Chignard M, Touqui L (2003) Surfactant protein-A and phosphatidylglycerol suppress type IIA phospholipase A2 synthesis via nuclear factor-kappaB. *Am J Respir Crit Care Med* 168: 692-699

Wüstneck N, Wüstneck R, Perez-Gil J, Pison U (2003) Effects of oligomerization and secondary structure on the surface behavior of pulmonary surfactant proteins SP-B and SP-C. *Biophys J* 84: 1940-1949

Wyllie J, Perlman JM, Kattwinkel J, Wyckoff MH, Aziz K, Guinsburg R, Kim HS, Liley HG, Mildenhall L, Simon WM *et al* (2015) Part 7: Neonatal resuscitation: 2015 International Consensus on Cardiopulmonary Resuscitation and Emergency Cardiovascular Care Science with Treatment Recommendations. *Resuscitation* 95: e169-201

Xu L, Yang Y, Zuo YY (2020) Atomic Force Microscopy Imaging of Adsorbed Pulmonary Surfactant Films. *Biophys J* 119: 756-766

Yasuoka S, Manabe H, Ozaki T, Tsubura E (1977) Effect of age on the saturated lecithin contents of human and rat lung tissues. *J Gerontol* 32: 387-391

Yazicioglu T, Mühlfeld C, Autilio C, Huang CK, Bär C, Dittrich-Breiholz O, Thum T, Pérez-Gil J, Schmiedl A, Brandenberger C (2020) Aging impairs alveolar epithelial type II cell function in acute lung injury. *Am J Physiol Lung Cell Mol Physiol* 319: L755-l769

Yeh TF, Chen CM, Wu SY, Husan Z, Li TC, Hsieh WS, Tsai CH, Lin HC (2016) Intratracheal Administration of Budesonide/Surfactant to Prevent Bronchopulmonary Dysplasia. *Am J Respir Crit Care Med* 193: 86-95

Yeh TF, Lin HC, Chang CH, Wu TS, Su BH, Li TC, Pyati S, Tsai CH (2008) Early intratracheal instillation of budesonide using surfactant as a vehicle to prevent chronic lung disease in preterm infants: a pilot study. *Pediatrics* 121: e1310-e1318

Yost CC, Soll RF (2000) Early versus delayed selective surfactant treatment for neonatal respiratory distress syndrome. *Cochrane Database Syst Rev*: Cd001456

Yu LM, Lu JJ, Chan YW, Ng A, Zhang L, Hoorfar M, Policova Z, Grundke K, Neumann AW (2004) Constrained sessile drop as a new configuration to measure low surface tension in lung surfactant systems. *J Appl Physiol (1985)* 97: 704-715

Yu S-H, Possmayer F (1993) Adsorption, compression and stability of surface films from natural, lipid extract and reconstituted pulmonary surfactants. *Biochim Biophys Acta* 1167: 264-271

Zarbock R, Kaltenborn E, Frixel S, Wittmann T, Liebisch G, Schmitz G, Griese M (2015) ABCA3 protects alveolar epithelial cells against free cholesterol induced cell death. *Biochim Biophys Acta* 1851: 987-995

Zasadzinski JA, Alig T, Alonso C, De La Serna JB, Perez-Gil J, Taeusch HW (2005) Inhibition of pulmonary surfactant adsorption by serum and the mechanisms of reversal by hydrophilic polymers: theory. *Biophys J* 89: 1621-1629

Zhang P, Villanueva V, Kalkowski J, Liu C, Pham T, Perez-Salas U, Bu W, Lin B, Liu Y (2019) Polyunsaturated Phospholipid Modified Membrane Degradation Catalyzed by a Secreted Phospholipase A2. *Langmuir* 35: 11643-11650

Zou C, Butler PL, Coon TA, Smith RM, Hammen G, Zhao Y, Chen BB, Mallampalli RK (2011) LPS impairs phospholipid synthesis by triggering β-transducin repeat-containing protein (β-TrCP)-mediated polyubiquitination and degradation of the surfactant enzyme acyl-CoA: lysophosphatidylcholine acyltransferase I (LPCAT1). *J Biol Chem* 286: 2719-2727

Zuo YY, Alolabi H, Shafiei A, Kang N, Policova Z, Cox PN, Acosta E, Hair ML, Neumann AW (2006) Chitosan enhances the in vitro surface activity of dilute lung surfactant preparations and resists albumin-induced inactivation. *Pediatr Res* 60: 125-130

Zuo YY, Veldhuizen RA, Neumann AW, Petersen NO, Possmayer F (2008) Current perspectives in pulmonary surfactant—inhibition, enhancement and evaluation. *Biochim Biophys Acta* 1778: 1947-1977